University of Tennessee, Knoxville

TRACE: Tennessee Research and Creative Exchange

Doctoral Dissertations

Graduate School

8-2004

Crystallization of Polyamide 66 Copolymers at High Supercoolings

Xiaoping Guan
University of Tennessee - Knoxville

Follow this and additional works at: https://trace.tennessee.edu/utk_graddiss

 Part of the Other Engineering Commons

Recommended Citation

Guan, Xiaoping, "Crystallization of Polyamide 66 Copolymers at High Supercoolings. " PhD diss., University of Tennessee, 2004.
https://trace.tennessee.edu/utk_graddiss/2272

This Dissertation is brought to you for free and open access by the Graduate School at TRACE: Tennessee Research and Creative Exchange. It has been accepted for inclusion in Doctoral Dissertations by an authorized administrator of TRACE: Tennessee Research and Creative Exchange. For more information, please contact trace@utk.edu.

To the Graduate Council:

I am submitting herewith a dissertation written by Xiaoping Guan entitled "Crystallization of Polyamide 66 Copolymers at High Supercoolings." I have examined the final electronic copy of this dissertation for form and content and recommend that it be accepted in partial fulfillment of the requirements for the degree of Doctor of Philosophy, with a major in Polymer Engineering.

Paul J. Phillips, Major Professor

We have read this dissertation and recommend its acceptance:

Joseph E. Spruiell, Roberto S. Benson, John R. Collie

Accepted for the Council:

Carolyn R. Hodges

Vice Provost and Dean of the Graduate School

(Original signatures are on file with official student records.)

To the Graduate Council:

I am submitting herewith a dissertation written by Xiaoping Guan entitled "Crystallization of Polyamide 66 Copolymers at High Supercoolings". I have examined the final electronic copy of this dissertation for form and content and recommend that it be accepted in partial fulfillment of the requirements for the degree of Doctor of Philosophy, with a major in Polymer Engineering.

Paul J. Phillips
Major Professor

We have read this dissertation
and recommend its acceptance:

Joseph E. Spruiell

Roberto S. Benson

John R. Collier

Accepted for the Council:

Anne Mayhew
Vice Chancellor and
Dean of Graduate Studies

(Original signatures are on file with official student records.)

CRYSTALLIZATION OF POLYAMIDE 66 COPOLYMERS AT HIGH SUPERCOOLINGS

A Dissertation
Presented for the
Doctor of Philosophy
Degree
The University of Tennessee, Knoxville

Xiaoping Guan

August 2004

ACKNOWLEDGEMENTS

First, I am especially indebted to my advisor Dr. Paul J. Phillips who has led me into fascinating field of polymer physics. He has always been patient to my wondering thoughts and been supportive during every step of my graduate studying. I am much honored to have Dr. Joseph E. Spruiell, Dr. Roberto S. Benson and Dr. John R. Collier to serve in my doctoral committee because each of them has been very actively involved in the relative research fields before. Their expertise and advice are indispensable for the successful completion of this dissertation studies.

Secondly, I would like to thank Dr. Kevin M. Kit for generously granting me access to DMA instrument and I have benefited tremendously from his wonderful lecture and warmhearted support. I especially appreciate Ms. Shelley Ling, Dr. Joseph E. Spruiell and Dr. J. S. Lin of Oak Ridge National Laboratory for their helpful advises on X-ray experiments. I also appreciate the quality and efficient DSC experiments of Mr. Tom Malmgren and Dr. Marek Pyda in Chemistry Department.

Finally, I would like to thank Sandy and Carla for their patience and kindness in preparing numerous paperwork for me from the first day I came to Knoxville; thank Frank and Randy for meeting my never satisfied appetite of nitrogen; thank Stephen, Greg, Mike and Doug for helping me fix the instruments. I am very grateful to many friendly staffs and fellow students during my graduate studies here. I especially appreciate many discussion and help from Anita Dimeska, Dr. Stein Schreiber, Dr. John Wagner, Dr. Samir Abu-Iqyas and Rahul Patki.

ABSTRACT

Crystallization kinetics and morphologies of a series of random copolymers of PA 66 (or Nylon 66) have been investigated at high supercoolings. Optical microscopy with rapid cooling apparatus was employed to observe spherulitic morphologies and measure growth rates. Final spherulitic morphologies of PA 66 and copolymers could be changed with increasing supercoolings from impinged spherulites to isolated spherulites with decreasing size until total amorphous.

Spherulite growth results indicated that the rates of crystallization of PA 66 copolymers were reduced with increasing content of comonomer, and crystallization was moved to lower temperatures. The melting temperature, crystallinity, crystal structure and lamellar thickness of the PA 66 copolymers from different cooling conditions were studied with Differential Scanning Calorimetry (DSC), Wide Angle X-ray Diffraction (WAXD), and Small Angle X-ray Scattering (SAXS).

Even though no temperature plateau is detected in the cooling curve, the spherulite growth of PA 66 at high supercooling is still found to be linear with time. This is attributed to a steady temperature gradient existing at the growth front. The spherulite growth kinetics of PA 66 across the whole supercooling range could be affected by the interaction of chain diffusion rate (into growth front), nucleation rate and latent heat diffusion (from growth front) at different crystallization temperatures. The morphology and melting behavior of PA 66 crystals can be explained by the behavior of H-bonding with increasing temperatures.

Dynamic mechanical relaxation behavior of PA 66 copolymers with different spherulitic morphologies were examined and compared with those of polyethylene copolymers to reveal the relationship between morphologies and dynamic mechanical relaxations.

TABLE OF CONTENT

LIST OF TABLES

LIST OF FIGURES

CHAPTER 1. INTRODUCTION

1.1. Brief background of PA 66 crystallization

Copolymerization is an effective way to change the polymer process window; many copolymers are synthesized to modify the crystallization behavior and control the final crystal morphology. These copolymers also provide a special window to help us clarify the crystallization behavior of homopolymers. This method was demonstrated to be very effective in clarifying the crystallization mechanism of polyethylene, especially when the crystallization of the copolymers is studied over a wide range of supercooling or pressure, which are two of the most important parameters of polymer processing. Our particular interest in this research is to study the crystallization behavior of random copolymers of PA 66 at high supercoolings.

The diverse spherulitic morphology of PA 66 has been studied by several authors (Khoury 1958, Lovinger 1978a, Magill 1966, Mann & Roldan-Gonzalez 1962, Ramesh et al 1994a). The crystallization kinetics of positive spherulites have been reported (Burnett & McDevit 1957, Harvey & Hybart 1971, Lindegren 1961, McLaren 1963, Stouffer et al 1996). Bulk crystallization of random copolymers of PA66/6, PA 66/6T (hexamethlyene terephthalamide) were also studied (Harvey & Hybart 1971).

Detailed studies were made of the spherulite growth kinetics, melting temperature and lamellar thickness (Schreiber 1998) of copolymers of PA 66 with 6T (hexamethlyene terephthalamide), 6I (hexamethlyene isophthalamide) and 6 at isothermal crystallization conditions (up to 220 ^{o}C). The lamellar thickness (about 1.5-2 chemical repeat units) of PA 66 did not change with the crystallization temperature as secondary nucleation

predicted. After a free energy simulation, it was found that the critical nucleus required for secondary nucleation (by chain folding along growth surface) is unrealistically big (31.4 unit cells even at 200°C), therefore it was concluded that PA 66 should crystallize with surface roughening mechanism by directly folding into melt due to H-bond as suggested for PA 66 positive spherulites (Lovinger 1978b).

1.2. Research objectives

In this study, we will extend the crystallization studies of PA 66 and copolymers to much higher supercoolings by taking advantage of rapid cooling method (Ding & Spruiell 1996). The initiative objectives are:

1) To extend the growth rates of PA66 copolymer to higher supercoolings and to see if they follow surface roughening mechanism;

2) To develop the surface roughening theory for PA 66 copolymers in terms of changing growth front shapes;

3) To explain the morphology and lamellar thickness of PA 66 copolymer at different supercooling using surface roughening theory;

4) To relate the melting behavior and dynamic mechanical relaxation behavior to structure and morphology.

In addition, two more objectives are derived during the process of experiments:

5) To develop a new thermal model for the spherulite growth front and test this temperature model in a system (PET) that undergoes secondary nucleation;

6) To re-evaluate the big picture of crystal growth mechanism over a wide range of supercoolings.

CHAPTER 2. LITERATURE REVIEW

2.1. Polymer crystallization kinetic theories

2.1.1. Basic thermodynamics in crystallization

Thermodynamics of phase transition provides the base for us to understand the driving force of crystallization as well as the minimum thickness for stable lamella (Armistead & Goldbeck-Wood 1992).

2.1.1.1. Driving force of crystallization

The free energy difference of phase transition at temperature T can be expressed as

$$\Delta G_f = \Delta H_f - T\Delta S_f \qquad (2.1)$$

The free energy decrease provides the driving force for crystallization. At the equilibrium melting temperature $T_m°$, the free energy of melt and crystal are equal ($\Delta G_f = 0$). Therefore, the entropy of fusion at $T_m°$ can be expressed as

$$\Delta S_f = \frac{\Delta H_f}{T_m^o} \qquad (2.2)$$

For small supercoolings, both ΔH_f and ΔS_f are approximately independent of the temperature. The free energy difference can be written as a function of supercooling ΔT (see Figure 2.1).

$$\Delta G_f = \Delta H_f \left(1 - \frac{T}{T_m^o}\right) = \Delta H_f \frac{\Delta T}{T_m^o} \qquad (2.3)$$

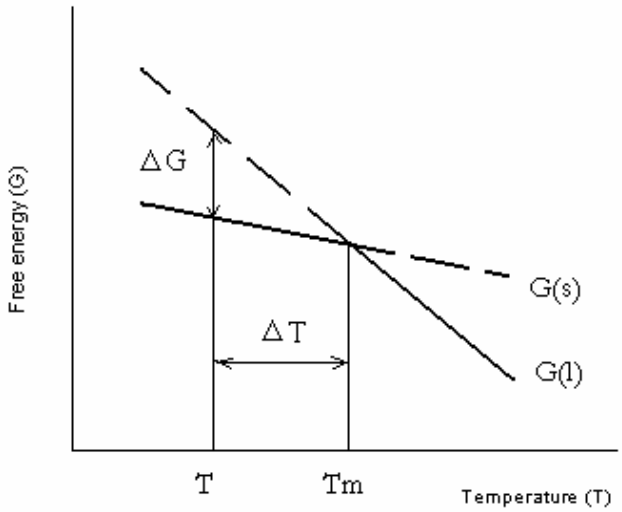

Figure 2.1 Schematic diagram of thermodynamic of polymer crystallization.

2.1.1.2. Critical lamellar thickness (or stem length)

Even though the free energy difference provides the driving force for crystallization, it does not always happen immediately, especially at the early stage of crystallization (nucleation). This is because the surface tension of newly formed crystal (nucleus) can increase the free energy. Therefore, the crystallization can occur only after the nucleus reaches some critical size, when the free energy decrease from phase transition exceeds the free energy increase from the surface tension.

This critical size is usually expressed as critical radius in metals, but it is expressed as critical stem length due to the unique lamellar morphology of polymer crystals. The total free energy of polymer crystal-melt system (see Figure 2.2) can be expressed as:

$$\Delta G_{Tot} = -\rho abl\Delta G_f + 2\sigma_e ab + 2\sigma al + 2\sigma bl \qquad (2.4)$$

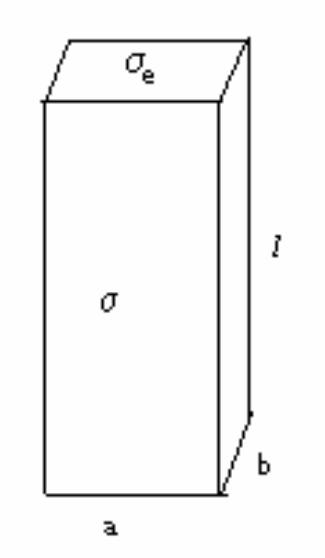

Figure 2.2 Schematic drawing of surface free energy of polymer crystal.

If surface free energy of lamella folding surface is much greater than that of lateral surface ($\sigma_e >> \sigma$), the contribution of lateral surface free energy can be ignored. Then the critical stem length can be expressed as

$$l^* = \frac{2\sigma_e}{\rho \Delta G} = \frac{2\sigma_e T_m^o}{\rho \Delta H_f \Delta T} \qquad (2.5)$$

This shows that the critical lamellar thickness varies inversely with the supercooling. We can rearrange equation 2.5 to get the melting temperature needed for a given lamellar thickness *l*:

$$T = T_m^o \left(1 - \frac{2\sigma_e}{\rho \Delta H_f} \frac{1}{l} \right) \qquad (2.6)$$

This is actually the well-known Gibbs-Thomson Equation.

2.1.2. Kinetic theories of pure metals and small molecules

In general, there are two different types of solid/liquid interface: atomic rough interface usually associated with metallic systems; and an atomic flat interface associated with non-metals. Due to the different atomic/molecular structure, continuous growth process is observed for rough interface; lateral growth process is usually observed in flat interface (Porter & Easterling 2001). This rough/flat interface could be the result of different magnitude of free energy decrease during the phase transition.

2.1.2.1. Diffusion controlled growth (Rough surface)

In this case, the driving force is very strong, and there is no nucleation barrier at any supercooling for rough surface. Since determining factor of crystallization is transport of mass or heat to or from the interface, the growth rate is to be expected to be linear to ΔT.

$$v = k_1 \Delta T \qquad (2.7)$$

Usually k_1 value is so high that supercooling of only a fraction of a Kelvin can achieve normal growth rate. The solidification process is therefore a diffusion-controlled process. Growth rate of pure metals are controlled by the heat diffusion, whereas growth of alloys is controlled by solute diffusion. It can be assumed that the atoms can be accepted at any sites in metals.

2.1.2.2. Interface controlled growth (smooth surface)

Usually materials with high entropy of fusion prefer to form atomically smooth (closely packed) interface, which could be the result of small driving force (ΔG) of

crystallization. Atoms prefer to join the ledges than attach to the smooth interface because the former position will result much lower increase of interfacial energy. Depending on how the ledges are formed, there are three different ways of lateral growth.

Surface Nucleation

Analogous to the forming of nucleus of critical size in homogeneous nucleation, a stable two-dimensional nucleus can be formed on the smooth interface. This process is usually called as *surface nucleation* (or secondary nucleation) to differentiate from primary nucleation. Once nucleated, it spreads rapidly over the interface.

The growth rate of the interface will be governed by the surface nucleation process. This can be expressed by

$$v \propto \exp(-k_2 / \Delta T) \qquad (2.8)$$

This is the case of the classical nucleation crystallization. It was later extended further to consider the relative value of nucleation rate (i) and spreading rate (g) in polymer crystallization (Lauritzen & Hoffman 1973). Overall growth rate is determined by the competition of nucleation and growth.

Regime I: spreading is much faster than nucleation

$$v_I \equiv b_o i L \qquad (2.9)$$

Regime II: more than one nucleus exists on the growth face; thus growth rate depends on both.

$$v_{II} \equiv b_o (2ig)^{1/2} \qquad (2.10)$$

Regime III (kinetic roughening): no nucleation barrier at high supercooling; growth rate depends on spreading rate.

$$v_{III} \equiv b_o i n_{III} a_0 \qquad (2.11)$$

It should be mentioned that kinetics roughening is different from the rough surface growth in that 1) growth rate in kinetic roughening is still determined by the surface nucleation rate; 2) atom adding direction is still parallel to the interface rather than normal to the interface as in the rough surface growth.

Spiral Growth (Screw Dislocation)

The screw dislocation exists as crystal defect can work as the ledge of step required for the lateral growth. The atoms add on to the step with an equal rate along the step, the step will develop into a growth spiral. It was shown that growth rate (Porter & Easterling 2001) of interface could be expressed as

$$v = k_3 (\Delta T)^2 \qquad (2.12)$$

Spiral growth is also observed in polymer solution crystallization, but the spiral growth occurs on the folding surface rather than the lamella growth direction that is always normal to the folding plane.

Growth from Twin Intersections (Twinning)

When two crystals in different orientations are in contact, the interface at the twin boundary can act as a source of new step to facilitate a growth mechanism just like spiral growth. The growth rates of different growth mechanism were shown in Figure 2.3.

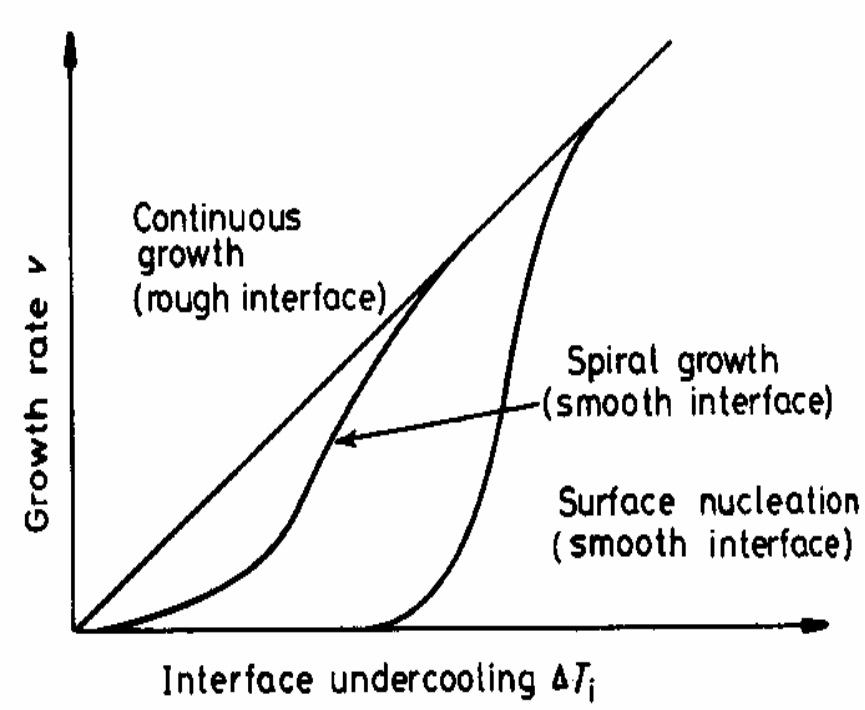

Figure 2.3 Comparing different growth kinetics on atomically rough and smooth surfaces. (Porter & Easterling 2001)

2.1.3. Growth phenomena in polymer crystallization

Before proceeding to discuss the growth mechanism of polymer crystallization, it is meaningful to recall some of the important features of polymer crystallization.

The most striking feature of polymer crystal (PE) is the chain folding mechanism in lamellae. Chain folding in polymer will be understandable if comparing with the extended chain crystals of paraffin, since polymers are just long chains consisting of many single monomers.

The crystallization behavior of polymers therefore should be very similar to the packing of monomers in terms of the interaction between the crystal motifs, whereas the constraint effect of chain on the crystal units should not be ignored. Other than the chain folding, the dependence of growth rate and the lamellar thickness on crystallization temperature (or supercooling) are also unique features of polymer crystallization.

2.1.3.1. Typical growth rate of polymer at different crystallization temperature

It was found in many isothermal kinetics studies that spherulites grow at a constant rate for a given temperature, except slowing down towards the end of the crystallization (Keller 1968). In general, the growth rates of polymers are found to increase with supercooling first, and then reach to a maximum value at some temperature between melting point (Tm) and glass transition temperature (Tg), finally the growth rate decrease with the supercooling. A typical growth rates plot versus crystallization temperature of polyamides is shown in Figure 2.4.

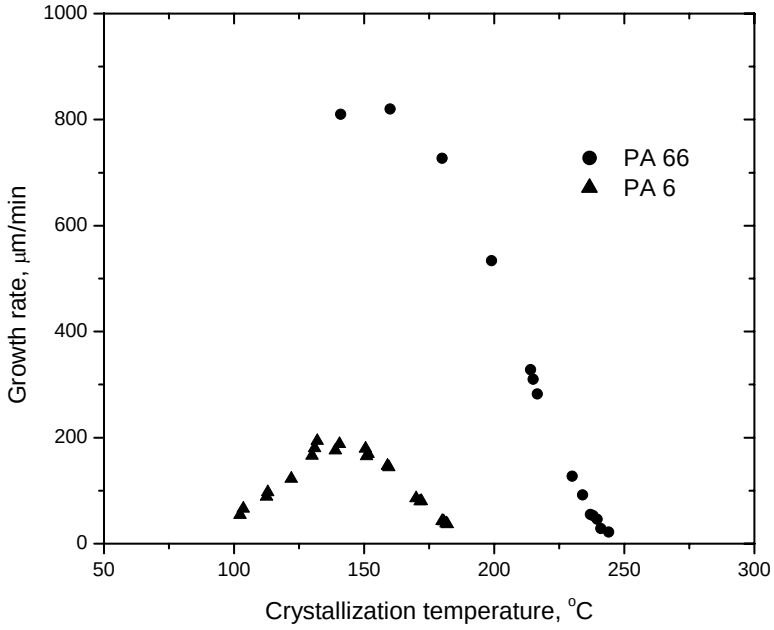

Figure 2.4 Spherulitic growth rates versus crystallization temperature for PA66 and PA6. (Burnett & McDevit 1957).

This bell shape growth rate plot is usually explained by the competition between (surface) nucleation process and (chain) diffusion process during the crystallization of polymer at different crystallization temperature. At high crystallization temperature (low supercooling) the nucleation is the controlling process, small supercooling results in slow growth rate; while at low crystallization temperature (high supercooling) diffusion is controlling process, the limited mobility limits the overall growth rate.

Such a curve can be easily predicted by simple model following such an equation (Phillips 1990):

$$G = G_0 \exp(-\frac{\Delta F^*}{kT}) \exp(-\frac{\Delta U^*}{kT}) \qquad (2.13)$$

Where G is the grow rate at temperature T, G_0 is a pre-exponential factor, ΔF^* is the free energy of forming critical nucleus, and ΔU^* is the activation energy of chain segment jump process.

2.1.3.2. Lamellar thickness versus crystallization temperature

It was observed (Keller 1968) that the crystallization temperature determined the fold length of crystal in polyethylene solution crystallization; the fold length is higher for higher crystallization temperature.

It was found later that lamellar thickness is only determined by the crystallization temperature in the same polymer-solvent system (see Figure 2.5.).

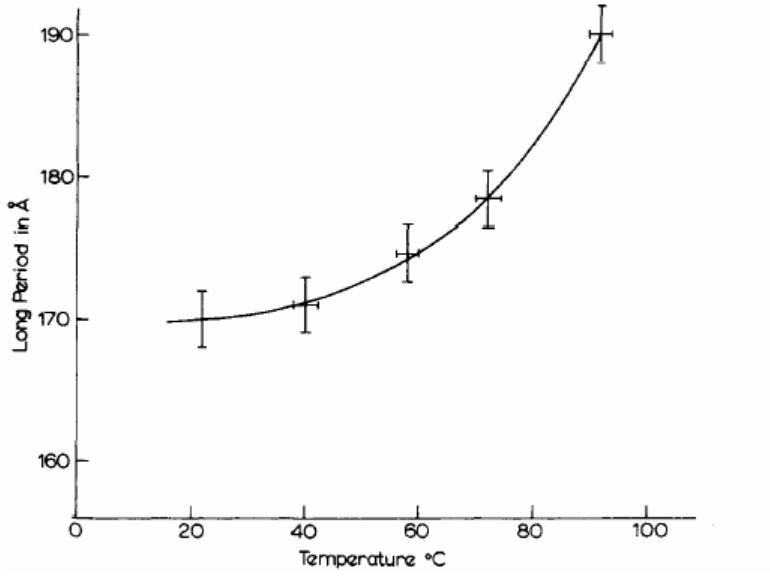

Figure 2.5 Lamellar thickness of polyethylene increased with crystallization temperature. (Keller 1968)

2.1.4. Secondary (or surface) nucleation theory of Lauritzen-Hoffman

All theories are developed to explain experimental results; so is the second nucleation theory. The early experimental results of polymer crystallization in solution are 1) growth rate is proportional to exp (-1/ΔT) and 2) observed crystals are facetted, 3) chain folding morphology in single crystal. All of these suggested characteristic nucleation controlled behavior.

With a flux-based kinetics treatment, chain folding mechanism was incorporated into the nucleation theory (Lauritzen & Hoffman 1973) to explain the free energy barrier, as well as the crystallization temperature dependence of lamellar thickness and growth rates.

The surface nucleation model (Hoffman & Miller 1997) is shown schematically in Figure 2.6. The first stem is the most difficult to attach onto the smooth growth front due to high free energy barrier, which is associated with surface free energies of two the lateral surfaces just formed.

After the successful attachment of the first stem, the new stems can be rapidly added to the “niche” on both sides of the first stem by the chain folding process. The work of forming fold can be balanced by the free energy of fusion of stems filling the niche. After the substrate spreading process, growth front advances by the layer thickness of b_0. The repeat process of nucleation-substrate completion therefore leads to a growth rate G.

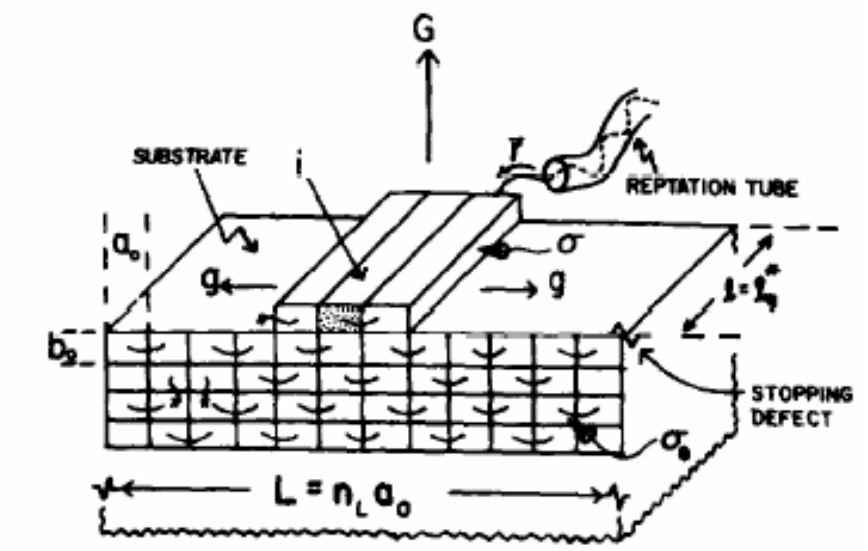

(a)

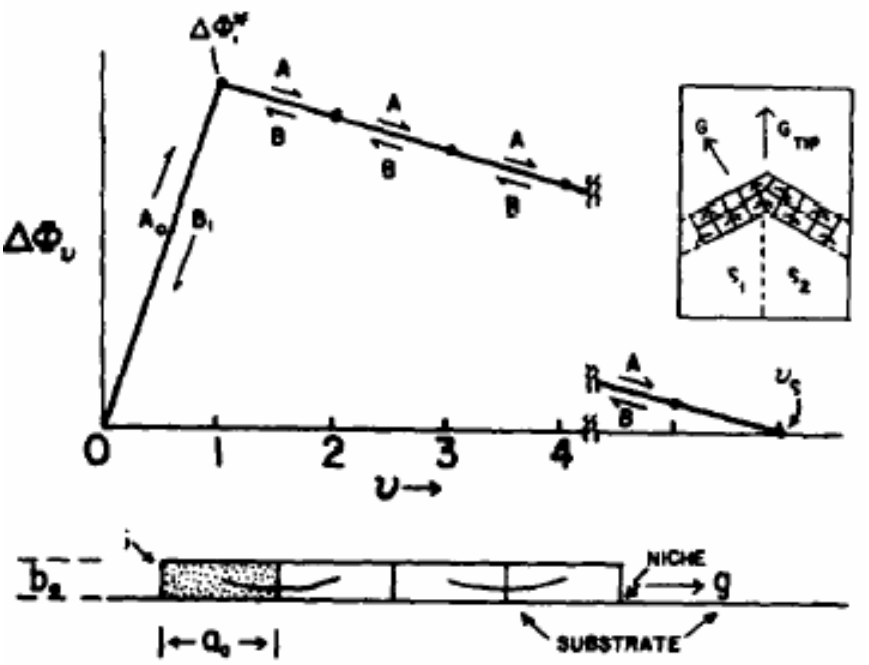

(b)

Figure 2.6 Secondary nucleation models: a) Physical path; b) Free energy barrier. (Hoffman & Miller 1997)

2.1.4.1. Thickness of the crystal

Based on the equation 2.14 derived from flux based treatment, it was suggested that the average lamellar thickness is determined by the net rate of the passage over the barrier, therefore the lamellar thickness is kinetically determined (Hoffman & Miller 1997). However, it should be mentioned that the thermodynamic origin of the free energy barrier makes such an argument very doubtful.

$$\langle l \rangle_{av} = \frac{\int_{2\sigma_e/\Delta F}^{\infty} lS(l)dl}{\int_{2\sigma_e/\Delta F}^{\infty} S(l)dl} = \frac{2\sigma_e}{\Delta F} + \delta l = \frac{2\sigma_e T_m^o}{\Delta H_f (T_m^o - T)} + \delta l \qquad (2.14)$$

2.1.4.2. Growth rate regime theory

By introducing a retardation factor into both nucleation rate and spreading rate, the growth rate of polymer at different regime (Hoffman & Miller 1997) can be written in a general form, which actually always contain the contributions of diffusion effect and nucleation as discussed in the growth rate – crystallization temperature dependence.

$$G = G_o \exp\left\{\frac{-Q_D^*}{RT}\right\} \exp\left\{\frac{-K_g}{T_c \Delta T}\right\} \qquad (2.15)$$

in which G_0 is a factor in the units of cm/s and nucleation constant, depending on the regime the value of K_g has the form of

$$K_{gI} = 2K_{gII} = K_{gIII} = \frac{4b_0 \sigma \sigma_e T_m^0}{\Delta H_f k} \qquad (2.16)$$

The schematic descriptions of regime I, II and III are shown in Figure 2.7. Regime I is the classical nucleation situation with the spreading rate much greater than the nucleation rate; Regime II occurs when the two rates are comparable; Regime III occurs when the nucleation rate is much greater than the spreading rate.

The regime transition behavior of growth rate can be checked by plotting log G + $\Delta U^* / kT$ versus $1/T\Delta T$ where ΔT is the supercooling. Therefore, this plot actually singles out the effect of diffusion contribution to the growth rate, and the slope is related to the contribution of nucleation.

The growth rated plot (see Figure 2.8a) and regime plot (see Figure 2.8b) demonstrate typical regime transitions in linear polyethylene.

2.1.5. Spherulite phenomenological theory of Keith-Padden

It was noticed that three general features always existing in spherulite-forming materials (Keith & Padden 1963): 1) arrays of fibrillar crystal habit inside spherulites; 2) non-crystallographic fiber branching; 3) impurities in small molecules forming spherulites.

Then a phenomenological spherulite formation theory was proposed that fibrillar structures were caused by the diffusion of impurities, which were rejected preferentially by the growing crystals. The impurities in high polymers are considered as non-crystallizable species, such as low molecular weight, atatic, and highly branched components.

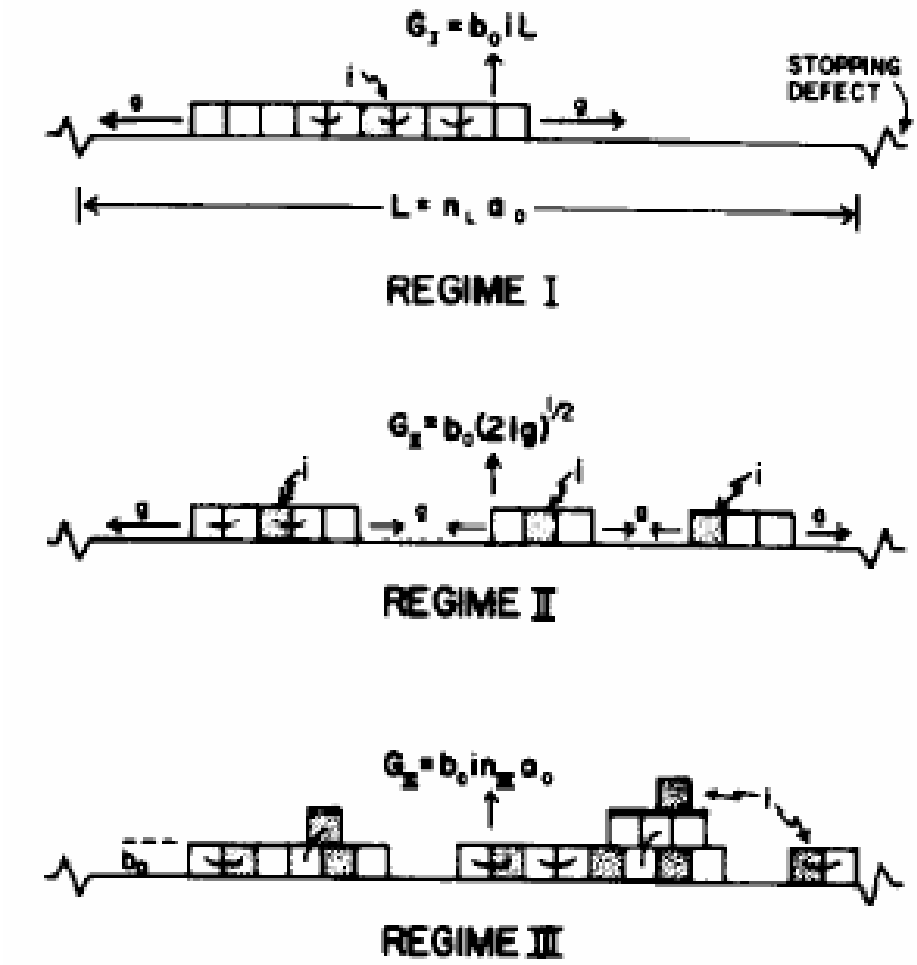

Figure 2.7 Schematic description of growth behavior change in Regime I, II, III. (Hoffman & Miller 1997)

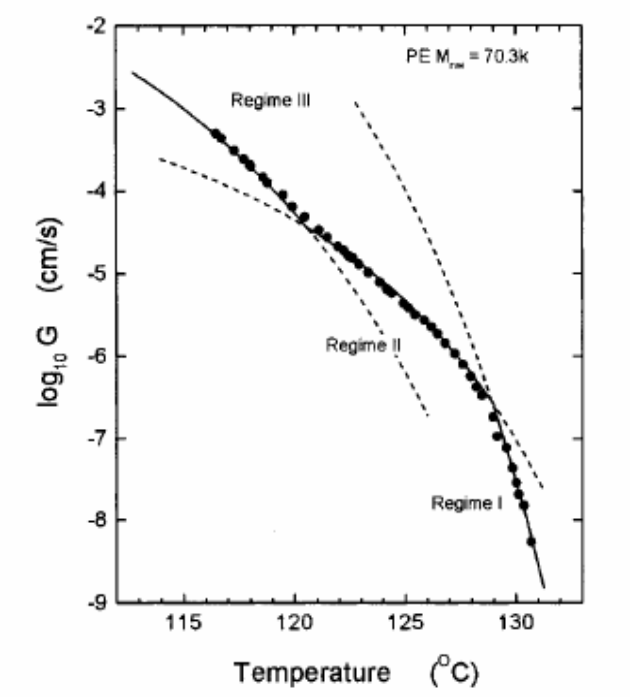

(a)

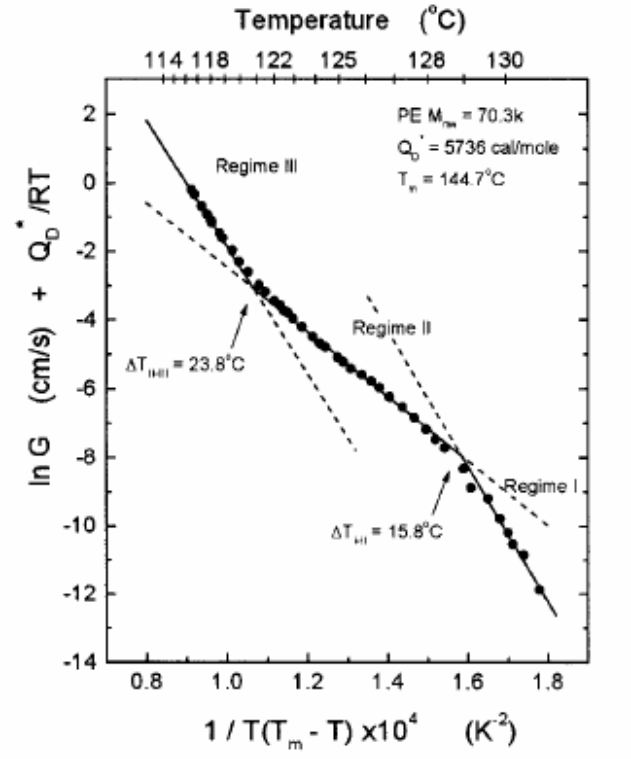

(b)

Figure 2.8 A linear polyethylene shows typical three regimes behavior during melt crystallization: a) growth rate; b) regime plot. (Armistead & Hoffman 2002).

This theory can well explain the coarseness (δ, “diameter” of fibrillar texture) with the relation δ=D/G, where D is the diffusion coefficient and G is radial growth rates. In spite of the success in explaining spherulitic morphology, the “impurities” assumption might just be a convenient assumption in polymer systems migrating from small molecules.

Also the linear growth rates in polymers could not be explained with this theory, because unusual parabolic growth ($R \propto t^{1/2}$) was found in crystallization of polymer system containing impurities of small molecular weight components (Keith & Padden 1964b).

2.1.6. Rough surface growth theory

2.1.6.1. Surface roughening with “entropy barrier” of Sadler-Gilmer

Sadler and Gilmer noticed that many crystals exhibited rounded face and even ‘leaf-shaped’ morphologies, which tend to occur at higher temperature than the facetted crystals (Sadler & Gilmer 1984). They proposed that it could be the result of surface roughening since the steps on the growth surface could be generated by thermal fluctuations at higher temperature, see Figure 2.9.

For classical rough surface growth, the growth rate should be proportional to the supercooling (ΔT). However the growth rates in polymers are proportional to exp (-1/ΔT), which imply the existence of growth barrier. This barrier is suggested to be of entropy origin due to the fact that crystalline stems are connected to one another in macromolecules (Sadler & Gilmer 1986).

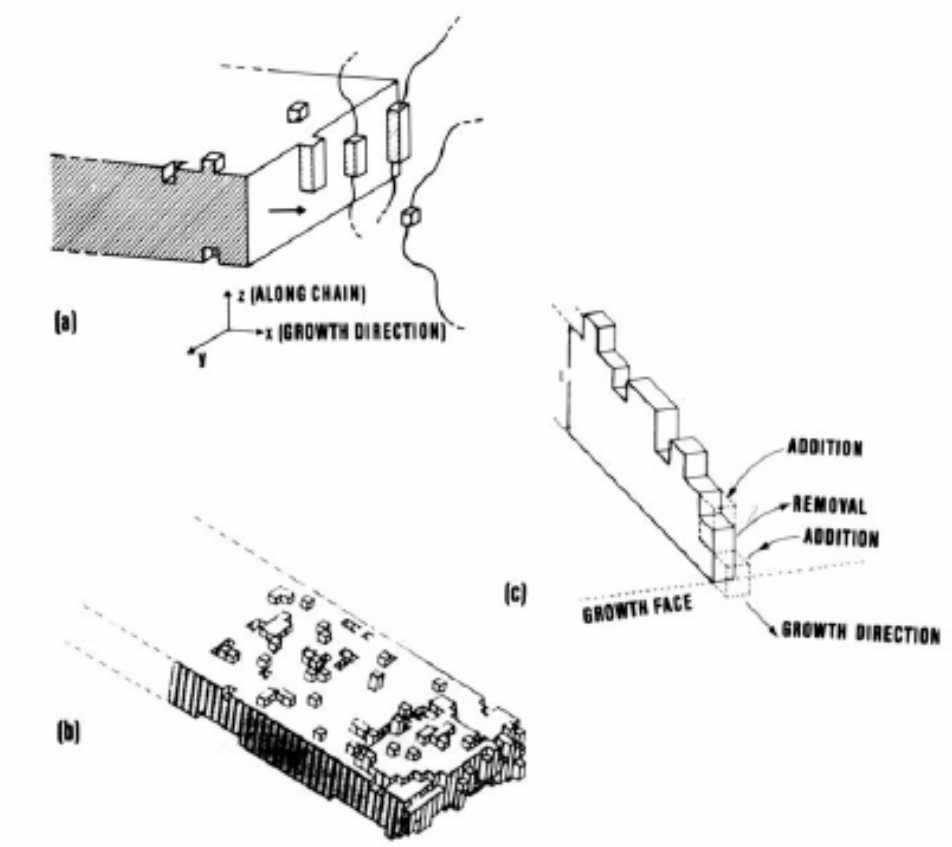

Figure 2.9 Schematic drawings of surface roughening model (Sadler & Gilmer 1986): a) Three-dimensional model; b) simulated crystal; c) two-dimensional model

Even though stems can be attached onto the crystal surface without energetic barrier, molecular chains still need further detach-attach process of some stems to form thermodynamic stable stems. Therefore, fluctuations into and out of the unviable state create an entropy barrier to crystal growth.

By suitable choice of binding energy, computer simulation did reproduce the main experimental trends both for lamellar thickness and for growth rate, see Figure 2.10. This rough surface theory seems reasonable in the physical process of stem attaching process and can explain the crystals growth behavior of low molecular weight PE and PEO (For low Mw PE and PEO, growth rates seem to be linear with the ΔT).

There existed some growth rate kinetics results of extended chain in low Mw poly (ethylene oxide) (Point & Kovacs 1980), low molecular weight polyethylene (Leung et al 1985) and paraffin (n- $C_{94}H_{190}$) (Hoffman 1985), as shown in Figure 2.11.

The growth rate is with good linear relationship with crystallization temperature in the extended chain region close to melting temperature, which could imply the rough surface growth mechanism and the disguising effect of chain folding.

Since it is very difficult to obtain clear experiment evidence for a roughening transition, the validity of roughening transition in polymer cannot be checked directly. Usually roughening theory has been applied to crystals with only nearest neighbor interaction and free to add or subtract units anywhere on the surface (Armistead & Goldbeck-Wood 1992).

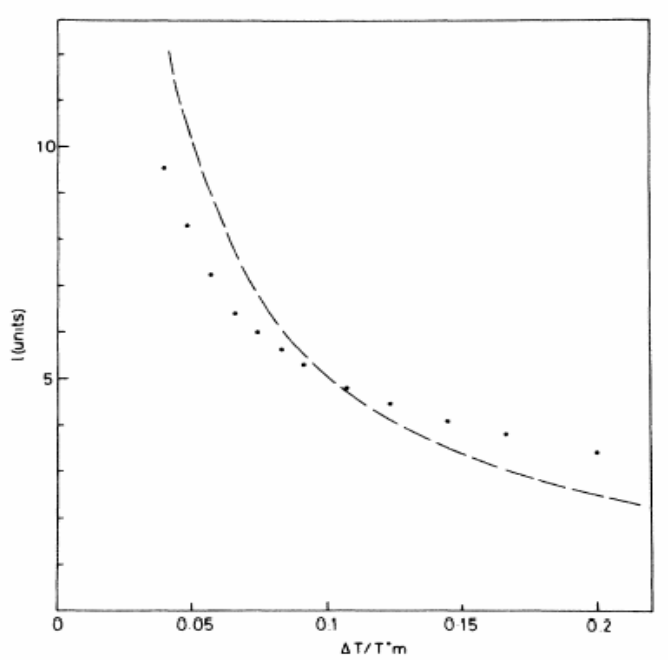

(a)

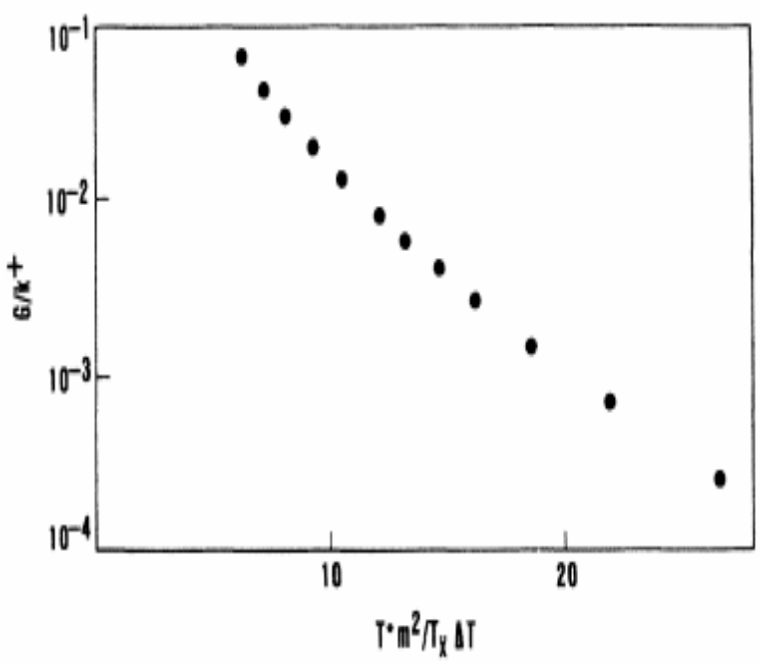

(b)

Figure 2.10 Simulation results from surface roughening model (Sadler & Gilmer 1986): a) lamellar thickness; b) growth rate

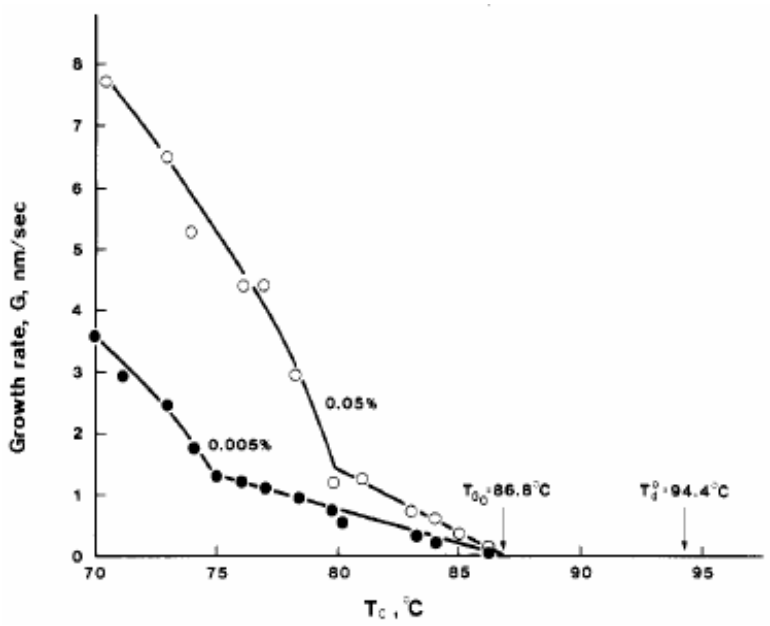

(a)

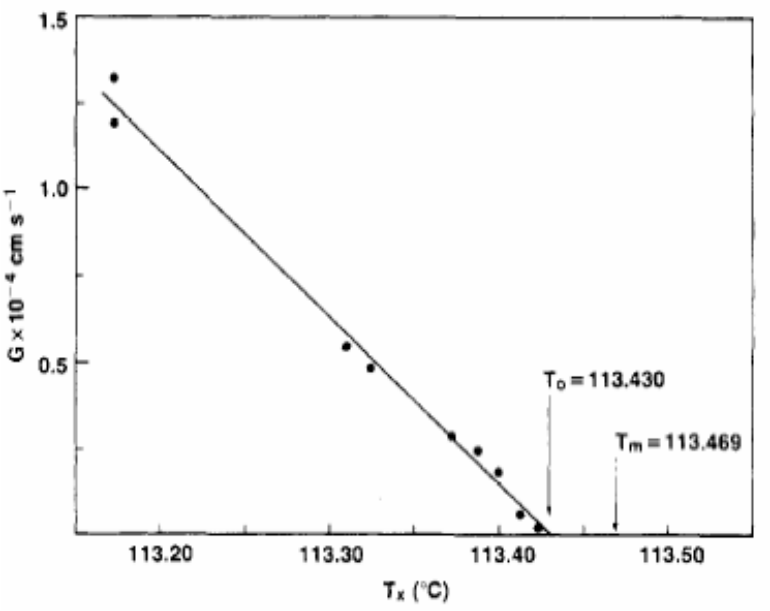

(b)

Figure 2.11 Linear growth rate versus crystallization temperature in extended chain region: a) PE3100 (Leung et al 1985); b) (~$C_{207}H_{416}$) (Hoffman 1985).

2.1.6.2. Surface roughening in PA 66 proposed by Schreiber-Phillips

Spherulitic growth rates of PA66 and a series of PA 66/6T copolymers were measured (Schreiber & Phillips 1998) with the crystallization temperature ranging from 220°C to 255 °C (see Figure 2.12). It was found that the growth rates of copolymers were almost indistinguishable from PA 66 homopolymer between 220 and 240 °C but were higher than those of homopolymer over 240 °C. When all of these growth rates were plotted on the regime plot, it was found unexpectedly that the growth rates of copolymers follow a straight line while those of PA 66 homopolymer just deviated slightly from the straight line at higher temperatures. This is obviously at variance with the secondary nucleation theory.

Lamellar thickness (see Figure 2.13) and melting temperature for crystals prepared at corresponding crystallization temperatures were also carefully measured. It was found that those values just slightly increased with crystallization temperatures. The widely used Gibbs-Thomson equation could not give reasonable equilibrium melting temperatures.

Considering the high surface free energy of H-bonding (110 ergs/cm^2) (Schreiber 1998), a simulation of free energy gave unrealistically big sizes of critical nucleus for secondary nucleation. Therefore it was suggested that crystallization of PA 66 and PA66/6T copolymers should follow surface roughening mechanism, which was in accordance with the viewpoint of H-bonding sheet arranging along spherulites radius (Lovinger 1978b).

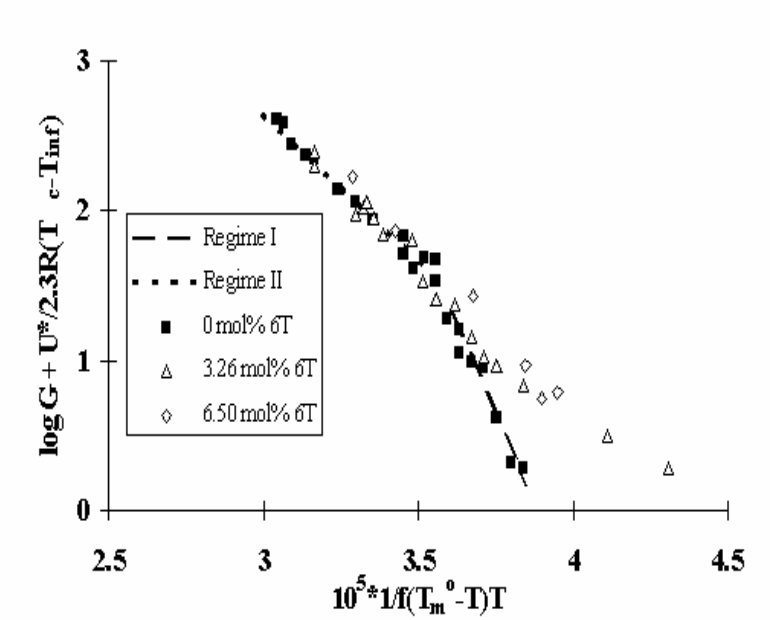

Figure 2.12 Regime plot of PA 66 and PA66/6T copolymers (Schreiber 1998).

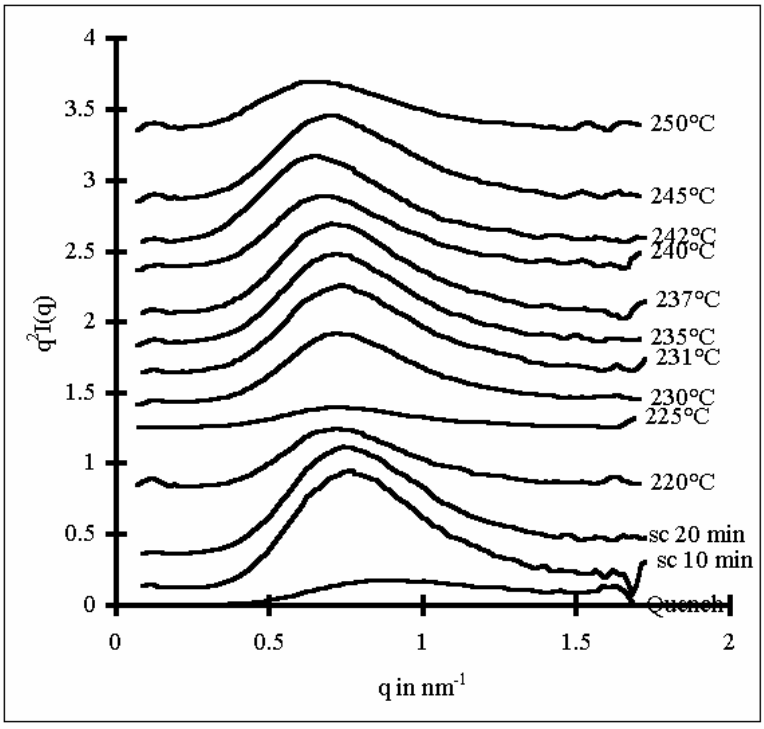

Figure 2.13 Lorentz Corrected Small Angle X-Ray Scattering Curves of PA 66 (Schreiber 1998).

2.2. A summary of structures and properties of PA66

2.2.1. Molecular structures and conformation

2.2.1.1. PA 66 chemical structure

The primary chemical structure of PA 66 is the recurring amide group, -CONH-, in the backbone. It can be visualized as the continuous condensation product of hexamethylene diamine and adipic acid, as shown in Figure 2.14. Strong hydrogen bond (H-bond) can be formed between the NH group and CO groups. This is the most important feature affecting the crystal structure of PA 66.

2.2.1.2. Molecular conformation in stable crystal

Since the NH group is essentially planar due to its partial double –bond character, the PA-66 molecule maintains the planar zigzag conformation as polyethylene, as shown in Figure 2.15. In PA 66, adjacent molecules are always parallel due to the molecular center symmetry. Intermolecular H-bonds can connect neighboring chains to form extended planar sheets containing H-bonds. In turn, H-bonded sheets stack with each other to form triclinic crystal structure.

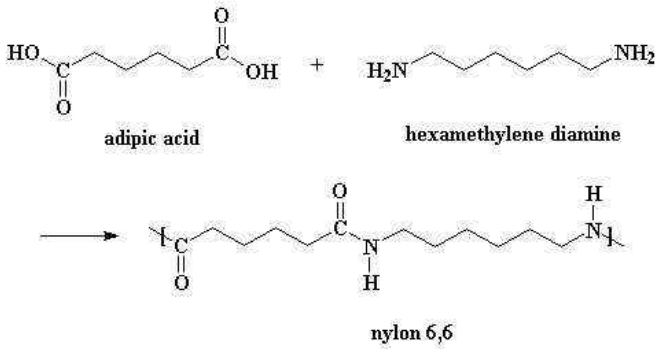

Figure 2.14 Schematic of polymerization and chemical structure of PA 66.

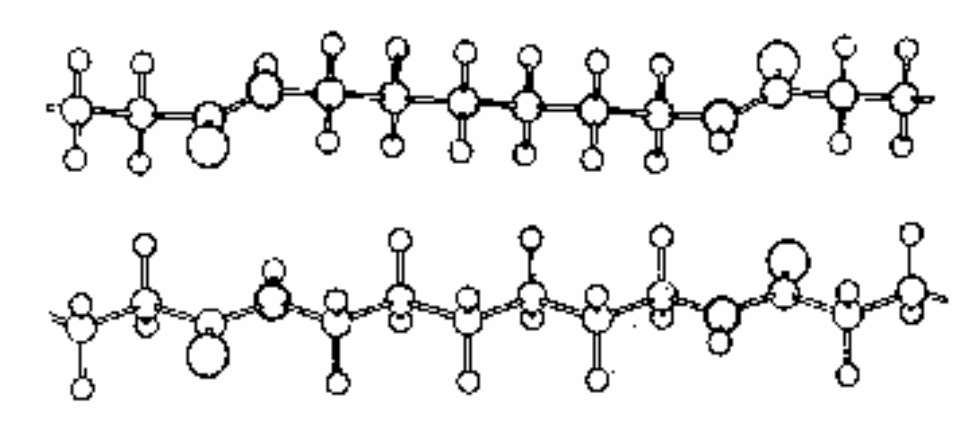

Figure 2.15 Molecular conformation in PA 66 crystal (Geil 1963).

2.2.2. Crystal structure of PA66

Figure 2.16 is a perspective drawing to show the chain arrangement inside a unit cell of α structure (Bunn & Garner 1947). There is only one chemical repeat in each unit cell, because the four chains on the edge of unit cell are actually shared by four unit cells.

The neighboring molecules are shifted by one methylene in *c*-axis to form intermolecular hydrogen bonded, planar H-bond sheets are in *a*-*c* or (010) plane (see Figure 2.17a). For the α structure, the hydrogen bonded sheets stack together by shifting 3 methylenes distance in c-axis to form stable polar interactions.

It is should be noticed that the chain direction (c-axis) is inclined to the basal plane (001) by an angle about 42°. Bunn also proposed that alternative packing of H-bonded sheets (see Figure 2.17b) could give the β structure, which should be a two-molecule triclinic cell.

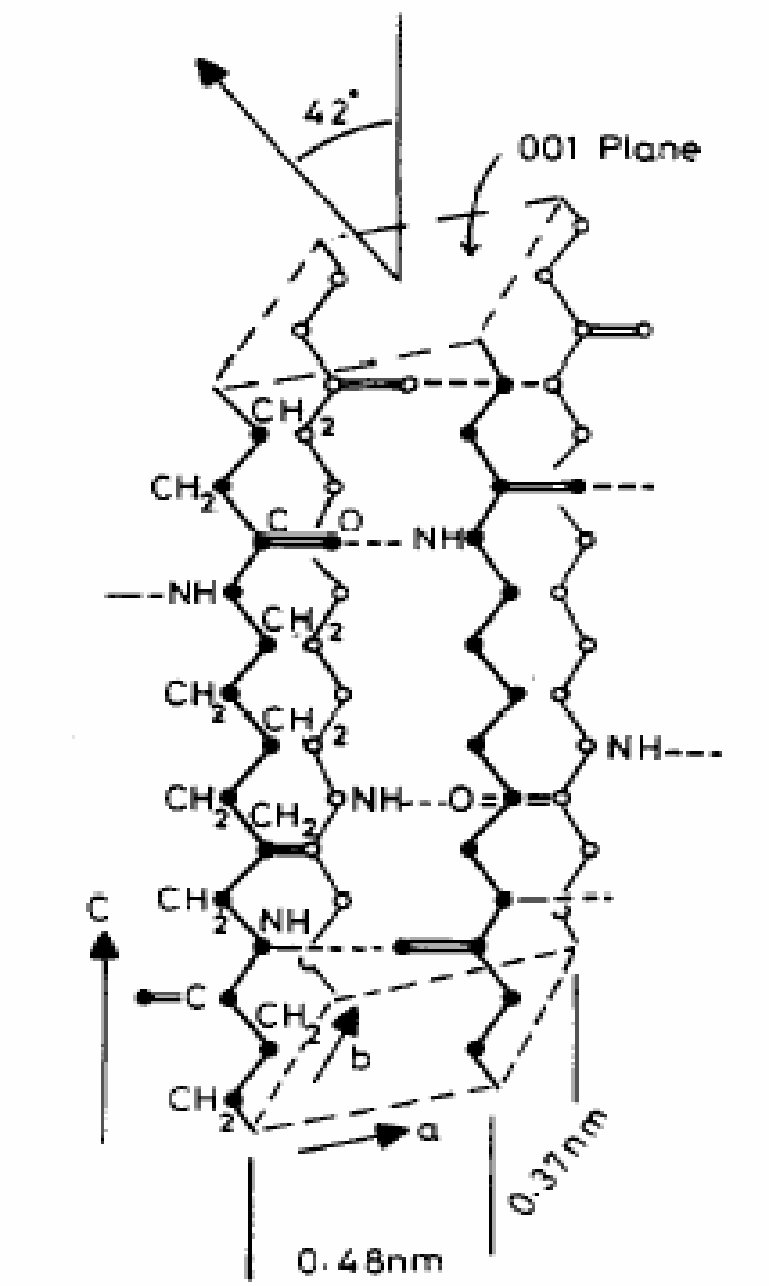

Figure 2.16 Packing of PA 66 molecules in the triclinic unit cell (Bunn & Garner 1947).

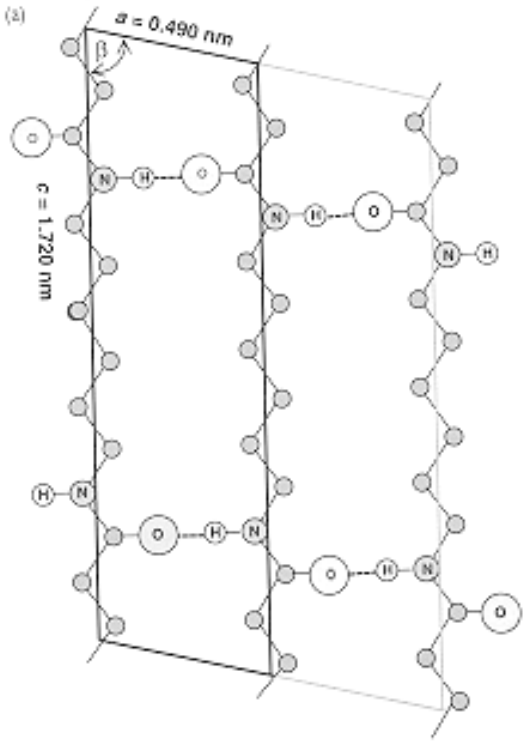

(a)

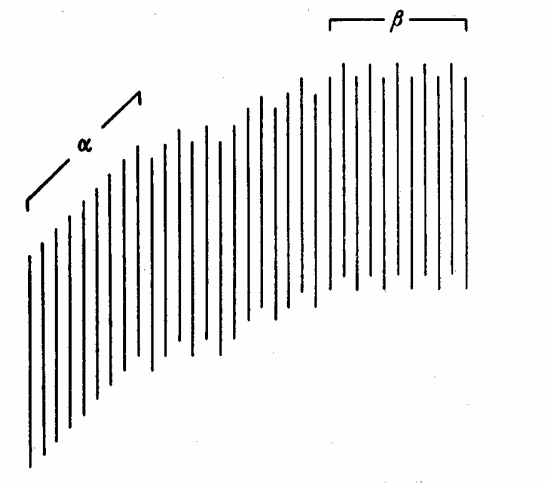

(b)

Figure 2.17 Packing of PA 66 molecules into H-bonding sheets (Bunn & Garner 1947): (a) H-bonding sheets; (b) Stacking of sheets.

2.2.3. PA66 single crystals from solutions

The structures of polymer crystals above the dimension of unit cell is usually called morphology (Kohan 1995), which can be studied by the distinctive shapes observed in different micrographs using different microscope (EM, OM and AFM).

Of course, other methods can also provide indirect sight into these structures, such as small angle scattering, thermal analysis, and spectroscopy.

2.2.3.1. Lamellar Structure

Lamellar single crystal is the thin-layer crystal formed by folding of polymer chain during the crystallization (Keller 1968), which is usually grown from dilute solution. PA66 single crystals are usually lathe shaped and often aggregate into sheaves (Cooper et al 1998), an electron micrograph of PA 66 lamellae is shown in Figure 2.18.

By Wide angle and low angle X-ray analyzes of Nylon 66 single crystal mats, it was found (Dreyfuss & Keller 1970) than chains within each lamella are inclined at substantial angle (~ 40^{o}) to the fold surfaces. The hydrogen-bonded sheets were found to run along the long axes of the crystals.

In general, regular chain folding on specific plane is determined by the minimization of surface free energy as in polyethylene; but for PA66 it is determined by the specific interactions (H-bonds) between the chains.

An ideal chain folding mechanism was proposed involving 3.5 repeat units for the crystalline core, as shown in Figure 2.19.

Figure 2.18 Lamellar structure of PA 66 single crystal (Geil 1960).

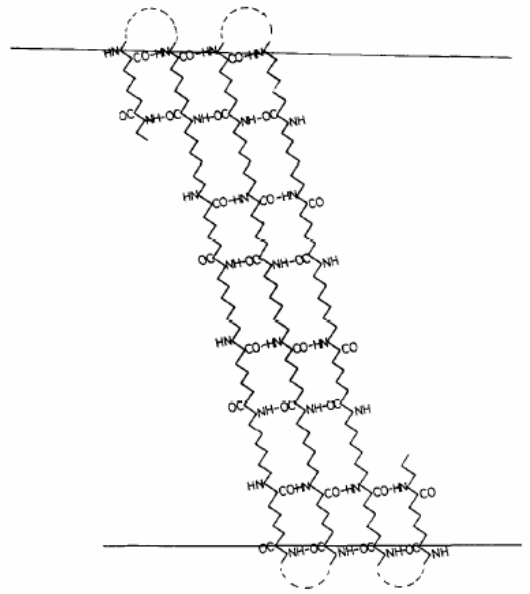

Figure 2.19 Ideal chain folding inside PA 66 lamella crystal with four repeat units (Dreyfuss & Keller 1970).

2.2.4. PA66 spherulites from melt crystallization

2.2.4.1. Spherulitic structures

Optically negative and positive spherulites in polyamides were first reported in PA 610 (Brenschede 1949), negative spherulites in PA 66 were prepared later (Boasson & Woestenenk 1956). The different birefringence under polarized microscope can be accounted for by the spherically symmetrical arrangement of uniaxial (refractive) index ellipsoids (Keller 1959) as shown in Figure 2.20.

Spherulites show positive birefringence when the larger refraction index is in the radial direction; spherulites show negative birefringence when the larger refraction index is in the tangential direction. PA 66 crystals are inherently birefringent due to the alignment of the H-bonded sheets along the crystal axis. In PA 66, α' is the refractive index for light vibration perpendicular to molecular sheet, β' is the refractive index for light vibrating in the H-bond sheet and perpendicular to molecular chains (i.e. along the C=O bonds), γ' is the refractive index for light vibrating along the molecule chains.

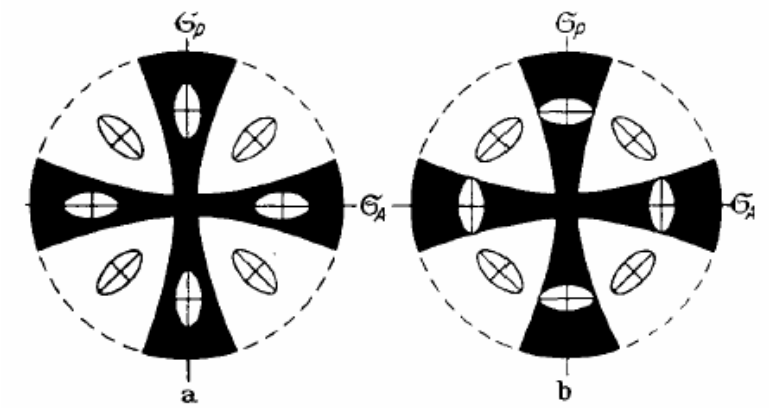

Figure 2.20 The birefringence of spherulite explained with uniaxial ellipsoids (Keller 1959): a) Positive spherulite; b) Negative spherulite.

The value for the three refractive indices were determined (Bunn & Garner 1947) to be $\alpha' = 1.475$, $\beta' = 1.525$, $\gamma' = 1.565$. The maximum refractive index is therefore in the chain direction and the higher value (β') in the H-bond sheet is due to general higher index for light vibration along the double bond (C=O).

Therefore, a spherulite will be birefringent if some axis of the crystal is parallel to the spherulite radius. The different birefringence in PA 66 is mainly due to orientation of H-bond sheet with respect to radius, as will be discussed later.

The comprehensive work (Khoury 1958, Magill 1966) summarized the formation of four different types of spherulites. Figure 2.21 shows the spherulite birefringence at different temperature for several polyamides.

Positive Spherulites

Positive spherulites are usually encountered when crystallization temperatures are below 250 °C. Three different features could be observed with decreasing crystallization temperature: 1) Axialites or fibrillar spherulites are formed between 250° C and about 235 °C; 2) Ringed (or banded, zig-zag extinct) spherulites are usually formed between 235 °C and 220 °C; 3) Non-ringed spherulites can be formed with increasing supercooling below 220 C.

A fibrillar spherulite at lower supercooling is shown in Figure 2.22a; and the crystal habits at different stages of forming process are shown in Figure 2.22b.

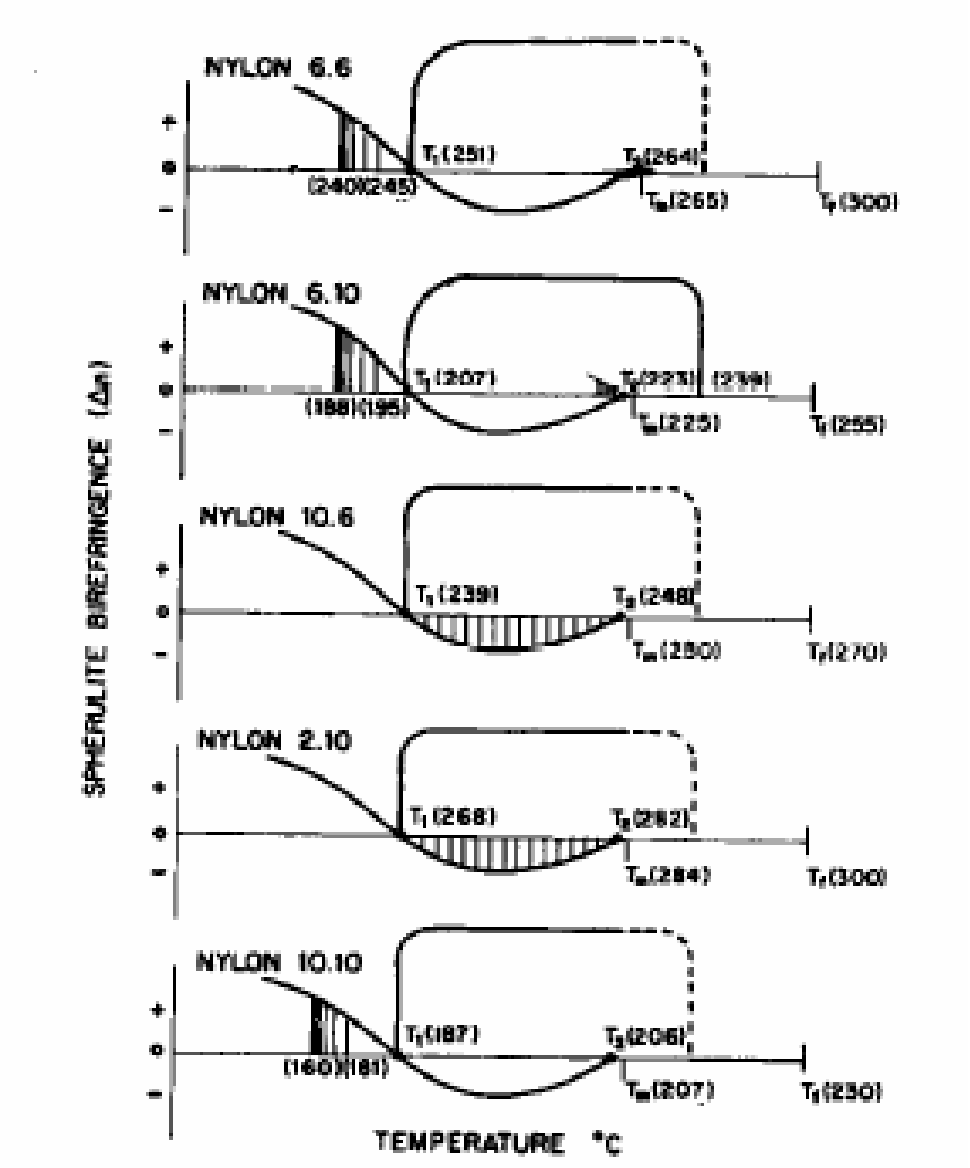

Figure 2.21 Spherulite birefringence of polyamides changes with crystallization temperature (Magill 1966).

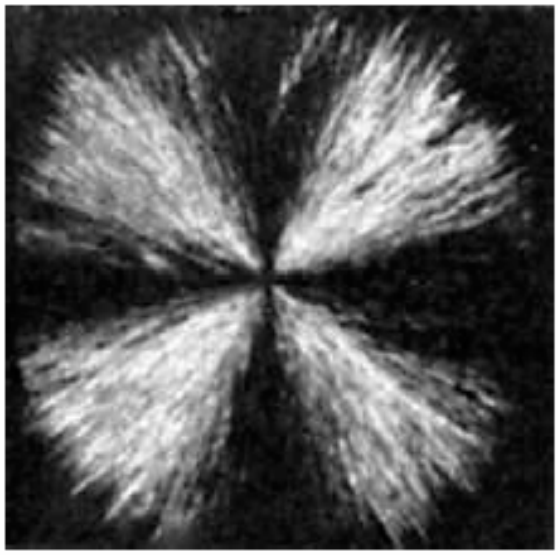

(a)

(b)

Figure 2.22 Positive spherulites of PA 66: a) under optical microscope; b) electron micrograph shows forming of fibrillar positive spherulites (Khoury 1958).

Negative Spherulites

Negative spherulites can be grown between 250 °C (T_1) and 264 °C (T_2) and the magnitude of the birefringence decreases when crystallization approaching both limits, as shown in Figure 2.23. Negative spherulites usually have higher optical melting points than the positive spherulites. It was reported (Khoury 1958) that the growth rates of negative spherulites decreased with increasing crystallization temperature in this zone, as shown in Figure 2.24.

Birefringent Aggregate

Birefringent aggregates were normally found to form and grow simultaneously with negative spherulites when the polymer chips were rapidly heated to temperature between 255 °C and 270°C, and held between 250 °C and 264 °C for crystallization. Such an example (Boasson & Woestenenk 1957) was shown in Figure 2.25. Spherulite aggregates were found to be strong birefringent but without definite optical sign, whose growth rates was about 1.5 times those of negative spherulites.

Non-birefringent Spherulites

Non-birefringent (or zero birefringent) spherulites were observed at two limit temperatures (T_1=250 °C and T_2=264 °C) of the negative spherulites growth zone. They were named (Magill 1966) as T_2-type non-birefringent and T_1-type non-birefringent respectively because they were actually different: T_2-type appeared to be randomly constituted, whereas T_1-type showed preferred orientation with respect to radial direction.

One of the T2-type non-birefringent spherulites is shown in Figure 2.26.

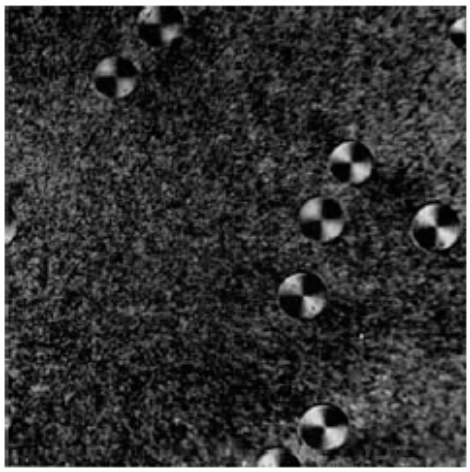

Figure 2.23 Negative spherulites crystallized at 256°C with λ/4 plane (Boasson & Woestenenk 1957).

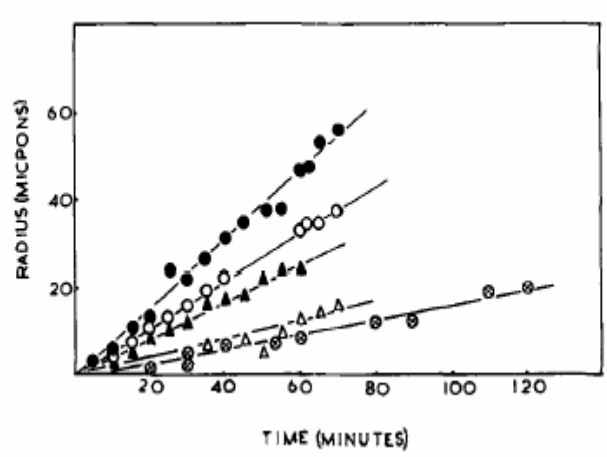

Figure 2.24 The growth rate of negative spherulites at 257, 259, 261, 263, 265 °C. (Khoury 1958).

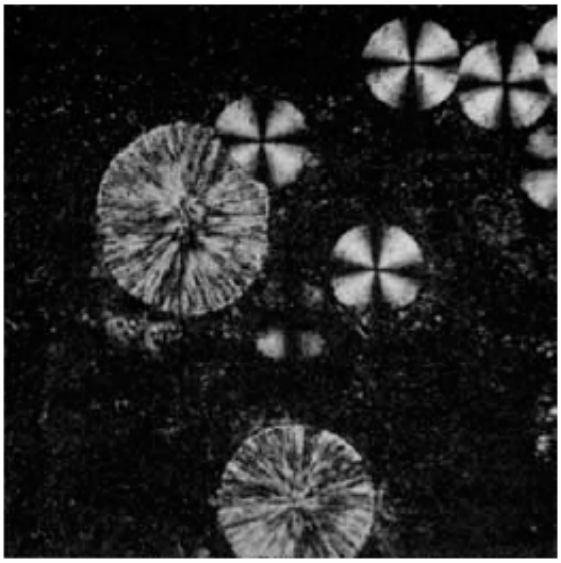

Figure 2.25 Spherulite aggregates grow simultaneously with negative spherulites (Boasson & Woestenenk 1957).

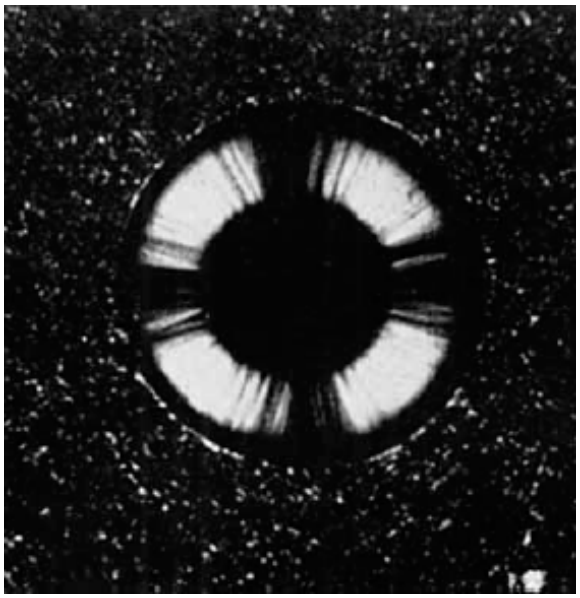

Figure 2.26 PA66 complex spherulites with non-birefringent center (264 °C) negative overgrowth at 257°C, with further overgrowth also formed at 264 °C (Magill 1966).

T1-type non-birefringent is elusive in experiments due to their small size and high nucleation rate at the lower crystallization temperature.

2.2.4.2. Amorphous structure and crystallinity of PA66

Amorphous structure

The structure information of amorphous of PA 66 should be very important considering the lower crystallinity of PA 66 comparing with PE (30-70%). Generally the fully amorphous phase is perceived as totally random without any significant structure following the concept of random coil conformation in the melt (Flory 1969). This might be true for the polymers such as polyethylene; but the situation could be different due to the strong H-bonds.

Quenched PA 66 was studied by Starkweather et al (Starkweather et al 1963). They found that the diffraction pattern contained with a single equatorial peak sharper than that of melt, see Figure 2.27. It also appeared different from the high temperature pseudo-hexagonal by the absence of (002) and its broad peak. Then quenched structures were proposed as a structure comparable with liquid crystals with only one-dimensional order.

Actually, the structure of amorphous PA 66 was demonstrated in many other experiments. NMR experiment shows that considerable H-N groups are keeping associated in the amorphous phase of PA 66 (Hirschinger et al 1990). At low crystallinity, DSC gives crystallinity values significantly higher than those from WAXD (Khanna & Kuhn 1997).

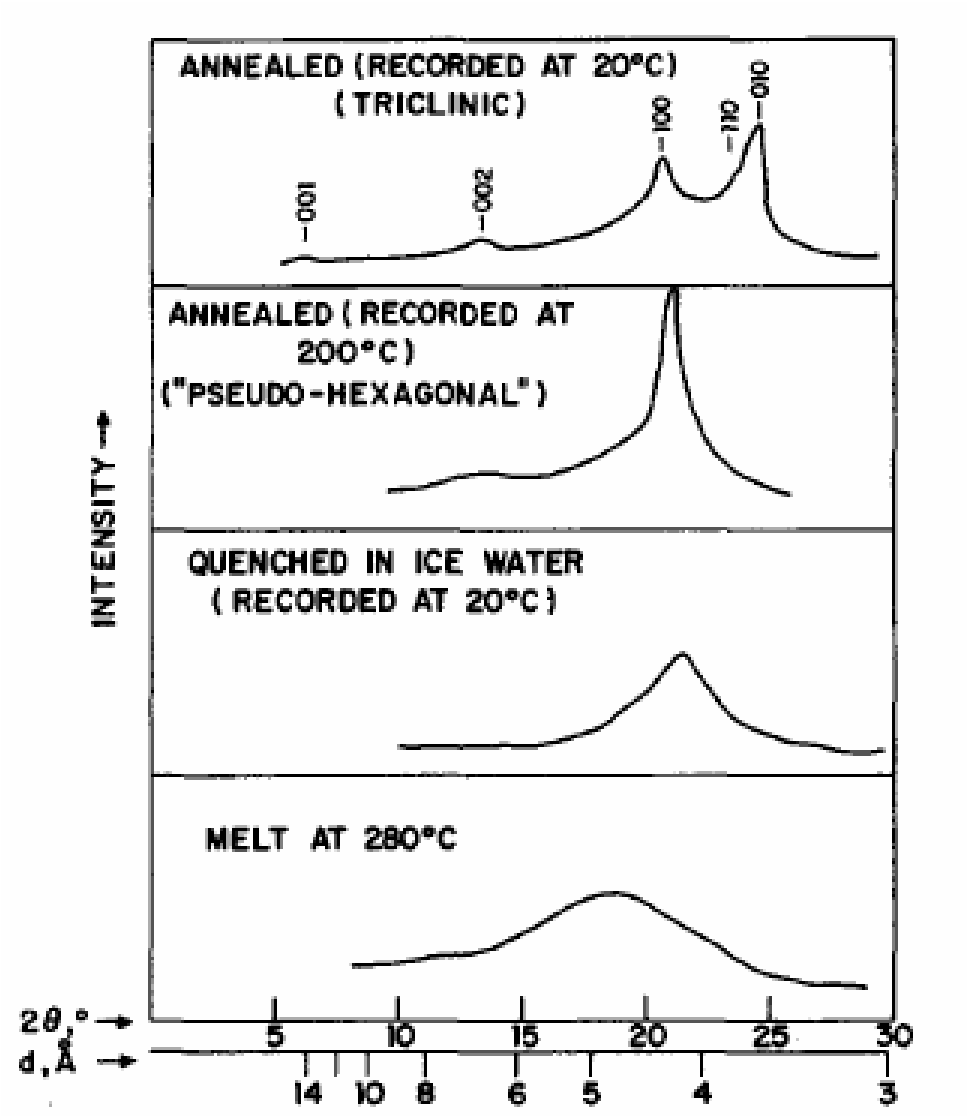

Figure 2.27 Comparison of X-ray diffraction patterns of PA 66 at different states (Starkweather et al 1963).

Crystallinity

If the structure of amorphous phase does exist, the crystallinity in PA 66 should be an index of the overall order of packing rather than the amount of three-dimensional order as existing in the triclinic unit cell.

2.2.5. Long period from Small Angle X-ray Scattering

2.2.5.1. Long periods of single crystal at different crystallization temperatures

As described in last part, Dreyfus and Keller reported that the long spacing kept constant (original mat 58-59 Å reducing to 53-54 Å after heat treatment) at considerable range of temperatures (Dreyfuss & Keller 1973). The values were significantly lower than the value of 100-180 Å for polyethylene, which was attributed to the large decrease of free energy as a result of H-bonding.

However it should be mentioned that long spacing of PA 66 could be increased continuously only after 250 °C (from 58 Å to 90 Å) when single crystals were annealed at high temperature (Koenig & Agboatwalla 1968).

It was first reported that the long spacing of PA 66 single crystals prepared from 1,4-butanediol solutions could be increased *continuously* after crystallization temperature was over 140 °C (Hinrichsen 1973); while long spacing did keep constant value of 54 Å at low crystallization temperatures (see Figure 2.28a). Result of annealing at high temperature showed that long spacing also increased *continuously* with annealing temperatures as reported before (Koenig & Agboatwalla 1968) (see Figure 2.28b).

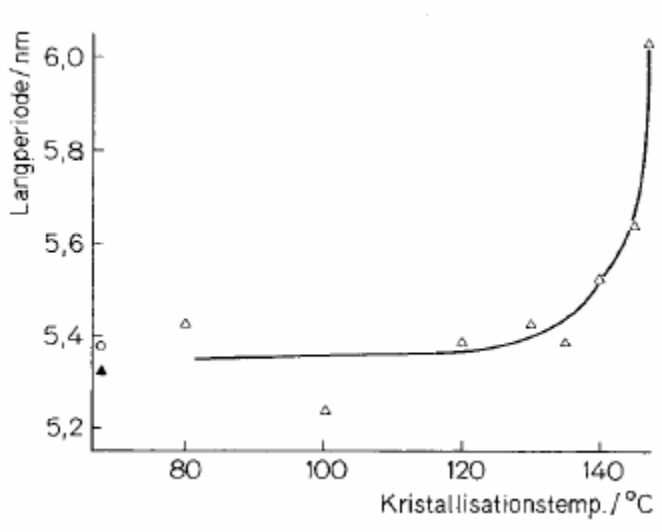

(a)

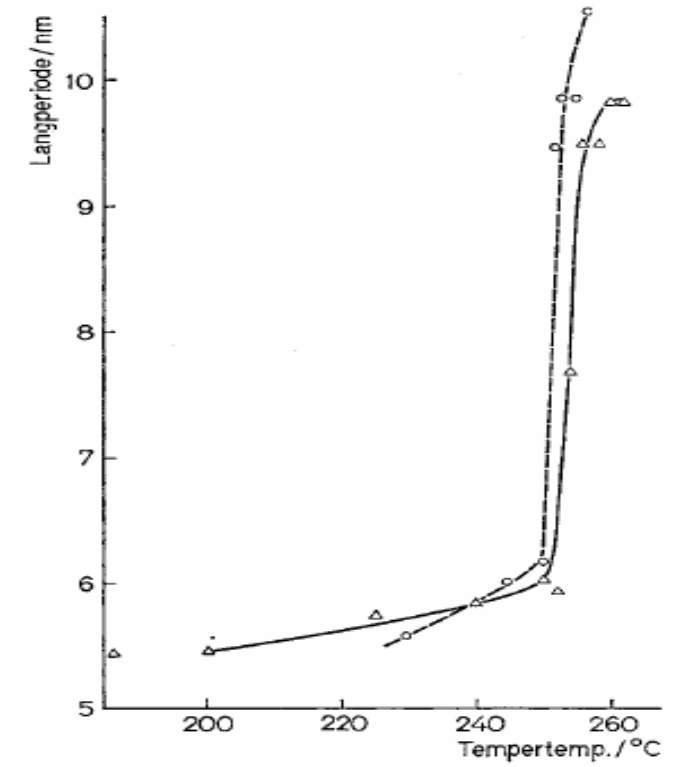

(b)

Figure 2.28 Change of long period in PA 66 lamella (Hinrichsen 1973) with temperature: a) solution crystallization temperature; b) annealing temperature.

After careful checking the long spacing values of (Hinrichsen 1973), one can find that they actually match those values expected with step increase of long spacing by ½ repeat unit from the base value of 54 Å. This should not be unexpected if one accepts the view that the chain folding can be readily formed by amide folds and acid folds.

Interesting DSC results were also reported for the single crystals with continuous long spacing (Hinrichsen 1973). Two peaks were found in each case; the magnitude and temperature both increased continuously in the low temperature peak while they both keep nearly constant in the high temperature peak. Different heating rates are also used to study the melting the single crystal of the same long spacing, and the high temperature peak was found to sharpen probably due to the annealing effect.

It was later confirmed (Magill et al 1981) that the increase of long spacing in PA 66 single crystals maintained a “quantized” feature i.e. 5 and 6 repeat units. Extensive DSC studies revealed that low melting peak became increasingly prominent with increasing heating rates, which showed typical character of reorganization process. They also found that melting curve of single crystals prepared at lower temperature (about 4 repeat units) showed double peaks while the single crystal with longer spacing from crystallization at higher temperature or annealing showed only one peak. Therefore, they tended to explain the high melting peak as the result of reorganization into more stable structure from the first peak due to annealing.

It should be pointed out that both the double melting peaks and continuous long spacing are still compatible with the concept of “quantized” lamellar thickness. First, we

should bear in mind that both small angle X-ray and DSC only give statistically average representation of the whole crystal system. Secondly, it is very possible for lamellae to exist in either of the “quantized” structures due to local environment, especially in the transition state. Finally, even the ¼ repeat unit steps in the average long spacing could be readily accounted for if PA 66 single crystal can fold by either amide fold of acid fold. The apparent single melting peak can also be reasonably resolved into one small peak at lower temperature and one strong peak at a constant high temperature.

It was established (Mitomo 1988) that different melting peaks from DSC corresponded amazingly well to different “quantized” lengths of stems, which was etched down from single crystals by hydrolysis in HCl and examined with Gel Permeation Chromatography (GPC).

2.2.5.2. Lamellar thickness in bulk crystallized PA 66 crystal

Long periods were reported in the range of 56-108 Å in the PA66 bulk crystals (Starkweather et al 1963), which were prepared by annealing at an elevated temperature after ice-water quenching from melt (‘annealing after quenching’) or by quickly cooling from melt to an elevated temperature, holding for 15 min then quenching with ice-water (‘hot quenching’).

At the same temperature, hot quenching produced larger long period than annealing after quenching (See Figure 2.29). It should be mentioned that long period keep increasing with time (5 s to 1 min) when annealing at 250 °C, probably indicating some solid-state transition.

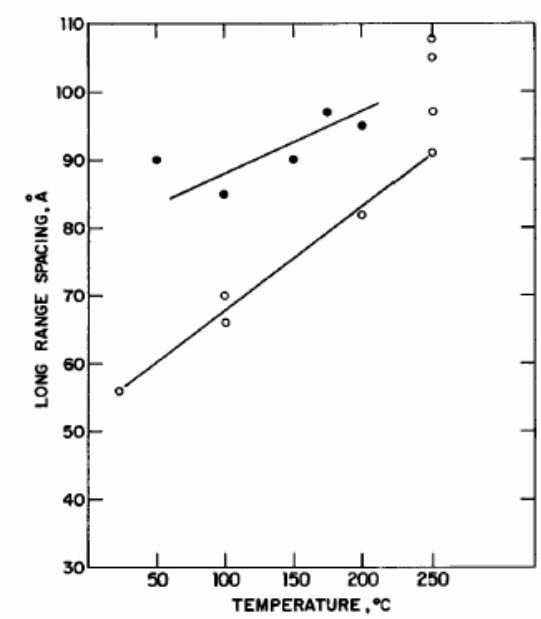

Figure 2.29 Long periods in bulk PA 66 crystals (Starkweather et al 1963): 1) by annealing after quenching in ice water (open circles); 2) by hot quenching (filled circles).

The SAXS long periods in PA 66 melt-crystallized spherulites have been determined (Schreiber 1998), which were isothermally prepared at crystallization temperatures below 250 °C, i.e. the temperature range of positive spherulite. It was found that the long period increased slightly with the crystallization temperature from 84.2 Å at 220 °C to 97.4 Å at 250 °C. After analyzing the SAXS intensity with correlation functions, it was found that the total crystal thickness kept nearly constant (just over 25 Å or 2 repeat units) with crystallization temperatures but core thickness increased somehow.

2.2.5.3. What if lamellar thickness is quantized?

Although it is still unknown whether the lamellar thickness of PA 66 exists with integral number of repeat units, it is reasonable to expect that the lamella with exact repeat units could be stable due to H-bond. Therefore, it is interesting to summarize the lamellar thickness, melting temperature and possible repeat units number, see table 2.1.

Table 2.1 Lamella thickness, melting temperature and possible quantized repeat units.

Repeat units		(Hinrichsen 1973)	(Magill et al 1981)	(Mitomo 1988)	Remark
n	l=12.8* n Å / l=13.5* n Å	l /T_m	l /T_m	l /T_m /N_G	
3.5	44.8/47.3			57.2/250/3.73	In HCOOH
4	51.2/54.0	54/240/260	54/254	62.8/254/4.09	In 1,4-butanediol
4.5	57.6/60.8	60.75/250/258			
5	64.0/67.5	67.53/252/264	67/265	68.2/264/5.18	Tm of "+" ?
5.5	70.4/74.3			76.4/267/	
6	76.8/81.0		76 /?		
6.5	83.2/87.8				
7	89.6/94.5			93.4/274/7.04	In Glycerol
7.5	96.0/101.3			98.0/277/	
8	102.4/108				

Note: 12.8 Å is the projection of one repeat unit on lamella normal; Dreyfuss and Keller showed constant lamellar thickness with 4 repeat units, 54 Å /4=13.5 Å (Dreyfuss & Keller 1973).

2.2.6. Melting studies with Differential Scanning Calorimetry

The melting behavior of PA 66 is the field with the most controversy. Probably this is due to the unique structure and morphology because of the H-bonding, and the possible structure transitions of PA 66 during the heating process caused on the other side. Therefore, only some typical DSC results of bulk crystallized PA 66 will be presented here with unique features identified.

2.2.6.1. Melting curves of the positive spherulites

Typical melting curves of positive spherulites, as shown in Figure 2.30a, for the usual situation of cooling to room temperature after isothermal crystallization process for specific time. Usually multiple endotherms are observed as a function of crystallization temperature. Three endotherms are clearly shown and usually identified as: 1) *Annealing peak*: the low temperature endotherm always occurs at about 10 °C above Tc, which is probably due to the melting of thin crystals formed during the space-filling crystallization (Stouffer et al 1996); 2). *Melting Peak*: the middle endotherm also increases with Tc but at a slower rate, its magnitude increases with crystallization temperature; 3) *Re-crystallization (or reorganization) peak*: the high temperature endotherm remains at an extraordinary constant temperature, probably due to its stable structure or associate to some very cooperative transition.

The relationship between the last two peaks could be revealed clearly when PA 66 crystals isothermally crystallized for 1 hr were melted immediately (Schreiber & Phillips 1998) without cooling to room temperature, see Figure 2.30b.

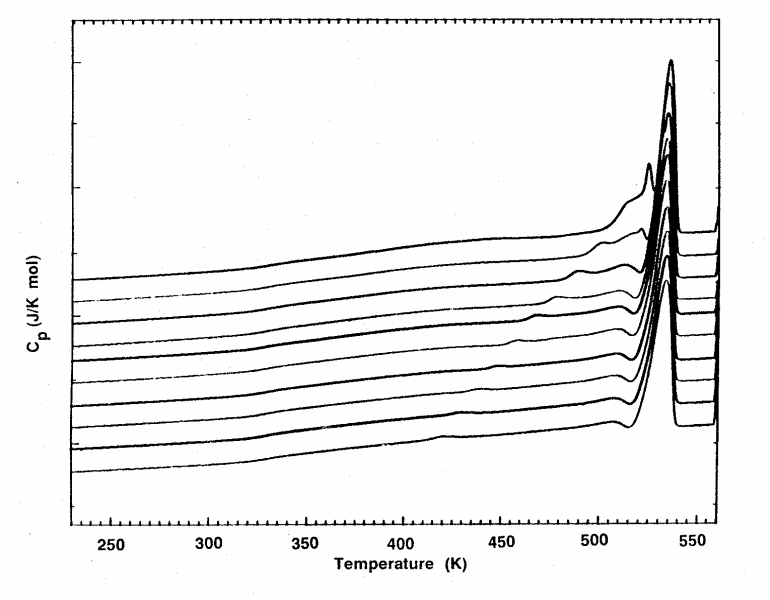

(a)

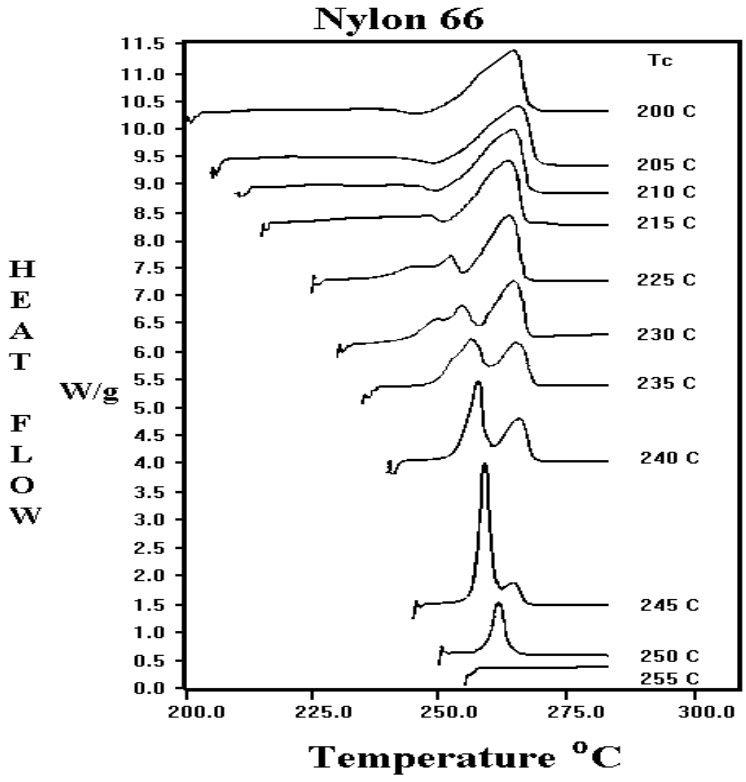

(b)

Figure 2.30 The typical melting curves of isothermally prepared crystals: a) cooling to room temperature (Xenopoulos & Wunderlich 1991); b) directly after crystallization process.(Schreiber & Phillips 1998).

When the crystallization temperature increases to 235 °C, the annealing peaks merge with the melting peak (in the middle). The magnitude and peak temperature of this single peak both increase with crystallization temperatures up to 250 °C, while the magnitude of re-crystallization peak decreased.

The small melting peak shows low (thermal) crystallinity, which seems to agree with the low (density) crystallinity as reported by (Starkweather et al 1963). It probably implies that crystallization ability of the PA 66 dramatically decreased at 250 °C.

2.2.6.2. Melting curves of negative spherulites

Complete studies on the melting behavior of negative spherulites were performed (Ramesh et al 1994b) after successfully reproducing negative spherulites in the DSC with a special temperature-time program.

Surprisingly, the higher melting peak was found to increase *continuously* with the crystallization temperature, see Figure 2.31. They were categorized into two different types due to slightly different exotherms behavior during the immediate cooling process following the crystallization.

2.2.6.3. Does Hoffman-Weeks method still work?

The sharp melting peak temperatures of PA 66 crystals prepared in isothermal crystallization were then plotted versus crystallization temperature as Hoffman-Weeks method, as shown in Figure 2.32. It is clearly demonstrated that melting behavior of PA 66 are distinctly different between positive spherulites and negative spherulites.

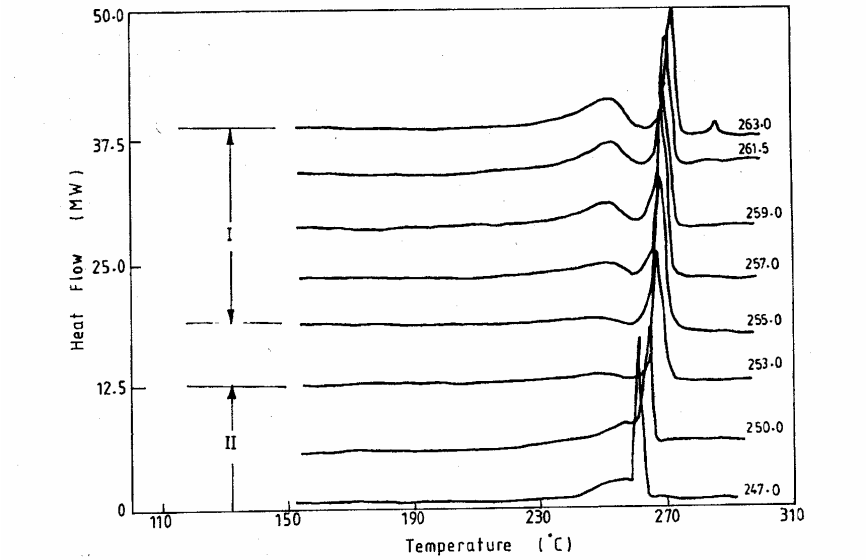

Figure 2.31 Melting curves of PA 66 negative spherulites after cooling to room temperature (Ramesh et al 1994b).

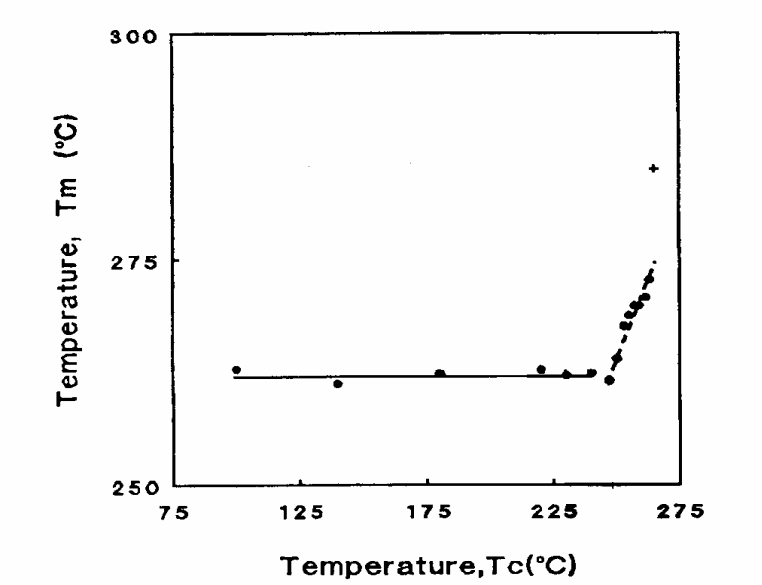

Figure 2.32. Dependence of the melting temperature on crystallization temperature for PA 66 (Ramesh et al 1994b).

This is very similar to the long period increase in solution crystallized PA 66 (as-crystallized or annealed). If the lamellar thickness actually increases with the crystallization temperature, the melting behavior of PA 66 crystals can be rationalized as below:

In the positive spherulites of PA 66, the original lamellar thickness might actually increase with the crystallization temperature, but it is metastable for kinetic reason during crystallization and thus subjected to reorganize into stable crystals, like the stable thickness with 4-repeat units in single crystal, during the melting process. Therefore, the original crystal is actually partial melted at first, subsequent melting of the stable structure results in the strong and constant melting peak.

In the negative spherulite of PA, the lamellar thickness increases with the crystallization temperature, but it is more stable due to its lamellar thickness being larger than the stable structure. Therefore, the melting process of the lamellae can complete only in one step without formation of stable structure.

2.2.7. Dynamic mechanical relaxations behavior

It is meaningful to present some dynamic mechanical result by (Starkweather & Jones 1981) here, because it not only complete the picture of all the transition and relaxation temperatures in PA66 but also give a critical view of the crystal state after 250°C. Dynamic relaxations correspond to the long-range motions of molecules (Stockmayer 1973). The γ relaxation (about -125°C) is usually related to the motions of short methylene sequence. The β relaxation (about -60 °C) is present in PA 66 sample

containing water, the related motion is not clear. The α relaxation (about 80 °C) is believed to relate to the motion of chain segments in the amorphous phase (Starkweather 1995).

The flexural modulus and loss tangent of powder extruded and injection molded PA 66 samples are shown in Figure 2.33 *a* and *b* respectively. The modulus is shown to drop significantly around 250°C, implying the beginning of fluidity. This temperature, termed as T_f (Takayanagi 1974), might be related to the beginning of the continuous increase of long period when annealed at different temperatures. If this is the case in partial melting in 250 °C, the reorganization process (to stable structure) should involve the chain motion of long-range character.

Some interesting effect of these transitions will be mentioned here. Melt rheological properties of PA 66 was found by (Starkweather & Jones 1981) to change dramatically close the melting temperature of PA 66 (265 °C), see Figure 2.34.

At 260 and 265 °C, two different slopes were found in log-log shear stress vs. shear rate plot: 0.41 was found at lower shear rate and a small rheological exponent at higher shear with 0.17 at 260 °C, essential zero at 265 °C, which clearly show plastic behavior. A typical melt viscosity behavior was observed at 270 °C.

A discontinuity was found to occur at 188 ^{o}C in the slope of the growth rate curve of PA 610 (see Figure 2.35), and was speculated to relate to Brill transition temperature of PA610 (Lindegren 1961).

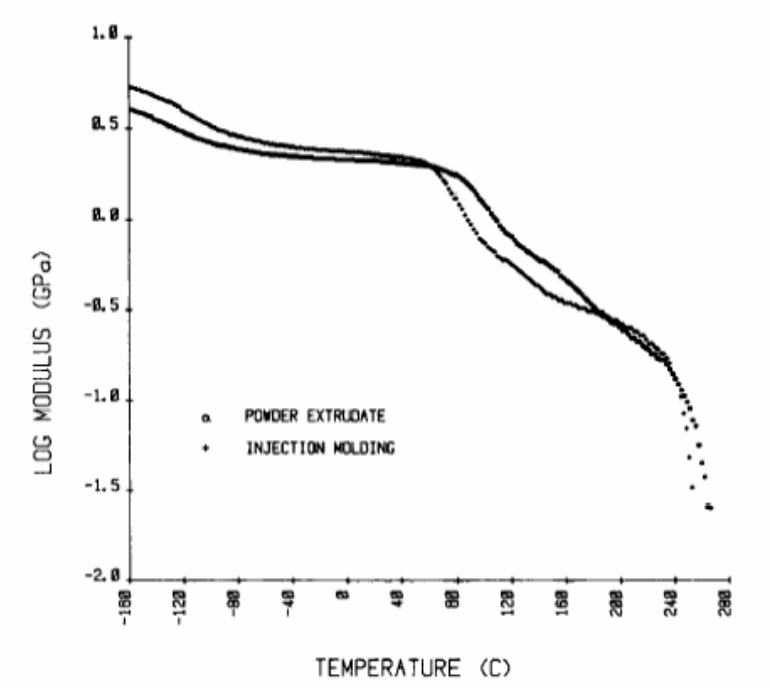

(a)

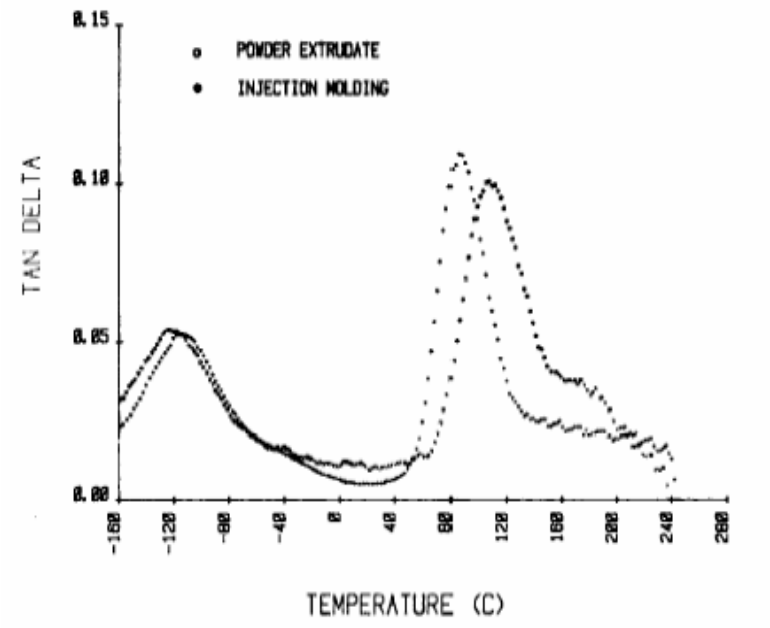

(b)

Figure 2.33 Dynamic mechanical behavior of PA 66: a) flexural modulus; b) loss tangent (Starkweather 1995).

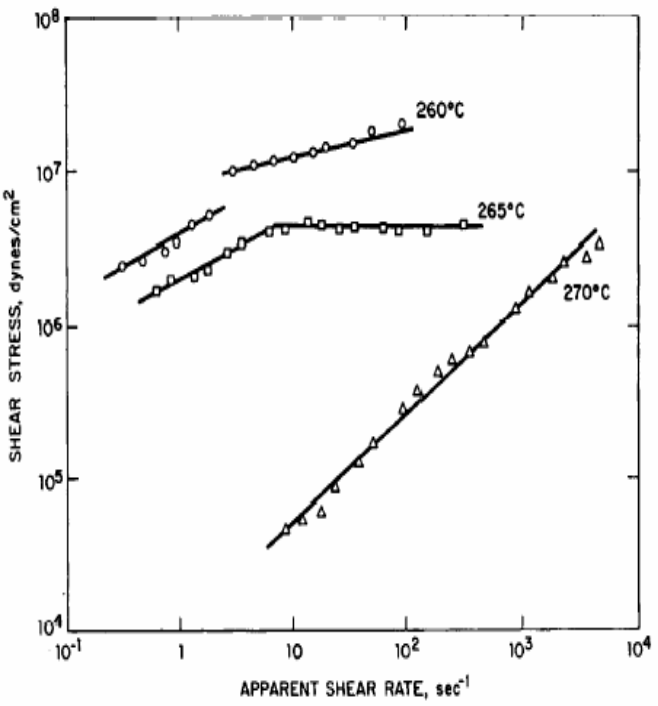

Figure 2.34 Rheological properties of PA66 below around melting temperature. (Starkweather & Jones 1981)

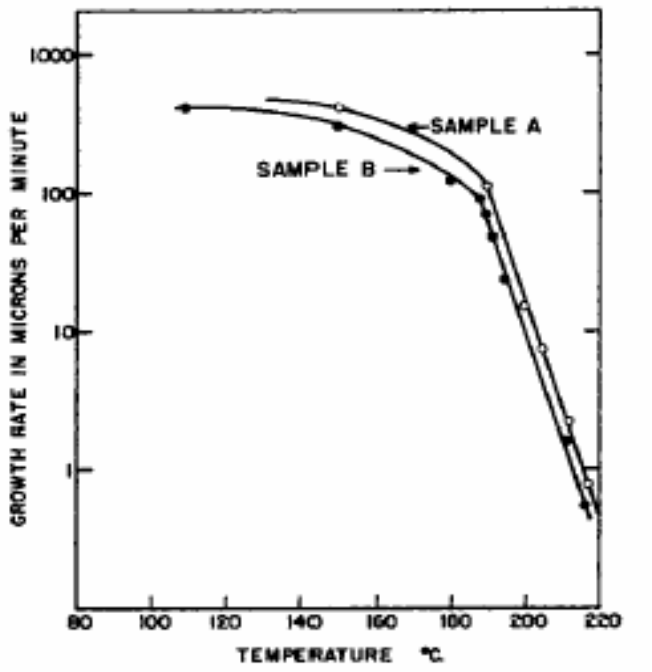

Figure 2.35 Growth rate of positive spherulites in PA 66 (Lindegren 1961).

2.3. Approaches to understand the crystallization of PA 66

2.3.1. Tailoring molecular structure with random copolymers

The strategy of studying the crystallization and melting behavior of homopolymer by comparing with a series of copolymers were successfully applied to polyethylene and PA 66 in our group. In general, the most striking effect of incorporation of comonomer is that the ability to crystallize and crystallinity of random copolymers will be lower than those of homopolymer. PA 66 copolymers with low comonomer contents will be used to comparatively study the crystallization and melting behavior of PA 66.

2.3.1.1. Chemical structures

Three different series of PA 66 (hexamethylene adipamide) random copolymers are 1) PA66/6T (hexamethylene terephthalamide as comonomer); 2) PA66/6I (hexamethylene isophthalamide as comonomer) and 3) PA66/6 (caprolactam as comonomer), respectively. The chemical structures of these copolymers are presented in Figure 2.36.

2.3.1.2. Isomorphous copolymer PA 66/6T

Isomorphous systems are characterized as crystallizing into the same morphology by the comonomer. The melting points of such copolymer were found to change monotonically with composition in PA 66/6T system (Edger & Hill 1952), see Figure 2.37.

This was attributed to the similar distances between carboxyl groups (differ by only 0.31 Å) and powerful hydrogen bonding force, as shown in Figure 2.38, which can bring the *p*-phenylene linkage into the line of chain.

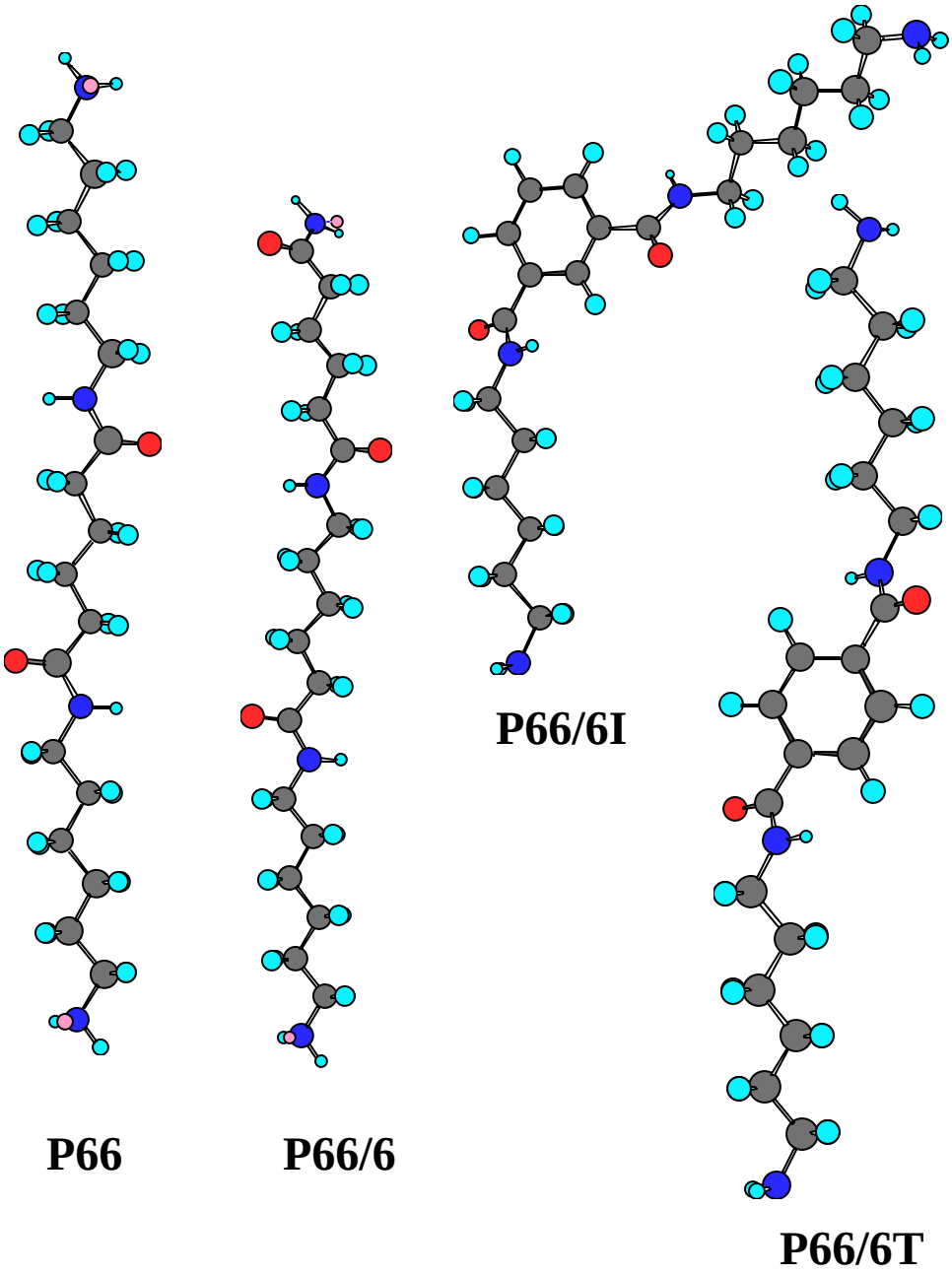

Figure 2.36 Chemical structures of PA66, PA66/6, PA66/6I and PA66/6T.

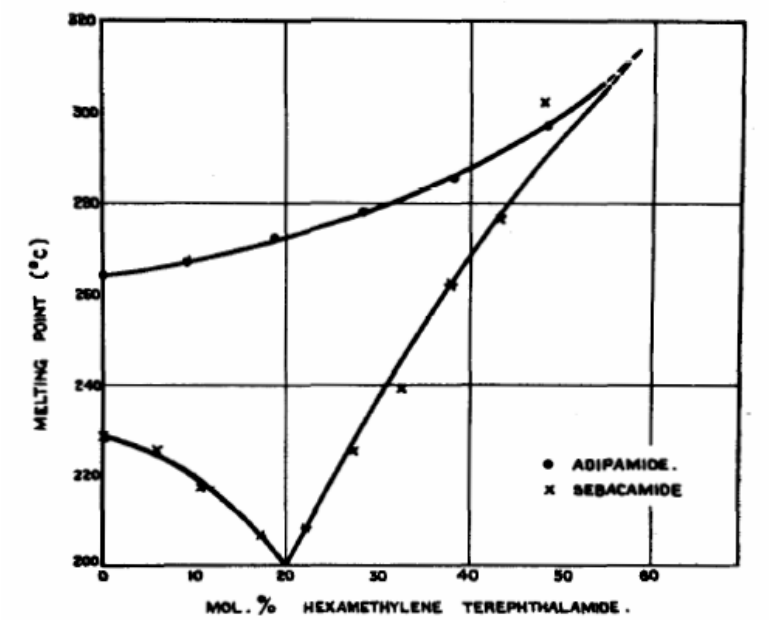

Figure 2.37 The isomorphism phenomenon shown in melting points of PA 66/6T copolymers (Edger & Hill 1952)

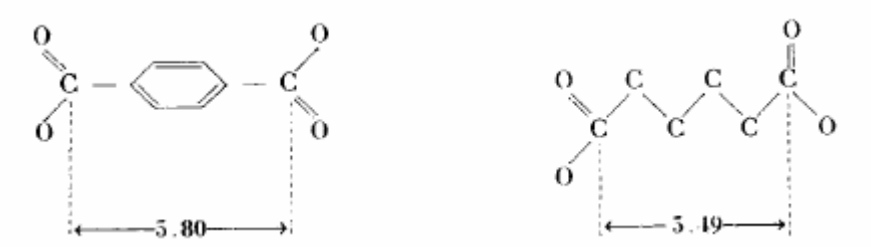

Figure 2.38 Isomorphism of PA 66/6T explained from the close distance between 6T and 66 (Edger & Hill 1952).

By adopting the Dipole Plane (formed across the chain by adjacent hydrogen bonds) Model, it was (Yu & Evans 1959) further identified that isomorphism can occur when the amide linkage of comonomer coincides with the lattice point on the next dipole plane or on the next dipole plane without exact coincidence.

Two conditions must be met for the comonomer to be present isomorphously (Figure 2.39): 1) The distance between the functional groups must be the same; 2) The orientation of the comonomer units the crystal must be correct.

2.3.1.3. Change the average sequence length of PA 66

For the random copolymers, the average sequence length of PA 66 can be easily manipulated by changing the comonomer content. For the PA66/6 copolymer, crystallizable PA 66 sequences decrease with the increasing PA 6 content. These copolymers could be useful to explore the crystallization behavior of PA 66 by studying lamellar thickness - temperature dependence.

2.3.2. Extending to higher supercooling with rapid cooling method

2.3.2.1. Original Ding-Spruiell rapid cooling method

In order to simulate the crystallization of *i*-PP in melt spinning process, an experiment method was developed to study the non-isothermal crystallization process of polymer at cooling rate up to 5000 °C/min (Ding & Spruiell 1996).

The major features of the method include a gas hot-stage that could be cooled down rapidly by quickly switching heat nitrogen gas to cool nitrogen gas.

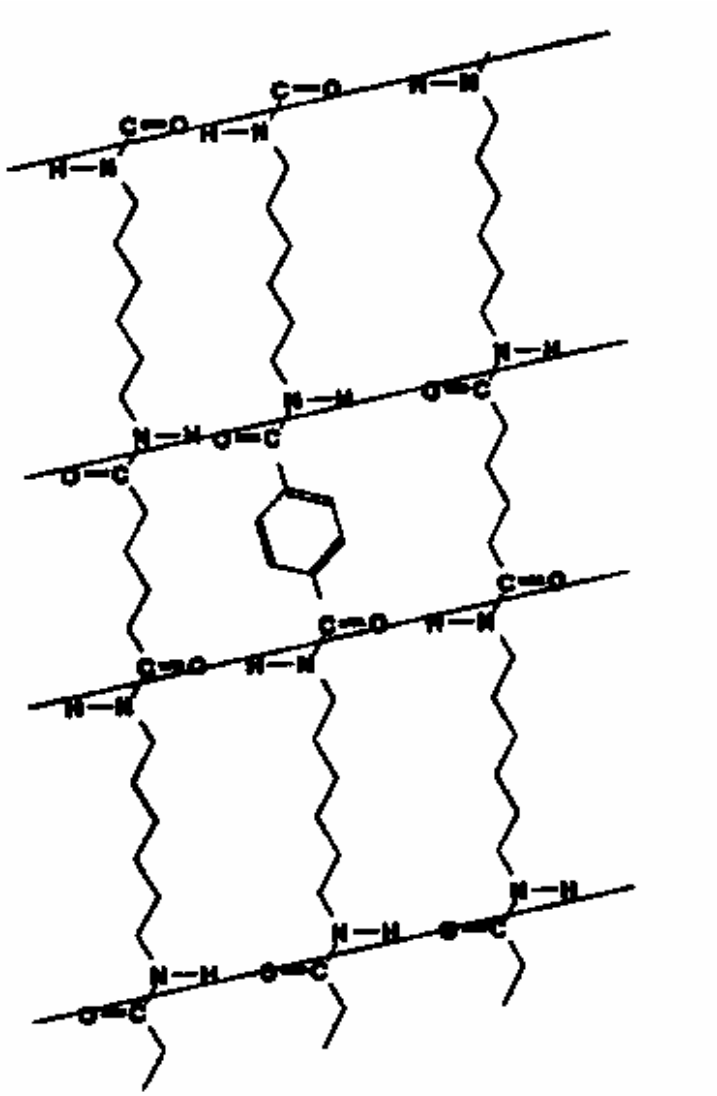

Figure 2.39 Possible isomorphous replacement in PA 66/6T copolymer (Kohan 1995)

A fine thermocouple (to record instant temperature) imbedded directly in polymer film that in turn is sandwiched by two cover glasses and an optical microscope with video and light intensity recording systems. The details of the setup will be given later in the experimental section.

Some very unconventional results were found by this unconventional experiment method. As shown in Figure 2.40, first the temperature versus time cooling curve at different cooling rate always showed a plateau and the plateau temperature decreased with increasing cooling rate.

Careful check of the light intensity and spherulite optical micrographs then revealed that the plateau corresponding to the linear spherulite growth process (see Figure 2.41 for details).

This discovery was extraordinary because it was the first time to confirm that polymers can maintain the constant temperature during the phase transition just like metals and small molecules, as suggested by the modeling of heat transfer during quenching of crystalline polymer (Sifleet et al 1973).

This temperature plateau was attributed to the balance effect of rapid release of latent heat with the heat dissipation by cooling medium (Ding & Spruiell 1996). It also provides unprecedented opportunities to measure spherulites growth rates at much lower crystallization temperatures (i.e. higher supercoolings), which could not be approached before with conventional hot-stage microscope method.

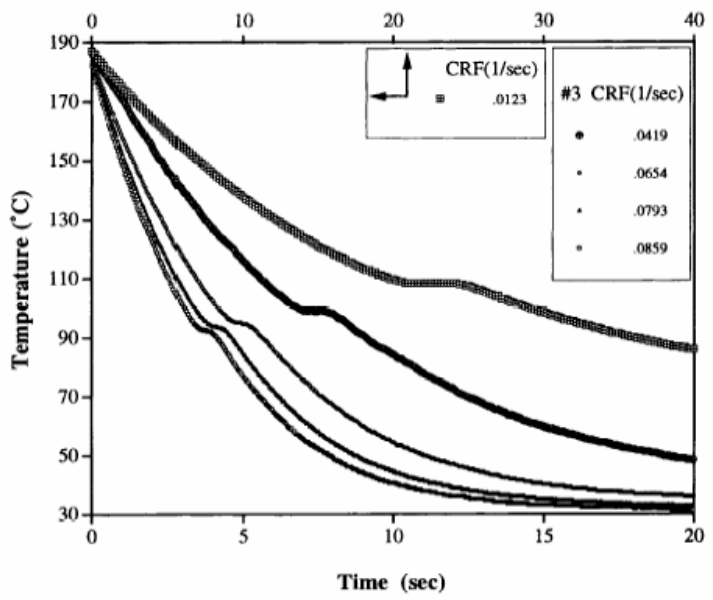

Figure 2.40 Cooling curves of iPP at different cooling rates (Ding & Spruiell 1996).

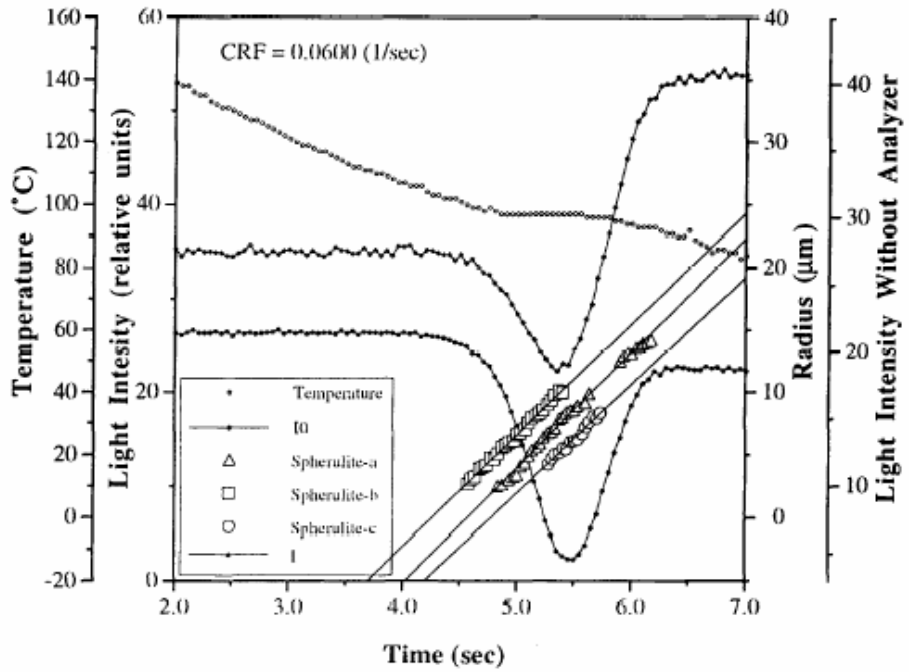

Figure 2.41 The temperature, light intensities and spherulites radius simultaneously recorded by rapid cooling method. (Ding & Spruiell 1996).

2.3.2.2. Application of "pseudo-isothermal" crystallization in polyethylene

The plateau was always present during the rapid cooling process of polyethylene. Therefore rapid cooling method was successfully used (Wagner et al 1999) to measure the growth rates at higher supercooling for a series of polyethylene and 1-octene copolymers. As shown in Figure 2.42a, the lowest crystallization temperature of linear polyethylene was extended from normal 120°C to as low as 90°C by making use of the "pseudo-isothermal" crystallization at the plateau temperatures.

With the regime analysis, the linear polyethylene was found for the first time to present a regime II to regime III transition at 120.8°C in addition to a regime I to regime II transition at 125.6°C, as shown in Figure 2.42b. The regime transitions lent strong support to the secondary nucleation mechanism in the crystallization of polyethylene.

The regime plots of polyethylene and copolymers were found to merge at extreme higher supercooling, which might reveal a common nucleation mechanism for different copolymers (Wagner & Phillips 2001).

2.4. Hypotheses and test schemes

2.4.1. Temperature hypotheses at spherulite growth front

To measure the growth rate at high supercooling, first we should deal with the temperature hypothesis in the rapid cooling methods. The temperature hypothesis has experienced an evolution process with the proceeding of preliminary experiments on PA 66 and the developing of understanding on heat diffusion in polymers.

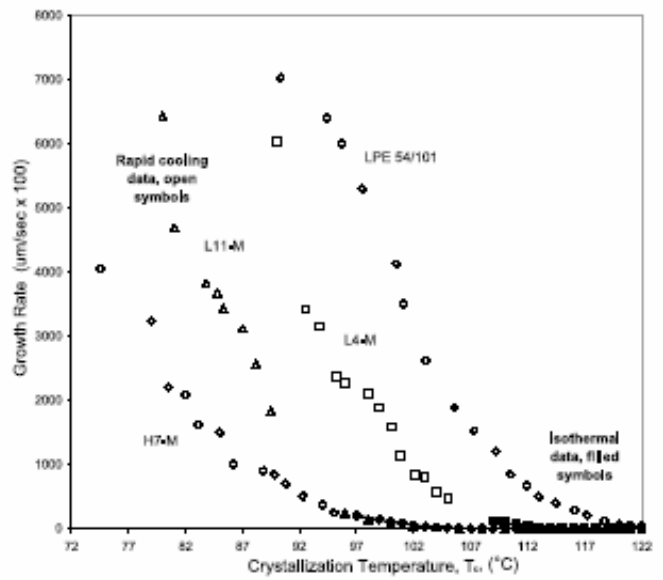

(a)

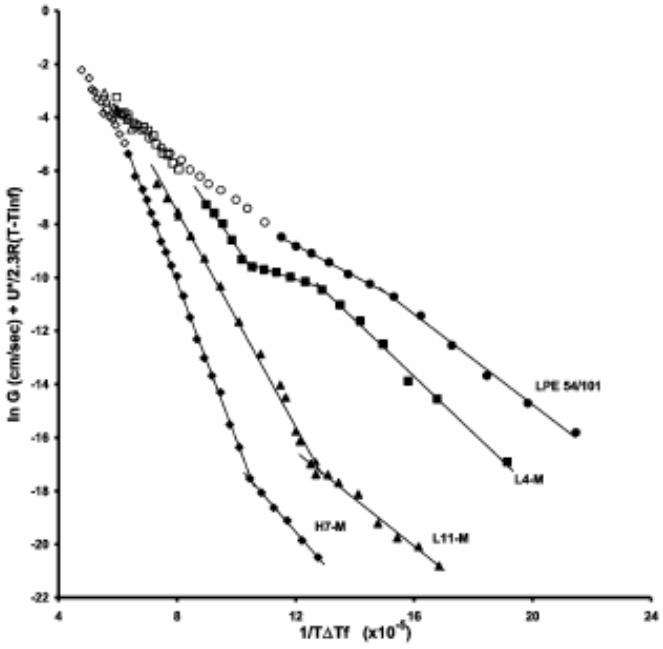

(b)

Figure 2.42 Growth kinetics of linear polyethylene and 1-octene copolymers from rapid cooling methods (Wagner & Phillips 2001). a) linear growth rates; b) regime plots.

2.4.1.1. Temperature plateau could also occur in PA 66

As it was described in the literature on the rapid cooling method, the temperature plateau discovered in PP, PE lead us to assume that a temporary isothermal ("pseudo-isothermal") condition in the sample could always be maintained by the rapid release of crystallization heat for semi-crystalline polymers. Therefore, reliable spherulite growth rates could be acquired even at higher supercoolings, which will then be used in kinetics regime analysis together with isothermal growth rates.

Unfortunately, the plateau has never been present in the cooling curve of PA66, even though a change of slope could be detected occasionally in very thick (~150 μm) samples. Nevertheless, it was clearly observed that spherulites were growing under optical microscope, and recorded light intensity showed significant increase. Similarly, no plateau could be detected in the rapid cooling of PET either. Therefore, it was concluded that the pseudo-isothermal is impossible in PA 66 and PET, probably due to the lower crystallinity and slower growth rates comparing to those of PE and PP.

2.4.1.2. Temperature is constant in the microenvironment around growth front.

After carefully measuring spherulite diameters in a wide range of time, it was found that the spherulites surprisingly still keep linear growth behavior even without the temperature plateau. Therefore, it was believed that there must be an isothermal "micro-environment" around the spherulites to keep the linear growth rates, while even imbedded thermocouple could only show us the average system temperature instead of the real temperature at the growth front. After taking the derivative of temperature over

time, it was found that a plateau did present in the dT/dt versus time curve. An infrared thermograph of PE did reveal uneven temperature distribution in system during non-isothermal crystallization without further details on the growth front due to poor resolution. Temperature average in a large area demonstrates that a plateau did exist in the cooling curve, as recorded with thermocouple. It seemed that the harmony was found again between temperature and growth rate.

2.4.1.3. Temperature gradient is steady at growth front due to poor heat diffusion

During the process of summarizing the preliminary results, it was found from textbooks on thermal diffusion (Lock 1994, Naterer 2000) that constant growth rate during the cooling was a very normal phenomenon in metals. But this constant growth rate is not due to the constant temperature at growth front as we have always expected in polymer but due to the steady *temperature gradient* at growth front for poor heat diffusion in the melt (see Figure 2.43). Poor conductivity of polymer comparing to metals makes accumulation of latent heat at growth front even more possible.

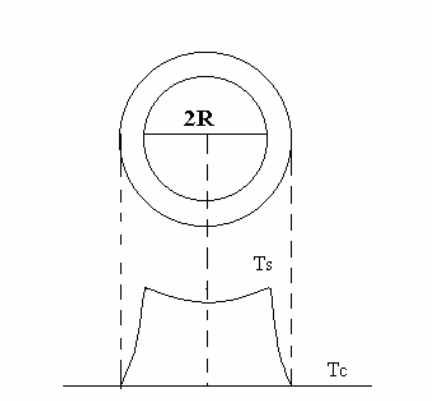

Figure 2.43 Schematic of steady temperature gradient around spherulite growth front.

Therefore the growth rate of PET over a wide range of high supercoolings were measured, spherulites radius still maintain good linear relation with time, even comparable with the situation of “isothermal” crystallization. Therefore, the hypothesis was formed that the linear growth rates of PA 66 and PET at higher supercoolings were the result of steady temperature gradients due to control of heat diffusion.

The implications of temperature gradient hypothesis in spherulite growth front are significant and not limited to the crystallization rates. Latent heat accumulation near lamellae folding surface could prevent further crystallization, there results in lower crystallinity and significant secondary crystallization afterward in PA 66. Temperature gradient due to poor conductivity could also be responsible for the wide melting range of polymers as observed in DSC.

2.4.2. Spherulite growth mechanism in PA 66 is surface roughening

The hypothesis of surface roughening in PA66 was mainly based on the regime analysis, lamellar thickness, melting temperature and simulation of critical nucleus size on PA 66 and PA 66/6T copolymer by (Schreiber 1998), as described before. It was the major motivation of this research to test this hypothesis with growth kinetics at higher supercooling and develop the possible physical path in terms of growth surface changing. From this point of view, it is different from the temperature gradient hypothesis, which is the working hypothesis to measure growth rates at higher supercoolings.

Due to unique H-bonding in the PA 66, it probably seems to be the most appropriate candidate to grow by surface roughening. The constant lamellar thickness

(and melting temperature) at wide range of supercoolings breaks the convention of lamellar thickness controlled by the chain folding as expected by secondary nucleation. The simulation of critical nucleus further supports the notion because the critical nucleation size required for secondary nucleation is unrealistic big.

However, as a kinetic theory, surface roughening hypothesis in PA66 ultimately need the verification of experimental growth rates at a wide range of supercoolings. The present growth kinetics data are too limited, and the absence of regime transitions in copolymer cannot disapprove the possibility of secondary nucleation because they could belong to only one regime. The growth kinetics should also be tested against the kinetics specific to surface roughening derived in metals and small molecules with consideration of long chain character of polymer.

On the other hand, one should be very cautious to define the kinetics mechanism solely based on regime analysis, since the apparent regime transitions could be due to some effects other than nucleation effect. We should thoroughly characterize the crystallization behavior and morphology of PA 66 with respect to supercoolings and molecular structures first before we could make any meaningful judgment.

2.4.3. Lamellar thickness and spherulite morphology determined by surface roughening

This hypothesis is suggested based on extrapolation from the experimental results of Schreiber based on the surface roughening hypothesis. The test on this hypothesis will be helpful to discern the surface nucleation hypothesis.

2.4.3.1. Lamellar thickness does not change much at higher supercoolings

Based on the Schreiber's result of lamellar thickness (Schreiber 1998) and the literature on solution crystallization (Dreyfuss & Keller 1973), it seems reasonable to expect that lamellar thickness will keep almost constant even at higher supercooling without controlling effect of secondary nucleation. The lamellar thickness can be easily checked with the SAXS, using the same method of Schreiber.

2.4.3.2. Lamellar thickness changes with average sequence length

This hypothesis is mainly based on the potential effect of comonomer on ability of molecule to form periodic H-bonding. For isomorphic PA 66/6T copolymer, such an effect could be ignorable if only H-bonding periodicity is considered.

For PA 66/6I and PA 66/6I, the change on lamellar thickness could be expected. If they were excluded from crystal due to preference to form stable crystal only with PA 66 segments, the lamellar thickness will be decreased.

On the other hand, if they were included into the crystal due to rapid growth at high supercooling, thus formed crystals should have the similar thickness as PA 66 homopolymer. However, the growth rates should decrease significantly due to smaller driving force because of less H-bonding content. The including model should be preferred considering the poor mobility of chain stem at high supercooling. The melting temperature could decrease in both situations: the former due to decrease of lamellar thickness, the latter due to small heat of fusion.

2.4.3.3. Non-isomorphic PA 66 copolymer with high content comonomer could be easier to quench

By the same logic as lamellar thickness, PA 66/6T copolymers could maintain similar driving force due to isomorphism; therefore have similar morphology as PA 66 homopolymer. The PA 66/6I and PA 66/6 copolymer should be easier to quench due to difficulty to find crystallizable PA 66 segments in excluding model, or due to lower driving force including model.

2.4.4. Melting temperatures and relaxation temperature correspond to comonomer and supercooling

This hypothesis is the reasonable result that would be expected from the hypothesis on lamellar thickness and morphology. Melting temperature should be the same for the same copolymer at different cooling rates if the lamellar thickness does not change much even at higher supercoolings. However, the melting temperature should be different for different copolymers because of the lamellar thickness because of difference in H-bonding regularity. In the light of the dynamic relaxation results on ethylene / 1-octene copolymers, relaxation temperatures, especially α and β, should change with lamellar thickness and crystallinity acquired by different copolymer at different supercooling temperature.

If the α relaxation (about 80°C) is related to amorphous phase only (Starkweather 1995), the relaxation temperature will slightly change while the magnitude will significantly decrease with crystallinity. If α is also related to the crystalline phase (such as interfacial phase), the relaxation temperature should also increase with crystallinity significantly. Since the molecules mechanism of β relaxation (about -60°C) is not

decided yet, it could be attributed to the motion of molecules in pure amorphous phase or to the methylene segment motion as counterpart of the glass transition temperature (about -37°C) in polyethylene. Such a motion could be possible considering the bigger distance between methylene segments.

2.4.5. Thermal diffusion could contribute to crystallization kinetics transitions in PA 66

Since the hypothesis of steady temperature gradient due to thermal diffusion was taken as working hypothesis and also have the surface roughening as the target hypothesis, it is necessary to expect what overall growth behavior will be expected if these two hypotheses are both confirmed to be true from experimental results. If the molecules are added onto the growth surface directly with only local adjustment in the roughening mode, the chain diffusion limitation could be ignored. Regime transitions in PA 66 could be simply accounted for with the interaction between roughening growth rate and heating diffusion rate.

Roughening growth rate will increase with increasing supercoolings while thermal diffusion capability of melt will decrease with increasing supercoolings. Regime I: the overall growth rate is roughening controlled, fibrillar spherulites formed (in axialites form at early stage). Regime II: roughening controlled growth with heat diffusion perturbation; ringed spherulites are formed due to probably growth front twisting to avoid local high temperature. Regime III: Fully heat diffusion controlled growth due to steady temperature gradient formed at growth front, (see Figure 2.44). The experiment schemes to test hypotheses are summarized in Table 2.2.

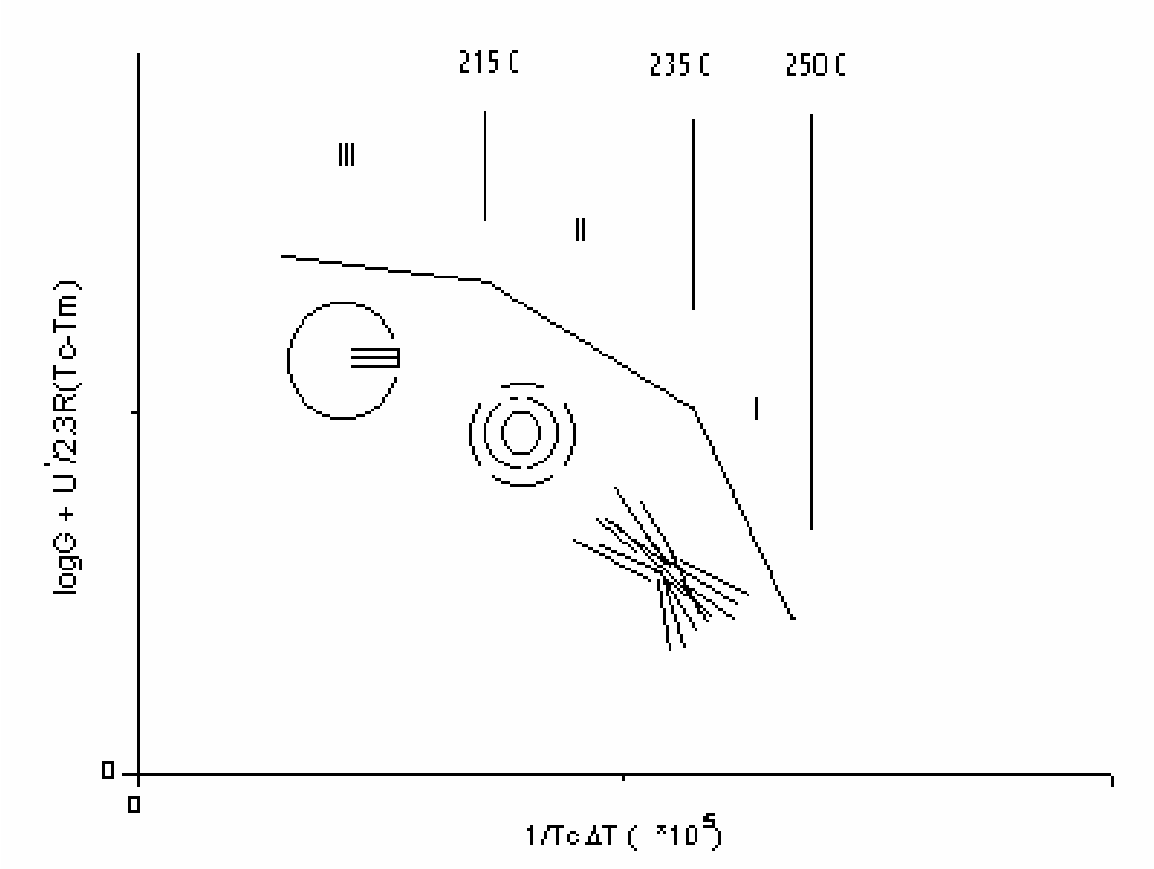

Figure 2.44 Schematic description of regime transition in PA 66.

Table 2.2 Summary of experiments proposed for hypotheses test

Objectives	Hypotheses	Test schemes	Results
1. To measure growth rate at higher ΔT	a) Plateau in T~t curve	Rapid cooling curve	No plateau!
		Linear growth	Linear
	b) Micro-T constant	Infrared imaging	Suggest T gradient
	c) dT/dt steady	Check PET growth	No plateau, linear growth
2. PA 66 surface roughening (PE secondary nucleation)	a) Rough surface	Microscope	-
	b) G linear with ΔT	Plot G ~ ΔT	Not really
	c) σ_e low ?	Gibbs-Thompson	-
3.Lamellar thickness and spherulite morphology	a) Constant *l* with ΔT	SAXS	Constant
	b) l ~ *comonomer*	SAXS	*l* decr. with incr.content
	c) Increase amorph.	OM & WAXD	Unimpinged, low Xc
4. Melting and relaxations behavior	a) Tm ~ *l*	DSC	Tm constant
	b) T_α ~Xc	DMA	-
5. Heat Diffusion also contributes to regime transitions	a) Heat diff. universal	Simulate diff. ~ ΔT	-
	b) Similar kinetics trans	Plot log G ~ ΔT	Three trans, different trend
	c) Morphology	POM	Axial, ringed, non-ringed

CHAPTER 3. EXPERIMENAL PROCEDURES

3.1. Materials

A series of random copolymers of hexamethylene adipamide (66) with either hexamethylene terephalamide (6T), or hexamethylene isophalamide (6I) or caprolactam (6) were used in this study. For the sake of simplicity, the samples were coded by the comonomer name and the weight content of comonomer. Therefore, the PA 66/6T copolymer with 3.3 wt% 6T was coded as PA6T03.

These samples were kindly provided in the form of pellets by former Monsanto Chemical Company (now Solutia). The Table 3.1 below shows the code names and concentration of copolymers (measured by Solutia), and melting temperature at the heating rate of 10 °C/min (Schreiber 1998).

A series of metallocene catalyzed ethylene/1-octene copolymers were also studied with DMA for comparison with relaxation behavior of PA 66 copolymers. The polyethylenes synthesized using metallocene catalysts were kindly provided by the Dow Chemical Company. Typical molecular characteristics are listed in Table 3.2.

3.2. Sample preparations

Thin film sample (50 μm) for kinetics measurement at higher supercooling were prepared by solution casting for clear spherulites images under optical microscope. Polymer solutions were first cast onto a 150 °C hot plate from 2 (w/v) % polymer solutions in formic acid (88 %), and vacuum dried at 90 ºC for 24 h to remove the residual solvent.

Table 3.1 Molecular characteristics of PA 66 random copolymers

Sample code	Comonomer Wt %	Comonomer Mol %	Mw by GPC	Tm (Peak) ^{o}C
PA 66 (Vydyne21)	0%	0%	25,000	269.32
PA 6T03	3.3%	2.8%	18,000 to 24, 000	266.96
PA 6T06	6.5%	5.5%	18,000 to 24, 000	267.71
PA 6T09	9.7%	8.3%	18,000 to 24, 000	266.43
PA 6T12	12.9%	11.1%	18,000 to 24, 000	267.33
PA 6I12	12.9%	11.1%	18,000 to 24, 000	253.48
PA6I16	16.1%	13.9%	18,000 to 24, 000	250.24
PA 66 (lab batch)	0%	0%	18,000 to 24, 000	268.87
PA606	6.0%	11.3%	18,000 to 24, 000	254.44
PA610	10.5%	19.0%	18,000 to 24, 000	249.43
PA616	16.0%	27.6%	18,000 to 24, 000	239.17
PA621	21.0%	34.7%	18,000 to 24, 000	230.64

Table 3.2 Molecular characteristics of metallocene polyethylenes samples.

Sample	M_n g/mol	M_w g/mol	M_w/M_n -	Branch/ 1000C	Comonomer mol %	Density g/cm^3	T_m °C
LPE38	38,200	77,600	2.03	0	0	0.9512	131.5
L-04	27,300	59,900	2.19	3.98	0.79	0.9365	122.7
L-11	21,200	43,700	2.06	10.86	2.15	0.9195	110.2
L-24	21,800	46,900	2.15	24.04	4.58	0.8975	95.4
L-37	23,000	46,300	2.01	36.73	6.89	0.8861	81.3
L-53	29,200	69,000	2.36	53.21	9.58	0.8700	51.4

Polymer films for DSC, SAXS, WAXS and DMA experiments were prepared with a Wabash hot press. Polymer pellets were vacuum dried at 100 °C for 24 h prior to compression molding, pellets were first melted at approximately 20 °C above the melting temperature for 5 min and pressed at 10 MPa for 3 min, then left cooling between mold plates to room temperature. The final film thickness was between 90-120 μm. Crystallization experiments at high supercoolings were then carried out with Ding-Spruiell rapid cooling methods.

3.3. Rapid-Cooling method

Linear spherulite growth rates were measured using a polarized optical microscope (Nikon Eclipse E600 POL) with video camera and Ding-Spruiell rapid cooling hot-stage (see Figure 3.1). Samples were held at 20 °C above the respective optical melting temperature for 5 min and then rapidly quenched to the crystallization temperatures. Simultaneously, temperature of sample was recorded from a fine thermal couple (25.4 μm) embedded in the thin polymer film sample (50 μm).

3.3.1. Spherulitic growth rates

Since no temperature plateau could be detected in the cooling curves, the crystallization temperatures were referred to the temperature corresponding to the onset of the crystallization, which could be detected by light intensity. The spherulite growth rates were determined by first plotting spherulite radius with time; linear growth rates of several spherulites were then averaged to represent the growth rate of one crystallization temperature.

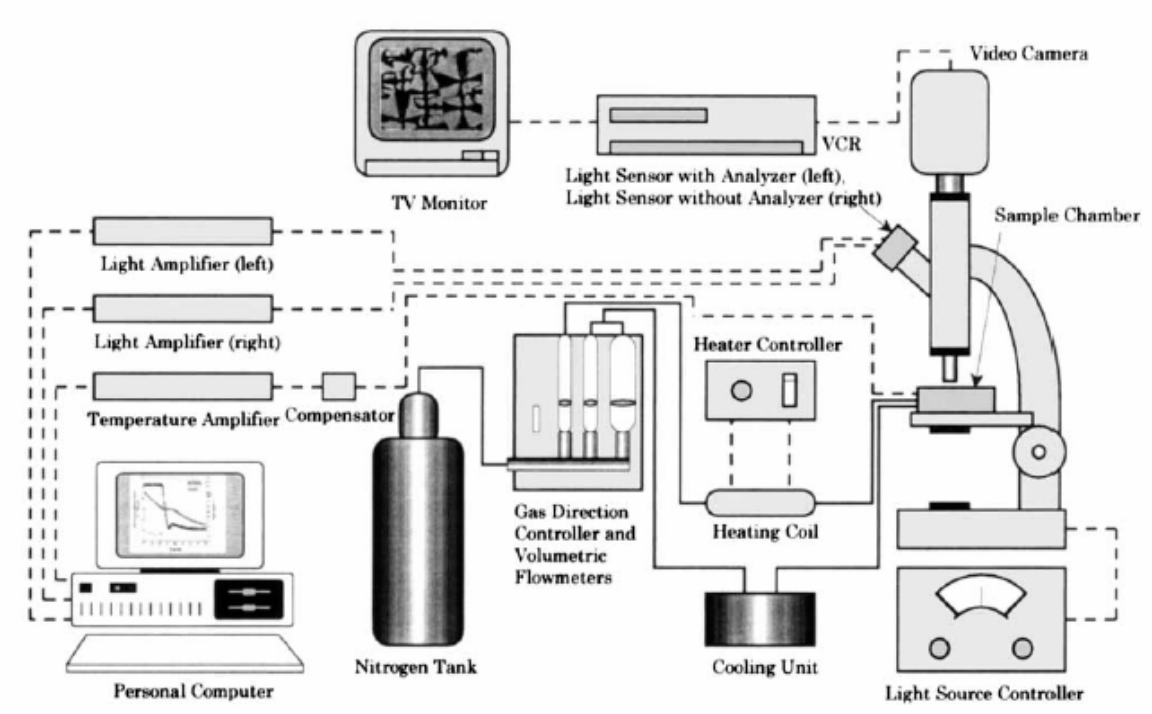

Figure 3.1 A schematic of rapid cooling apparatus (Ding & Spruiell 1996).

3.4. Wide Angle X-ray Diffraction (WAXD)

WAXD studies were carried out using Philips Diffractometer in the reflection mode with Cu Kα radiation, λ = 0.1542 nm. The operating voltage and current are 35 kV and 40 mA respectively, and calibration was done using a silicon standard (2θ = 24.465°).

3.4.1. Resolve reflections by profile fitting

Reflection integrated intensities were determined by deconvolution of the diffraction peaks into a series of peaks by Philips Profit software.

3.4.2. Calculate X-ray crystallinity

The percent of crystallinity was calculated from the relative areas of the amorphous and two major crystalline peaks with equation below:

$$W_{c,x} = \frac{A_{(010)} + A_{(110)}}{A_{(Amorp.)} + A_{(010)} + A_{(110)}} \qquad (3.1)$$

3.5. Small Angle X-ray Scattering (SAXS)

SAXS patterns were measured with a three pin-hole small angle X-ray scattering system in University of Tennessee recently constructed by Molecular Metrology. A 2-D detector was used for scattering pattern image acquisition.

The lamellar thickness could be determined from the application of Bragg's law on Lorentz corrected intensity or from the first maximum of 1-D correlation functions.

An explicit MathCAD data treatment program developed by Schreiber (Schreiber 1998) was used in this research, therefore only major processes will be described here.

3.5.1. Long period from Bragg's law (reciprocal space)

The long period can be obtained from Lorentz corrected SAXS intensity profiles using Bragg's law with the assumption that semi-crystalline polymer is a two-phase system with sharp boundary between alternative crystalline and amorphous phases. Bragg's law is given by:

$$n\lambda = 2d\sin\theta \qquad (3.2)$$

Where, d is spacing of crystalline plane, 2θ is scattering angle, λ is the wavelength of X-ray. In Small Angle X-ray Scattering, the scattering intensity (I) is usually recorded versus scattering vector ($q = 4\pi\sin\theta/\lambda$). Therefore, an alternative form of Bragg's law is preferred as below:

$$d = \frac{\lambda}{2\sin\theta} = \frac{2\pi}{(4\pi\sin\theta)/\lambda} = \frac{2\pi}{q} \qquad (3.3)$$

The long period L (corresponding to spacing d in wide angle) can be determined from the q_{max}, which corresponds to the maximum scattering intensity in the Lorentz corrected intensity profiles.

$$L = \frac{2\pi}{q_{\max}} \qquad (3.4)$$

Using the two-phase semi-crystalline model, the lamellar thickness (*l*) can be calculated from long period by multiplying volume crystallinity (Xc), which could be determined from DSC, density measurement or WAXD.

$$l = L * X_c \qquad (3.5)$$

Since the long period determined from Lorentz corrected intensity curve is the weighted average of semicrystalline polymer (Vonk 1988), the corresponding lamellar thickness is also a weighted average value. It should also be mentioned that this method not only assumes the ideal two-phase model but also assume a homogeneous lamellar structure.

However, in real polymer systems from bulk crystallization, there exists transition (or interfacial) zone between crystalline phase and amorphous phase; and there also exists distribution of lamellar thickness and spacing. Therefore, alternative method of one-dimensional correlation is usually used.

3.5.2. Lamellar thickness from one-dimensional correlation function (real space)

A graphical extrapolation procedure was proposed (Strobl & Schneider 1980a, Strobl & Schneider 1980b)to determine lamellar structure parameters based on the properties of the *correlation function*, which can be obtained by Fourier transformation of the scattering curve.

$$K(z) = \frac{1}{2v}\int_0^\infty I_{LC}(q)\cos(qz)dq \qquad (3.6)$$

Since scattering data from SAXS experiments are only in the range of 0.11 $nm^{-1} < q < 1.5\ nm^{-1}$, extrapolations to $q = 0$ and to $q \rightarrow \infty$ are necessary for the Fourier transformation.

At low q, a linear connection between origin and the first measured points was used; for $q \rightarrow \infty$, Porod's law ($I \propto q^{-4}$) was used and further checked in a log$I(q)$-log$q$ plot for accuracy.

A schematic view of correlation function of semicrystalline polymer is shown in Figure 3.2. Long period (L) can be determined as the first maximum of one-dimensional correlation function after zero.

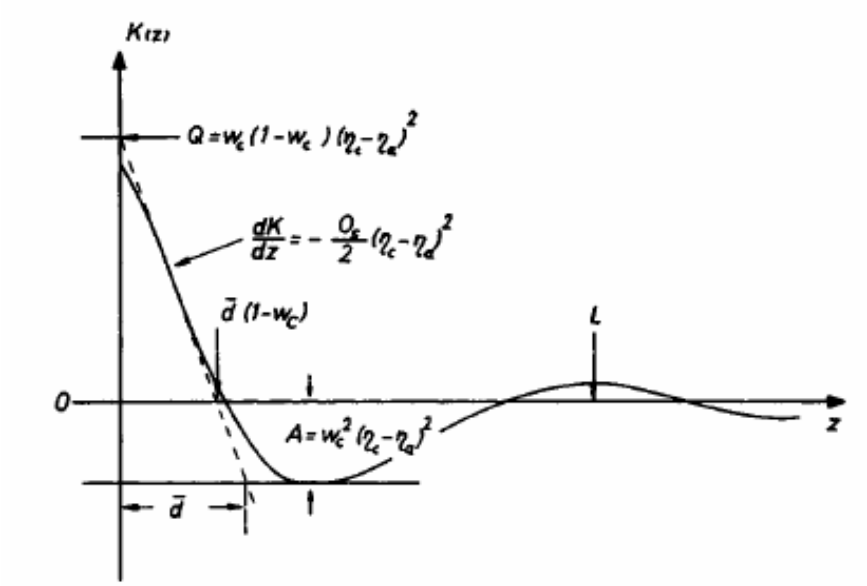

Figure 3.2 Schematic of *Self Correlation Triangle* (Strobl & Schneider 1980b).

A straight section exists in the "self-correlation" range of (0 < Z <d), which reflects the electron density correlation within a lamella (Strobl & Schneider 1980b). The constant slope is related to the specific inner surface O_s:

$$\frac{dK}{dz} = -\frac{O_s}{2}(\eta_c - \eta_a)^2 \qquad (3.7)$$

When extrapolated to Z = 0, the intercept gives the invariant of "corresponding ideal two-phase structure" for the real lamellae.

$$Q = w_c(1 - w_c)(\eta_c - \eta_a)^2 \qquad (3.8)$$

A number average lamellae thickness ($\bar{d}$) can be determined as the point where the extrapolated straight section meets with the horizontal base line:

$$A = -w_c^{\,2}(\eta_c - \eta_a)^2 \qquad (3.9)$$

and the correlation function K(z) reach to zero when

$$z_0 = \bar{d}(1 - w_c) \qquad (3.10)$$

3.6. Differential Scanning Calorimetry (DSC)

Melting behavior was characterized with a Thermal Analyst 2910 DSC (from TA Instrument) with a liquid nitrogen-cooling accessory in Polymer Characterization Laboratory of University of Tennessee. The heating scans were performed with a heating rate of 10 °C /min. Dry nitrogen gas with a flow rate of 20 ml/min was purged through

the DSC cell to prevent the thermal degradation. The temperature and heat flow was calibrated with the heat of fusion of indium (28.45 J/g). The peak temperatures were determined as the melting temperatures.

3.6.1. DSC crystallinity

The thermal crystallinity was calculated by the ratio of experimental heat of fusion (ΔH_f) to heat of fusion for 100% crystalline PA66 (ΔH_f^o =255.41 J/g) from ATHAS data bank (Xenopoulos & Wunderlich 1991).

$$X_h = \frac{\Delta H_f}{\Delta H_f^0} \qquad (3.11)$$

3.7. Dynamic Mechanical Analyzer (DMA)

Dynamic mechanical properties were studied using a Dynamic Mechanical Thermal Analyzer DMTA V ^{TM} of Rheometric Scientific in rectangular tension mode. Specimens are of the following dimension: length 25 mm, width 5 mm, and thickness around 0.120 mm.

The storage modulus, loss modulus and loss factor were measured using a sinusoidal tensile strain of 0.05% with 0.1% static strain to keep automatic tension. The temperature range was from –100 to 150 ^{o}C and the frequencies employed were 0.1, 0.3, 1, 3, 10 and 30 Hz.

CHAPTER 4. RESULTS

4.1. Spherulitic growth rates of PA66 copolymers

4.1.1. PA 66/6T copolymers

The spherulitic growth rates of PA 66 and PA66/6T copolymers at different crystallization temperatures are shown in Figure 4.1. Growth rates from rapid cooling experiments and isothermal crystallization with Mettler hot-stages are represented with different symbols. A peak in the growth rate vs. crystallization temperature can be observed for each polymer, which clearly demonstrated the effectiveness of rapid cooling approach to reach growth rates at high supercoolings.

With increasing content of 6T in PA66/6T copolymers, growth rate peak value almost does not change at all. Since the magnitude of growth rate changes significantly across several decades, the relationship between crystallization rates and supercooling are more clearly represented in a logarithm plot of growth rate, see Figure 4.2. Growth rates appear as three distinct stages with decreasing crystallization temperature. First, a linear relationship can be clearly observed between Log G and Tc for the high crystallization temperatures (low supercoolings).

When the crystallization temperatures decrease further (under 238 °C for PA 66), the growth rate deviates from the original line but still follows a straight line with a decrease slope. It should be mentioned that this change of slope is actually corresponding to the optical morphology changing from axialites (or elliptical) structure to spherulitic structures for each of the polymers, which is also generally observed at the regime I/II transition of secondary nucleation (Hoffman & Miller 1997).

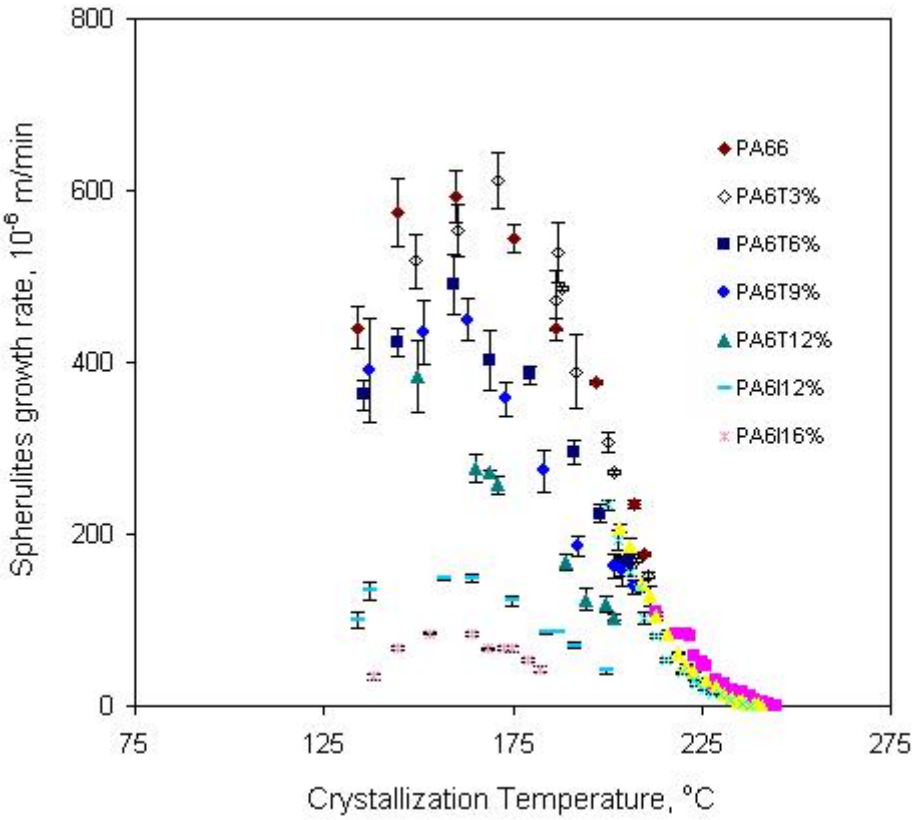

Figure 4.1 Spherulitic growth rate of PA66/6T and PA66/6I copolymer versus crystallization temperature.

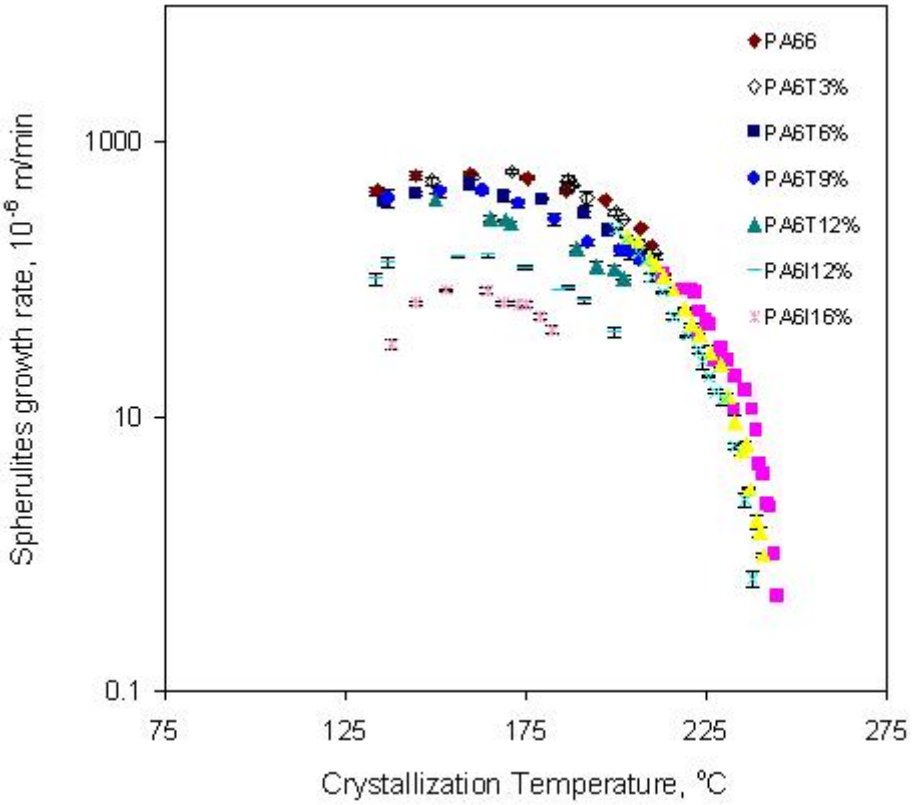

Figure 4.2 Logarithm of spherulite radius growth rate of PA 66/6T copolymers versus crystallization temperature.

When the crystallization temperatures decrease further, generally determined with rapid cooling method, the growth rates deviate from the linear relationship again. A change of ringed / non-ringed spherulitic structure in optical morphology is usually found at this transition temperature. The growth rates flatten out at the location close to the growth rate maximum; then decrease with further decrease of crystallization temperature.

4.1.2. PA 66/6 copolymers

The spherulitic growth rates of PA 66 and copolymers at different crystallization temperatures are shown in Figure 4.3. Growth rates from rapid cooling method and isothermal crystallization are represented with solid and open symbols, respectively. A peak in the growth rate vs. crystallization temperature plot can also be observed for each polymer, which showed the effectiveness of rapid cooling approach to reach high supercoolings. The peak temperature for PA66 is around 159.8 ^{o}C, which is close to the average of T_g (80 ^{o}C) and T_m (263 ^{o}C) of PA 66.

The peak position moves to lower temperature with increasing content of PA6, with peak value of 149.8 ^{o}C for PA606 and 142.0 ^{o}C for PA 610, respectively. The crystallization temperatures of copolymers were found to move to lower temperature at equivalent cooling condition, and growth rate is significantly reduced with decreasing average sequence length of PA66 at the same time.

The change of crystallization rates with supercooling were more clearly represented in the logarithm plot of growth rate, see Figure 4.4. A linear relationship can be clearly observed between Log G and Tc for the high crystallization temperatures.

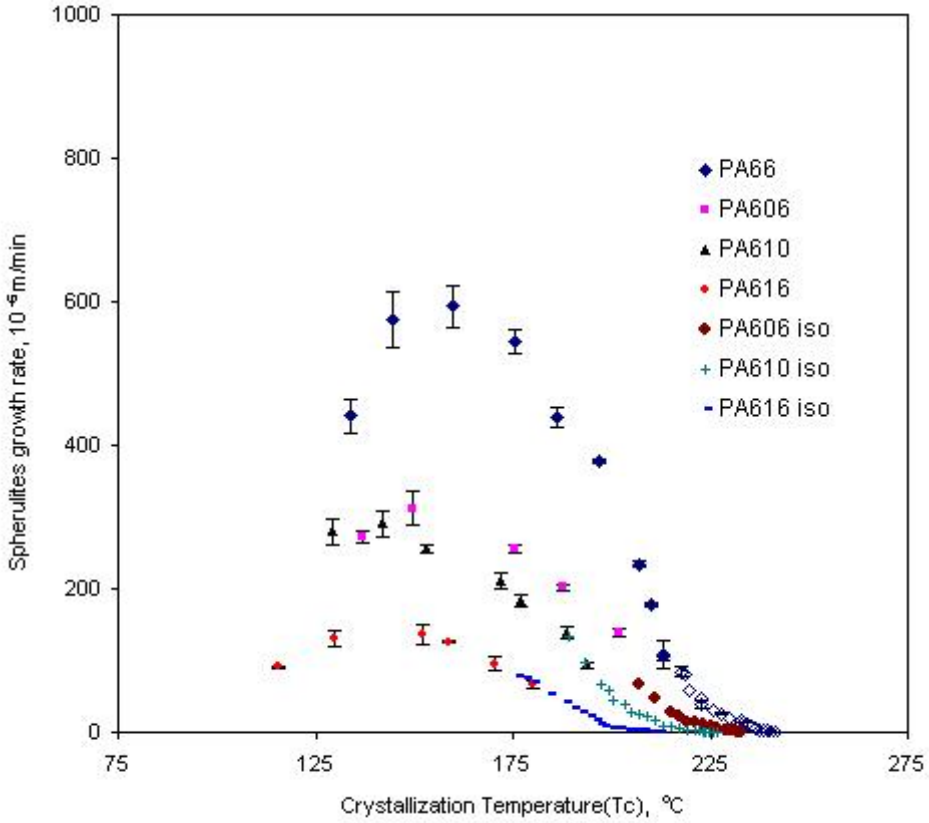

Figure 4.3 Spherulite growth rate of PA 66/6 copolymers versus crystallization temperature.

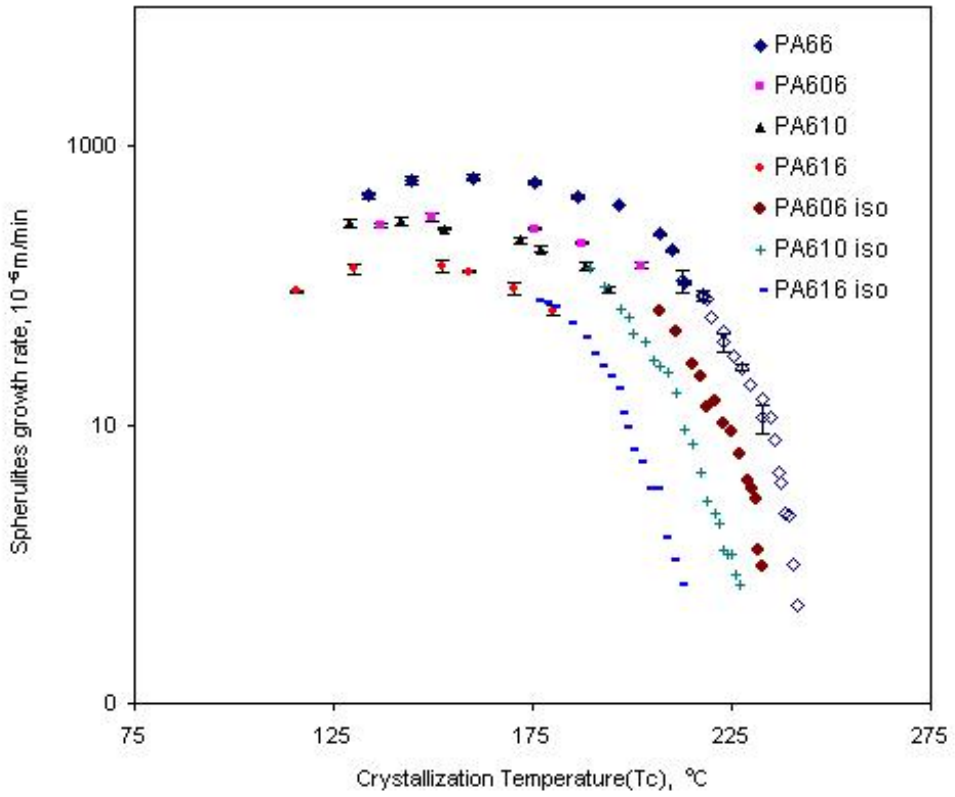

Figure 4.4 Logarithm of spherulite radius growth rate of PA 66/6 copolymers versus crystallization temperature.

As observed in PA66/6T copolymers, a second linear relationship with smaller gradient exists for lower crystallization temperatures. For the growth rate at higher supercooling measured with rapid cooling method, the growth rates were found to flatten out instead of following linear relationship.

Similar to the observations in PA66/6T copolymers, axialites/spherulite and ringed/non-ringed spherulites transition were corresponding to the two transitions in growth rate kinetics.

4.2. Spherulitic morphology formed at high supercoolings

PA 66 copolymers at higher supercoolings not only showed significantly different growth rates, but also showed diverse spherulitic morphologies, which can be changed from impinged spherulites at high crystallization temperature to isolated spherulites, then to completely amorphous optical morphology by changing the cooling conditions, see Figure 4.5.

In general, PA 66 and copolymers form impinged spherulites at higher crystallization temperature. The spherulite sizes decrease with the decreasing crystallization temperatures, while the spherulite numbers increase simultaneously because of increasing homogeneous nucleation. PA66/6T copolymers appear similar spherulitic morphology as PA 66 homopolymer does.

PA66/6 copolymers have smaller spherulite size than PA 66 homopolymer at equivalent cooling conditions (cooling rates), which might be the result of decreasing crystallization ability that has been shown in the slower growth rate in Figure 4.3.

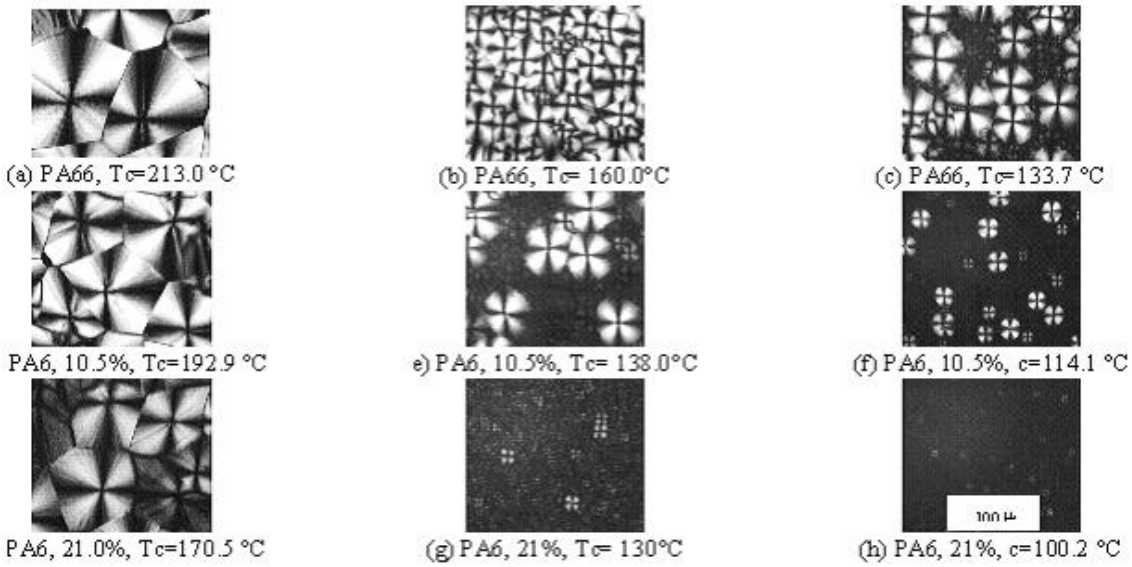

Figure 4.5 Spherulites of PA66 and PA6 copolymer observed under Polarized Optical Microscopy (with X20 objective).

4.3. Crystal structure from Wide Angle X-ray Diffraction

4.3.1. PA 66/6T and PA66/6I copolymers

Generally, two diffraction peaks exist in PA66 crystals: a lower angle peak (around 20°) from the diffraction of (100) plane and a higher angle peak (around 24°), which is actually the convolution of diffractions from (110) and (010) planes. It was determined that the diffraction angle of (100) is at 20.36° and the combination (010)/(110) peaks at 24.09/24.43 in X-ray diffraction (Bunn & Garner 1947). The (100) diffraction is related to the chain distance within H-bonding sheet; while (110)/(010) doublet is related to the inter-sheet displacement. Sometime a weak peak due to (002) is also observed around 10° for PA 66 with high crystallinity, which is usually related to the diffraction of folding plane in the lamellae.

Wide angle X-ray Diffraction patterns of PA66 crystals formed at different supercoolings are shown in Figure 4.6. It is found that both peak position and magnitude of (100) diffraction does not change much with decreasing crystallization temperature; while (010)/(110) diffraction moves to lower angle and peak intensity decreases at the same time. Therefore, the H-bonding structures between neighboring chains should be well preserved at increasing supercooling whereas the displacement between H-bonding sheets increases somehow.

Wide angle X-ray Diffraction patterns of PA66/6T copolymers are shown in Figure 4.7 (3wt% 6T), Figure 4.8 (6wt% 6T), Figure 4.9 (12wt% 6T) for increasing content of 6T comonomer.

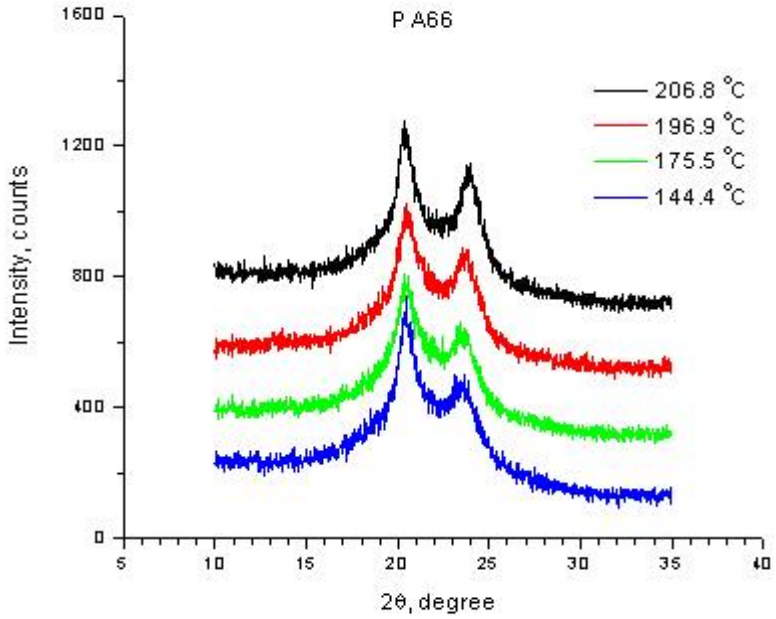

Figure 4.6 Wide Angle X-ray Diffraction patterns of PA 66 at high supercoolings.

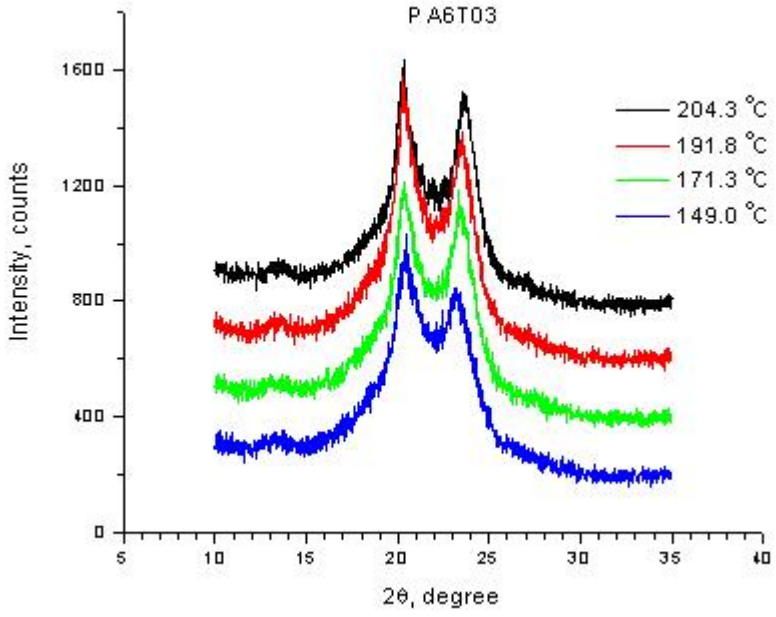

Figure 4.7 Wide Angle X-ray Diffraction pattern of 3 wt% PA 66/6T copolymer at high supercoolings.

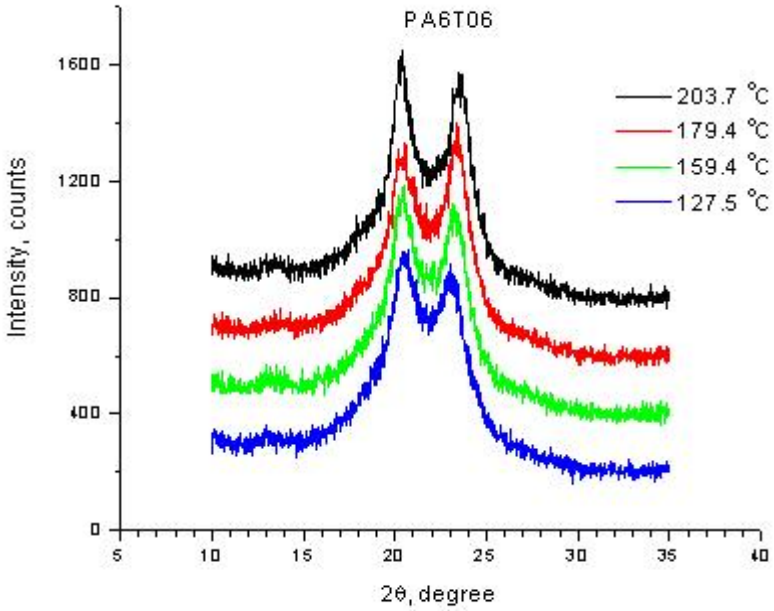

Figure 4.8 Wide Angle X-ray Diffraction pattern of 6 wt% PA 66/6T copolymer at high supercoolings.

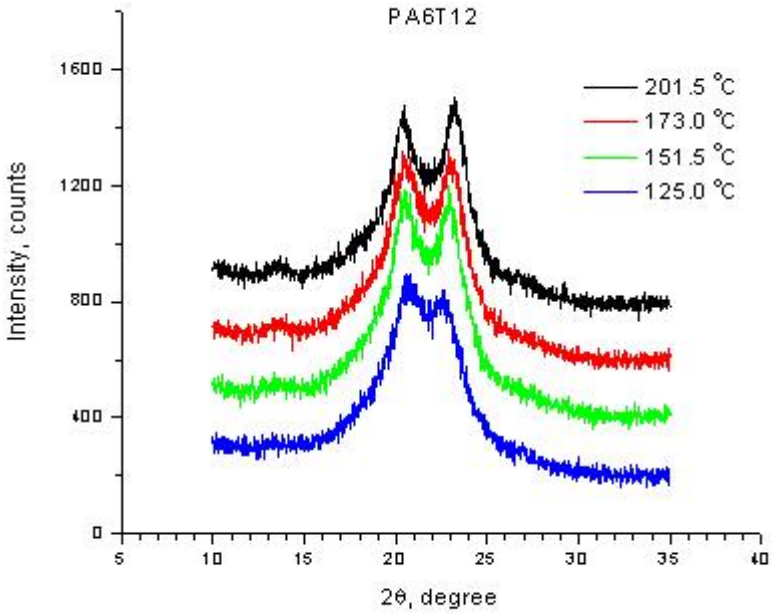

Figure 4.9 Wide Angle X-ray Diffraction pattern of 12 wt% PA 66/6T copolymer at high supercoolings.

Basically, all of them have similar peak position and peak intensity as PA 66 homopolymer, and the higher angle peak (inter-sheet distance) also shows similar tendency of decreasing with increasing crystallization temperature as observed in PA66. However, there are two distinct features in PA 66/6T copolymers: 1) (200) diffraction is more clearly observable around 12°; 2) the intensity of (010)/(110) peak is stronger relative to (100) peak than in PA66, and this tendency increases with the 6T content.

In 12 wt% PA 66/6T copolymer, the magnitude of (010)/(110) peak overpasses that of (100) peak. The change of relative magnitude could result either from the variation of chain distance within H-bonding sheet or from the increasing content of regular H-bond sheet in the system; both of them could be attributed to the inclusion of 6T repeat units into lamellar crystal.

The implications of these features will be further discussed related to the co-crystallization and to possible nucleation effect of the planar benzyl ring in 6T in the part of discussions.

Wide angle X-ray Diffraction patterns of 12 wt% PA66/6I crystals formed at increasing supercoolings are shown in Figure 4.10. Obviously, the diffraction patterns are much closer to PA 66 than PA 66/6T copolymers. At high supercooling, the (010)/(110) peak intensity decrease significantly with decreasing crystallization temperatures. Apparently, only one strong (100) peak exists in the diffraction pattern with a very weak (010)/(110) shoulder. It should be mentioned that the corresponding optical micrograph shows amorphous super-structure.

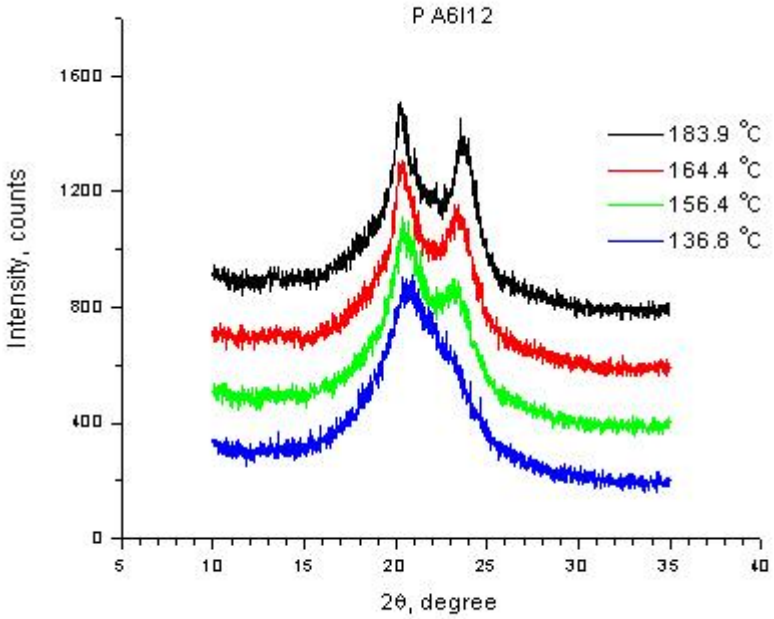

Figure 4.10 Wide Angle X-ray Diffraction pattern of 12 wt% PA 66/6I copolymer at high supercoolings.

4.3.2. X-ray diffraction pattern of PA 66/6 copolymers

Wide angle X-ray Diffraction patterns of PA66/6 copolymers are shown in Figure 4.11 (6 wt% PA6), Figure 4.12 (10 wt% PA6), and Figure 4.13 (21% PA6). In general, the diffraction patterns are changing with the supercooling similar to those of PA 66 and PA 66/6I copolymers. With increasing PA 6 content, (010)/(110) peak intensity decreases and the resulting crystallinity also decreases significantly. Only a single amorphous peak can be observed at very high supercooling, which is consistent with the observation of spherulitic morphology with optical microscopy. The asymmetry of amorphous peak is probably due to the ubiquitous one-dimensional H-bonding structure existing between neighboring chains.

4.3.3. Summary of WAXD results

In summary, both diffraction angle and intensity of (010)/(110) doublet decrease with increasing supercooling for PA66 and all copolymers. The (100) peak basically maintains its peak position as long as the crystallinity is detectable with WAXD. The PA 66/6T copolymers show stronger (002) diffraction and (010)/(110) diffraction and have higher crystallinity value comparing to PA66 homopolymer, PA66/6I and PA66/6 copolymers. The crystallinity determined from relative area of diffraction peak is consistent with spherulitic morphology by optical observation.

The resulting peak position, integrated area and crystallinity from peak deconvolution procedure are listed in Table 4.1 for PA 66 homopolymer and copolymers at different supercoolings.

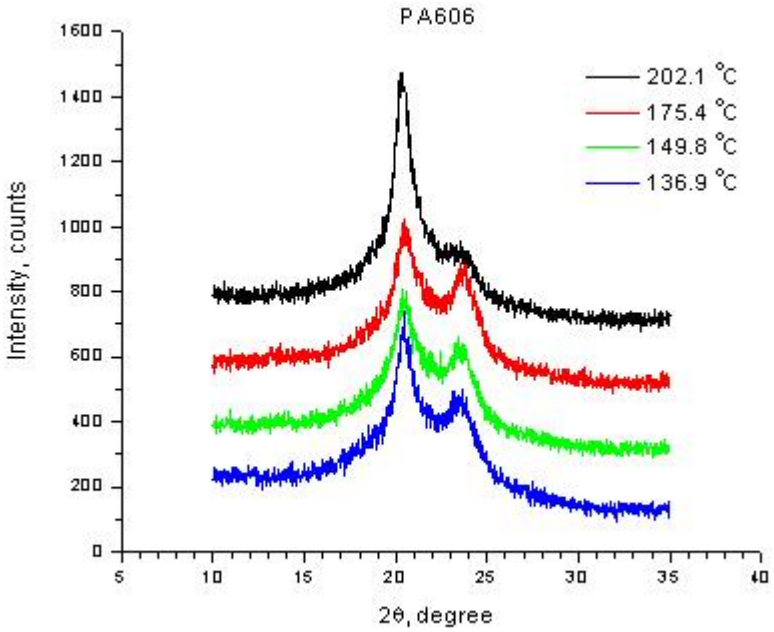

Figure 4.11 Wide Angle X-ray Diffraction pattern of 6 wt% PA 66/6 copolymer at high supercoolings.

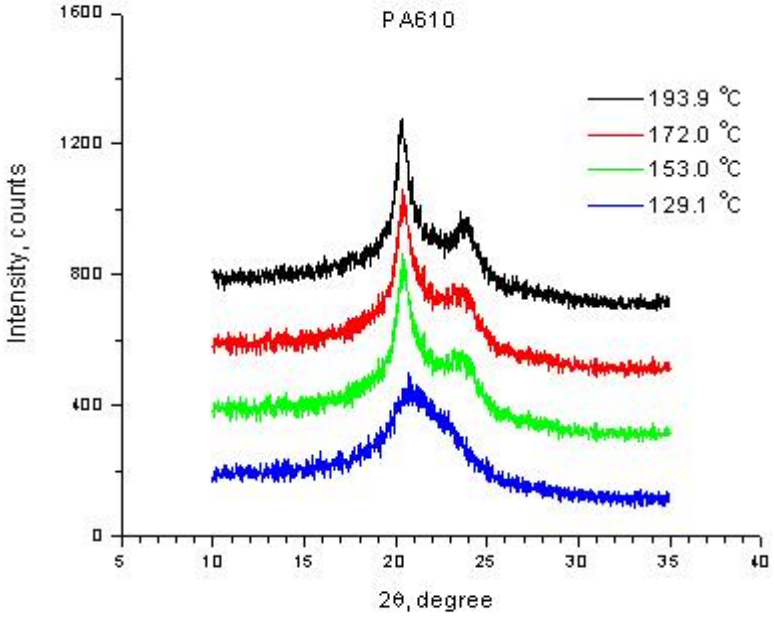

Figure 4.12 Wide Angle X-ray Diffraction pattern of 10 wt% PA 66/6 copolymer at high supercoolings.

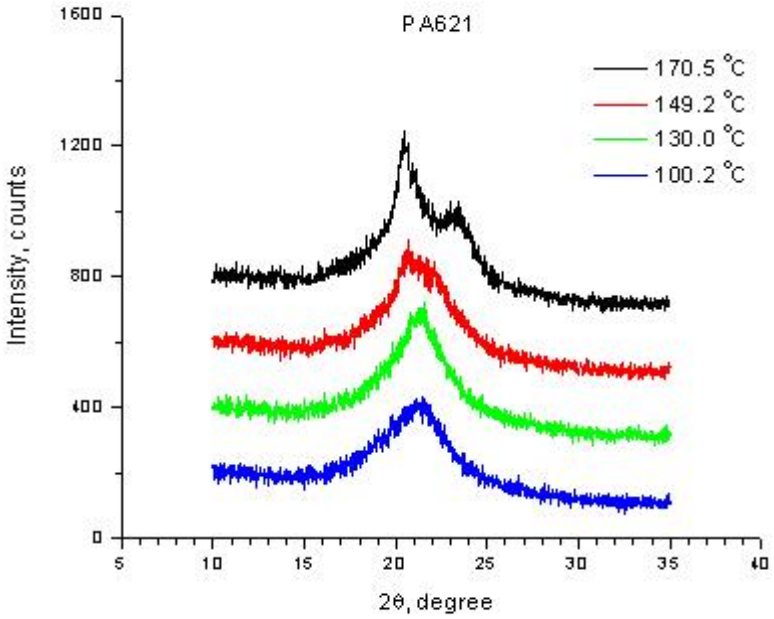

Figure 4.13 Wide Angle X-ray Diffraction pattern of 21 wt% PA 66/6 copolymer at high supercoolings.

Table 4.1 Summary of WAXD parameters of PA66 copolymers

Sample	Cool flow	Tc °C	$2\theta_{(100)}$ °	$2\theta_{(100)/(010)}$ °	$d_{(100)}$ Å	$d_{(100)/(010)}$ Å	Xc %
PA 66	0	206.8	20.3912	23.9751	4.352	3.709	34.96
	10	196.9	20.4897	23.7855	4.332	3.738	32.38
	40	175.5	20.4529	23.656	4.339	3.759	31.67
	150	144.4	20.4281	23.6606	4.345	3.758	27.04
PA6T03	0	204.3	20.2865	23.7206	4.375	3.748	38.08
	10	191.8	20.3521	23.5787	4.361	3.771	35.81
	40	171.3	20.3622	23.5299	4.358	3.778	35.99
	150	149.0	20.397	23.4243	4.351	3.795	30.85
PA6T06	0	203.7	20.3467	23.6127	4.362	3.765	39.21
	10	179.4	20.4061	23.4645	4.349	3.789	36.06
	40	159.4	20.3864	23.3803	4.353	3.802	31.47
	150	127.5	20.450	23.2337	4.340	3.826	24.06
PA6T12	0	201.5	20.3728	23.3021	4.356	3.815	31.06
	10	173.0	20.4345	23.1852	4.343	3.834	25.79
	40	151.5	20.4427	23.0947	4.341	3.849	24.03
	150	125.0	20.5267	22.9599	4.324	3.871	14.01
PA6I12	0	183.9	20.2852	23.7866	4.375	3.738	31.48
	5	164.4	20.3506	23.5759	4.361	3.771	29.03
	10	156.4	20.456	23.4704	4.339	3.788	26.32
	40	136.8	20.6078	23.4704	4.307	3.788	6.78
PA606	0	202.1	20.3603	23.8072	4.359	3.735	31.23
	10	175.4	20.4801	23.6727	4.334	3.756	29.97
	40	149.8	20.5448	23.128	4.320	3.843	21.62
	150	136.9	20.5072	23.849	4.328	3.729	4.53
PA610	0	193.9	20.3404	23.8861	4.363	3.723	30.07
	10	172.0	20.4169	23.7157	4.347	3.749	27.04
	40	153.0	20.4209	23.7265	4.346	3.748	24.73
	150	129.1	20.6911	23.2249	4.290	3.827	7.60
PA621	0	170.5	20.4688	23.5713	4.336	3.772	25.15
	10	149.2	20.6308	22.9277	4.302	3.876	7.73
	40	130.0	-	-	-	-	-
	150	100.2	-	-	-	-	-

4.4. Lamellar structure from Small Angle X-ray Scattering

4.4.1. PA 66/6T and PA66/6I copolymers intensity profiles

The SAXS intensity profiles of PA 66 and PA66/6T copolymer are shown in Figure 4.14 (PA66), Figure 4.15 (PA6T, 3%), Figure 4.16 (PA6T, 6%), Figure 4.17 (PA6T, 12%) and Figure 4.18 (PA6I, 12%), respectively. The scattering intensities of the polymers are found to decrease with supercooling, which is consistent with optical spherulitic morphology and the crystallinity results from wide angle X-ray diffraction.

For PA 66 homopolymer and PA66/6T or PA66/6I copolymers, the position of scatting intensity maximum (q_{max}) remains relatively constant agreeing with previous findings (Schreiber 1998) at higher crystallization temperatures with conventional isothermal crystallization method on the same copolymers. It appears that the percent crystallinity of these polymers also does not change significantly with supercoolings.

4.4.2. PA 66/6 copolymers intensity profiles

The SAXS intensity curves of PA 66 and PA66/copolymer are shown in Figure 4.19 (PA6, 6%), Figure 4.20 (PA6, 10%) and Figure 4.21(PA6, 21%), respectively. The scattering intensities of the polymers are found to decrease with supercooling. For PA66/6 copolymers, the position of scatting intensity maximum (q_{max}) increases slightly with increasing supercooling, corresponding to the gradually un-impinged spherulitic structure therefore with much lower crystallinity value. It seems that long period is somehow related to the crystallinity in PA 66 as reported in the quenched PA66 samples (Starkweather et al 1963).

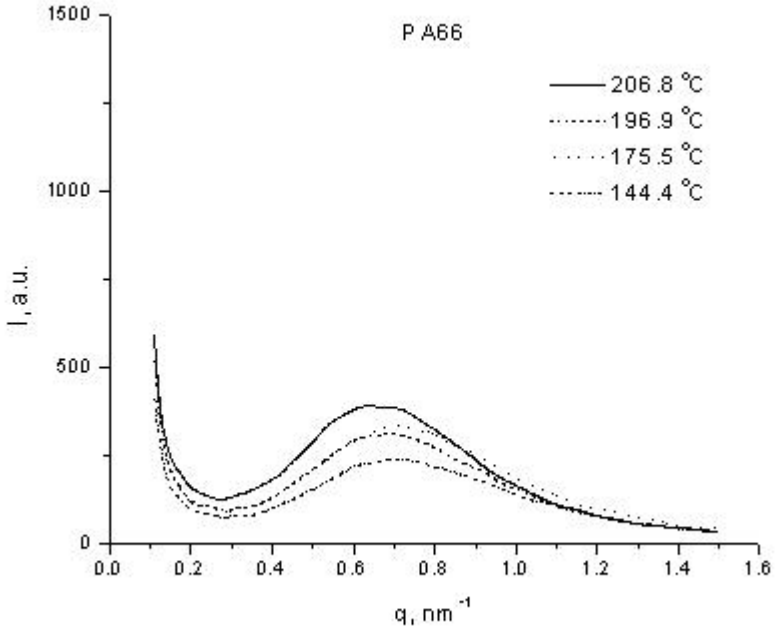

Figure 4.14 Small Angle X-ray Scattering curves of PA 66 homopolymer at high supercoolings.

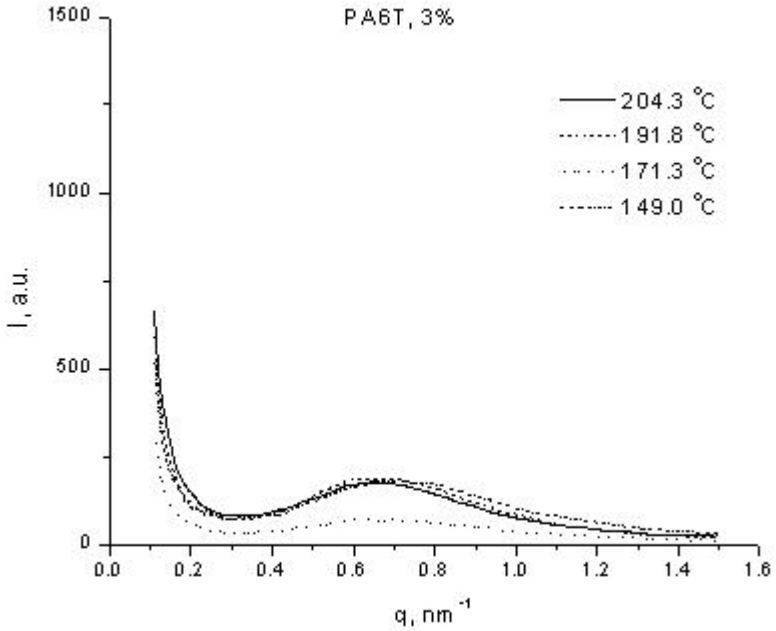

Figure 4.15 Small Angle X-ray Scattering curves of 3 wt% PA 66/6T copolymer at high supercoolings

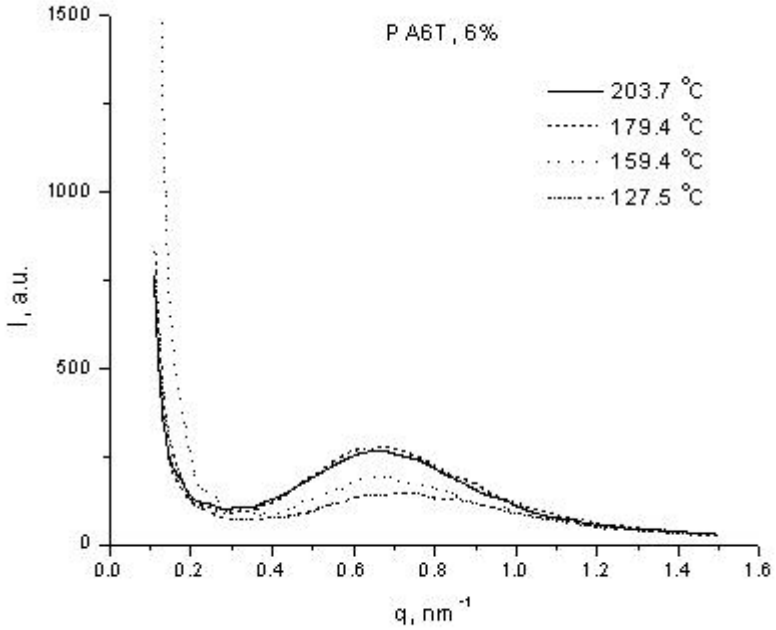

Figure 4.16 Small Angle X-ray Scattering curves of 6 wt% PA 66/6T copolymer at high supercoolings

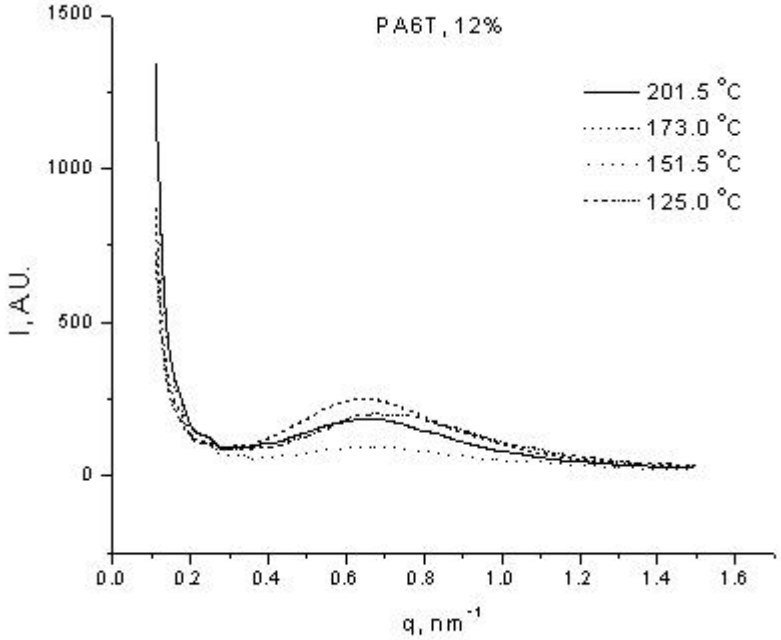

Figure 4.17 Small Angle X-ray Scattering curves of 12 wt% PA 66/6T copolymer at high supercoolings

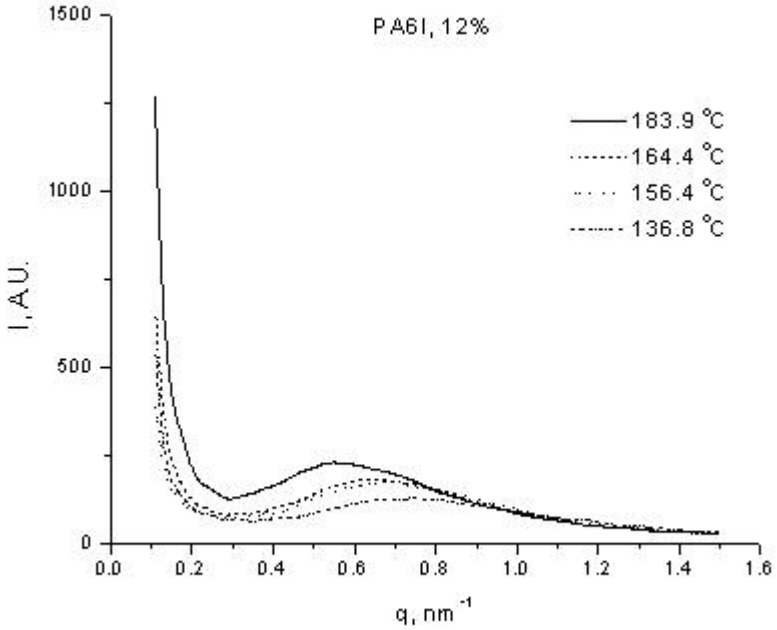

Figure 4.18 Small Angle X-ray Scattering curves of 12 wt% PA 66/6I copolymer at high supercoolings.

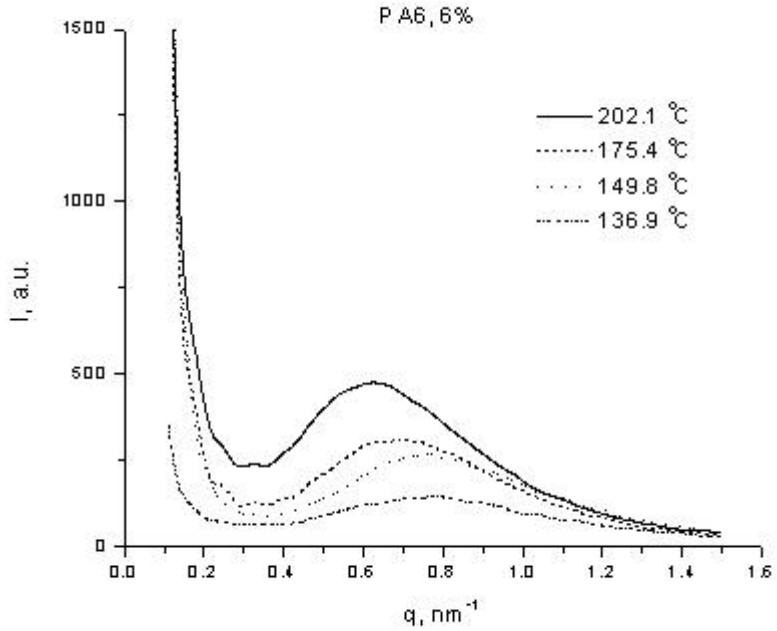

Figure 4.19 Small Angle X-ray Scattering curves of 6 wt% PA 66/6 copolymer at high supercoolings.

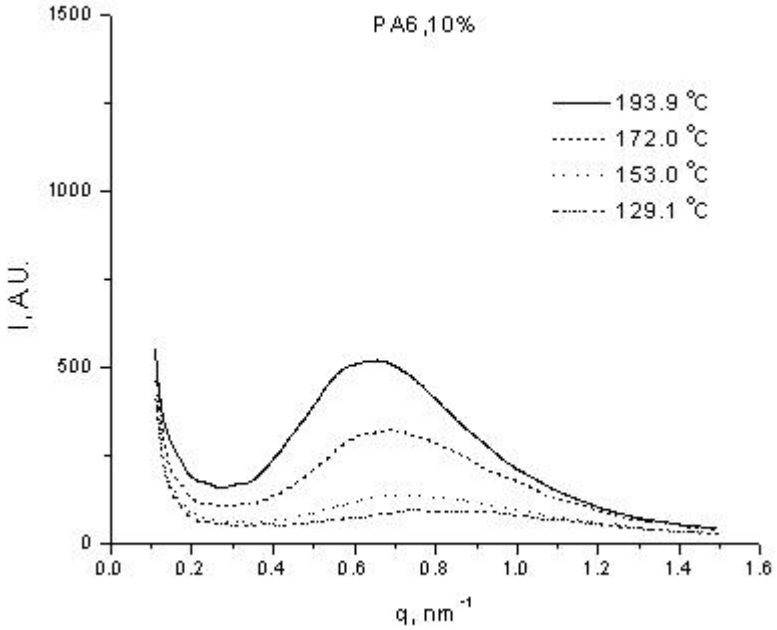

Figure 4.20 Small Angle X-ray Scattering curves of 10 wt% PA 66/6 copolymer at high supercoolings.

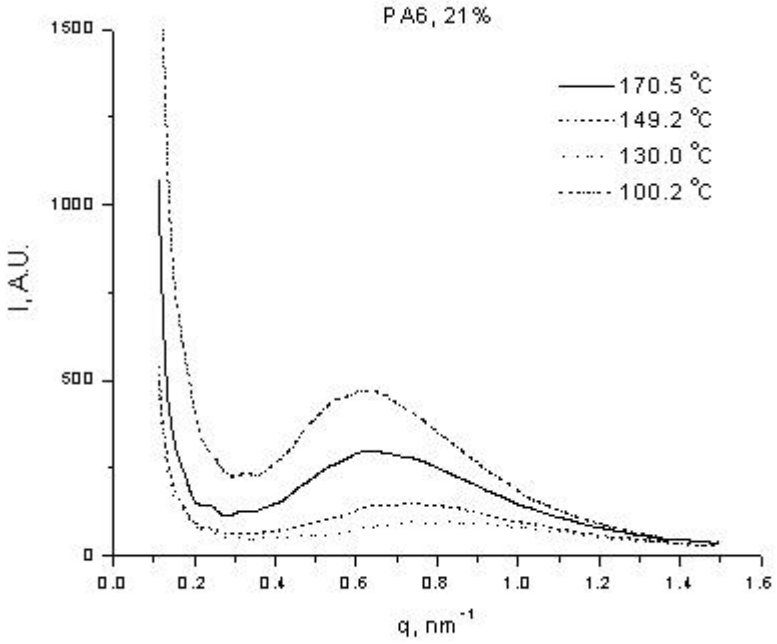

Figure 4.21 Small Angle X-ray Scattering curves of 21wt% PA 66/6 copolymer at high supercoolings.

If this is the general case, then it is not difficult to understand the relatively constant long periods in PA66 and PA66/6T copolymer (at the range of supercooling accessible with rapid cooling methods), whose crystallinity is relatively constant in the range of 30% - 35%.

4.4.3. One dimensional correlation function

The one dimensional correlation function analyses give more direct indications of the long periods in the real space and the results are shown in Figure 4.22 (PA66), Figure 4.23 (PA6T, 3%), Figure 4.24 (PA6T, 6%), Figure 4.25 (PA6T, 12%) and Figure 4.26 (PA6I, 12%). The long period of PA66, corresponding to the position of maximum $K_1(Z)$ value, was found to decrease only slightly with decreasing crystallization temperatures, which is consistent with Schreiber's results of isothermal crystallization at higher temperatures as well.

The one dimensional correlation function analyses of PA66/6 copolymer are shown in Figure 4.27 (PA6, 6%), Figure 4.28 (PA6, 10%) and Figure 4.29 (PA6, 21%). The long period of PA66, corresponding to the position of maximum $K_1(Z)$ value, was found to decrease only slightly with decreasing crystallization temperatures.

4.4.4. Summary of SAXS results

The scattering intensity decreases with the increasing supercooling for all the polymers studied. The long period determined from both Bragg equation and one-dimensional correlation function is relatively constant, which confirms the observation of Schreiber at higher crystallization temperature.

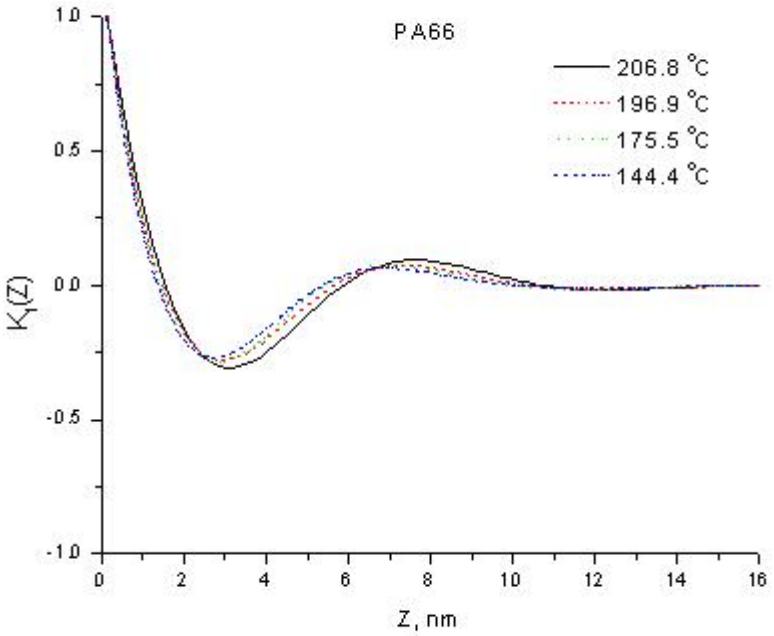

Figure 4.22 1-D correlation function of PA66 at high supercoolings.

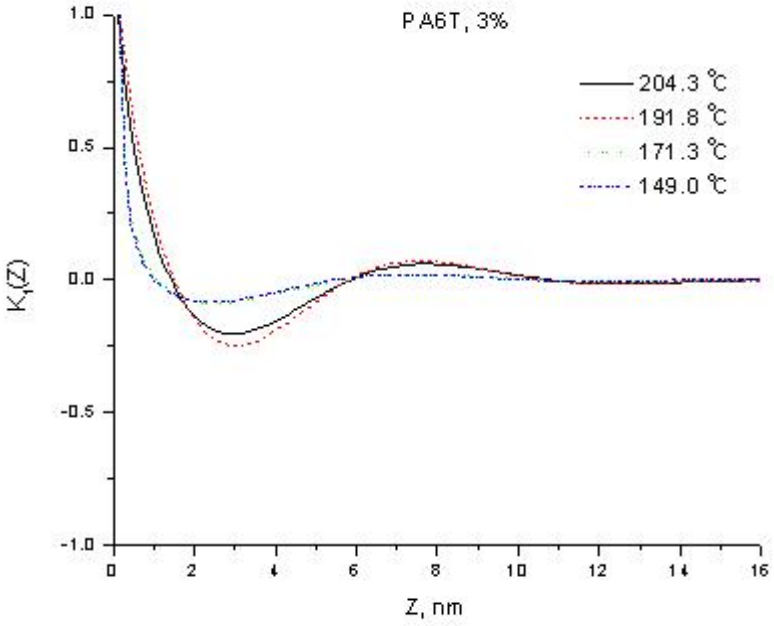

Figure 4.23 1-D correlation function of 3 wt% PA 66/6T copolymer at high supercoolings

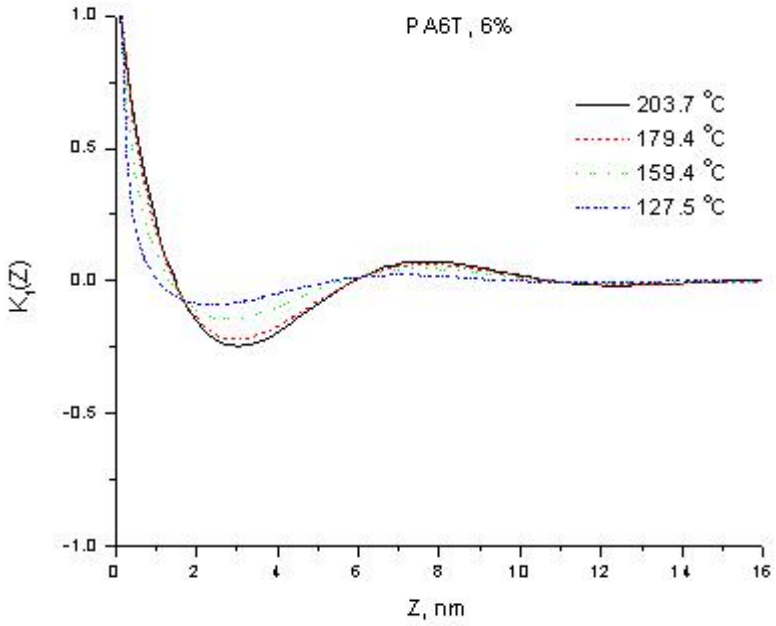

Figure 4.24 1-D correlation function of 6 wt% PA 66/6T copolymer at high supercoolings

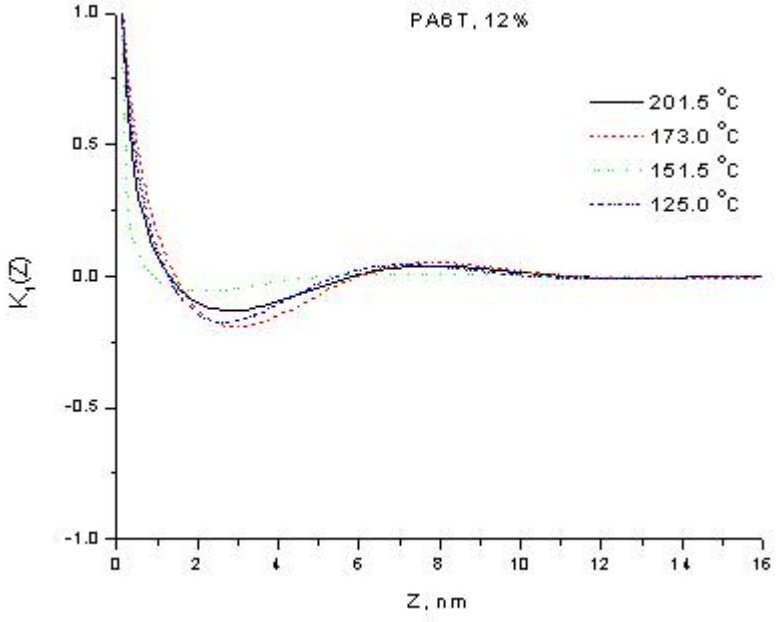

Figure 4.25 1-D correlation function of 12 wt% PA 66/6T copolymer at high supercoolings

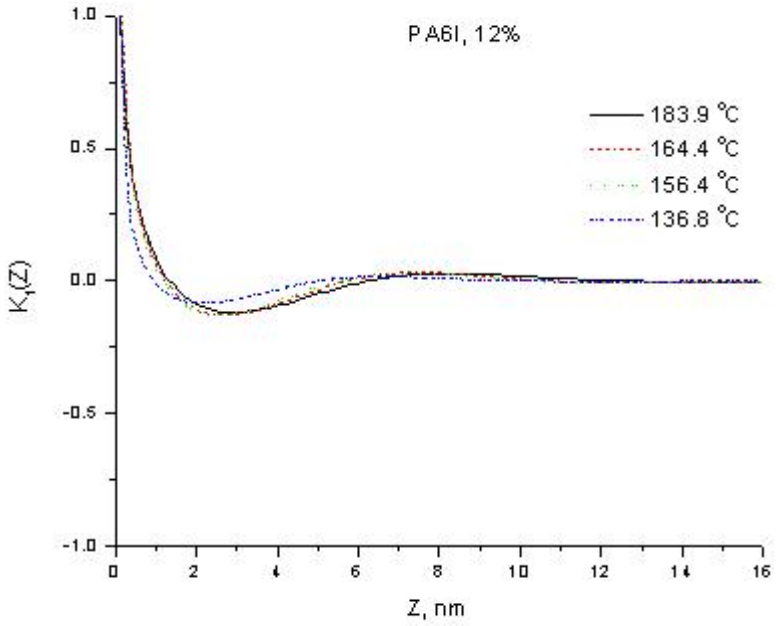

Figure 4.26 1-D correlation function of 12 wt% PA 66/6I copolymer at high supercoolings

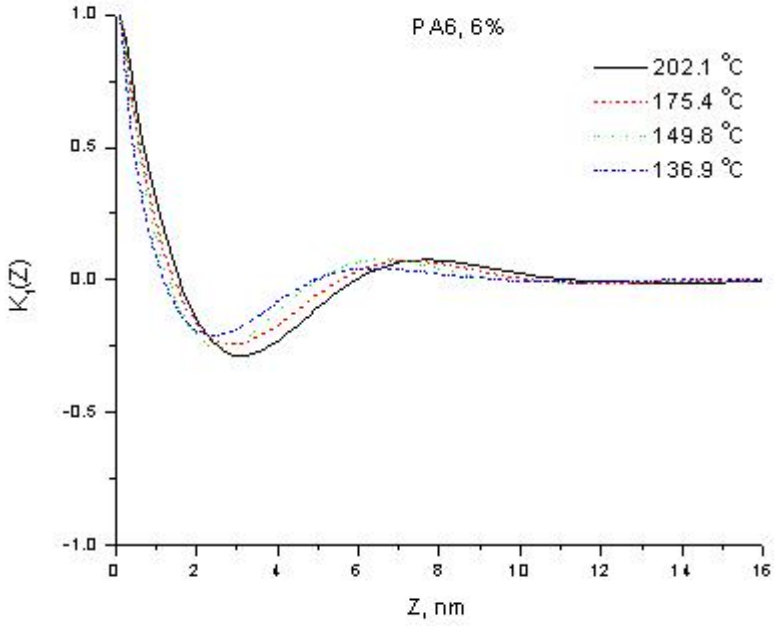

Figure 4.27. 1-D correlation function of 6 wt% PA 66/6 copolymer at high supercoolings

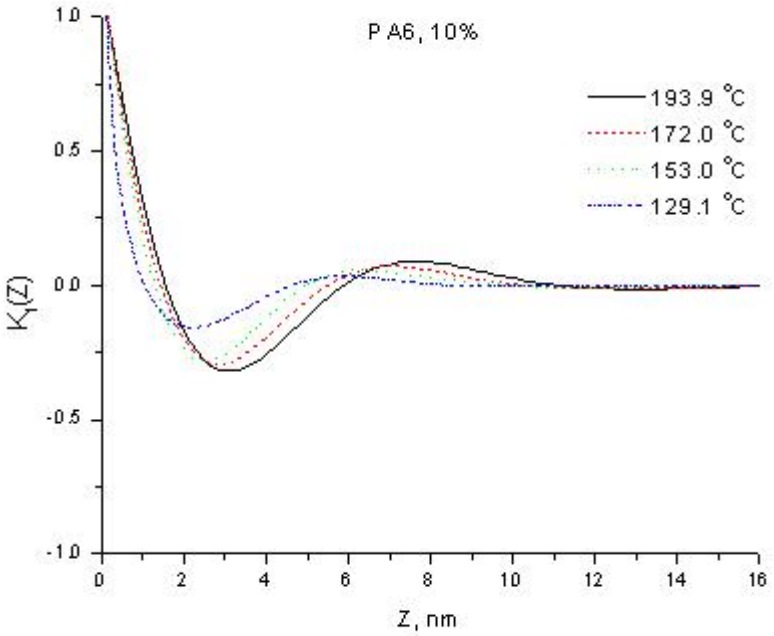

Figure 4.28 1-D correlation function of 10 wt% PA 66/6 copolymer at high supercoolings

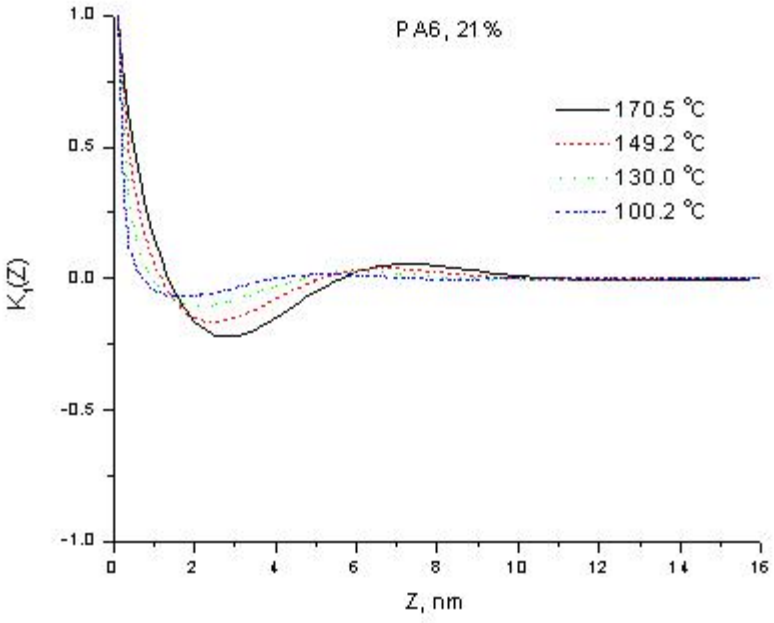

Figure 4.29 1-D correlation function of 21 wt% PA 66/6 copolymer at high supercoolings

The long periods of PA66/6 copolymer decrease more significantly with increasing supercooling comparing to those of PA66/6T copolymers. This feature seems to correspond to the occurrence of gradual un-impinged spherulitic structure as observed in optical micrograph, as well as the lower bulk crystallinity shown by Wide Angle X-ray diffraction. Table 4.2 lists the specific value of crystallinity and long periods estimated from Bragg equation and one-dimensional correlation function.

4.5. Melting behavior studied with DSC

The DSC was used to study to the melting behavior of the crystal phase in PA 66 and copolymers formed at different supercooling. On the one hand, melting studies provide morphological information for the crystal structure as the reverse process of crystallization; on the other hand, melting behavior gives indications of the chain behavior at different temperatures.

It should be stated that the melting process is a very complicated process; the original crystal structure might change (such as lamella thickening observed in PE, cold crystallization in PET) during the heating process. Therefore, extra caution is necessary for the accurate interpretation of the crystal morphology from melting. For the melting process of PA66/6 copolymers, it should be mentioned that isolated spherulites maintain their size until the melting point, and no obvious spherulitic structure change (as in PET) has been observed with optical microscopy at the similar heating rate as that of DSC. A clear cold crystallization peak has been reported just above glass transition temperature for PA66 samples quenched with liquid nitrogen (Xenopoulos & Wunderlich 1990).

Table 4.2 Summary of SAXS result for PA 66 and copolymers at high supercoolings

Sample	**Cool Cond.**	**Tc °C**	**$Xc_{(WAXD)}$ %**	**$L_{(Bragg)}$ Å**	***lc*** **Å**	**$L_{(1-D)}$ Å**	**$Xc_{(1-D)}$ %**	**$lc_{(1-D)}$ Å**	**$la_{(1-D)}$ Å**
PA 66	0	206.8	34.96	7.6755	2.68	7.5931	31.95	2.23	5.36
	10	196.9	32.38	7.7705	2.52	7.3687	30.44	2.05	5.32
	40	175.5	31.67	6.9085	2.19	7.0433	29.47	1.92	5.12
	150	144.4	27.04	6.9085	1.87	6.9152	25.35	1.78	5.14
PA6T03	0	204.3	38.08	7.8775	3.00	7.7391	37.27	2.57	5.17
	10	191.8	35.81	7.8775	2.82	7.5931	34.38	2.33	5.26
	40	171.3	35.99	6.8031	2.45	7.4471	35.82	2.46	4.99
	150	149.0	30.85	7.4836	2.31	7.3011	30.81	2.29	5.01
PA6T06	0	203.7	39.21	8.0934	3.17	7.7391	37.77	2.50	5.24
	10	179.4	36.06	8.0904	2.92	7.7391	35.12	2.41	5.33
	40	159.4	31.47	7.6755	2.42	7.4471	31.18	2.47	4.98
	150	127.5	24.06	7.1272	1.73	7.0928	24.0	2.34	4.75
PA6T12	0	201.5	31.06	7.4836	2.32	7.7391	30.85	2.57	5.17
	10	173.0	25.79	8.0904	2.09	7.8852	25.26	2.08	5.81
	40	151.5	24.03	5.6209	1.35	6.9973	24.00	2.23	4.77
	150	125.0	14.01	7.1728	1.00	7.0958	13.76	1.58	5.52
PA6I12	0	183.9	31.48	8.3151	2.62	8.3232	31.30	2.71	5.61
	5	164.4	29.03	7.6755	2.23	7.4471	28.87	2.46	4.99
	10	156.4	26.32	7.1728	1.89	7.2322	26.18	2.19	5.04
	40	136.8	6.78	6.5631	0.44	6.531	6.77	1.30	5.23
PA606	0	202.1	31.23	8.0885	2.53	7.6702	28.48	2.13	5.54
	10	175.4	29.97	7.4663	2.24	7.2441	28.60	2.04	5.20
	40	149.8	21.62	6.5084	1.41	6.5148	20.24	1.59	4.92
	150	136.9	4.53	6.870	0.31	6.3941	4.36	1.22	5.17
PA610	0	193.9	30.07	8.0904	2.43	7.7391	26.49	2.02	5.72
	10	172.0	27.04	7.3615	1.99	7.0958	24.76	1.84	5.26
	40	153.0	24.73	6.5631	1.62	6.403	22.55	1.64	4.76
	150	129.1	7.60	5.6209	0.43	5.9116	7.50	1.22	4.69
PA621	0	170.5	25.15	7.1728	1.80	7.3687	24.28	1.89	5.48
	10	149.2	7.73	6.9085	0.53	6.6591	23.83	1.80	4.86
	40	130.0	~ 0	5.7089	0.00	6.1406	-	-	-
	150	100.2	~ 0	4.9770	0.00	4.9163	-	-	-

Since the sample prepared in this study is kept at room temperature after cooling with nitrogen gas to room temperature, such a “cold crystallization” peak certainly does not appear in this melting study. In a word, the cold crystallization (in amorphous phase) and apparent spherulitic structure developing are not involved in the melting process of PA66.

These phenomenon are not unexpected in the light of result of constant lamellar thickness of single crystal at a wide range of annealing temperature (Magill et al 1981, Starkweather et al 1963). Nevertheless, lamella thickening could occur at higher temperature, probably above 250 °C, as observed in these annealing studies.

4.5.1. PA 66/6T and PA66/6I copolymers

The melting behavior of the PA66 homopolymer and PA 66/6T copolymers formed at high supercoolings are shown in Figure 4.30 (PA66), Figure 4.31(PA6T03), Figure 4.32 (PA6T06), Figure 4.33 (PA6T09), Figure 4.34 (PA6T12), Figure 4.35 (PA6I12) and Figure 4.36 (PA6I16).

First, one common feature among all these curves is the apparent single peak with a constant peak temperature at different forming supercoolings. Though the single peak is not symmetric, which generally have a long edge at low temperature side and sharp edge at high temperature side, which might imply a convolution of several melting peaks.

Secondly, the constant temperature has different dependence of comonomer content dependence for PA66/6T copolymers and PA66/6I. For PA66/6T copolymers,

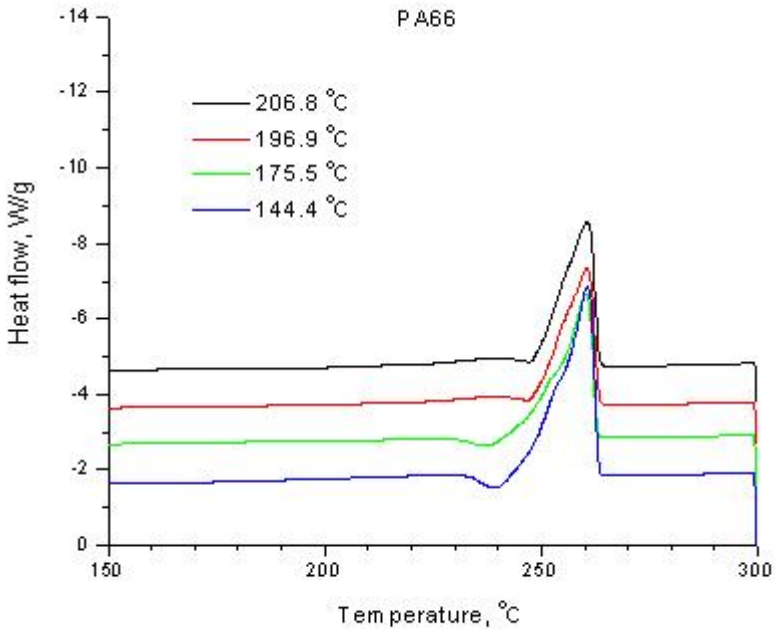

Figure 4.30 Melting curves of PA 66 crystals formed at high supercoolings

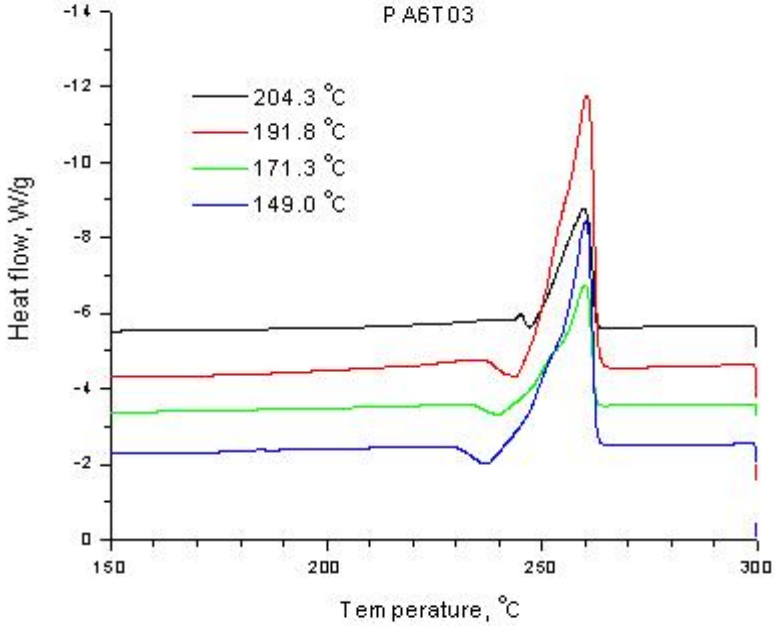

Figure 4.31 Melting curves of 3 wt% PA 66/6T crystals formed at high supercoolings.

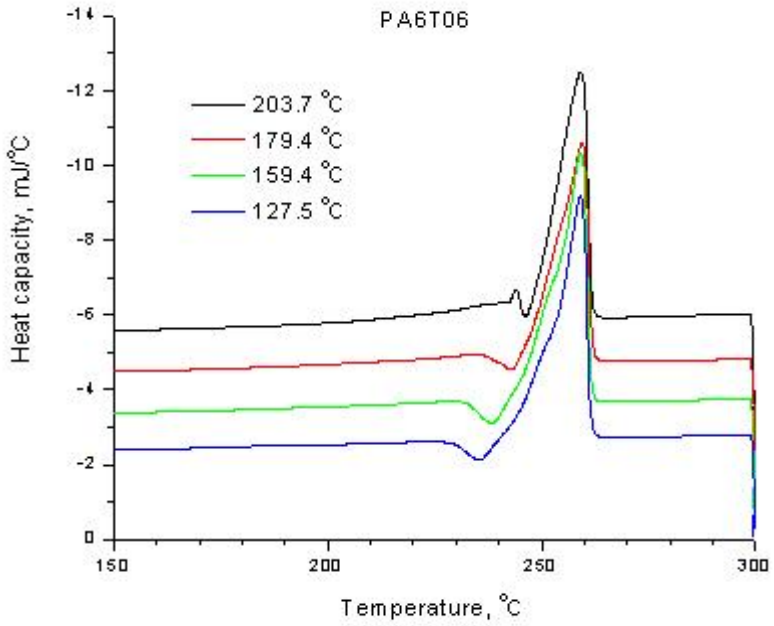

Figure 4.32 Melting curves of 6 wt% PA 66/6T crystals formed at high supercoolings

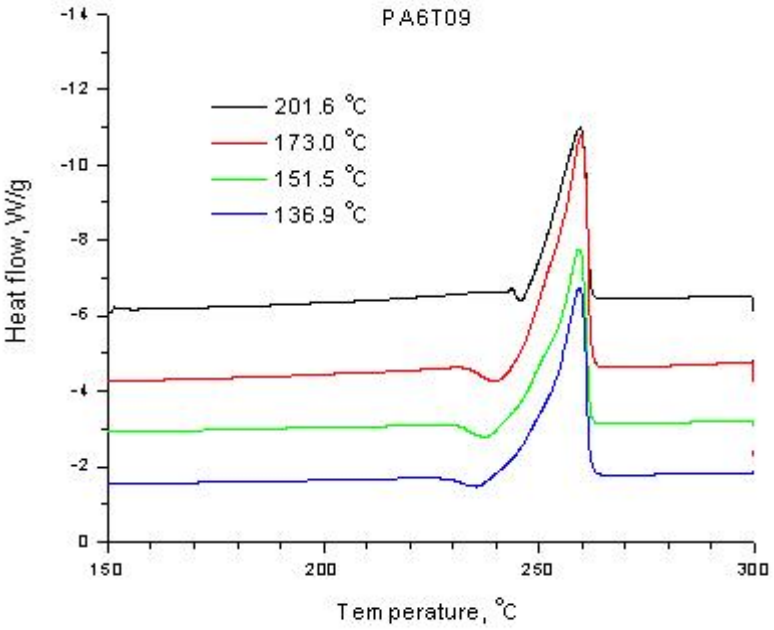

Figure 4.33 Melting curves of 9 wt% PA 66/6T crystals formed at high supercoolings

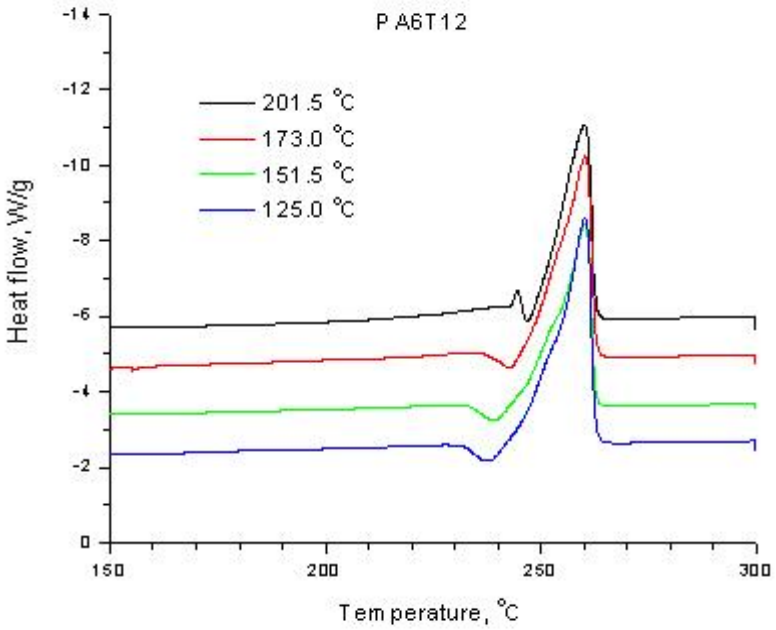

Figure 4.34 Melting curves of 12 wt% PA 66/6T crystals formed at high supercoolings

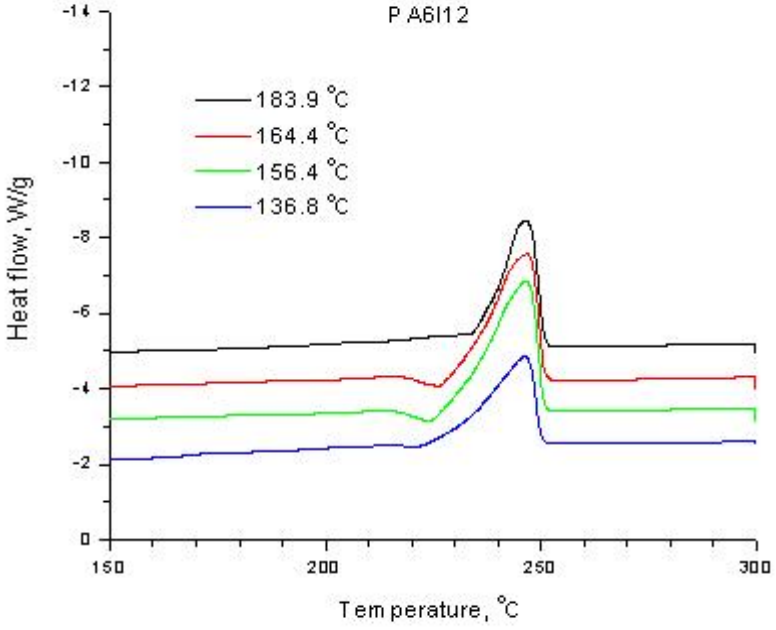

Figure 4.35 Melting curves of 12 wt% PA 66/6I crystals formed at high supercoolings

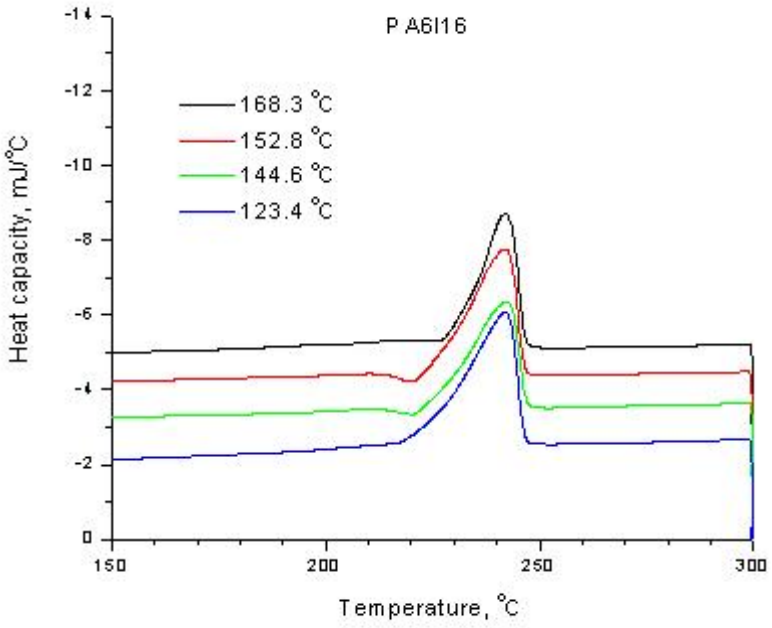

Figure 4.36 Melting curves of 16 wt% PA 66/6I crystals formed at high supercoolings

the constant peak temperatures and peak shapes for all of them are the same as PA 66 homopolymer (262 °C) independent of increasing comonomer content. This could be the result of isomorphous crystallization of 6T and 66 (Schreiber 1998).

For PA66/6I copolymers, the constant peak temperature decreases with increasing content of 6I component with a peak value of 246°C for PA6I12 and 242°C for PA6I16. This is consistent with the tendency of Flory equation (Flory 1949) that predicts the depression of melting temperature of copolymer with comonomer excluded from the crystal.

With increase of supercooling, a shoulder gradually increases at the low temperature side of the single peak. An endothermic peak also shows up just after the beginning of the melting, which might corresponding to the perfection of crystal during the heating process.

4.5.2. PA 66/6 copolymers

The melting curves of the PA66/6 copolymers formed at high supercoolings are shown in Figure 4.37 (PA606), Figure 4.38 (PA610), Figure 4.39 (PA616) and Figure 4.40 (PA621). The melting behavior of PA66/6 copolymers is similar to those of PA 66/6I copolymers.

First, the melting curves also show the apparent single peak with a constant peak temperature at different forming supercoolings. Though the single peak is not symmetric, that might imply a convolution of several melting peaks.

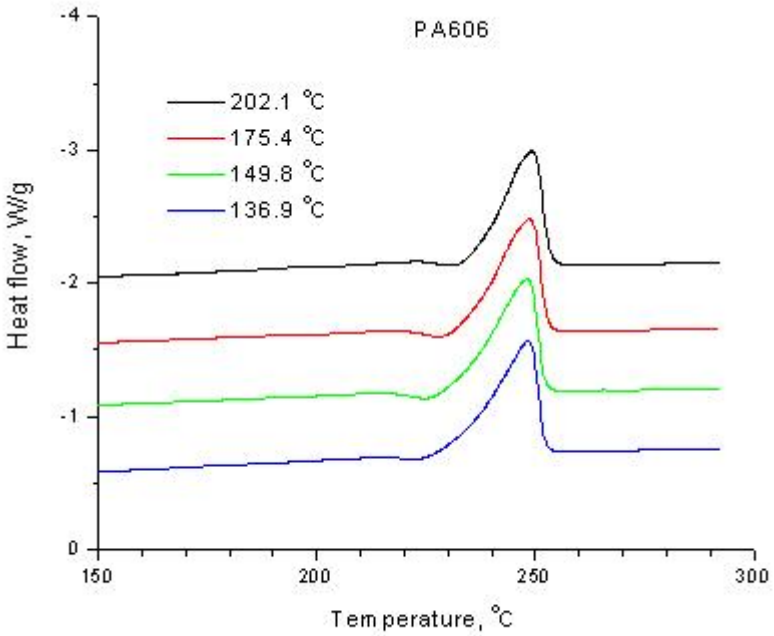

Figure 4.37 Melting curves of 6 wt% PA 66/6 crystals formed at high supercoolings

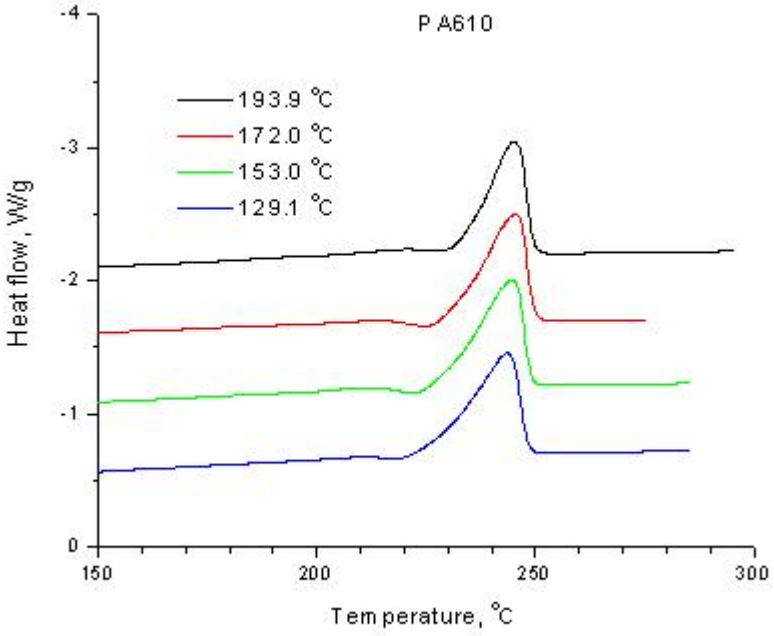

Figure 4.38 Melting curves of 10 wt% PA 66/6 crystals formed at high supercoolings

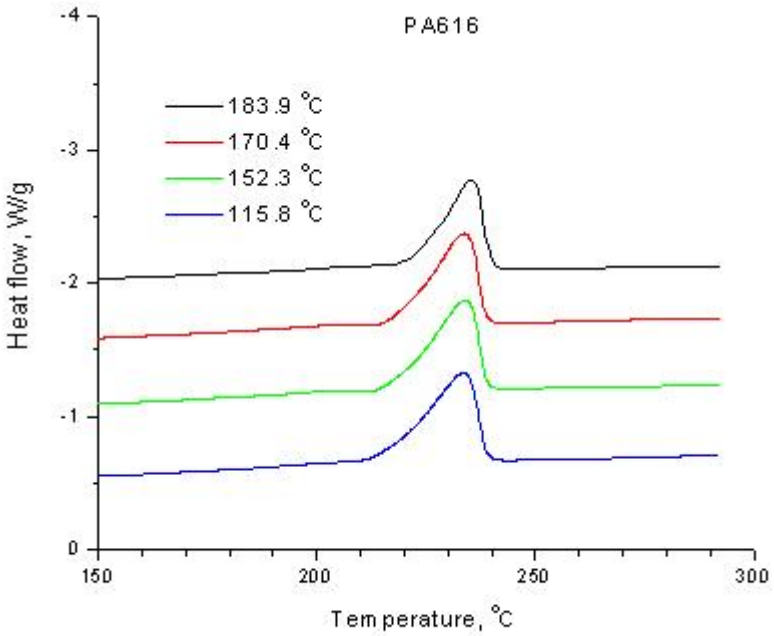

Figure 4.39 Melting curves of 16 wt% PA 66/6 crystals formed at high supercoolings

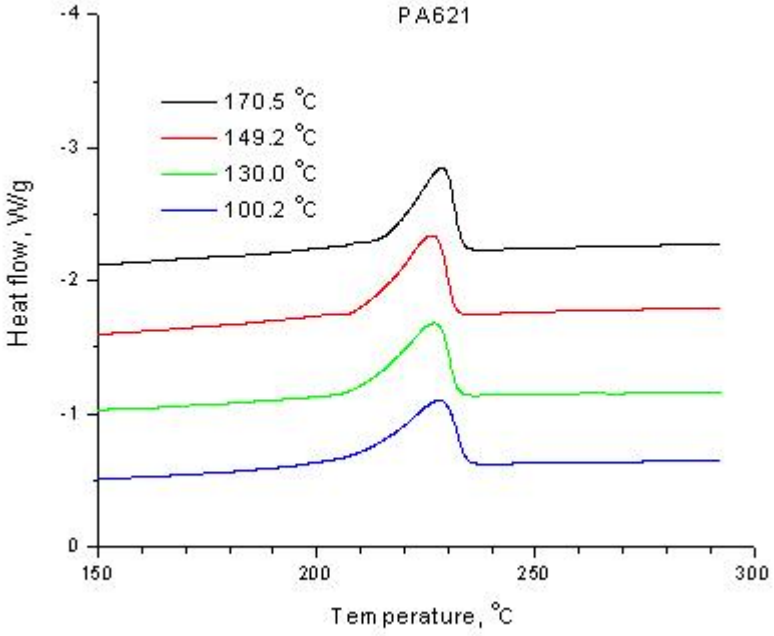

Figure 4.40 Melting curves of 6 wt% PA 66/6 crystals formed at high supercoolings

Secondly, the constant peak temperature for PA66/6 copolymers decreases with increasing content of PA6 component with a peak value of 249°C for PA606, 245°C for PA610, 234°C for PA616 and 228°C for PA621, respectively. This is also consistent with the tendency expected from Flory equation (Flory 1949) that predicts the depression of melting temperature of copolymer with comonomer excluded from the crystal.

With increase of supercooling, the general peak shape does not change significantly as in PA66/6T copolymers. And the endothermic peak does not clearly show up just after the beginning of the melting as in PA66/6T copolymers, which might be due to the less crystallization ability for the necessity of excluding PA 6 comonomer from the crystal or less driving force by disturbing the H-bonding structure.

4.5.3. Effect of heating rates

In view of the apparent single peak in all these polymers, change of heating rate was tried to distinguish the melting peaks. The heating curves of the PA66 specimens from the same cooling conditions are plotted in Figure 4.41 for heating process at a range of heating rate of 5, 10, 20, 40 °C/min, respectively.

It is clearly shown that basically still single peak appears at increasing heating rate, though the peak shape tends to more symmetric and move to lower temperature slightly. In addition, the endothermic peak does not show up at high heating rate, which tends to support the existence of a recrystallization/reorganization process at the beginning of melting process. A heating rate of 10 °C/min was used since the obvious failure to separate the melting peak at higher heating rate.

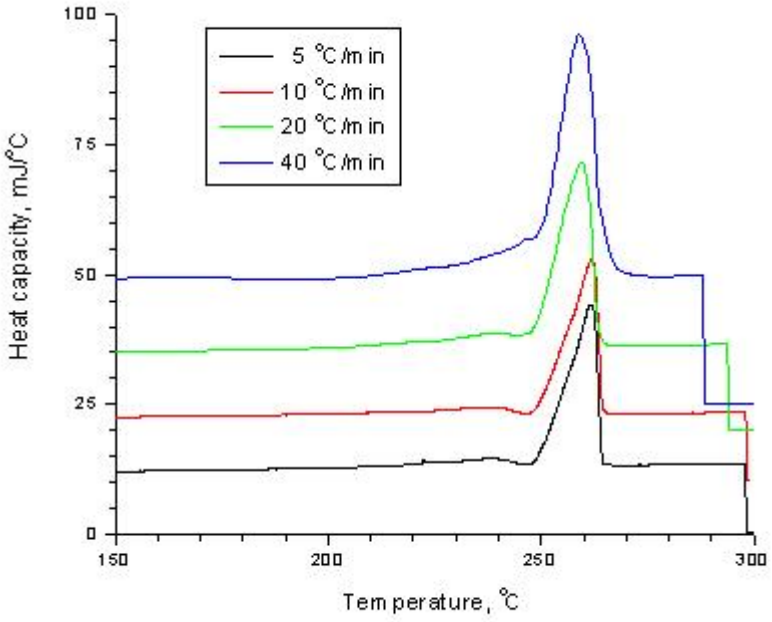

Figure 4.41 Effect of heating scanning rate for PA 66 crystals formed at high supercoolings

4.5.4. Summary of DSC results

In general, single asymmetric melting peak is observed in the melting process of crystals of PA66 homopolymer and copolymers formed at high supercoolings. The melting peak value is kept at constant for each polymer in spite of increasing supercoolings.

The constant melting peak of PA66/6T copolymers are of the same value as that of PA66 homopolymer, independent of the comonomer content change that might be the result of the isomorphism.

However, the temperature value of the constant melting peak tends to decrease with the increasing content of the comonomer in PA66/6I and PA66/6 copolymer, which is consistent with the melting temperature depression as predicted by the Flory equation for the comonomer exclusion model.

Crystal perfection is present during the melting process of the PA66 and copolymers, while it is not significant in the PA66/6 and PA66/6I copolymer comparing to PA66/6T copolymers.

Table 4.3 summarizes the specific value for the melting temperatures, heat of fusion as well as the crystallinity estimated. For PA66/6T copolymer the ΔH_f^o values of PA66 is used assuming fully inclusion model. ΔH_f^o of the copolymer for the PA66/6 copolymers is calculated with a linear exclusion model. ΔH_f^o of PA66 and PA6 are taken as 255.41 J/g and 229.78J/g, respectively (Xenopoulos & Wunderlich 1990).

Table 4.3 Summary of DSC results of PA66 and copolymers.

Sample	Cryst. Condition	Tc °C	Tm(Peak) °C	ΔH J/g	Xc %
PA66	5 C/min	206.8	262.46	66.33	25.97
	10 C/min	206.8	262.78	65.39	25.60
	20 C/min	206.8	260.88	66.06	25.86
	40 C/min	206.8	261.44	63.10	24.71
PA 66	0	206.8	260.74	69.55	27.23
	10	196.9	260.65	70.86	27.74
	40	175.5	260.45	67.22	26.32
	150	144.4	260.89	66.10	25.88
PA6T03	0	204.3	259.57	72.50	28.39
	10	191.8	260.47	68.37	26.77
	40	171.3	260.01	67.89	26.58
	150	149.0	260.17	66.07	25.87
PA6T06	0	203.7	259.49	70.88	27.75
	10	179.4	259.84	67.80	26.55
	40	159.4	259.39	65.55	25.66
	150	127.5	259.36	64.17	25.12
PA6T12	0	201.5	260.01	64.34	25.19
	10	173.0	260.21	60.33	23.62
	40	151.5	260.08	58.94	23.08
	150	125.0	260.12	59.76	23.40
PA6I12	0	183.9	246.43	51.16	20.03
	5	164.4	246.82	52.08	20.39
	10	156.4	246.53	52.19	20.43
	40	136.8	246.27	57.12	22.36
PA606	0	202.1	249.16	54.78	21.58
	10	175.4	248.75	54.52	21.47
	40	149.8	248.16	56.88	22.41
	150	136.9	248.35	59.76	23.54
PA610	0	193.9	245.17	56.49	22.34
	10	172.0	245.43	53.21	21.04
	40	153.0	244.81	56.39	22.30
	150	129.1	243.61	58.16	23.00
PA616	0	183.9	235.37	47.31	18.82
	10	170.4	233.78	49.06	19.52
	40	152.3	234.07	50.73	20.18
	150	115.8	233.58	55.92	22.25
PA621	0	170.5	228.61	50.87	20.34
	10	149.2	226.34	51.03	20.40
	40	130.0	226.86	49.44	19.77
	150	100.2	228.06	50.77	20.30

4.6. Dynamic mechanical behavior studied with DMA

4.6.1. Dynamic mechanical behavior of polyethylene copolymers

4.6.1.1. Effect of branching content

The dynamic mechanical results of linear polyethylene and copolymers show that the storage modulus decreases with the increasing branch content see Figure 4.42 and Figure 4.43. The beginning of significant loss moves to lower temperature while the percent of the loss also increases with the branch content.

The loss factor curves show continuous changing in α and β relaxations with increasing supercooling. On the one side, the β relaxation peak decrease in intensity from the most significant peak in L53 to a weak shoulder in L11, then to a barely detectable tail in L04 and finally disappeared in linear polyethylene with decreasing branch content, and the β relaxation temperature also moves to slightly higher temperature, Figure 4.44, as reported (Clas et al 1987).

On the other side, the α- relaxations decrease in intensity and move to lower temperature with increasing branch content. But the behavior of α relaxation is more complicated due to coexistence of the two different mechanisms α_1 and α_2. α_2 seems to move from very close to melting peak in linear polyethylene to much lower in L24, while the relative intensity of α1 (to α2) decrease with the increasing branch content so that α2 is apparent in L11 and L24. The assignment of the α_1, α_2 and β will be discussed later with results of different frequency (activation energy) and those of different sample crystallization temperatures.

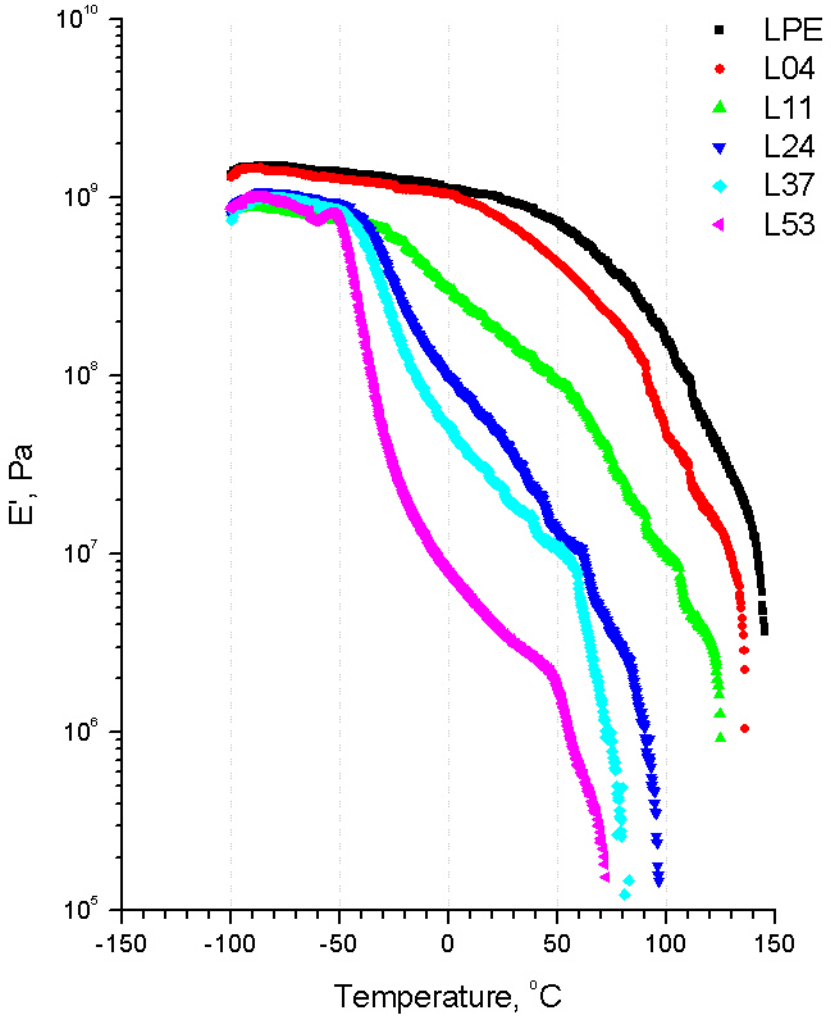

Figure 4.42 Dynamic mechanical behavior of polyethylene copolymers at 1Hz: Storage modulus (E')

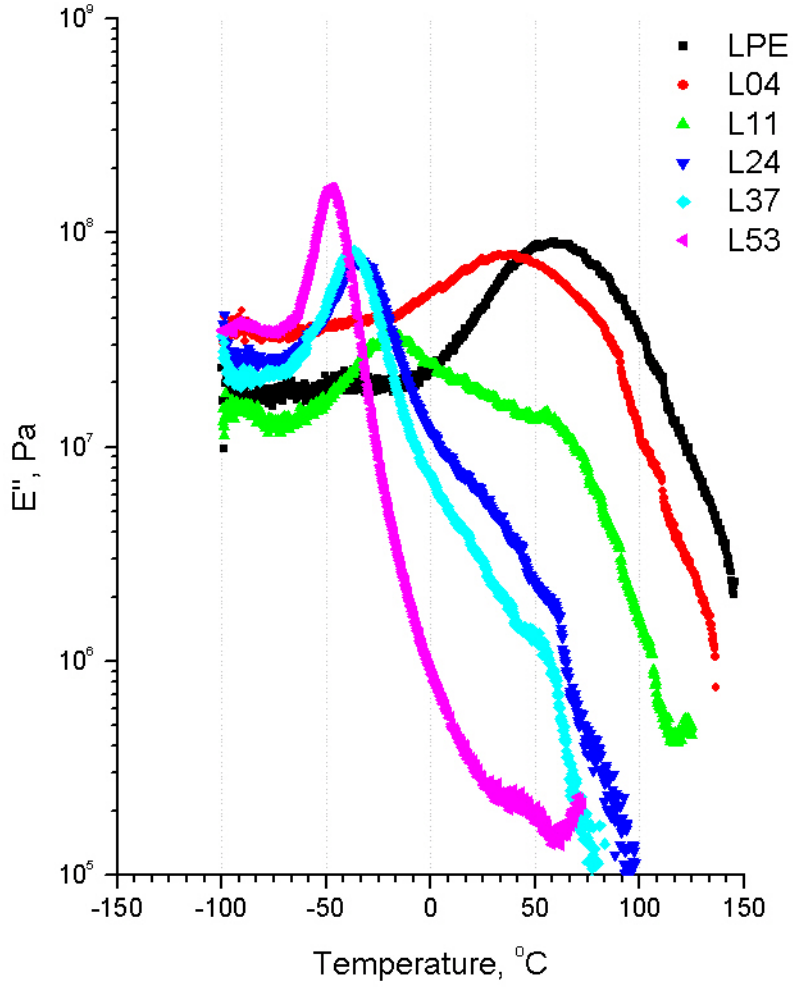

Figure 4.43 Dynamic mechanical behavior of polyethylene copolymers at 1Hz: Loss modulus (E')

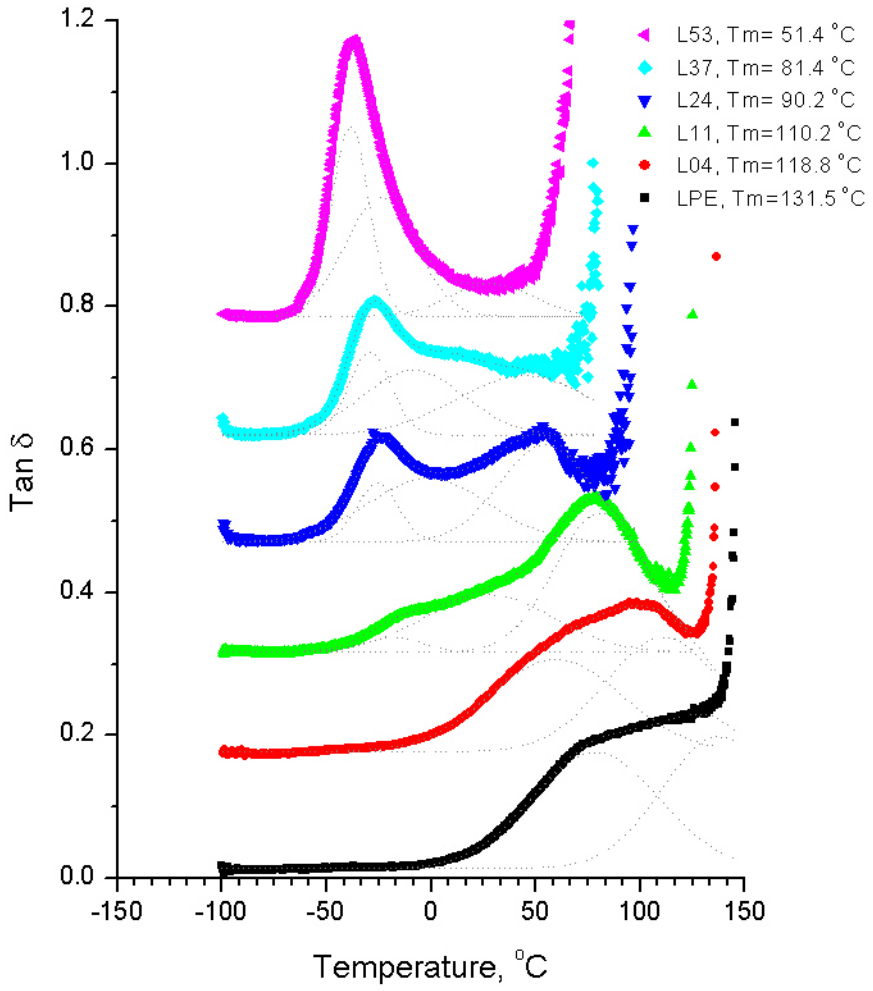

Figure 4.44 Dynamic mechanical behavior of polyethylene copolymers at 1Hz: Loss factor (shifted for clarity)

4.6.1.2. Dynamic mechanical relaxation of polyethylenes prepared at different cooling rates.

After studying the effect of branch content on the mechanical relaxation, we get the general picture of the relaxation behavior in the polyethylene copolymers. To further explore the effect of the structure and morphology on the dynamic mechanical properties of polyethylene, we need to understand the relaxation behavior of the same materials with different spherulites morphology, degree of crystallinity, lamellar thickness.

It was first reported that the α relaxation temperature of quenched samples occur at 20 ^{o}C lower than that of slowly cooled samples (Flocke 1962). Rapid cooling method was proved to be very effective in tailoring the polymer morphology (Guan & Phillips 2003) in terms of the spherulite size, crystallinity, and lamellar thickness. The loss factor curves of the linear polyethylene and copolymers prepared at different cooling rates are presented in Figure 4.45. For linear polyethylene, the results are consistent with reports on the relaxation behavior of quenched samples, while we also got access to the intermediate quenching stages thanks to the controlled quench of rapid cool method. For the air cooled LPE, the loss factor curve shows a typical two-stage increase, which is generally attributed to the overlapping of α_1 peak and α_2 peak.

With increasing cooling rates, the rising edge moves slightly to the lower temperature and also turns steeper, which could be the result of the lower α_1 relaxation temperature and stronger intensity. With increasing cooling rate, the second stage change from increase to level off, even decrease at higher cooling rates and clearly show two peaks, which could be due to the lower α_2 relaxation temperatures and lower intensity.

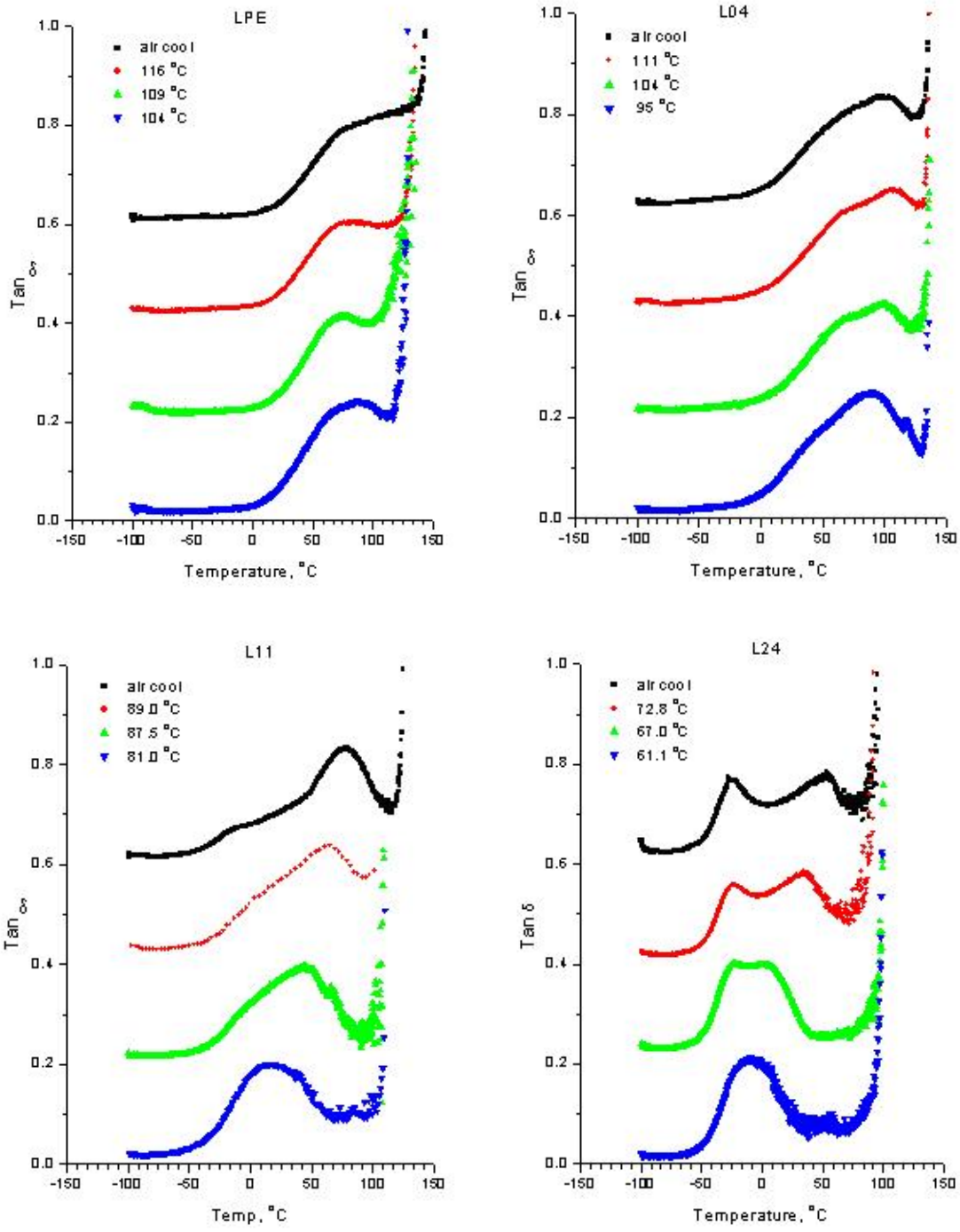

Figure 4.45 The loss factors of Polyethylenes prepared at different supercoolings.

For L04 samples, two relaxation peaks are always apparent from loss factor curve due to the small lamellar thickness. α_1 and α_2 relaxations show similar tendency with increasing cooling rate as LPE. A slightly increasing loss factor can be observed between –50 and 0 ^{o}C which may be sign of very weak β relaxations.

L11 and L24 show striking change in relaxation peaks, which are consistent with the significant change of crystal morphologies because of the increasing cooling rate. For air cooled L11 sample, a small peak is clearly visible between –50 and 0 ^{o}C, which has been assigned as β relaxations, the highest relaxation peak (α_2) is also clearly as the strongest peak while the originally strongest peak of α_1 are shadowed by the convolution of β and α_2 peaks.

With increasing cooling rate, α_2 relaxation moves to lower temperature and shows weaker peak intensity. The rising edge of the loss factor curve turns steeper and steeper, which is the sign of stronger α_1 relaxation as shown in LPE and L04 (maybe also result of the stronger β relaxation).

Air-cooled sample of L24 show much stronger β relaxations and weaker α_2 relaxations compare to L11, α_1 relaxation is almost invisible, but its existence can be inferred by deconvoluting the sharp β and α_2 relaxations.

It should be noticed that the β relaxation temperature does not change significantly with increasing cooling rates, while α relaxation temperature apparently decreases with supercooling.

4.6.2. Dynamic mechanical relaxation behavior of PA66 copolymers

Similar strategies were performed on the series of PA 66 copolymers in order to investigate the effect of crystal structures on relaxation behavior. Since it was well known that water (H_2O) can significantly affect the relaxation behavior of PA66 by forming H-bonding with amide group (Starkweather 1995), all of the samples were vacuum dried at 90 °C overnight before the DMA experiment to reduce the effect of moisture. Trace amount of water may still affect the DMA measurements in this study during the handling of samples in the atmosphere as well as the system cooling process.

4.6.2.1. Effect of comonomer type on mechanical relaxation behavior

The dynamic mechanical results for PA66 and copolymers show that the storage modulus decreases with increasing comonomer content (see Figure 4.46). The modulus of all of these polymers except PA610 does not distinguish from each other within the experiment error. A small transition is observed around –60 °C, which should be the β relaxation of PA66. The beginning of significant loss, corresponding to the α relaxation (usually related to glass transition), is at the same temperature (around 50 °C in E′ plot) except PA610, whose transition begins at around 20 °C.

It appears that the incorporation of aromatic 6T (homopolymer Tg = 125 °C) and 6I (homopolymer Tg = 118 °C) comonomer does not significantly change the glass transition temperature of PA66 copolymers at the low content (up to 12 wt%), even a higher glass transition temperature is expected from the higher Tg of aromatic homopolymer provided the copolymer is miscible with PA66.

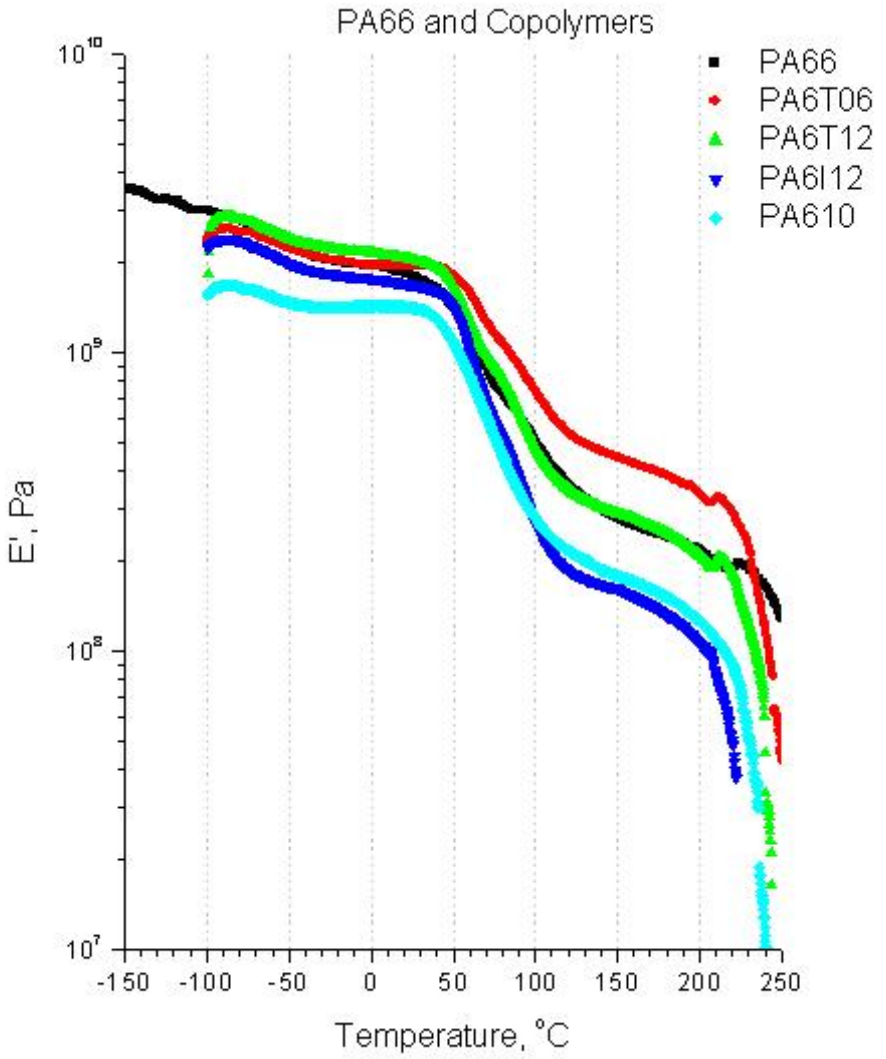

Figure 4.46 Dynamic mechanical behavior of PA 66 copolymers at 1Hz: Storage modulus (E')

Whereas the PA610 shows significantly lower glass transition temperature, this is reasonable considering the lower glass transition temperature of PA6 (Tg = 48°C) and also the relatively higher molar concentration in PA610.

After the glass transition, PA6T06 shows higher residual storage modulus than PA66 homopolymer, but PA610 show lower residual storage modulus. This might be correlated to the higher crystallinity in PA6T06 due to nucleation effect and lower crystallinity in PA610 probably due to the interruption of the H-bonding structure.

The α and β relaxation are more clearly shown in curves of loss modulus (E") and loss factor (Tanδ) of PA66 and copolymers as shown in Figure 4.47 and Figure 4.48. A small β relaxation clearly exists at –60 °C for each copolymer as shown in the E' plot.

A peak shown around 0°C only in PA66, which should be attributed to experiment error since no significant transition observed in the E' plot and it is only shown in this samples. A sharp α relaxation temperature is observed around 80°C for PA66. PA6T06, PAT12, PA6I 12 has slightly higher relaxation temperature, whereas PA610 has a lower α relaxation temperature around 75°C.

4.6.2.2. Effect of supercoolings on mechanical relaxation of PA 66 copolymers

The spherulitic morphology of PA66 copolymers was shown to change dramatically with the supercooling in a manner similar to that observed in polyethylene copolymers.

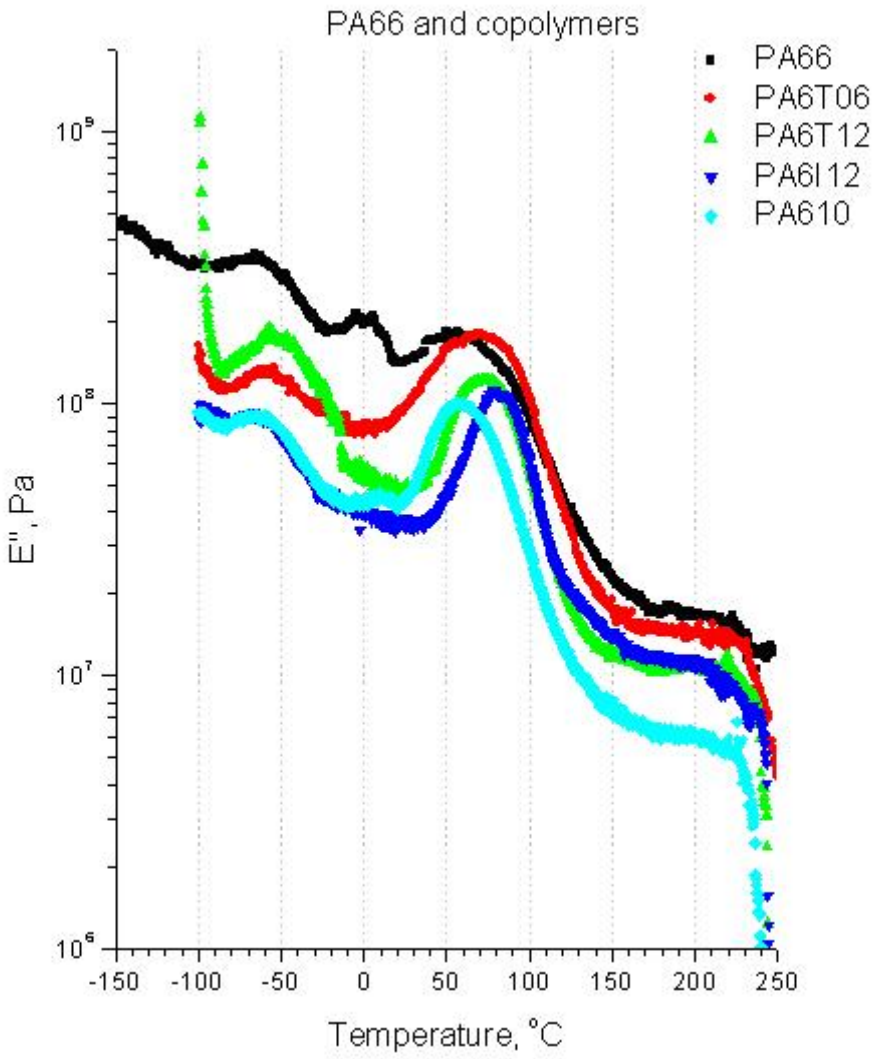

Figure 4.47 Dynamic mechanical behavior of PA 66 copolymers at 1Hz: Storage modulus (E")

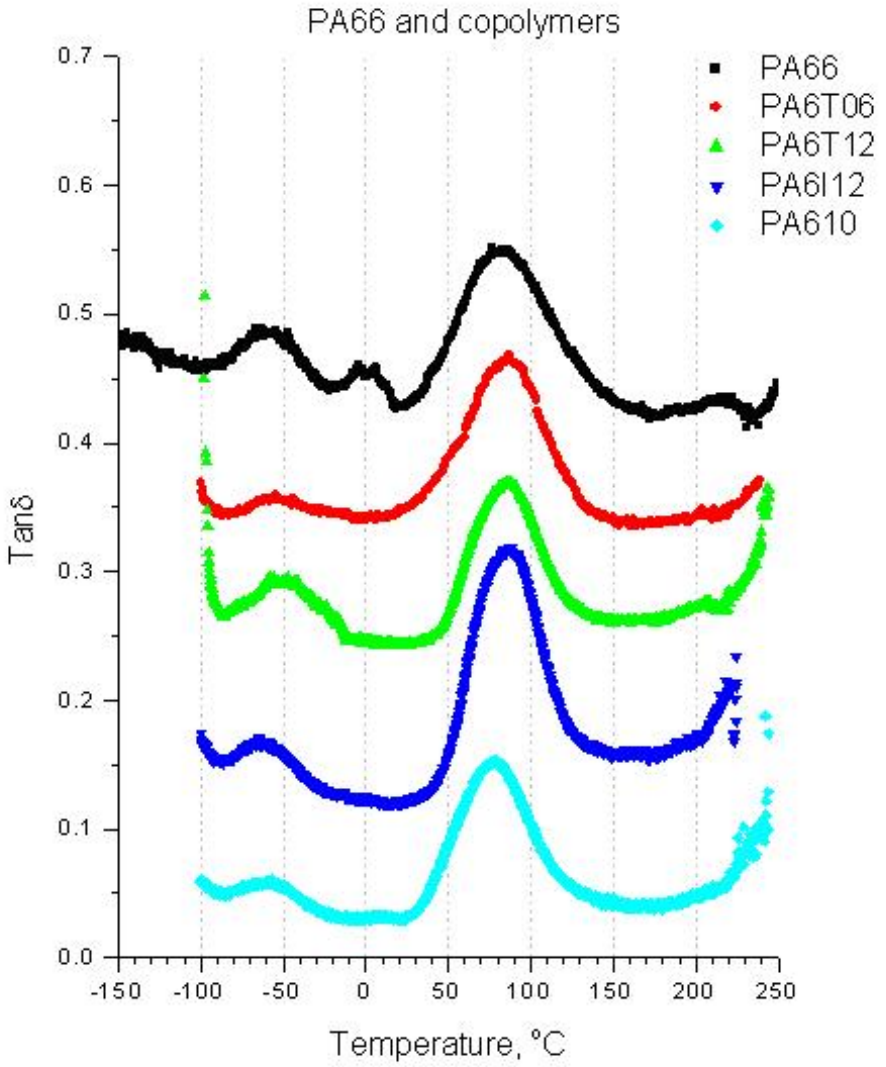

Figure 4.48 Dynamic mechanical behavior of PA 66 copolymers at 1Hz: Loss factor (Tanδ, shifted for clarity)

It was expected that the diverse morphology would have some effects on the dynamic relaxation behavior of PA66 copolymer. Unfortunately, the significant change of relaxation behavior was not observed in the PA66 and copolymers.

The relaxation behavior was shown in Figure 4.49 for PA66, PA6T12, PAI12 and PA610, respectively. It is clear that the α relaxation did not show as significant change as in polyethylene copolymers. Generally, the α relaxation shows up as single peak and the relaxation peak value move to the lower value with increasing supercooling.

Another feature is that the α relaxation peak also tends to sharpen with increasing supercooling. No further effort was given for the deconvolution of the α relaxation because it was deemed that not clear feature available for meaningful separation of the peak.

The specific relaxation results for PA66 and copolymers are listed in Table 4.4.

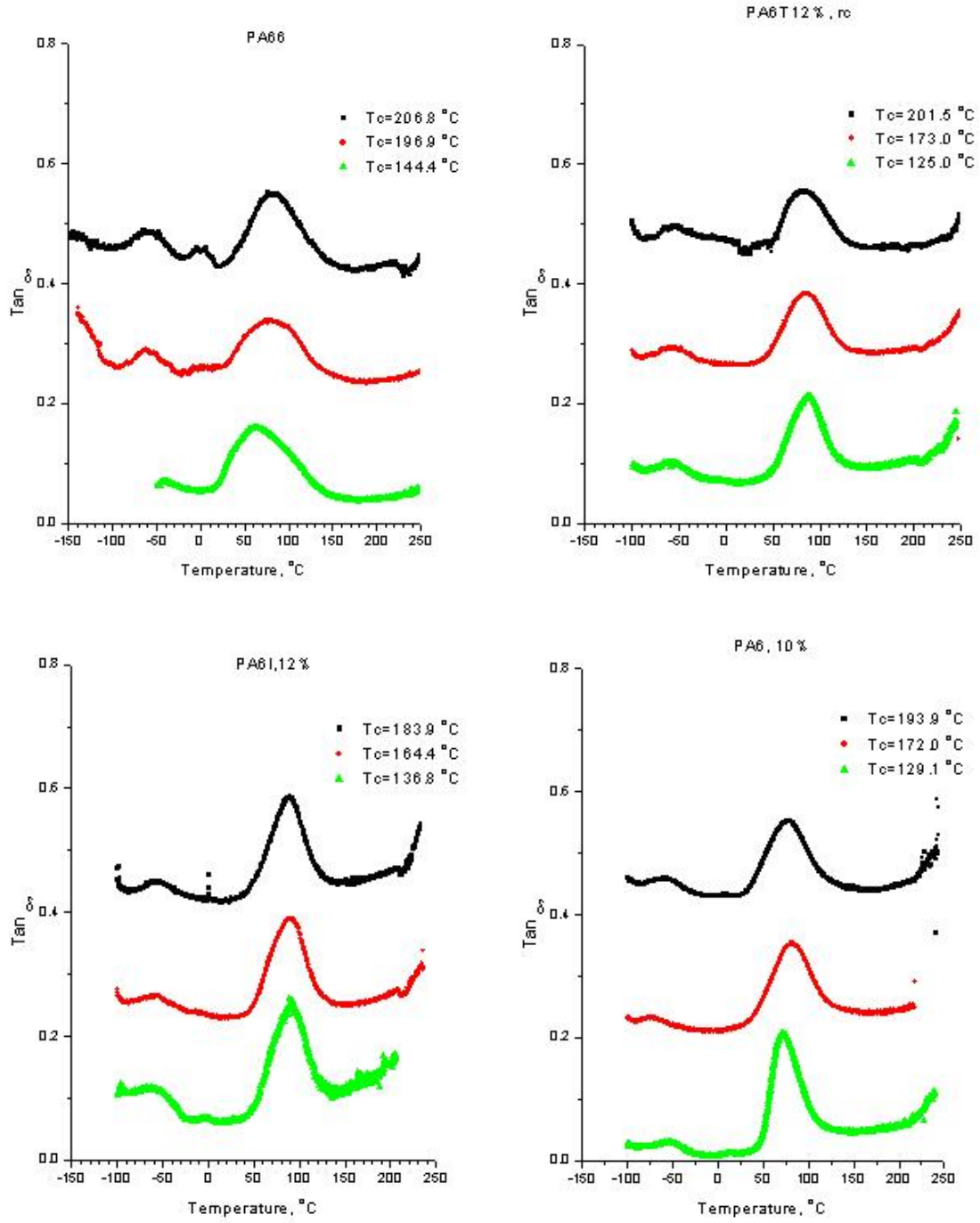

Figure 4.49 The loss factors of PA66 and copolymers prepared at different cooling rates.

Table 4.4 Relaxation temperature of PA 66 and copolymers

Sample	Cryst. condition	Tc °C	Tm °C	Xc %	T_β °C	T_α °C
PA 66	Air cool	-	260.74	27.23	-58.23	82.20
PA6T06	Air cool	-	259.49	27.75	-56.07	87.49
PA6T12	Air cool	-	260.01	25.19	-53.71	85.39
PA6I12	Air cool	-	246.63	20.03	-60.98	91.28
PA610	Air cool	-	245.17	22.34	-57.04	78.60
PA66	0	206.8	260.74	27.23	-56.88	82.20
	10	196.9	260.65	27.74	-58.23	80.77
	150	144.4	260.89	25.88	-	62.06
PA6T12	0	201.5	260.01	25.19	-54.29	83.44
	10	173.0	260.21	23.62	-56.30	84.9
	150	125.0	260.12	23.40	-58.33	86.71
PA6I12	0	183.9	246.43	20.03	-54.82	89.50
	5	164.4	246.82	20.39	-56.84	90.83
	40	136.8	246.27	22.36	-59.52	90.02
PA610	0	193.9	245.17	22.34	-57.58	77.54
	10	172.0	245.43	21.04	-70.13	81.92
	150	129.1	243.61	23.00	-72.86	72.03

CHAPTER 5. DISCUSSIONS

In this chapter, the experimental results are discussed relating to the current knowledge on the polymer crystallization kinetics, morphology, melting and relaxation.

First, the existence of temperature gradient around spherulites is proposed from the experimental observation of linear growth rate in PA66 and PET at decreasing system temperatures. Thermal diffusion analysis further proves the possibility of steady temperature gradient. Since this part addresses the basic working hypothesis of growth rate measurement at high supercooling in this study, it is necessary to be discussed prior to kinetics consideration.

Secondly, the growth rates of PA66 copolymers measured at high supercoolings, in combining with growth rate data at low supercooling, are analyzed with respect to crystallization temperature (or supercooling). The kinetic analyses are completed with both the secondary nucleation theory and rough surface theory. The transitions of growth behavior are also discussed from the standpoints other than interface mechanism.

Thirdly, the crystal structure and morphology of PA 66 copolymers are discussed in terms of spherulitic morphology, crystal structure and lamellar structure. Thereafter, the melting behavior of PA66 copolymers over wide range of supercooling is interpreted relating to chemical structure and chain folding length.

Finally, mechanical relaxation behavior PA66 copolymers, comparing to that of PE copolymers, is discussed with respect to the understanding of crystal structure and morphology. Based on the dependence of relaxation temperature on the chemical

structure and supercooling, the molecular mechanisms of α relaxation and β relaxations are discussed.

5.1. Temperature gradient around spherulitic growth front at high supercoolings

5.1.1. Linear spherulitic growth

Heat diffusion has been known to be an important element in the crystallization of metal materials for decades (Raimo et al 2001). In the field of polymeric materials, it first called attention to researchers who worked on polymer engineering during efforts of modeling the polymer cooling process (mostly non-isothermal) to explain the existing experiment results. But most considerations were still limited to the macroscopic scale, such as correlating the release and diffusion of latent heat to the bulk crystallinity development (Eder et al 1990, Sifleet et al 1973, Sombatsompop et al 1999), analyzing the heat transfer to predict residual stress in molding parts (Benard & Advani 1995, Prabhu et al 2001), and modeling the structure development in the spinning line (Schultz 1991b, Tiller & Schultz 1984).

In the microscopic scale, the effect of heat diffusion on polymer melt crystallization was first considered by Schultz (Schultz 1991a). He also considered the effect of "solute" distribution, which is significant for the polymer systems with part of the contents excluded from crystalline phases.

Accompanying the introduction of this concept to studies of polymer crystallization, experimental results revealed the important role of heat diffusion. It was observed that the pulse growth of poly (3- hydroxy butyrate) (PHB) on the lamellar scale

by AFM (Hobbs et al 1998), which is at odd with the expected constant linear growth rate based upon second nucleation model. An excellent review was written on the role of thermal conductivity and its influence on the crystallization rate of spherulites (Raimo et al 2001).

Figure 5.1 shows the typical relationship of temperature to time during the crystallization process of PE in a rapid cooling experiment using an embedded micro-thermocouple. There is horizontal plateau on the T-t curve, which is due to the release of latent heat of fusion balancing the heat transfer to the cooling medium (Schultz 1991a). In the case of nylon 66 there was no horizontal plateau ever observed in the rapid cooling curves (see Figure 5.2). It is believed that this is due to the low crystallinity of nylon 66 and to its low crystallization rate. As was mentioned earlier, when effective nucleating agents are present in the polymer the horizontal plateau can be seen.

Instead, there was a plateau or a point of inflexion in the temperature derivative versus time curve over the time span in which an increase of light intensity occurred (see Figure 5.3). The temperature corresponding to the beginning of the temperature derivative – time curve disturbance was taken as the crystallization onset temperature. Studies of spherulitic growth rate showed that the growth rate was linear over much of the temperature drop measured by the embedded micro-thermocouple (see Figure 5.4). This observation clearly requires a constant crystallization temperature at the growth face. The measured temperature change in the film over the time period that spherulitic growth is measured is as much as 30^{o}C. Such a change in crystallization temperature would normally give rise to a change in spherulitic growth rate of an order of magnitude.

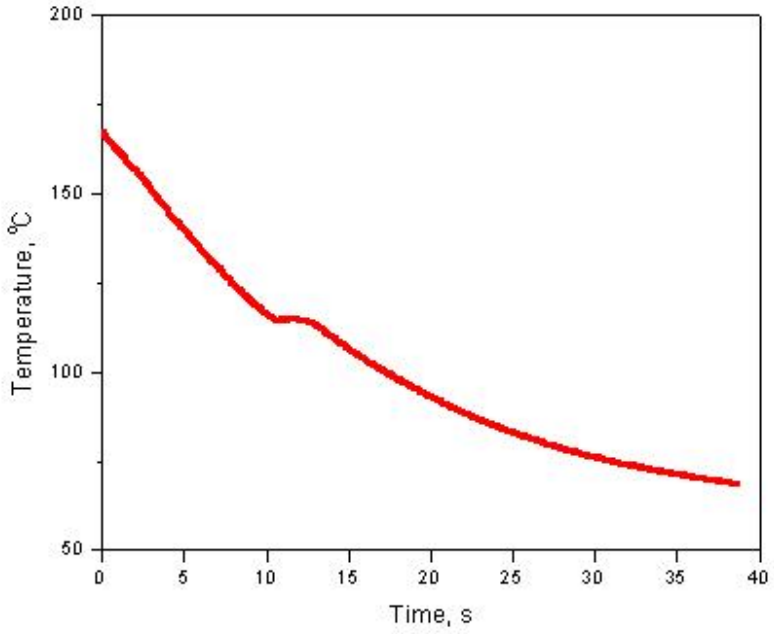

Figure 5.1 Typical cooling curve of polyethylene shows a horizontal plateau

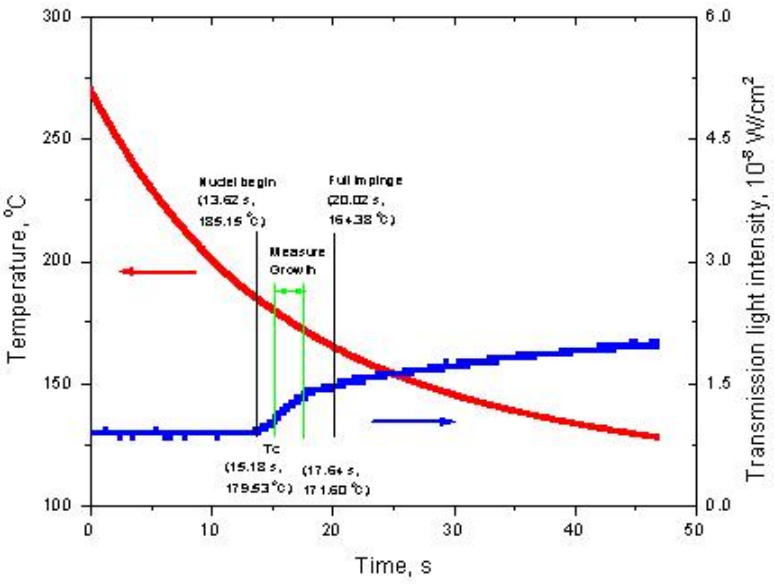

Figure 5.2 Temperature and light intensity vs. time during the rapid cooling of PA66.

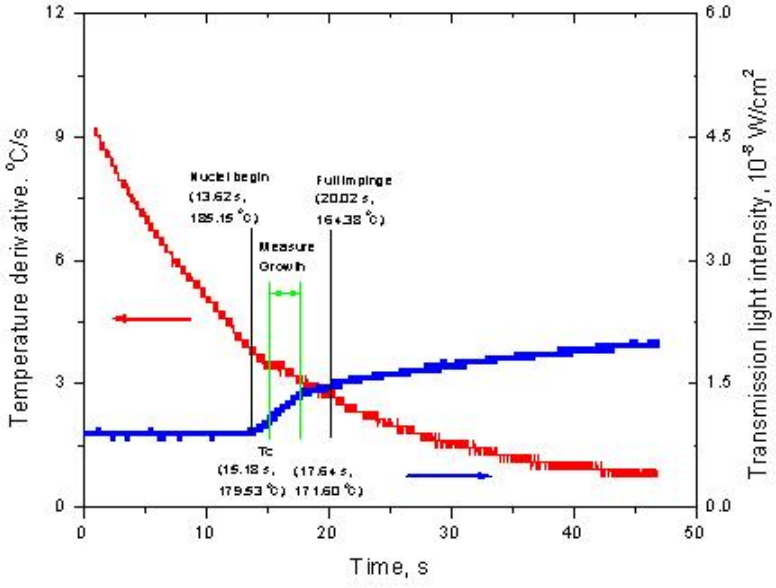

Figure 5.3 Temperature Derivative and Light Intensity vs. time during the rapid cooling of PA66

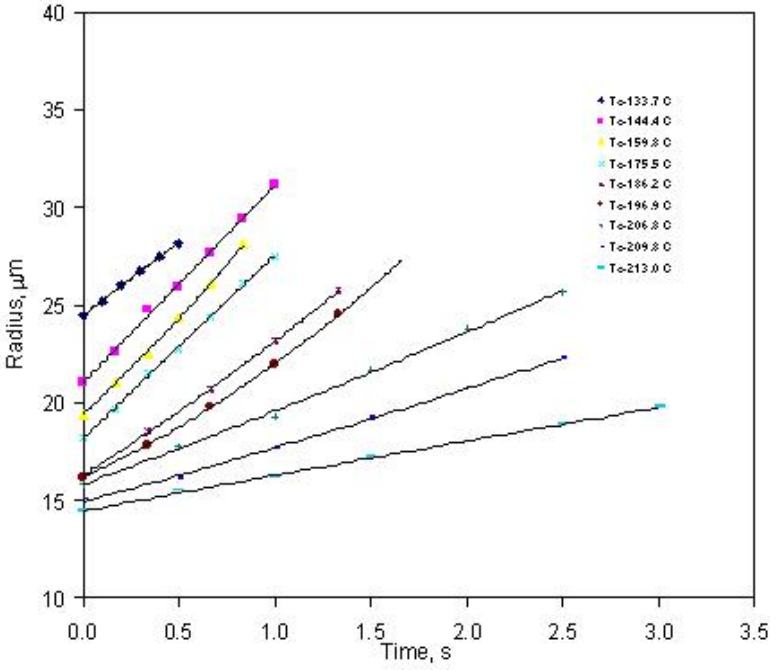

Figure 5.4 Linear relationship between radius of spherulites and crystallization time during crystallization of PA66

The light intensity kept increasing after the impingement of the spherulites, from which it is possible to infer the presence of a significant secondary crystallization process.

In order to explore this point further, first the instantaneous growth rate of a spherulite has been plotted as a function of crystallization time. In Figure 5.5 is shown the behavior of linear polyethylene. Shown is a plot of temperature measured by the embedded thermocouple as a function of time along with a plot of the point-to-point slope of the spherulite radius versus time curve, as a function of the same time range.

Clearly, for this material there is a direct correlation between measured temperature and time. When the temperature begins to drop the spherulite growth rate begins to increase. When PA66 is considered from the same point of view a somewhat different phenomenology is observed. In Figure 5.6 it can be seen that, although the temperature measured using the embedded thermocouple is decreasing at a constant rate of 5^{o}C/sec, the growth rate stays linear within the error bounds.

In order to explore the possibility of the data being generally characteristic of polymers, and not simply characteristic of a surface-roughening system, poly (ethylene terephthalate) has been studied.

The reason for this choice for material was simply that earlier bulk growth rate studies of the polymer using the rapid cooling equipment had discovered that samples containing nucleating agents showed a plateau region, but that plain samples did not. PET is a well-studied polymer and its growth rate dependence on crystallization temperature is well known.

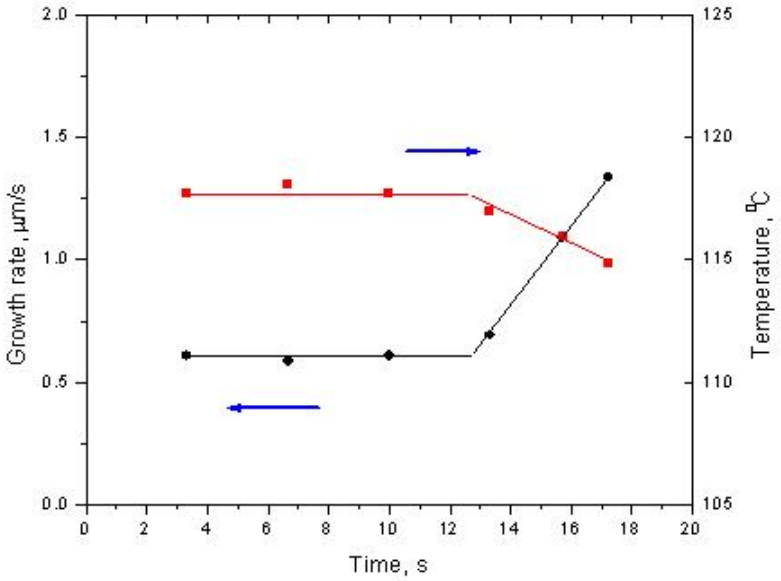

Figure 5.5 Growth rate and temperature change with time during rapid cooling of PE.

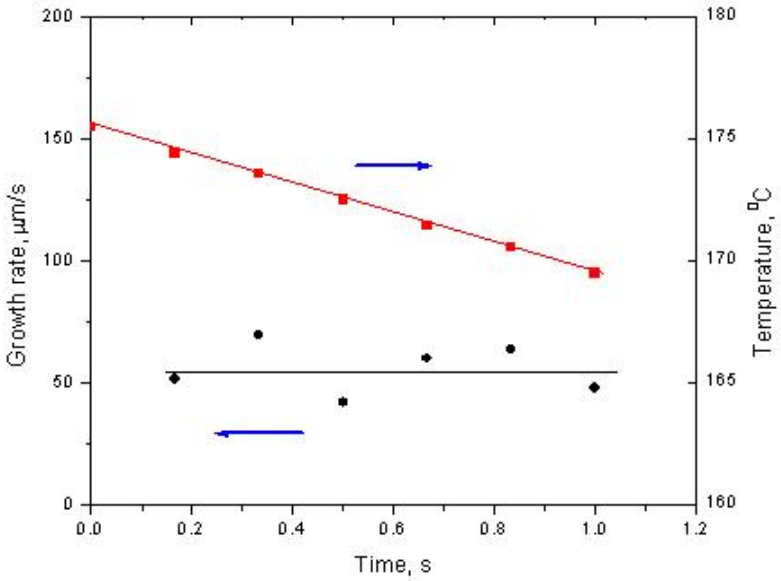

Figure 5.6 Growth rate and temperature change with time during rapid cooling of PA66.

A typical plot of temperature versus time, as measured using an embedded micro-thermocouple, during a rapid cooling experiment on PET is shown in Figure 5.7. Characteristic data of spherulite size versus crystallization time are shown in Figure 5.8, where it can be seen that approximately linear growth is observed, similar to what was seen for the nylon 66. The temperatures shown in the legend of Figure 5.8 are, as for the nylon 66, are the observed points of inflexion in the temperature – time curves. In some cases the growth curves are linear with time and in other cases the spherulite growth rate decreases slowly with time, presumably because the slower growth rate of the PET versus that of nylon 66 does not release enough thermal energy per unit time to maintain the isothermal state at the growth face.

An example of this behavior is shown in Figure 5.9 where although the temperature, as measured by the embedded micro-thermocouple, decreases in a linear fashion, the growth rate of the spherulite, although linear at first, begins to decrease slowly with time. The rate of decrease of growth rate is not of the order of magnitude that would be expected for a drop of 10 ^{o}C in growth temperature, based on the known behavior of PET. When the growth rates are plotted against the inflexion temperature, it is seen that the temperatures correspond to the diffusion-controlled side of the characteristic bell-shaped curve of PET (Figure 5.10). From the results presented above it is apparent that both nylon 66 and PET exhibit linear growth rates during rapid cooling and that the film temperature, as represented by an embedded micro-thermocouple, does not represent the actual crystallization temperature at the crystal growth face.

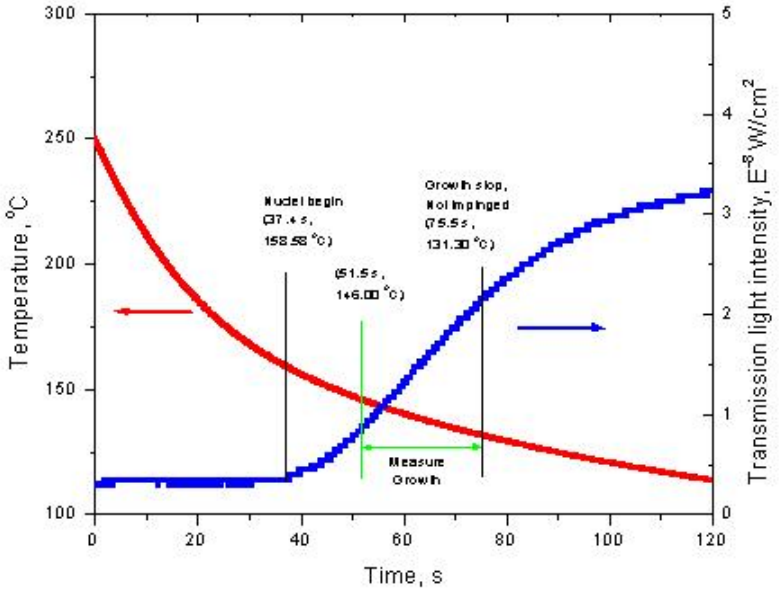

Figure 5.7 Plot of temperature vs. Time during the rapid cooling of PET

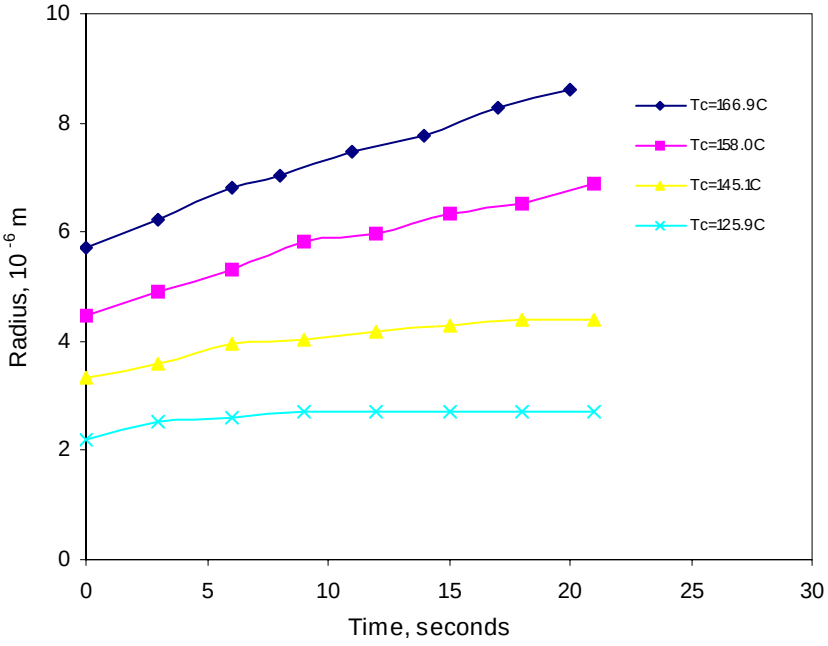

Figure 5.8 Spherulite radii vs. crystallization time during the rapid cooling of PET

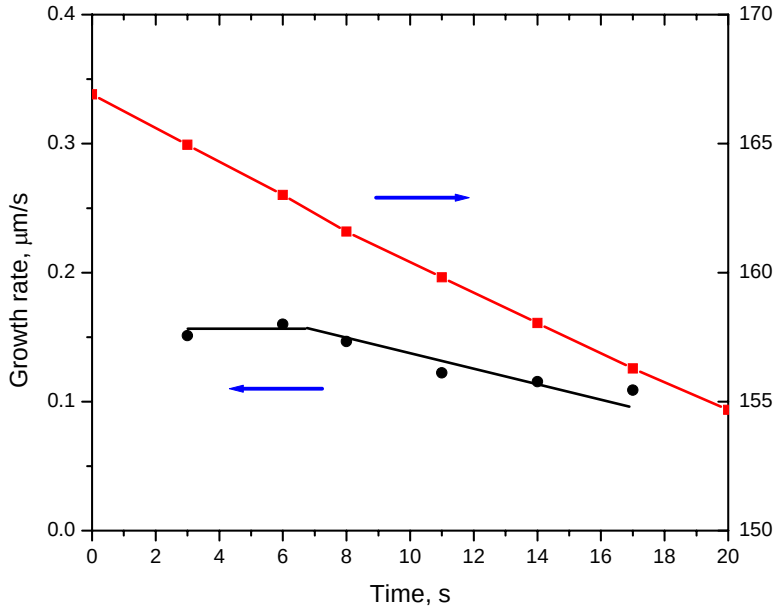

Figure 5.9 Growth rate and temperature change with time during rapid cooling of PET.

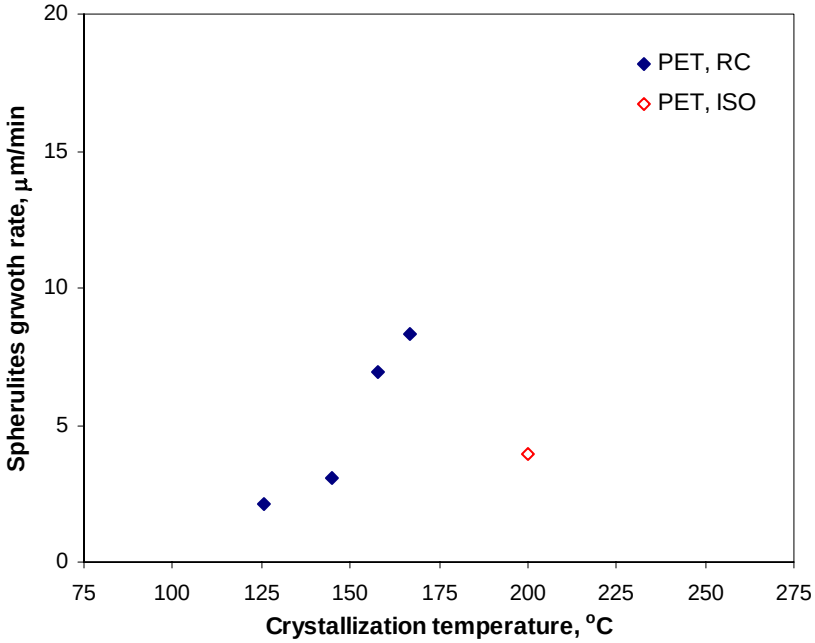

Figure 5.10 PET growth rates determined from the slope of radius-time curves

It is also apparent that the behavior cannot be sustained indefinitely and that there is a limit to the externally applied temperature that can be balanced by the released heat of fusion. It is also clear that the phenomenon can be sustained better by a more rapidly crystallizing polymer, such as PA 66, than the more slowly crystallizing PET.

The results of this study have profound implications for our understanding of polymer crystallization. If the temperature at the growth face is different for a relatively slow crystallization polymer such as nylon 66, then it must be significantly different for fast crystallization polymers, such as linear polyethylene and isotactic polypropylene.

In the case of these two polymers, the heat of fusion released during crystallization is large enough to maintain a constant temperature in the entire film, as measured by the embedded micro-thermocouple. Hence, the temperature at the growth face must be significantly higher than the measured value.

This temperature profile will have a form similar to that represented schematically in Figure 5.11. Such a profile means that the crystal will be annealed at temperatures significantly higher than the crystallization temperature for a considerable amount of time after its formation.

The consequence of this will be a rapid thickening and perfection process, which has been long recognized as occurring immediately after crystallization, but for which there has been no acceptable mechanism postulated, due to the assumption of an isothermal crystallization process.

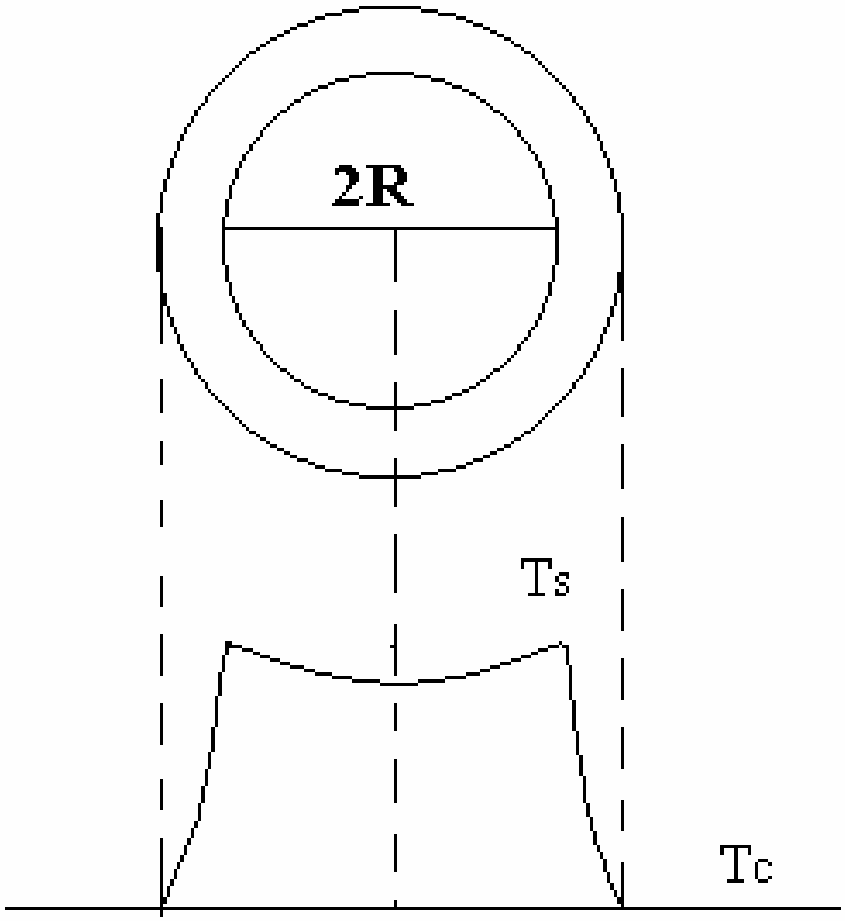

Figure 5.11 Schematic of temperature profile around growing polymer spherulite

The presence of a temperature gradient, similar to that shown in Figure 5.11, but not recognized as such, could also give rise to many false interpretations of experimental data, such as the presence of a meso-phase or an adsorbed phase on the crystal surface. A temperature greater than that of the crystallization temperature, in the crystal behind the growth front, could also lead to unnecessary assumptions about the internal mobility of the chains in the crystal.

These are just a few of the potential consequences of this finding and remain to be explored in detail. Indeed, it will be necessary to re-evaluate all our current beliefs about the crystallization process and the mechanisms of crystallization.

It should also be apparent that at conditions of growth at low supercooling the temperature gradient at the crystal-amorphous interface would be quite low and might be consistent with an isothermal assumption. However, it should be self-evident that a considerable amount of modeling of the temperature distribution and evolution during the crystallization process is necessary, before any real understanding of the situation can be obtained.

In summary, linear growth rates were found during the rapid cooling of nylon 66 and PET despite no temperature plateau in the cooling curve. Further instantaneous growth rate analysis revealed that temperature gradient at the growth front of spherulites led to the linear growth. This behavior shows that crystallization is controlled by a temperature gradient at the growth face, and not by the measured temperature. The results of this study have profound implications for our understanding of polymer crystallization.

5.1.2. Thermal diffusion analysis

The melt crystallization of polymers belongs to the classical problem of heat transfer with phase change: a solid growing into supercooled liquid. Due to the symmetry of spherulites, we can simplify the problem into a one-dimensional heat transfer problem with all heat transferred from interface into melt only (Schultz 1991a). The temperature profile around a spherulite is shown in Figure 5.11.

If we assume the temperature of the spherulite remains infinitesimally below T_f (phase change temperature) and the temperature of the supercooled melt far from the spherulite is Tc, "crystallization temperature", (supercooled melt temperature actually), then all of the latent heat of fusion at the interface will transfer into melt forming a temperature gradient around the spherulites.

HEAT RELEASE: Based on the energy balance of release of latent heat and diffusion of heat, the boundary condition at the crystal-melt interface can be written as:

$$\rho \Delta H_f \frac{dR}{dt} = -k \left. \frac{\partial T}{\partial r} \right|_R \qquad (5.1)$$

Left hand side is the latent heat release rate that increases with the growth interface growth rate. Right hand side is the heat transferred away by the melt that is proportional to the heat conductivity of the melt and temperature gradient at the interface.

HEAT DIFFUSION: The heat conduction in the melt before the interface is given as Fourier's Law:

$$\rho C_p \frac{\partial T}{\partial t} = k \frac{\partial^2 T}{\partial r^2} \qquad (5.2)$$

The temperature in the melt is intrinsically transient in the fixed coordinate system while temperature distribution in melt (near the interface) tends toward a steady solution in a coordinate system moving with the interface. This coordinate as r'= r-vt, θ = T-Tc, where v = dR/dt is the steady interface velocity.

$$\frac{\partial \theta}{\partial t} = \frac{k}{\rho C_p} \frac{\partial^2 \theta}{\partial r^2} = \alpha \frac{\partial^2 \theta}{\partial r^2} \qquad (5.3)$$

can be transformed into

$$\alpha \frac{\partial^2 \theta}{\partial r'^2} + v \frac{\partial \theta}{\partial r'} = 0 \qquad (5.4)$$

which has the solution

$$\theta(r') = \theta_I \exp\left(-\frac{vr'}{\alpha}\right) \text{ or } T - Tc = (T_f - Tc)\exp\left(-\frac{vr'}{\alpha}\right) \qquad (5.5)$$

The temperature gradient is therefore expressed as:

$$\frac{d\theta(r')}{dr'} = -\theta_I \frac{v}{\alpha} \exp\left(-\frac{vr'}{\alpha}\right) \qquad (5.6)$$

at the steady state, the temperature gradient at the crystal-melt interface is.

$$\left(\left.\frac{dT}{dr}\right|_R\right)_{steady} = \left.\frac{d\theta(r')}{dr'}\right|_0 = -(T_f - T_c)\frac{v}{\alpha} = -\frac{T_f - T_c}{\alpha / v} \qquad (5.7)$$

The ratio of diffusivity to interface propagation rate was defined (Schultz 1991a) as diffusion length (δ), which determines the gradient accompanying the temperature difference between crystal and melt at steady state.

$$\delta = \frac{\alpha}{v} \qquad (5.8)$$

In this work, temperature gradient at steady state is used as the critical condition to determine the spherulites growth kinetics.

- When $\rho \Delta H_f \frac{dR}{dt} < -k\left(\left.\frac{\partial T}{\partial r}\right|_R\right)_{steday}$, When the growth rate is very low, the latent heat can be transferred from the interface in time, the spherulites growth rate are controlled by the thermodynamic kinetics;

- When $\rho \Delta H_f \frac{dR}{dt} \geq -k\left(\left.\frac{\partial T}{\partial r}\right|_R\right)_{steday}$, when the growth rate is very high, the melt can not diffuse heat fast enough, the local heat accumulation will decrease the interface propagation rate to match with the heat diffusion rate, therefore the spherulite growth rates are controlled by the steady heat diffusion rate.

If the temperature gradient is a constant, the spherulite radius growth rate will be linear.

$$R(t) = \left(\frac{k}{\rho \Delta H_f}\left.\frac{\partial T}{\partial r}\right|_R\right)t + r_o \qquad (5.9)$$

Based on the concept of diffusion length, a conclusion has been drawn (Schultz 1991a) that thermal diffusion has no bearing on spherulitic crystallization by estimating the heat diffusion length (~ 10^3 cm) from the relative magnitude of diffusivity (10^{-3} cm^2/S) and spherulite growth rate (10^{-6} cm/S). However, several factors might justify the significant effects of thermal diffusion on the crystallization kinetics in PA66. 1) Our crystallization experiments were carried out at higher supercoolings, spherulite growth rates are in the range of (200 to 900) $\times 10^{-6}$ cm/s; 2) The role of heat diffusion may be promoted due to the unique molecular arrangement scheme in the spherulites of PA66. It was found that PA66 molecules form H-bond plane along the spherulites growth direction. This structure may cause PA66 to differ from other polymers in the heat diffusion capability.

In Figure 5.12, a scheme is proposed to relate the crystal structures to the possible heat diffusion path, growth rates and final lamellar morphology in polyethylene and PA66. It was known that PE molecules fold onto the growth front (110), stack along the growth direction (b axis) to form lamella (Phillips 1994), while PA 66 molecules fold in the H-bond plane into melt along the growth direction within the positive spherulites (Lovinger 1978b).

There exist three different thermal conductivities for the lamella crystals (k_c, $k_{//}$, $k_{\perp}$), which correspond to the k values in the chain axis, along the growth direction, normal to both growth direction and chain axis. The relative magnitudes are in the order of $k_c >> k_{//} > k_{\perp}$ in the PE lamella, but in the order of $k_c >> k_{\perp} > k_{//}$ in PA66 lamella due to H-bond plane.

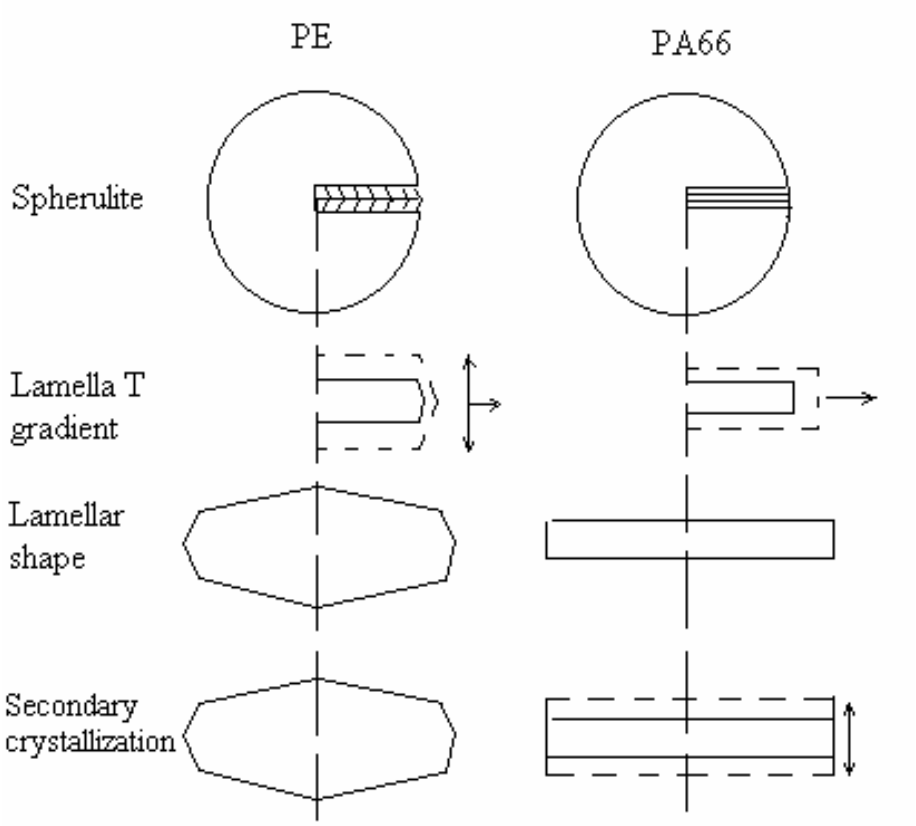

Figure 5.12 A scheme relates the crystal structures, thermal diffusion and crystal morphology.

Due to the usual lamella stack structure in spherulites, *c* axis cannot work as an efficient heat diffusion direction. It should be more efficient to diffuse the latent heat from the growth front to the pocket between lamellar stacks than diffuse along the growth direction ($k_{//} > k_{\perp}$) in PE spherulites; but more heat should be diffused to melt along the growth direction in the positive spherulites of PA66.

Obviously, the thermal diffusion in PE spherulites is more efficient than PA66 spherulites in transferring the latent heat from the growth front, because it not only has short diffusion distance by getting ride of heat locally, but also avoid the heat accumulation before the growth front, which might be major cause of thermal diffusion control of growth kinetics in PA66.

The different heat diffusion scheme is also consistent with the lamella shape and the relative higher content of secondary crystallization. The higher thermal conductivity normal to the growth direction provides the additional growth dimension in PE spherulites, which may account for the shape of growth front and the higher crystallinity. The poor thermal conductivity crosses the H-bond plane prevents the lamella growth normal to the growth direction, which may account for the low crystallinity and the strong secondary crystallization observed in the PA66.

The spherulites of PA 66 were found to increase linearly with time at higher cooling rate, which was explained by the effect of heat diffusion on kinetics. Based on the classical one dimensional heat diffusion of solid growing into supercooled liquids, temperature gradients of spherulite growth front were analyzed.

The critical condition at which spherulites growth rate change from thermodynamic kinetics to thermal diffusion kinetics was given. The significant effect of the heat diffusion on crystallization kinetics in PA66 was correlated to the H-bond planes in the positive spherulites, which make its crystallization kinetics prone to thermal diffusion controlled.

5.2. Crystallization kinetics of spherulitic growth

5.2.1. Chemical structure of comonomer on growth rates

5.2.1.1. Comonomer Inclusion (isomorphism in PA66/6T)

Due to the unique chemical structure (with amide group –CONH-) of PA66, the crystallization behavior of PA66 copolymers can be changed significantly from the PA66 homopolymer by modifying the H-bonding structure formation. However, there is an exception that 6T comonomer can co-crystallize with 66 components due to the similar repeat unit length as 66, which is the so-called crystallization isomorphism.

As shown in the results section, the melting temperatures of PA66/6T copolymers are found to be the same as PA66 and crystallization rates do not differentiate much from PA66 over a wide range of supercoolings, which basically agree with the previous isothermal results. It has been explained from the standpoint of maintaining H-bonding in PA66/6T copolymers due to isomorphism.

However, it should be mentioned that the PA66/6T copolymer did deviate from the PA66 at very low supercooling (above 239 °C) on growth kinetics. PA66 has lower crystallization rate comparing to PA66/6T copolymers and show an I/II type regime

transition in regime plot, whereas PA66/6T copolymers seem to stay within regime II. Based on this observation, it was proposed that PA66/6T copolymer should follow rough surface growth due to the projection of benzyl ring at the growth front (Schreiber 1998).

The verification experiment conducted in this research has shown that this is not exactly the case. At low supercooling range, the growth rate of PA66/6T copolymer tends to be higher than PA66, but there is still a weak transition at the temperatures close to 239 °C. The higher growth rates of PA66/6T are probably due to the nucleation effect by the existence of rigid benzyl ring in the chains. The relatively higher crystallinity value of PA66/6T copolymer might be another indications of this nucleation effect.

On the contrary, the growth rate of PA66/6T copolymers at high supercooling are slightly lower than those of PA 66 homopolymer and this tendency to be more obvious with the increasing of the 6T content. The growth rates of PA6T12 are clearly lower than PA66 homopolymer.

It might be helpful to understand kinetics reduction from the reduced chain diffusion capability of PA66/6T since chain diffusion must play an increasingly important role in the crystallization at higher supercoolings.

In general, the PA66/6T copolymers have almost the same growth rates as PA66 homopolymer over a wide range of supercoolings. Whereas their growth rates seem to be higher at very low supercooling probably due to the increased nucleation effect and lower at very high supercooling due to decreased chain diffusion ability, both could result from existence of the benzyl ring.

5.2.1.2. Comonomer exclusion

Crystallization kinetics of PA66/6 and PA66/6I copolymers appear to follow the conventional predictions for the situation of comonomer exclusion during crystallization. The growth rates of copolymer decrease significantly with the increasing content of comonomer. This rate decreasing effect can be understood from the concept of two consequent processes of the crystallization.

First, incorporation of comonomer will significantly decrease heat of fusion of copolymer due to the interruption of H-bonding formation. It is therefore expected that driving force of crystallization will reduce somehow.

Secondly, the growth rate will be further decreased due to the necessity of excluding comonomer to form stable lamellar stem consisting of only crystallizable PA66 segments. Undoubtedly, such a selection process will delay the interface proceeding.

5.2.2. Effect of supercooling on crystallization rates

After discussing the effect of the comonomer on crystallization kinetics, it is meaningful to check how specifically the growth rate of each copolymer depends on the crystallization temperatures or supercoolings.

It was the major objective of this research to explore the growth mechanism of PA66 copolymers by studying the supercooling dependence and chemical structure dependence of PA66 copolymers. The relationships between growth rate and supercooling for PA 66/6T copolymers and PA66/6 copolymer are shown in Figure 5.13 and Figure 5.14.

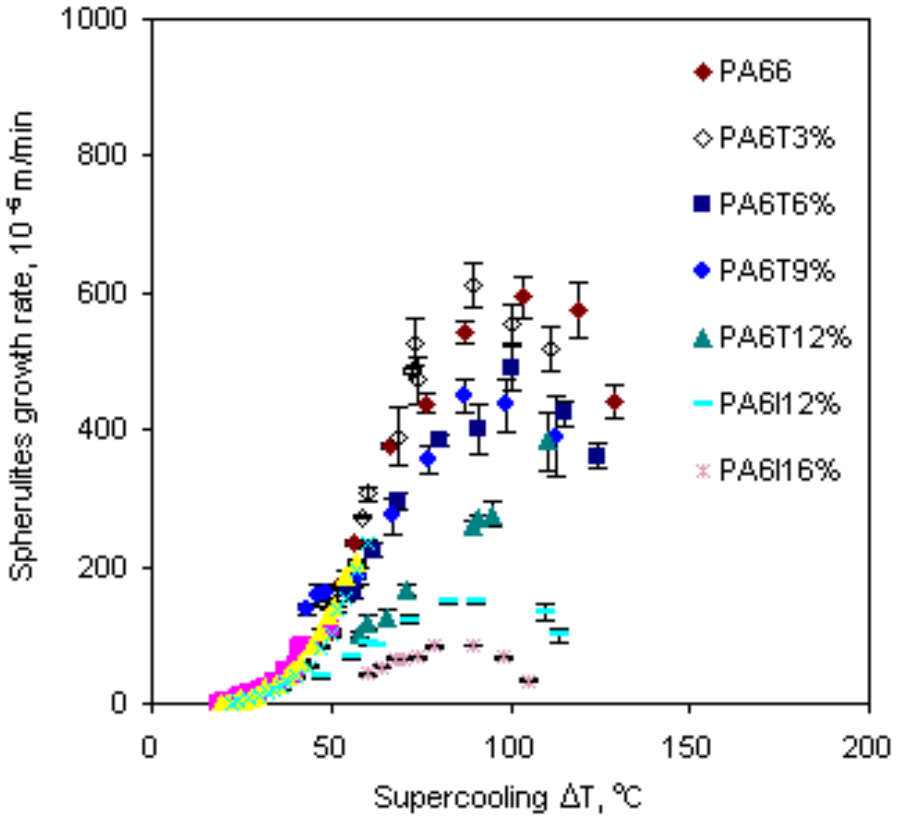

Figure 5.13 Growth rate of PA66/6T copolymers at different supercoolings.

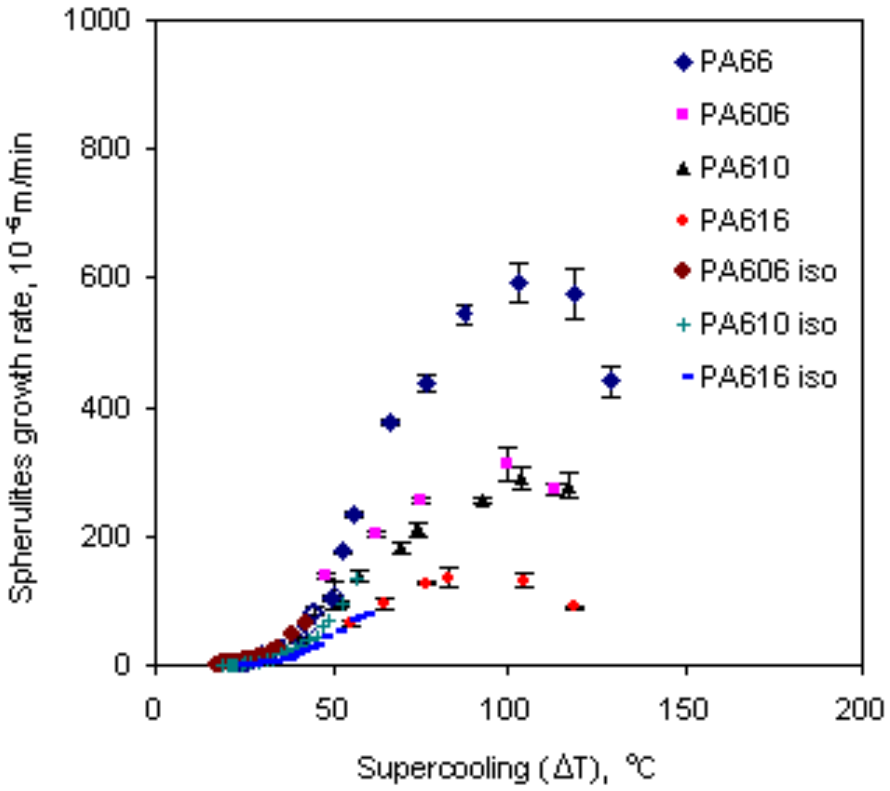

Figure 5.14 Growth rate of PA66/6 copolymers at different supercoolings.

To estimate the supercoolings, the specific constant melting peak temperatures of each polymer measured from DSC were normally used though an equilibrium melting temperature (301°C) is necessary, which was the value estimated from the Tm ~ *l*c with Gibbs-Thomson relationship in single crystals (Magill et al 1981). It just serves the purpose of estimating the driving force with the apparent melting points, as in the small molecules, for the convenience of comparison. The significance of equilibrium melting temperature will be discussed in detail in the section of regime analysis and melting behavior, respectively.

In general, growth rates of polyamides still appear as the "bell" shape in the growth rate versus supercooling plot, which is typical for nucleation-growth type kinetics (Magill 1962). Considerable supercooling is required for the beginning of the experimentally detectable growth rates. It is interesting to notice that the minimum supercoolings are almost the same (about 20°C) for different copolymer with the supercooling estimated from the apparent DSC melting point instead of the equilibrium melting temperature.

At low supercooling, the growth rates increase slowly with supercoolings (ΔT) and appear as an exponential relationship, which has been shown as straight line in the logarithm plot of growth rates to crystallization temperature before. Then spherulites growth rate increase much faster with supercooling after the supercoolings are beyond 30 °C. Finally, the growth rate will increase at much slower pace until it reaches a maximum growth rate before gradually decrease with the supercoolings. This might be attributed to

the increasing effect of chain diffusion at such high supercoolings crystallization conditions.

It is necessary to point out that the overall growth kinetics of PA66 copolymers do not seem to follow the rough surface growth mechanism over the wide range of supercoolings, as usually encountered in the crystallization of metals. First, a minimum supercooling is not required for the occurring of crystal growth for rough surface. Secondly, the rough surface growth should follow a linear relationship with supercoolings, at least for low supercooling range. However, an exponential relationship is found in PA66 and copolymers instead. Therefore, PA66 and its copolymers appear to follow a nucleation type growth mechanism in the range of low supercooling without precluding the possible rough surface kinetics at higher supercoolings.

Up to now, these preliminary impressions are solely based on the apparent growth kinetics and supercooling relationship. The discussion of the growth mechanism in PA66 will be discussed in more details comparing to the small molecules after excluding the chain diffusion effect with regime analysis.

5.2.3. Regime analysis of spherulitic growth rates

Secondary nucleation theory has originally been developed (Lauritzen & Hoffman 1960) to explain the growth kinetics of polyethylene single crystal growth in solution after the unprecedented wide recognition of chain folding conformation in PE single crystal (Keller 1957). It is basically the extension of a nucleation model developed for small molecules by Fisher and Turnbull (1949) with additional consideration of folding

conformation of PE chains in single crystals. It could provide satisfactorily quantitative explanations for the dependence of growth kinetics and lamellar thickness on supercoolings in polymer solution crystallizations.

Secondary nucleation theory was later transplanted to polymer melt crystallization, mostly based on the experimental observation that the growth rate and the lamellar thickness still depend on the supercooling in the same manner in the melt as in solution growth (Armistead & Goldbeck-Wood 1992). Considerable reservations still persist since it is well known that crystallization in bulk system, also called "solidification", is much more complicated than in solution or vapor phase (Cahn et al 1964) since diffusion is obviously a very important controlling factor.

In spite of the caution on the secondary nucleation mechanism, it provides a powerful tool for the quantitative analysis of growth rate and supercooling dependence in melt crystallization of polymers. The growth rates of PA66 and copolymer over a wide range of supercoolings will be analyzed with regime analysis in order to elucidate the growth kinetics over the wide range supercooling in this study. The general form of regime edition of the secondary nucleation equation (Phillips 1990) is expressed as:

$$G = G_0 \exp\left[-\frac{U^*}{R(T_c - T_\infty)}\right] \exp\left[-\frac{K_g}{T_c \Delta T f}\right] \qquad (5.10)$$

Where G is the linear growth rate, U* is the activation energy for transport of the segments to the crystallization site, R is the gas constant. Tc is the crystallization temperature and T_∞ is the temperature where all motions associated with viscous flow

cease, usually taken as Tg-30 K. ΔT is the supercooling. Tm^o-Tc. K_g is nucleation parameter and defined in three regimes as

$$K_{gI} = 2K_{gII} = K_{gIII} = \frac{4b_0\sigma\sigma_e T_m^o}{\Delta h_f^o k} \qquad (5.11)$$

f is a correction factor used to compensate for changes in Δh_f^o with temperature at high supercoolings, defined as $f = 2T/(T + T_m^o)$.

Effect of U value*

It has been well known that the value of U* can significantly affect the kinetics transition behavior in the regime plot. Unfortunately, the independent measurements of U* for polymers are scantly available, and it is even more difficult to obtain the diffusion activation energy for crystalline polymers under crystallization temperatures.

The value of U* is therefore often taken as universal value of 1500 cal/mol with some adjustment for the good of fit. The growth rates of PA66 homopolymer are plotted in Figure 5.15 to show how U* value will affect the regime transition behavior.

For the universal U* value of 1500 cal/mol, it is shown that three regimes will appear at the temperatures corresponding to the growth rate-crystallization temperature as shown in Figure 5.15. They will be labeled as Regime I, II, III corresponding to relative supercoolings just for the convenience of description, and they do not necessarily corresponding to the regimes in secondary nucleation. The first two regimes are close to be linear whereas the Regime III at high supercooling shows a little upward curvature close to growth rate maximum temperature.

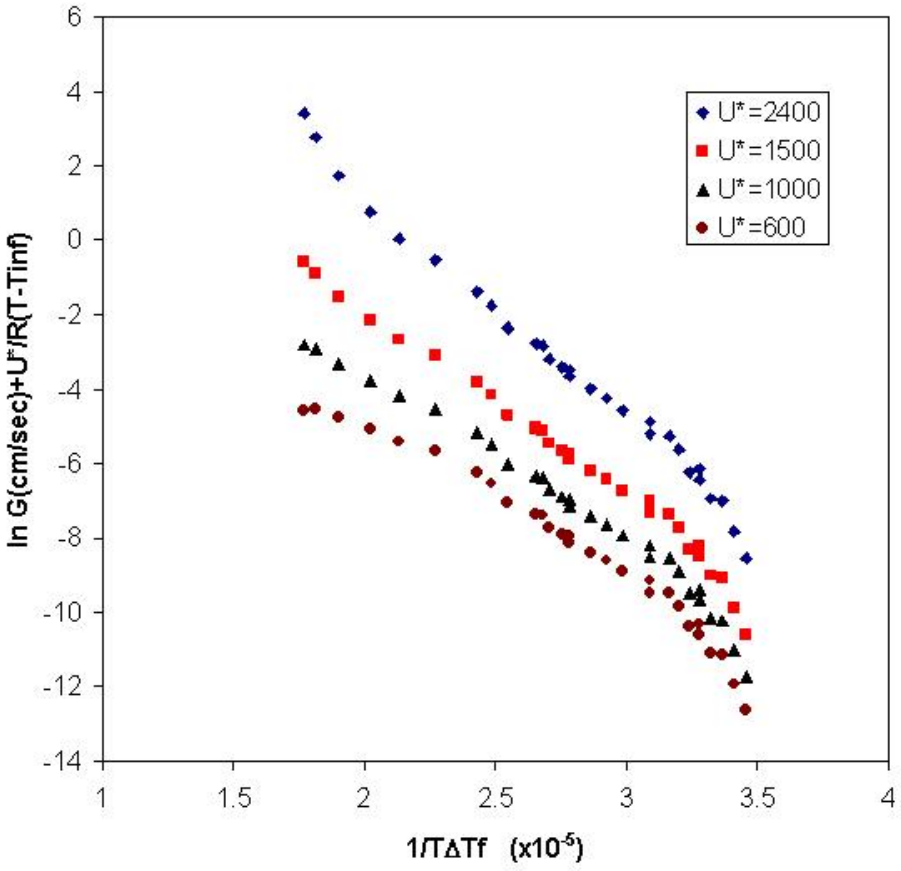

Figure 5.15 The effect of U* value on the regime transition of PA66 homopolymer (Tm^o=301 °C)

Such a tendency is more clearly shown with U* value of 2400 cal/mol. A U* value of 600 cal/mol for the regime analysis (Schreiber 1998) was used to remove the curvature for growth rated of lower crystallization supercooling obtained from isothermal crystallization (Regime II). It appears that this value does give a good linear fit for the regime I and II.

However, a downward curvature is usually observed around the growth rate maximum temperature in the contrary to the upward curvature with the U* value of 1500 cal/mol. Such a decrease of nucleation across the growth rate maximum is not expected from the view of nucleation-growth since nucleation rate is expected to keep increasing with the decreasing supercoolings.

A U* value of 1000 cal/mol was found to be able to remove any curvature across the growth rate maximum (regime III), therefore it was chosen for the further regime analysis of PA66 copolymers, assuming that all copolymer will have the same diffusion activation energy as PA66 homopolymer and that no nucleation mechanism change occurs around the growth rate maximum temperature.

Effect of Tm^o value

Due to the unique melting behavior of PA66, the equilibrium melting temperature has been uncertain for a long period. A Tm value of 272°C (545K) has been used for the kinetics analysis of PA66 (Magill 1962), which was actually the melting point of negative spherulites.

Another value of 280 °C has also been reported, which is usually estimated from the Hoffman-Weeks plot with middle melting temperature (Illers & Haberkorn 1971, Stouffer et al 1996, Wunderlich 1980).

With Gibbs-Thomson equation, the equilibrium melting temperature of PA66 was determined to be 301°C and heat of fusion of 61 cal/g (Magill et al 1981). Since the crystallization and melting behavior of PA66 does not follow conventional theories.

It is still debatable to determine which Tm^o is most appropriate for the kinetics analysis of PA66 melt crystallization. Therefore, the effect of Tm^o value on the regime transition is considered and shown in Figure 5.16.

Clearly, the Tm^o does not change the general transition behavior, which is expected from the mathematical terms of regime analysis. However, the slope changed because of the significantly different supercoolings estimated with different Tm^o. Thus it is believed that appropriate choice of U* value has more dramatic effect for the purpose of studying the regime transition behavior changing with the crystallization temperatures.

For the regime analysis of PA66 and PA66/6T copolymers, the same Tm^o of 301°C is used considering the crystallization isomorphism. For PA66/6 copolymer, it is either estimated with melting depression equation of Flory for PA66/6 copolymers for exclusion or estimated with a linear model with the Tm^o of PA6 taken as 260°C (Xenopoulos & Wunderlich 1990). Therefore, a U* value of 1000 cal/mol is always used without special mention in the following kinetics analysis.

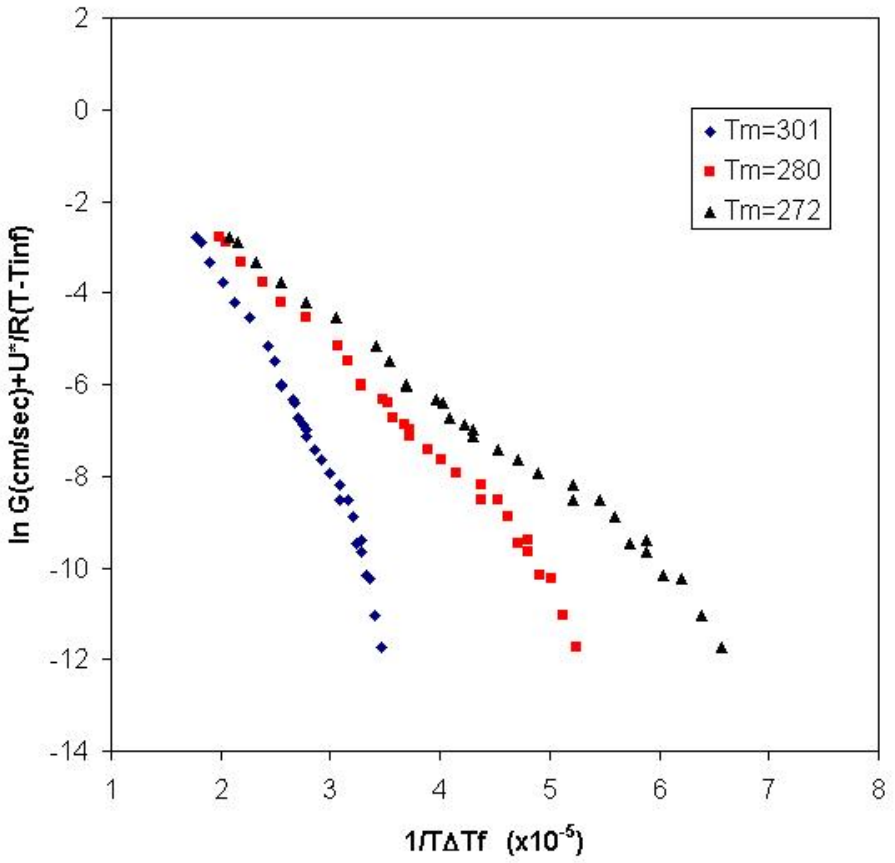

Figure 5.16 The effect of Tm^o value on the regime transition of PA 66 homopolymer (U*=1000 cal/mol)

5.2.3.1. Regime analysis of PA66/6T copolymers

The regime plot of PA66/6T copolymer is shown together with PA66 homopolymer in Figure 5.17. The growth rates of PA6T03 and PA6T06 have been completed to the low supercoolings as those of PA66. The U* value of 1000 cal/mol and the Tm^o value of 301°C are used for the regime analysis, based on the discussion of U* and Tm^o. Both PA66/6T copolymers show similar regime transition behavior. The curves of PA66/6T copolymers tend to shift to the lower value comparing to PA66 at equivalent supercooling, which could be the result of slightly increased diffusion activation energy or actual higher equilibrium temperature due to structure modification as discussed before.

A regime I/II transition also occurs at high crystallization temperature (around 239 °C), which is found to corresponding to the Axialite/Spherulite morphology changes under optical microscope. The ratio of the slope for regime I to regime II is close to 2, as described in secondary nucleation theory.

For Regime II/III transition, the slope of regime III was found to be smaller than that of regime II, which is different from an expected in for Regime II/III transition by one fold in secondary nucleation theory. This apparent dilemma does not appear unexplainable in the light of the analysis of thermal diffusion at high supercoolings. As it has been discussed, the linear growth rate of spherulites at high supercooling is possible due to the steady temperature gradient around spherulite rather than the nominal "isothermal" crystallization temperature.

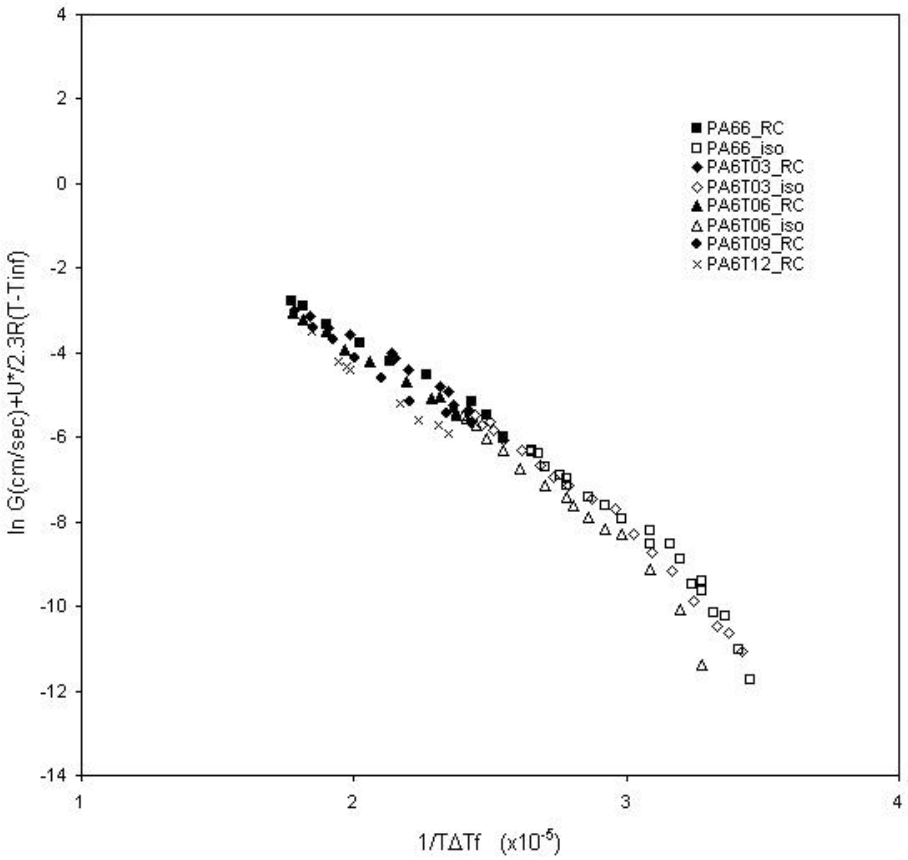

Figure 5.17 Regime plot of PA66/6T copolymer with U* =1000 cal/mol (Tm^o=301°C).

Therefore, the growth rate only represents the apparent spherulites interface growth rate but not actually the nucleation controlled interface growth rate as always assumed in secondary nucleation. It has been believed that thermal diffusion affected growth should still follow the interface controlled growth mechanism, such as nucleation controlled growth (Benard et al 1996).

5.2.3.2. Regime analysis of PA66/6 copolymers

PA66/6 copolymer crystallization is normally explained with exclusion mode (Harvey & Hybart 1970), which is also the expected mechanism from the analysis of melting points.

However, it is still not sure if the PA6 repeat-units are selectively excluded at the growth front or included first at growth front then excluded behind the growth front during the crystal perfection process. The latter mode is possible considering the high driving force at higher supercooling and not significantly different chemical structure between PA66 and PA6, which is considered as defect only from the standpoint of disturbing H-bonding formation and is totally different from the branch defects in polyethylene copolymers.

Therefore, the regime analysis of PA66/6 copolymers was performed with two sets of equilibrium melting temperatures estimated either from a linear inclusion model or Flory exclusion model. It was expected that such an analysis would shed some light on the crystallization mechanism of PA66/6 copolymers from the checking of growth kinetics.

- ***Inclusion mode***

The regime plot of PA66/6 copolymer with linear inclusion mode is shown together with PA66 homopolymer in Figure 5.18. The growth rates of PA606, PA610 and PA616 are completed to the low supercoolings with isothermal crystallization as PA66. The U* value of 1000 cal/mol is used as discussed before, and the T_m^o value of each copolymer is estimated from the Tm^o of PA66 (301°C) and that of PA6 (260°C) with linear interpolation.

It was shown that similar three regimes with decreasing crystallization temperature appeared in the regime plot. A regime I/II type transition also occurs at high crystallization temperature in PA66/6 copolymers (239°C for PA66, 229°C for PA606, 211°C for PA610 and 196°C for PA616), which confirmed the corresponding relationship with the Axialite/Spherulite morphology changes under optical microscope. The ratio of the slope for regime II to regime I is close to 2, as described in secondary nucleation theory.

For Regime II/III transition, the slope of regime III was also smaller than that of regime II, which is different from an expected increase by one fold in secondary nucleation theory. It is interesting to notice that regime plots of different copolymer tend to merge at very high supercoolings, as has been found before with ethylene/1-octene copolymers. This merging tendency was explained with the inclusion of hexyl branch into crystal in the ethylene/1-octene copolymers at high supercooling (Wagner & Phillips 2001). Such a tendency should be much more possible with PA66/6 copolymer due to the absence of the steric branch and structure similarity between PA66 and PA6.

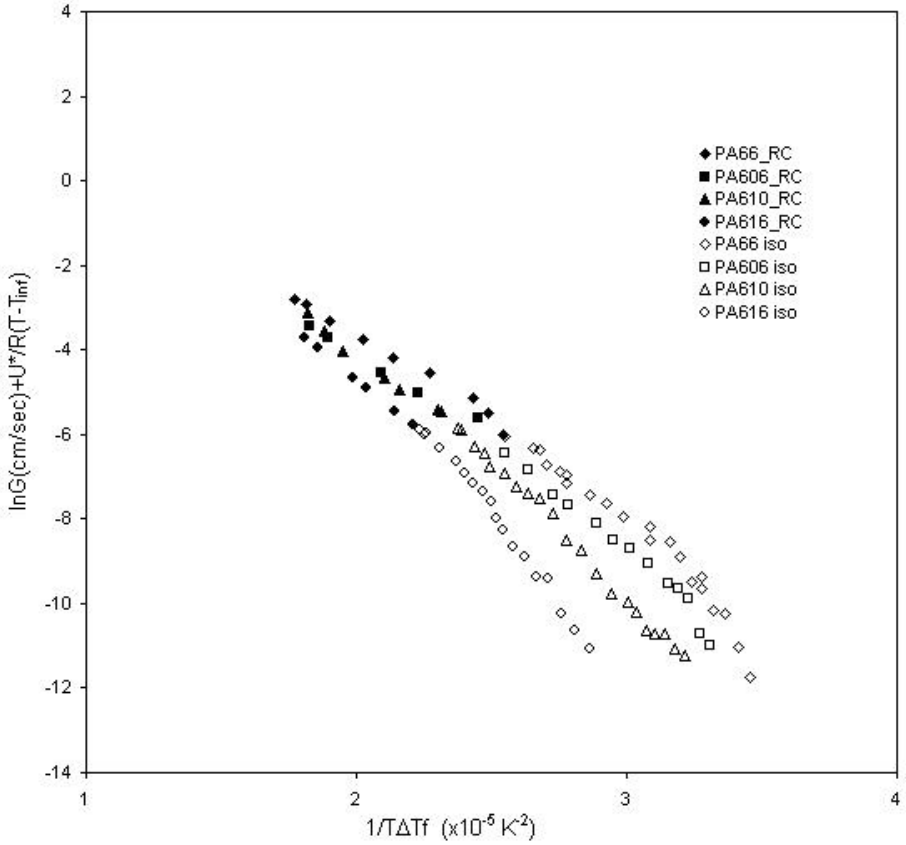

Figure 5.18 Regime plot of PA 66/6 copolymers with U*=1000 cal/mol (Tm^o estimated from inclusion mode)

Another salient feature is that the slope of PA66/6 copolymers are lower than PA66 homopolymer in each regime, which might indicate the decreasing driving force of copolymer due to the interruption of H-bonding formation.

- ***Exclusion mode***

The regime plot of PA66/6 copolymer with exclusion mode is shown together with PA66 homopolymer in Figure 5.19. The growth rates of PA606, PA610 and PA616 are completed to the low supercoolings with isothermal crystallization as PA66. The U* value of 1000 cal/mol is used as discussed, and the value of each copolymer is estimated from the Tm^o of PA66 (301°C) with the melting point depression equation due to Flory.

They still show similar three regimes with decreasing crystallization temperature in the regime plot, as it is expected from the discussion of the Tm^o effect. A regime I/II type transition also occurs at high crystallization temperature in PA66/6 copolymers (239°C for PA66, 229°C for PA606, 211°C for PA610 and 196°C for PA616.For Regime II/III transition, the slope of regime III was also smaller than that of regime II, which is different from an expected increase by one fold in secondary nucleation theory.

But the most significant feature is that the regime plots of PA66/6 copolymers seem to be closer to each other, therefore they show the same appearance as PA66/6T copolymers especially at high supercoolings. At regime I, the regime plot of each copolymer tends to begin to deviate from the common regime plot of high supercooling at the increasing value of supercooling with the increasing comonomer content.

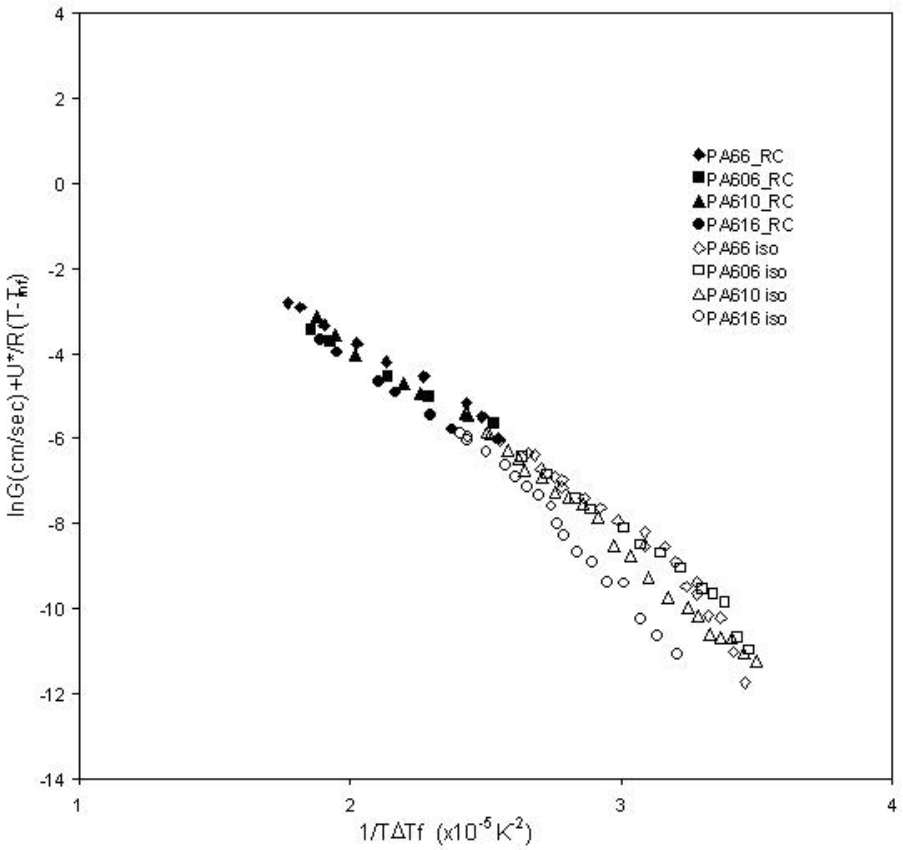

Figure 5.19 Regime plot of PA66/6T copolymer with U* =1000 cal/mol (Tm^o estimated from exclusion mode with Flory equation)

If this is really the case, the regime behavior of PA66/6 copolymer at high supercooling seems to imply that all the copolymer actually follow the same kinetics independent of the chemical structure, not just the appearance of merging tendency as observed in the regime analysis of PA66/6 copolymer with inclusion mode. And the delay of transition of the transition to higher supercooling could be explained from the decreasing driving force and heat of fusion at PA66/6 copolymer.

Since it has been established in all the polymers studied at low supercooling that the regime I/II transition is accompanied with Axialite/Spherulite morphology change, this plot seems to imply that the growth rate exhibited by spherulites does not represent the actual nucleation controlled interface growth rate of each lamella but represents a coordinated spherulite interface spreading rate. Obviously, such a transition behavior of growth rate could be explained from the effect of thermal diffusion. What else can better explain the appearance of circular interface in spherulites than the synchronic effect of thermal diffusion?

On the other hand, for crystallization at low supercooling (Axialites), the growth rate is much lower and thermal diffusion effect could be ignored as in solution crystallization. Each lamella can keep its own growth rate as controlled by the specific interface growth mechanism. Therefore, the observed growth kinetics at this regime tends to show the unique growth kinetics of lamellae determined by the specific chemical structure. The thermodynamic parameters derived from regime analysis are summarized in Table 5.1.

Table 5.1 Parameters derived from kinetic regime analysis

Activation Energy (cal/mol)	Sample code	Tm^o (K)	ΔHf (J/cm^3)	Regime I Ln G_o (cm/s)	Regime I Kg ($\times 10^5$ K^2)	Regime II Ln G_o (cm/s)	Regime II Kg ($\times 10^5$ K^2)	Regime III Ln G_o (cm/s)	Regime III Kg ($\times 10^5$ K^2)
Inclusion	PA66	574.15	224.04	23.18	10.27	4.48	4.45	1.04	2.97
U* =600	PA606	569.52	222.69	16.29	8.47	5.57	5.06	0.22	2.81
(Schreiber)	PA610	566.36	221.80	10.93	7.28	6.20	5.53	2.02	3.73
	PA616	562.83	220.45	13.42	8.90	7.22	6.33	1.91	3.99
Inclusion	PA66	574.15	224.04	25.32	10.45	7.09	4.77	6.90	4.65
U* =1000	PA606	569.52	222.69	18.59	8.68	8.35	5.43	6.31	4.58
	PA610	566.36	221.80	13.58	7.59	9.61	6.13	9.42	6.11
	PA616	562.83	220.45	16.52	9.36	11.20	7.14	10.94	7.11
Exclusion	PA66	574.15	224.04	25.32	10.45	7.09	4.77	6.90	4.65
U* =1000	PA606	566.38	210.60	16.97	7.81	7.56	4.96	5.86	4.26
Flory	PA610	560.73	201.64	11.47	6.39	8.29	5.29	8.41	5.40
	PA616	553.92	188.19	13.03	7.27	9.01	5.72	9.10	5.83
Co-crystal	PA6T03	574.15	224.04	14.48	7.25	7.10	4.81	6.25	4.38
Tm=574.15K	PA6T06	574.15	224.04	23.32	10.30	8.23	5.37	7.25	4.99

a_0=asinβ*sin66.25=4.37Å

b_0=bsinα=4.03 Å

5.2.4. Kinetics analysis with rough surface model

As introduced in the section of literature review, surface roughening has been proposed as the possible growth model of PA66 based on the consideration of its chain folding direction and constant lamellar thickness. However, it should be mentioned that there is not a well-developed analytical model for surface roughening growth since the model has been based on the computer simulation due to its origin of statistical mechanics.

Nevertheless, it has been shown (Chui & Weeks 1978), using linear response theory, that the growth rate should be linear with supercooling at small supercooling when Tc is over roughening transition temperature (T_R). Based on the conventional quasi-equilibrium model, the growth rate can be taken as the difference between the rate of arrival and departure rate at the interface (Armistead & Goldbeck-Wood 1992):

$$v = R_A^o \exp\left(-\frac{Q_A}{kT}\right) - R_D^o \exp\left(-\frac{Q_D}{kT}\right) \qquad (5.12)$$

Where Q_A and Q_D are the activation energies for the arrival and departure process, $Q_D - Q_A$ is the latent heat of fusion, ΔH. At equilibrium melting temperature (T_m), there is no growth, thus growth rate is zero. It can be derived that:

$$\frac{R_A^o}{R_D^o} = \exp\left(-\frac{\Delta H_f}{kT_E}\right) \qquad (5.13)$$

When equation 5.15 is substituted into equation 5.14, it follows that the growth rate of crystal can be express as:

$$v = R_A^o \exp\left(-\frac{Q_A}{kT}\right)\left[1-\exp\left(-\frac{\Delta H_f \Delta T}{kT_E T}\right)\right] \qquad (5.14)$$

for $T_I > T_R$, at small ΔT, the equation 5.16 can be simplified as

$$v = R_A^o \frac{\Delta H_f \Delta T}{kT_E T}\exp\left(-\frac{Q_A}{kT}\right) \qquad (5.15)$$

Therefore, the growth rate is approximately linear to the supercooling. For $T_I > T_R$, the growth rate approaches that given by classical nucleation theory, and the curves can be fitted by an exponential equation over a limited region (Jackson 1984):

$$v = v_o(\Delta T)^{\beta} \qquad (5.16)$$

On the log-log plot, the growth rate after diffusion correction should be linear to the supercooling, as shown in equation 5.17. The growth rates are shown in Figure 5.20 for different crystal roughness (T_I/T_R).

$$Logv = \log v_o + \beta \log(\Delta T) \qquad (5.17)$$

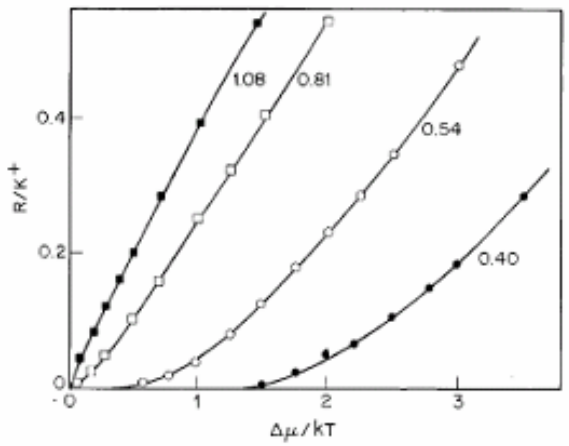

Figure 5.20 Normalized growth vs. chemical potential difference for different crystal surfaces (Jackson 1984).

With this rough surface analytical mode in mind, it should be meaningful to check the relationship between the interface growth rate (after diffusion correction) and the supercooling. Due to the obvious similar growth rate of PA66/6T copolymers to PA66 homopolymer, only PA66 and PA66/6 copolymers are considered for rough surface growth kinetics checking. The growth rate is corrected with the same diffusion activation energy (U*) of 1000 cal/mol and the supercoolings for copolymers are estimated from equilibrium melting temperature with linear inclusion model.

The reduce growth rates are plotted versus supercooling in linear plot (see Figure 5.21) and log-log plot (see Figure 5.22), respectively. It appears that the growth rate still show exponential relationship with supercooling even after the diffusion correction. The growth rates are expected to be zero up to 50 °C of supercoolings.

This exponential relationship is confirmed in the log-log plot. It is interesting that the growth rates clearly fall into three regions with increasing supercooling that is amazingly similar to the result of regime analysis. It seems that each of the region can be reasonably fitted into straight line. The decreasing slope with increasing supercooling seems to suggest that growth rates of PA66 and PA66/6 copolymers are changing from interface-controlled mechanism to the diffusion-controlled mechanism.

In summary, the growth rate of PA66 and its copolymer have exponential relationship with supercooling. The crystallization temperature in this study should be much lower than the surface roughening temperature (T_R).

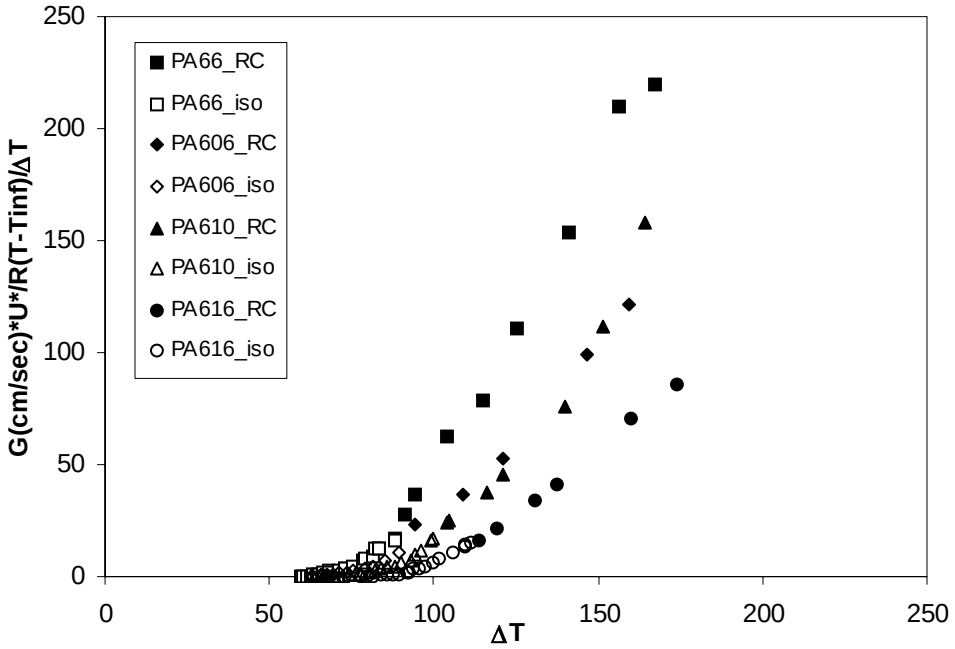

Figure 5.21 Reduced growth rate of PA66/6 copolymer as a function of supercooling.

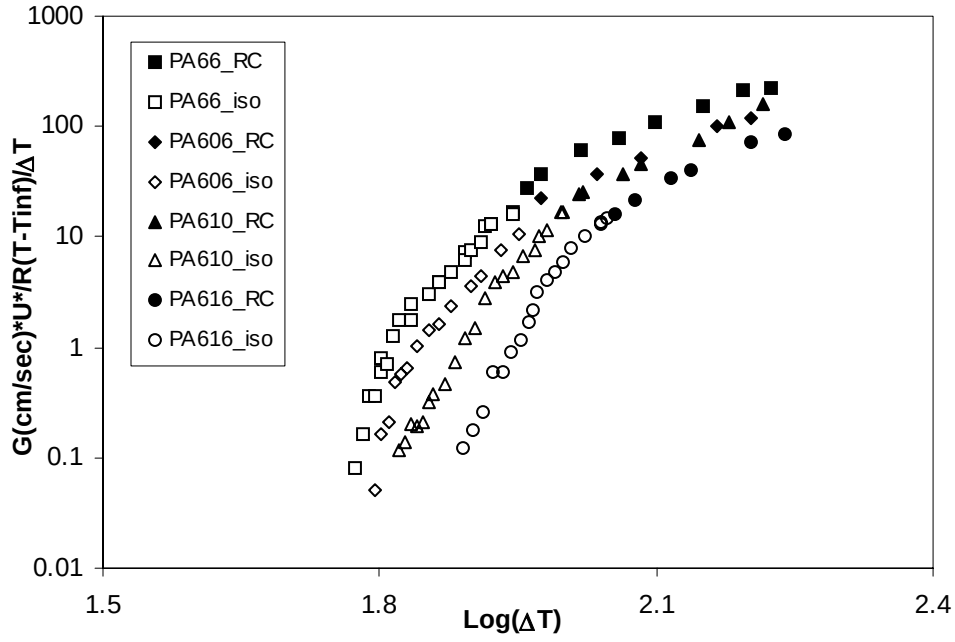

Figure 5.22 Reduced growth rate of PA66/6 copolymer versus supercooling in the log-log plot.

5.2.5. Possible origins of regime transition in PA66

After analyzing the growth rates of PA66 and copolymer with regime plot and simple kinetic model, it is meaningful to summarize the possible origins of the transitions in regime plot. Obviously, these transitions showed different tendency from the regime transitions described in the classic secondary nucleation mechanism. Alternative rough surface growth mechanism was actually proposed (Schreiber 1998) to explain the growth rate of PA66 positive spherulites based on the knowledge of the chain folding in the radial direction in positive spherulites. This is different from the direction perpendicular to the radial direction in polyethylene that was deduced from the X-ray studying of the crystal structure from zone-crystallized PA66 crystal by (Lovinger 1978b). Therefore, it is necessary to illustrate the possible causes of transition in regime plot start from the assumption used in the regime analysis as well as other concepts in small molecules.

First, it should be mentioned that the melt crystallization is a very complicated process compared to crystallization in solution and vapor. A lot of overlapping processes exist in the process of crystal growth, such as chain diffusion to the growth front, attachment/de-attachment onto the interface, chain conformation adjustment, diffusing away the produced latent heat and excluded species, crystal perfection or thickening. The growth kinetics is usually divided into *interface control* growth mechanism and *diffusion control* mechanism depending on the dominant rate controlling process, which is normally the slowest process under the specific condition.

The classic growth mechanism considers that growth rates are basically controlled by the surface nucleation and chain diffusion, which can well explain the bell shape

growth rate kinetics with the product of two Arrhenius type rates. At low supercooling, the nucleation process is the controlling process; at high supercooling, the diffusion is the controlling process. A growth rate maximum is therefore predicted with an intermediate supercooling. The basic assumption is that interface growth rate depends solely on the surface nucleation rate and chain diffusion rate, while other interface growth modes and diffusion processes of heat and un-crystallized species are ignored. Certainly, such a model can explain the overall crystallization rate in many systems with the beauty of physical simplicity.

5.2.5.1. Interface control mechanism

Secondary nucleation theory is essentially the extension of the classical surface nucleation theory in order to explain a transition of the interface growth rate, corrected for diffusion, at increasing supercooling in polymer solution crystallization. Since such a transition is unexpected with the classical surface nucleation theory, it was proposed that the interface growth rate should be attributed to not only *surface nucleation* rate (*i*) but also *surface spreading* rate (*g*) following the surface nucleation (Hoffman et al 1976). By the interaction of these two rates at interface, three different growth rate regimes will occur with increasing supercoolings in the regime plot. It should be mentioned that the surface nucleation has always been indispensable for the crystal growth. Secondary nucleation theory just amended the deficiency of surface nucleation theory at increasing supercoolings by including an additional factor (g).

Even earlier than that, however, it was found that crystal growth could occur at very low supercooling where classical surface nucleation theory predicts that no growth

should happen. It had been a mystery until Frank et al proposed (Burton et al 1949) that screw dislocation, which often exists at the growth front as defect, could provide niches for continuous interface growth without the necessity of surface nucleation. Similarly, twinning has also been proposed to be another interface rate control mechanism at low supercooling.

Contrary to the explanation of growth with screw dislocation, It was proposed (Jackson 1969) that crystal growth could simply occur on rough surface after a surface roughening transition temperature (T_R). Gilmer (Gilmer 1976) has tested this hypothesis with computer simulation, then Sadler and Gilmer (Sadler & Gilmer 1984, Sadler & Gilmer 1986) tried to explain the polymer crystallization kinetics with rough surface growth mechanism.

Only several experiments reveal the existence of surface roughening transition. It should be mentioned that such a transition often occurs at temperature close to the melting point and growth rate is expected to be linear with supercooling, which is in contrast to experimental observations of polymer crystallization. In viewing of the long chain structure of polymers, the feasibility of applying this hypothesis in polymer crystallization is a very controversial issue.

Certainly, any change of growth mechanism with supercooling will result in transition in regime plot. Nevertheless, such a change of growth mechanism has seldom been suggested from the present knowledge of growth kinetic and morphology polymers.

5.2.5.2. Diffusion control mechanism

When the supercooling is high enough, the nucleation rate will not be controlling process anymore. The diffusion processes are gradually becoming the dominant factor. It is well known that heat diffusion is the controlling process for the solidification of pure metal while diffusion of solute (impurity) is the controlling process for the solidification of metal alloys (Porter & Easterling 2001). However, as it was discussed before, both classic surface nucleation theory and secondary nucleation theory only considered the mass transport (chain diffusion) to the growth front.

Even for the mass transportation (chain diffusion), some uncertainties remain until now. In the classical surface nucleation theory, the diffusion term is expressed with an Arrhenius type term, which basically assumes that the diffusion term involved in melt crystallization can be estimated with a viscosity type relation (Ngai et al 2000). But it is known that the melt viscosity can only be well represented with Arrhenius type term at the temperature over Tg +100°C; while a W.L.F. type relation is found more appropriate to estimate the viscosity at temperature between Tg and Tg+100°C due to the increasing effect of free volume on diffusion at lower crystallization (Hoffman & Miller 1997).

Therefore it is usually recommended to use WLF type term to estimate the diffusion term for the regime analysis over a wide range of supercooling (Phillips 1990), which is also due to the lacking of the data on Arrhenius activation energy. Choosing value for the U* and Tm^o certainly could affect the regime behavior, as demonstrated in the discussion on the effect of U* and Tm^o value. The effect is especially significant for the high supercooling data.

What is more, there is argument that the diffusion process involved in the crystallization could actually be different from the diffusion expressed with viscosity (Ngai et al 2000). Viscosity may express the translational motion while the diffusion involved in melt crystallization could be due to self-diffusion, rotational diffusion or "reptation" diffusion for polymer (Hoffman & Miller 1997).

In spite of these uncertainties, it is reasonable to believe that regime analysis still provide a vital tool for the analysis of the growth kinetics of polymers, especially for the transition at low supercooling and when the transitions can be well correlated to the morphological observations.

Keith and Padden (Keith & Padden 1963) were the first to consider the effect of other diffusion effects on the crystallization of polymers. But probably due to their extensive experience in the solidification of metal alloys and polymer blends, most of the attention is put on diffusion away of un-crystallizable impurity from the growth front and the diffusion of latent heat was ignored because it was deemed less significant than the impurity diffusion. A phenomenological spherulite forming theory has been proposed based on this concept, but it could not account for the spherulites growth in pure polymer and small molecules. Slow growth rate in polymer is another reason for frequent dismissal of the effect of thermal diffusion.

Even though thermal diffusion has seldom been considered in polymer melt crystallization, its effect on the crystallization (or solidification) has been well recognized in the studying of morphology instability (Langer 1989, Sekerka 1968) and thermal

dendrite growth (Gill 1989, Glicksman & Lupulescu 2004) in small molecules. Thermal dendrite has been considered as the possible model of crystal growth in strained melt crystallization of polymers in order to explain the high crystallization rate during melt spinning (Tiller & Schultz 1984). However, it was believed that the growth rate in quiescent crystallization is too small (two orders of magnitude slower) comparing to the thermal diffusion limited interface growth rate, therefore nucleation-growth should still be the operating mechanism in spherulite growth. The observed linear spherulitic growth rate also seems to support the interface control since the interface propagation will be proportional to the square root of time. However this linear growth rate is also possible due to a steady temperature gradient around the spherulite as discussed in section 4.1, which has also been demonstrated by the simulation of temperature profile (Benard et al 1996). Even if the individual lamella growth still follows the interface control kinetics, the actual temperature is affected by the thermal diffusion and the overall growth rate of spherulite is not the simple manifestation of interface kinetics.

5.2.5.3. Smooth-rough transition at high supercoolings

Other than the possibilities of nucleation rate change in secondary nucleation and the diffusion effect, there is another theory that could explain the growth mechanism change. After reviewing the experiment data on the solidification of metals, organic, and inorganic compound, it was proposed that solidifications from pure melt would follow a lateral mechanism at sufficient small supercooling and follow continuous mechanism at large supercoolings after a transition regime (Cahn et al 1964). This transition of growth mechanism was predicted based on the diffuse interface model (Cahn et al 1964).

Such a transition of growth kinetics is shown schematically in Figure 5.23. The growth rate is corrected for the temperature dependence of diffusivity (with viscosity) and divided by supercooling in (a), only diffusion correction is done to show the growth rates in (b). At low supercooling ($\Delta T_K < \Delta T_K^{**}$), a classical dislocation is shown here to give a linear plot through the origin, whereas surface nucleation is also possible without such a linear relationship. At sufficiently high supercooling ($\Delta T_K > \Delta T_K^{*}$), the nucleation barrier disappears and the continuous mechanism will give a constant value independent of the supercooling. In the transition regime, the growth should still occur by lateral spreading mechanism, but the growth rate deviates from the classical equation and deviates in the direction of faster growth (Cahn et al 1964, Tiller 1991).

It should also be pointed out that whether such transition could be experimentally observed depend on the magnitude of diffuseness (g), which depends on the number of atomic (or molecular) layers comprising the transition from solid to liquid. It is possible that only continuous regime will be observed with small g; but continuous mechanism might not be reachable with large g. In the context of this mechanism transition in metals and small molecules, it is obvious that secondary nucleation theory of polymer crystallization did not consider the transition into continuous growth mechanism. This simple treatment was reasonable considering the relatively low supercooling range for the melt crystallization of polymers in the past; the nucleation barrier was always believed to be the controlling factor of polymer crystallization. The relatively higher supercooling for PA66 melt crystallization might be another justifications for considering such a transition.

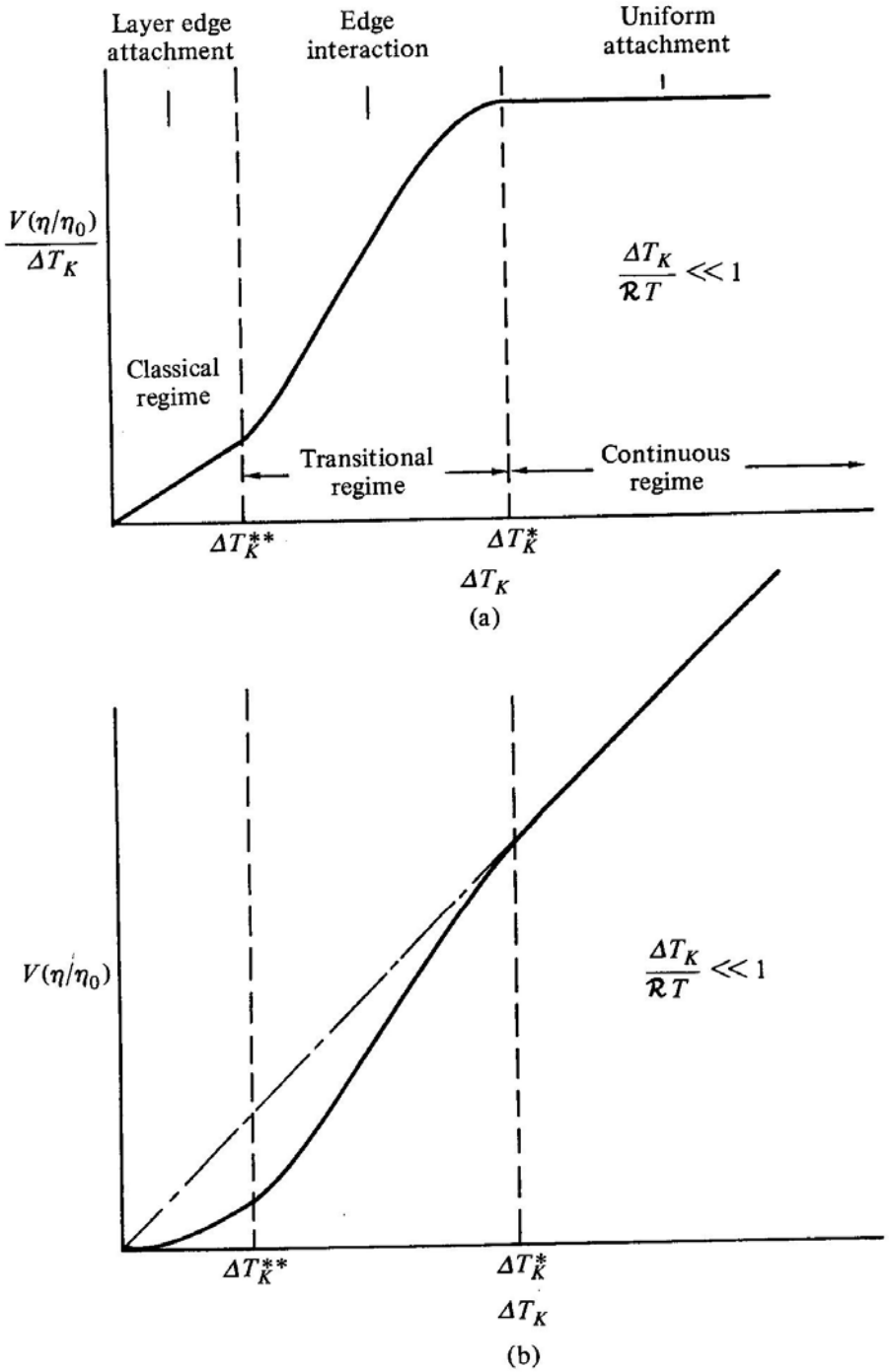

Figure 5.23 Theoretically predicated growth rate curves as function of supercooling, ΔT_K for interface with emergent dislocations (Tiller 1991).

Another observation on nucleation barrier in the secondary nucleation theory of polymer crystallization is the complication of the unique chain-folding conformation in polymer crystals. Secondary nucleation theory can be used to explain the dependence of chain folding length on supercoolings. But it was well known that the growth rate kinetics could change dramatically in low molecular weight PEO and PE crystallization with the change of quantized chain folding lengths (Hoffman 1985, Leung et al 1985, Point & Kovacs 1980).

In the melt crystallization of PA66, the chain folding direction is along the radial direction (Lovinger 1978b) and the lamellar thickness is also found to be independent of supercooling over a wide range of supercooling. Without the concern of nucleation barrier due to chain folding at high supercoolings, PA66 could very possibly follow the growth mechanism (such as rough surface growth) similar to metals and small molecules.

5.3. Crystal morphologies

5.3.1. Spherulites formation mechanism

As revealed in the growth kinetics, the transition of kinetics behavior is usually concomitant with the change of spherulitic morphology. It is therefore necessary to address the morphology forming process relating to the kinetics analysis as well as the current understanding of the spherulite forming.

5.3.1.1. Keith-Padden phenomenological theory (interface stability)

Based on the concept of interface instability (Tiller et al 1953) in metal alloy, a phenomenological model was proposed to explain the spherulite formation process (Keith

& Padden 1963). After summarizing the spherulitic structure, in minerals, polymers, organic compounds, inorganic compounds and liquid crystals, it was found that generally spherulites consisted of fibrillar crystals separated by uncrystallized melt and the fibrils exhibited non-crystallographic “small angle branching”.

In analogy to the cellular interface in metals, fibrillar structure was attributed to the unstable interface that was brought about by the diffusion of impurities from growth front. Small angle branching was believed to be the result of disordered surface nuclei at the growth front when diffusion length (δ) is sufficiently small.

Actually, it was noticed that the fibrils were commonly ribbon-like lamellar crystal in polymer spherulites whereas they were prismatic needle-like fibrils in non-polymeric spherulites. Even though diffusion of latent heat was known to control the growth rate of pure melt, it was believed to be insignificant in comparison to impurity diffusion based on following three reasons:

1) spherulitic growth rate is linear ($r \propto t$) rather than nonlinear ($r \propto t^{1/2}$) as in the case of latent heat diffusion control; 2) spherulitic growth rates in polymers and organic compounds are so slow ($G<10^{-3}$ cm/sec) that it requires only slight temperature gradient between crystal and melt to diffuse away the latent heat, therefore the system is taken as isothermal; 3) a modest increase in impurity content, a few percent, can reduce the growth rate significantly at any given temperature.

This model could semi-qualitatively explain the coarseness and lateral dimension of fibrils of PS and PP spherulites in terms of impurity layer thickness (δ) with one or

two orders of magnitude (Keith & Padden 1963). Nevertheless, this phenomenological model (Figure 5.24) has been controversial from its inception. First, it was well known highly purified hydrocarbons can also form spherulites. Secondly, the morphological studies (Bassett & Hodge 1981a, Bassett et al 1981) demonstrated that the proposed lamellar dimension and diffusion length (δ) relationship was inadequate to quantitatively explain their results.

It should be mentioned that a morphological stability theory was later developed (Mullins & Sekerka 1963, Sekerka 1968) considering the growing perturbation in terms of impurity, temperature gradient and interfacial energy.

The newer interface stability theory has been applied to polymer spherulites (Calvert 1983) and found that fibrillar size did vary with diffusion coefficient and growth rate in the same direction as Keith-Padden theory predicted but the variation is markedly less than the change of D/G probably due to the stability effect of interfacial energy.

5.3.1.2. Bassett morphological theory (lamellar divergence)

After extensive morphology studies (see Figure 5.25) of melt crystallized polyethylene with TEM, it was found (Bassett & Hodge 1981b) that lamellae were the major crystal habit inside the spherulites of polyethylene. Spherulites advance by the propagation of first-forming ("dominant") lamellae, which diverge and branch into melt as reported before in fracture surface studies (Geil 1963) and cis-polyisoprene (Edwards & Phillips 1975). Later forming ("subsidiary") lamellae were found to grow from existing dominant lamellae to fill the space between dominant lamellae.

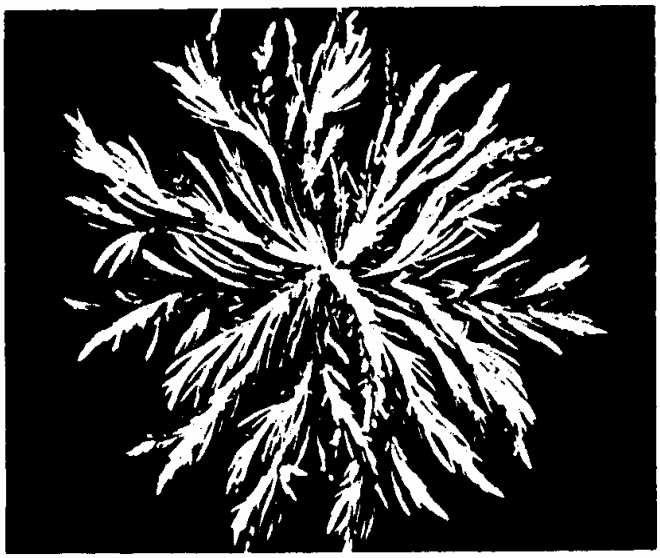

Figure 5.24 Fibrillar structure in spherulite of PP blend.
(Keith & Padden 1964a)

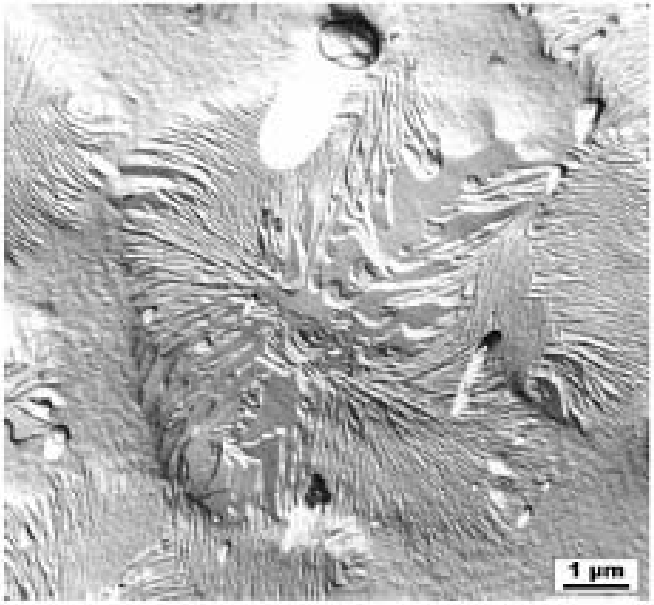

Figure 5.25 Lamellar construction of linear low density polyethylene spherulites.
(Bassett 2003)

Successive divergence of dominant lamellae is believed to generate spherulitic morphology. The branch point could be a giant screw dislocation or direct nucleation. The cause of spherulitic growth was originally proposed as repulsion pressure from cilia (Bassett & Olley 1984), i.e. uncrystallized portions of molecules partly attached to the lamellar surface, then poor packing of rough fold surface was also suggested as additional cause to explain the lamellar divergence in mono-disperse n-alkanes (Hosier et al 2000). It was shown that cellulation was not the cause of spherulitic growth since it could be imposed on normal spherulitic growth at a later stage (Abo el Maaty et al 1998).

5.3.1.3. Considerations from kinetics controlling

The change from spherulitic to axialitic structure was phenomenologically attributed to the reduced branching by Bassett. It was related to the profile change of dominant lamellae from “S” type to ridged or planar with (Bassett & Hodge 1981a, Bassett et al 1981) folding surface, which was explained by the growth front ordering before adding new layer of fold stems (Abo el Maaty & Bassett 2001).

It has been suggested that (Armistead & Hoffman 2002, Hoffman & Miller 1997) axialitic structure corresponded to the kinetics regime I with only one active nucleus on the growth surface and spherulitic structures corresponded to regime II with multiple nuclei on the growth surface, respectively. But the apparent difference of overall shapes between axialites and spherulites appears to imply that probably only one primary nucleation operates in the case of spherulites at high supercoolings whereas one lamella is more likely the precursor of the axialitic and finally elliptical structure.

5.3.2. Crystal structure and crystallinity

5.3.2.1. Effect of comonomer on crystal structure

As have been shown in results, the crystal structures of PA66 and copolymer at high supercoolings do not change significantly from those observed at low supercoolings. Whereas it was found that the crystallinity of PA66/6T copolymers tend to have higher crystallinity values than PA66/6 copolymers, even higher than PA66 polymer. A direct comparison of the X-ray diffraction patterns of those polymers is shown in Figure 5.26.

Two diffraction peaks always exist in all of the polymers, which indicate that inclusion of comonomer does not change triclinic structure. The only important feature is that relatively stronger (010)/(110) peak in PA66/6T, which is probably due to nucleation effect of benzyl ring in the PA66/6T copolymer. The substitute of hexamethyl group with benzyl ring should also stiffen the molecular chain conformation that would reduce the entropy of polymer melt. Therefore, the primary nucleation rate and growth rate should both increase because of this structure change.

In PA66/6 copolymers, contrary to the situation in PA66/6T or PA66/6I copolymers, molecular chains will be more flexible due to the reduced possibility of inter-molecule H-bonding formation, therefore higher entropy of melt is expected. At the same time, the heat of fusion will also be reduced as the result of this structure irregularity. It is therefore expected that nucleation and crystallization rate of PA66/6 will be lower than PA66 homopolymer. The spherulites of PA66/6 copolymers could not be fully developed at higher supercoolings, as demonstrated in optical micrographs.

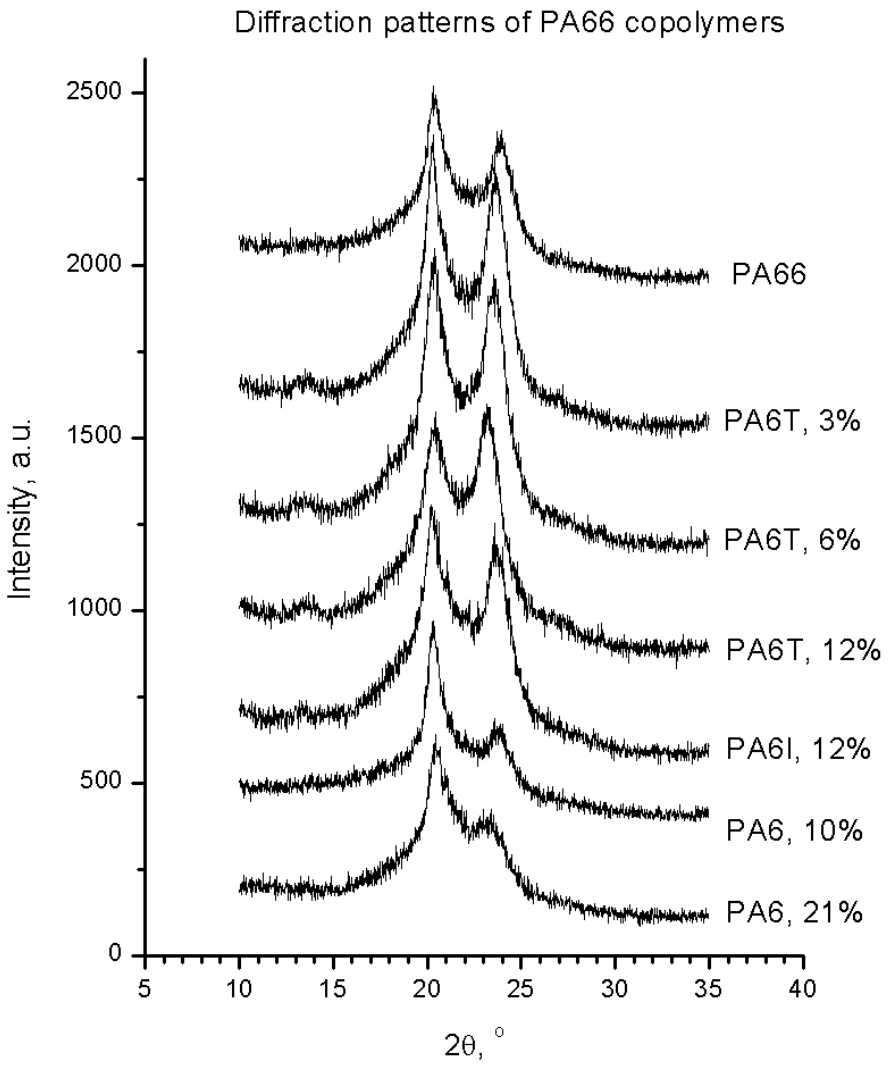

Figure 5.26 Comparison of Wide Angle X-ray Diffraction pattern for PA66 and copolymer prepared with equivalent cooling conditions.

5.3.2.2. Effect of supercooling on crystal structure

It should also be mentioned that the high supercooling does not change the crystal lattice significantly, even though the crystallinity could be changed dramatically with increasing supercoolings, which is generally due to the degree of completion for primary crystallization process. The diffraction angle (2θ) of the copolymers is plotted in Figure 5.27. The (100) diffraction angle, corresponding to chain distance within H-bonding sheets, is clearly constant over all the polymers at different supercoolings. It can be inferred that H-bonding structure is well maintained, which means that this constant distance could be maintained by isomorphism crystallization in PA66/6T copolymers or by exclusion of comonomer (PA6 or PA6I segments) from lamellar crystal in PA66/6 copolymers and PA66/6I copolymers. The (010)/(110) doublet seems to be more sensitive to the copolymer structure and supercoolings, which is probably related to long-order crystal structure perfection whereas (100) diffraction could be related to a short-order structure (say H-bonding between neighboring chains).

5.3.2.3. Comparison of crystallinity from WAXD and DSC

First, it should be mentioned that of percent crystallinity in PA66 usually based on the concept of linear interpolation between completely amorphous and crystalline phases. Density, heat of fusion and X-ray diffraction have commonly been used in the determination of percent crystallinity of polymers. The value of crystallinity in melt crystallized PA66 is usually less than 50% even when it actually shows the similar impinged spherulitic morphology as in polyethylene, which is probably due to the coarse fibrillar structure within the spherulites.

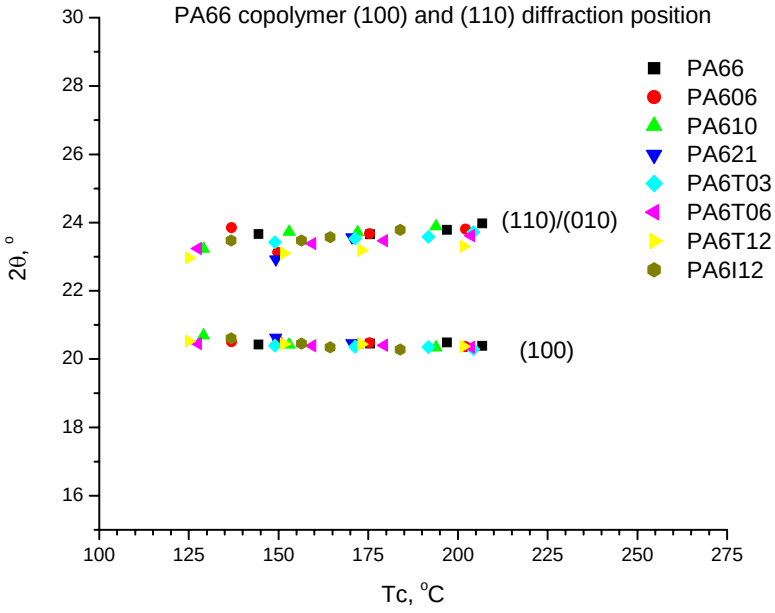

Figure 5.27 The X-ray diffraction peaks of PA66 and copolymers

Ideal density values of amorphous and crystalline phase can be extrapolated from infrared absorption and estimated from unit cell parameters (Starkweather et al 1963). The heat of fusion of 100% crystalline PA66 could be extrapolated from extrapolating experimental values of heat of fusion with density (45 cal/g) (Dole & Wunderlich 1959); estimated form Clapeyron equation through pressure-volume-temperature experiments (45.8 cal/g)(Starkweather et al 1984); or estimated from Gibbs-Thomson equation with melting temperature-lamellar thickness values of single crystal (62 cal/g) (Starkweather et al 1984). X-ray diffraction can give a direct estimate of percent crystallinity with reflection intensity of crystalline phase and amorphous phase, but the peak deconvolution procedure will involve some degree of arbitrariness.

The crystallinity values calculated from DSC and X-ray diffraction are both listed in Table 5.2 for comparison. X-ray diffraction tends to give a higher value for crystals with impinged spherulitic morphology than DSC method.

This could be attributed to the relatively high value of ΔH_f^o (62 cal/g) used here. For quenched PA66/6 structure, DSC gives a much higher crystallinity value while optical morphology and WAXD show highly amorphous structure. There are two possible reasons could explain the abnormal high values from the DSC: 1) heating process could induce crystallization or crystal perfection during DSC experiment; 2) one dimensional structure order (probably due to H-bonding between neighboring chains) exists in the apparent amorphous materials, which could contribute to the melting peak but could not be detected by X-ray diffraction.

Table 5.2 Comparison of crystallinity estimated from WAXD and DSC

Sample	Cool cond. mm/min	Tc °C	Tm °C	ΔH J/g	Xc(DSC) %	Xc(X-ray) %
PA 66	0	206.8	260.74	69.55	27.23	34.96
	10	196.9	260.65	70.86	27.74	32.38
	40	175.5	260.45	67.22	26.32	31.67
	150	144.4	260.89	66.10	25.88	27.04
PA6T03	0	204.3	259.57	72.50	28.39	38.08
	10	191.8	260.47	68.37	26.77	35.81
	40	171.3	260.01	67.89	26.58	35.99
	150	149.0	260.17	66.07	25.87	30.85
PA6T06	0	203.7	259.49	70.88	27.75	39.21
	10	179.4	259.84	67.80	26.55	36.06
	40	159.4	259.39	65.55	25.66	31.47
	150	127.5	259.36	64.17	25.12	24.06
PA6T12	0	201.5	260.01	64.34	25.19	31.06
	10	173.0	260.21	60.33	23.62	25.79
	40	151.5	260.08	58.94	23.08	24.03
	150	125.0	260.12	59.76	23.40	14.01
PA6I12	0	183.9	246.43	51.16	20.03	31.48
	5	164.4	246.82	52.08	20.39	29.03
	10	156.4	246.53	52.19	20.43	26.32
	40	136.8	246.27	57.12	22.36	6.78
PA606	0	202.1	249.16	54.78	21.58	31.23
	10	175.4	248.75	54.52	21.47	29.97
	40	149.8	248.16	56.88	22.41	21.62
	150	136.9	248.35	59.76	23.54	4.53
PA610	0	193.9	245.17	56.49	22.34	30.07
	10	172.0	245.43	53.21	21.04	27.04
	40	153.0	244.81	56.39	22.30	24.73
	150	129.1	243.61	58.16	23.00	7.60
PA621	0	170.5	228.61	50.87	20.34	25.15
	10	149.2	226.34	51.03	20.40	7.73
	40	130.0	226.86	49.44	19.77	0
	150	100.2	228.06	50.77	20.30	0

No matter what is the reason, the X-ray crystallinity seems to give a more accurate representation of three dimensional crystal structures in the samples of PA66 and PA66 copolymer formed at high supercoolings. Since crystallinity is used to account for the content of spherulitic structure because of copolymer structure and supercoolings, no further experimental efforts were carried out to determine the origin of high crystallinity value of DSC method for quenched samples.

It is clearly shown that percent crystallinity determined from X-ray diffraction decreases with increasing supercooling, and this tendency is especially significant for PA66/6I and PA66/6 copolymers. This has been discussed from the standpoint of slow crystallization rate as before. The possible nucleation effect in PA66/6T copolymers is indicated by the higher crystallinity comparing to those of PA66 homopolymer at relatively low supercoolings; while the possible effect on chain diffusion is shown in the lower crystallinity comparing to that of PA66 at higher supercoolings.

5.3.3. Lamellar structure

The lamellar structure of PA66 appears not change at the high supercoolings, the long periods determined from the maximum on Lorentz-corrected intensity profile and one dimensional correlation function are plotted in Figure 5.28 and Figure 5.29, respectively. The long period from isothermally (open symbols) crystallization measured before (Schreiber 1998) were also added for comparison. The long periods are found to slightly decrease with crystallization temperature at low supercooling, then flatten out with further increase of supercooling that is similar to the findings of long period in single crystals from solution crystallization (Hinrichsen 1973, Magill et al 1981).

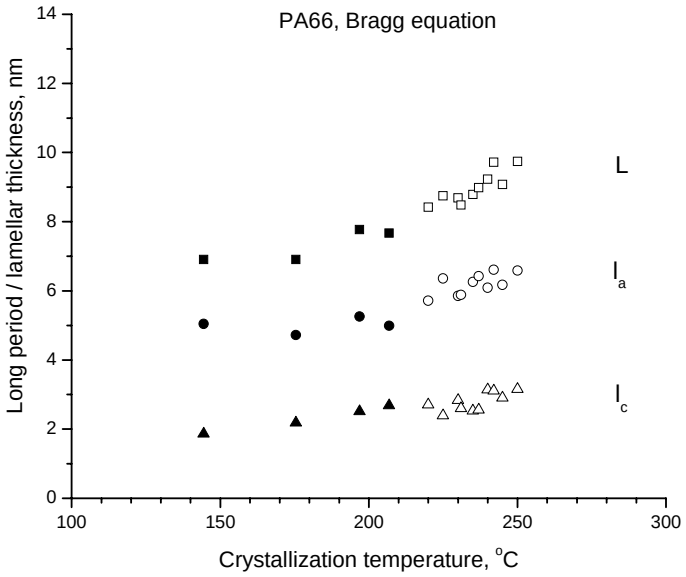

Figure 5.28 Lamellar structure of PA66 derived from Bragg equation.

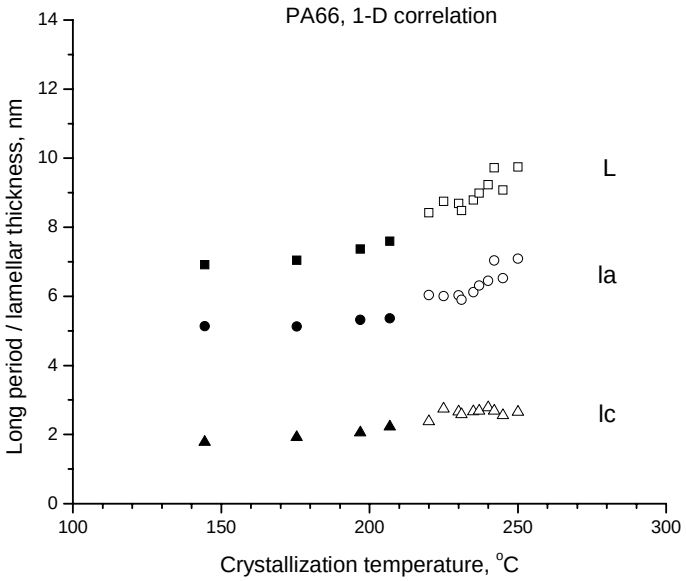

Figure 5.29 Lamellar structure of PA66 derived from 1-D correlation function.

It should be mentioned that long period usually correspond to the lamellar thickness in single crystal mats from solution crystallization (Dreyfuss & Keller 1973, Dreyfuss et al 1972). But in melt crystallization, long periods are usually taken as the distance between neighboring lamellae that include the lamellar thickness and amorphous thickness for two-phase model, or also interfacial layer in three phase model. The long periods of PA66 copolymers are plotted in Figure 5.30.

The copolymer structure does not affect the long periods significantly at the same crystallization temperature. In general, the long periods decrease little with the decreasing crystallization temperature, whose value is in the range of 6-10 nm as reported (Starkweather et al 1963) for the long periods of PA66 samples quenched from melt.

In the case of polymers with high crystallinity like PE and PP, such a model does give accurate estimate of the lamellar thickness that is consistent with lamellar thickness obtained from TEM and Raman.But in low crystallinity polymer like PET and PA66, the legitimacy of such a model is in question since it is well known that lamella are generally found widely separated from each other with significant amount of amorphous phase filling the space.

Finally, it should be mentioned that 1-D correlation function is also useful to determine the *electron density difference* ($\Delta\eta$) between crystalline phase and amorphous phase in addition to the lamellar thickness. Extensive studies had been conducted on the effect of comonomer structure and crystallization temperature on SAXS morphology of PA66 and its copolymers (Schreiber 1998).

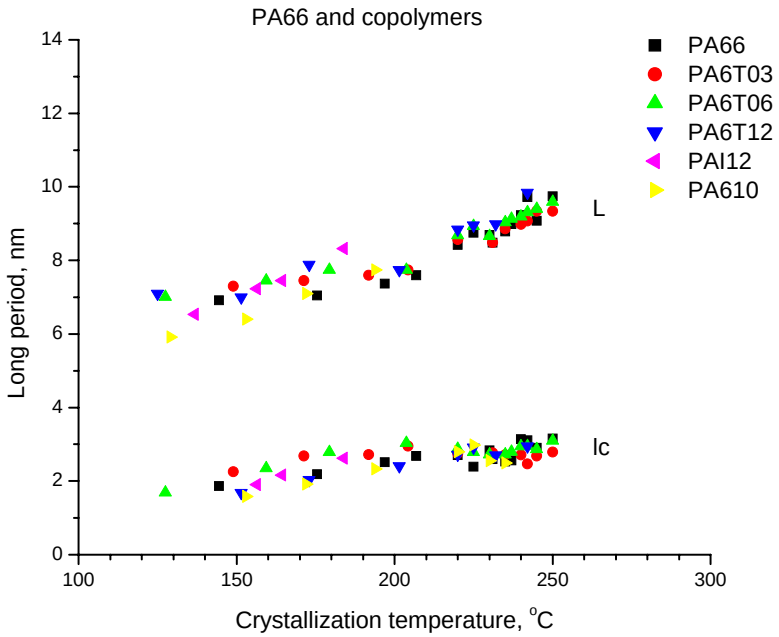

Figure 5.30 Long periods and lamellar thickness of PA66 copolymers.

In general, all copolymer, especially PA66/6I copolymer, had lower electron density difference comparing to PA66 homopolymer due to the increasing content of amorphous phase as well as the increasing perturbing effect of comonomer on H-bonding. Quenched samples usually had lower electron density difference than samples from isothermal crystallization at low supercoolings.

5.4. Melting behavior

5.4.1. Effect of comonomer on the final melting temperatures

It will be helpful to address the effect of copolymer content on the final melting temperatures in PA66 copolymers before discussing the effect of supercooling. It has been reported that the final melting temperature are relatively constant over a wide range of supercooling even though the magnitude of the final melting peaks decreases somehow with increasing supercoolings (Schreiber 1998).

Such phenomena have also been observed in the melting of crystals formed at high supercooling ranges for PA66 and its copolymers, as reported in the section of results. This is probably due to the complex crystalline transformation unavoidable during the heating of PA66 crystals.

When these constant melting temperatures are plotted versus the molar content of comonomer, as shown in Figure 5.31 it clearly shows that the PA66/6T copolymers have a relatively constant melting temperature independent of comonomer content while the PA66/6I and PA66/6 copolymer decrease linearly with the increasing content of comonomer.

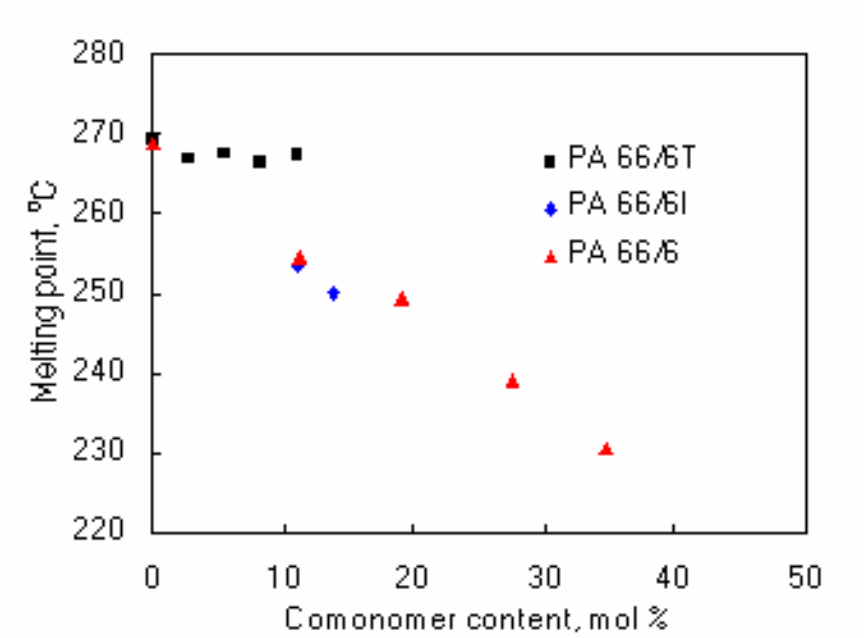

Figure 5.31 Melting point of as received PA66 copolymers versus comonomer content.

The different melting temperature dependence on comonomer content has been attributed to the isomorphism of PA66/6T copolymers; and attributed to the conventional exclusion mechanism of PA6 and PA6I segments from the PA66 crystal core by Schreiber. It is interesting to notice that PA66/6I and PA6I seems to follow the same linear relationship, which might imply that their melting temperatures could both be related to the average sequence length of crystallizable PA66 as described by the Flory melting temperature equations.

5.4.2. Crystallization temperature on melting temperatures

It seems clear that final melting points can be well explained with the existing theory. However, it is not the case on the issue of supercooling dependence of PA66 and copolymers. Apparently, only one melting peak can be observed in the melting curves of

PA66 and copolymers, which is in contrast to the increase of melting temperature with crystallization temperature usually observed in polyethylene. The obvious asymmetric shape and occasional endothermic transition in melting curves also seems to imply that melting process involves more than a simple mechanism. Therefore, it was determined that it should be helpful to elucidate the melting process of PA66 and copolymer with the additional studying on the melting behavior for crystals from lower supercoolings.

The melting behavior of PA66, PA6T06, PA6T12, PA6I12 and PA610 are shown in Figure 5.32, Figure 5.33, Figure 5.34, Figure 5.35 and Figure 5.36, respectively.

5.4.2.1. Asymmetric single peak at low Tc (Tc < 220^{o}C)

At the range of high supercoolings, only one peak is shown in the melting process of PA 66 and copolymers. Both isothermal crystallization (Schreiber 1998)and rapid cooling methods of this study were shown to be able to produce only single melting peak with a constant peak position. However, the single peak does not necessarily imply a simple crystal structure or melting process. The single peak is asymmetric with a large tail at lower temperature side, and a distinct shoulder can be observed at samples crystallized from very low Tc (144 ^{o}C of PA66).

Another feature that needs to be mentioned is the sharp edge of the single peak at the high temperature side. Therefore, it is possible that more than one peak overlapping into the asymmetric single peak. This asymmetric single peak could be explained with to a metastable crystal structure formed after melting original crystals during the heating process in DSC or existence of different crystal thickness population.

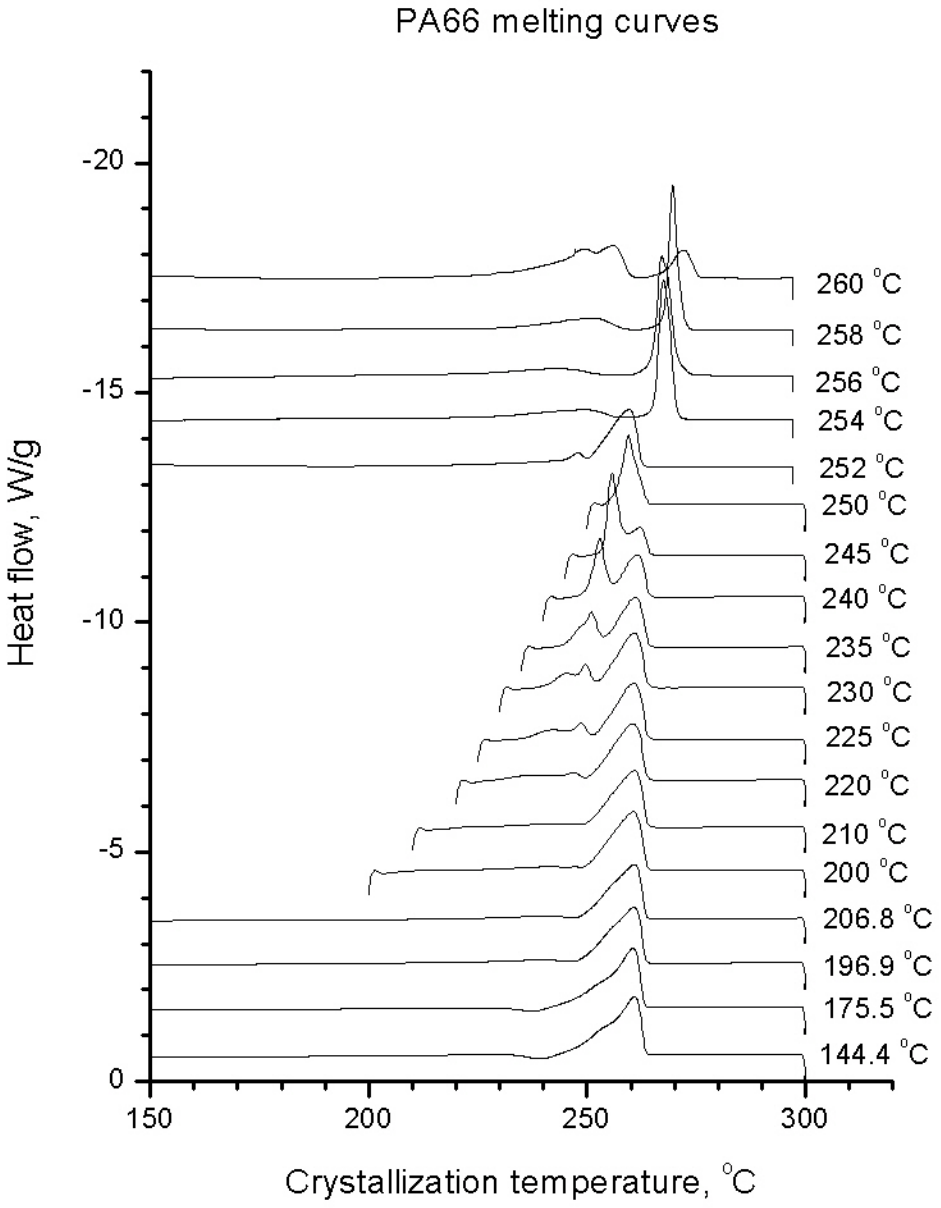

Figure 5.32 Melting temperatures of PA 66 prepared at different crystallization temperatures.

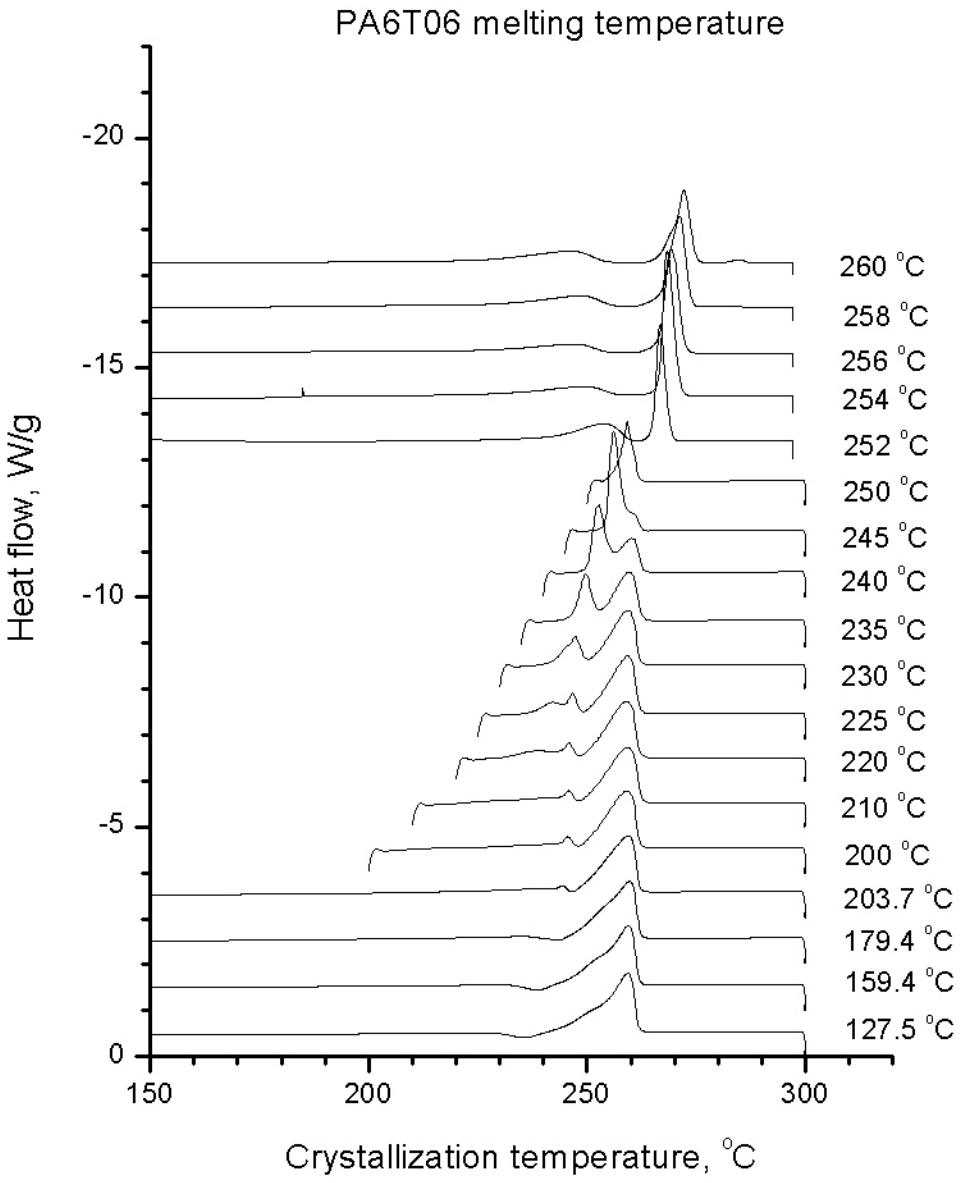

Figure 5.33 Melting temperatures of PA 6T06 prepared at different crystallization temperatures.

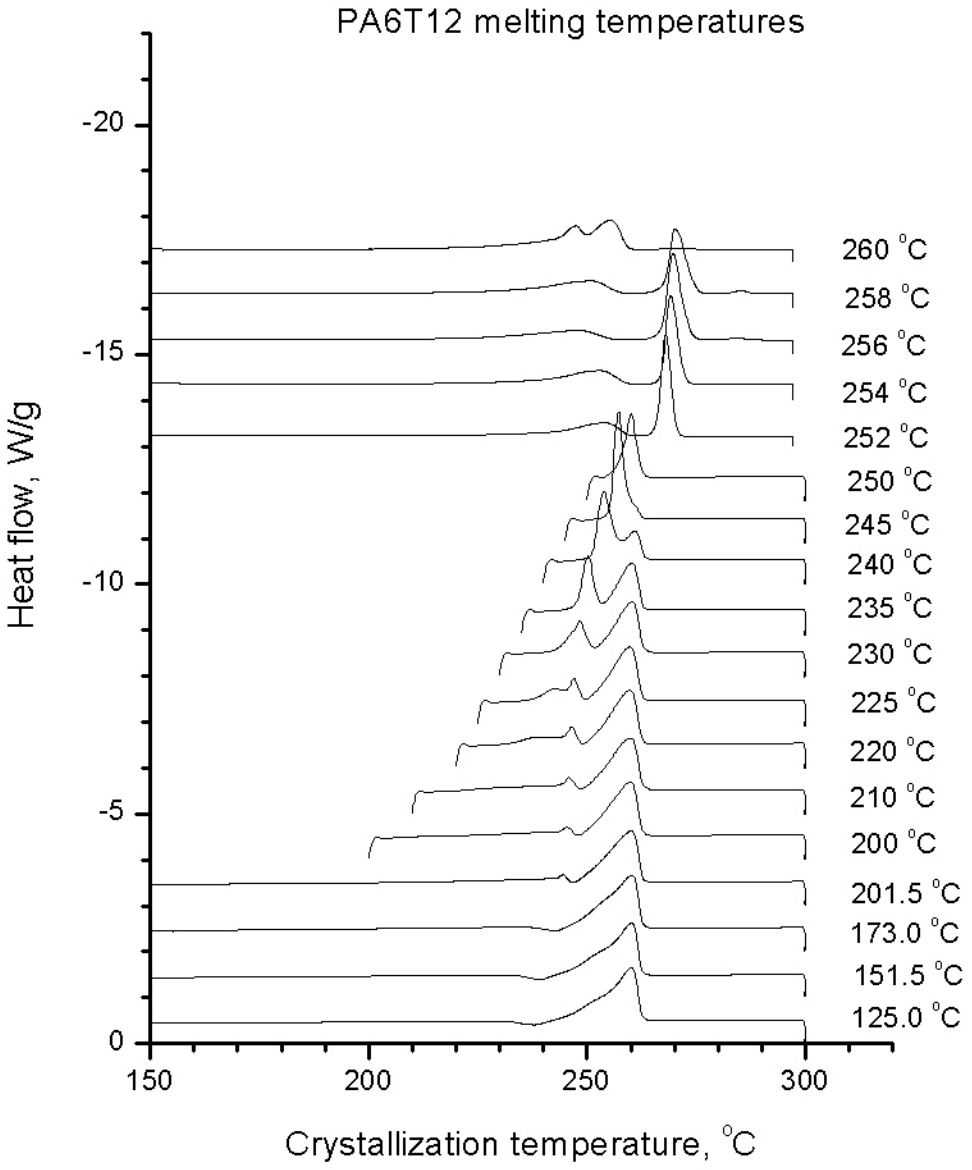

Figure 5.34 Melting temperatures of PA 6T12 prepared at different crystallization temperatures.

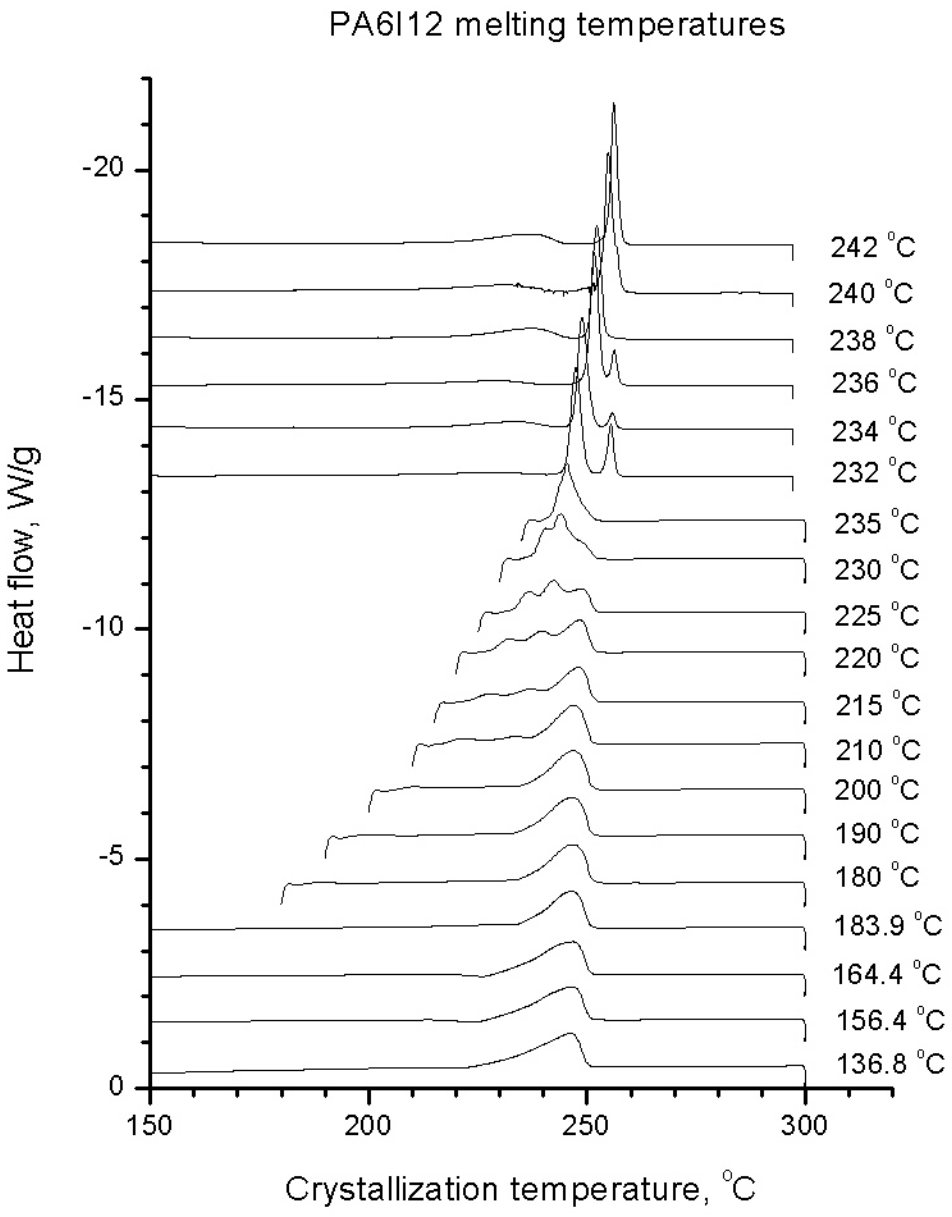

Figure 5.35 Melting temperatures of PA 6I12 prepared at different crystallization temperatures.

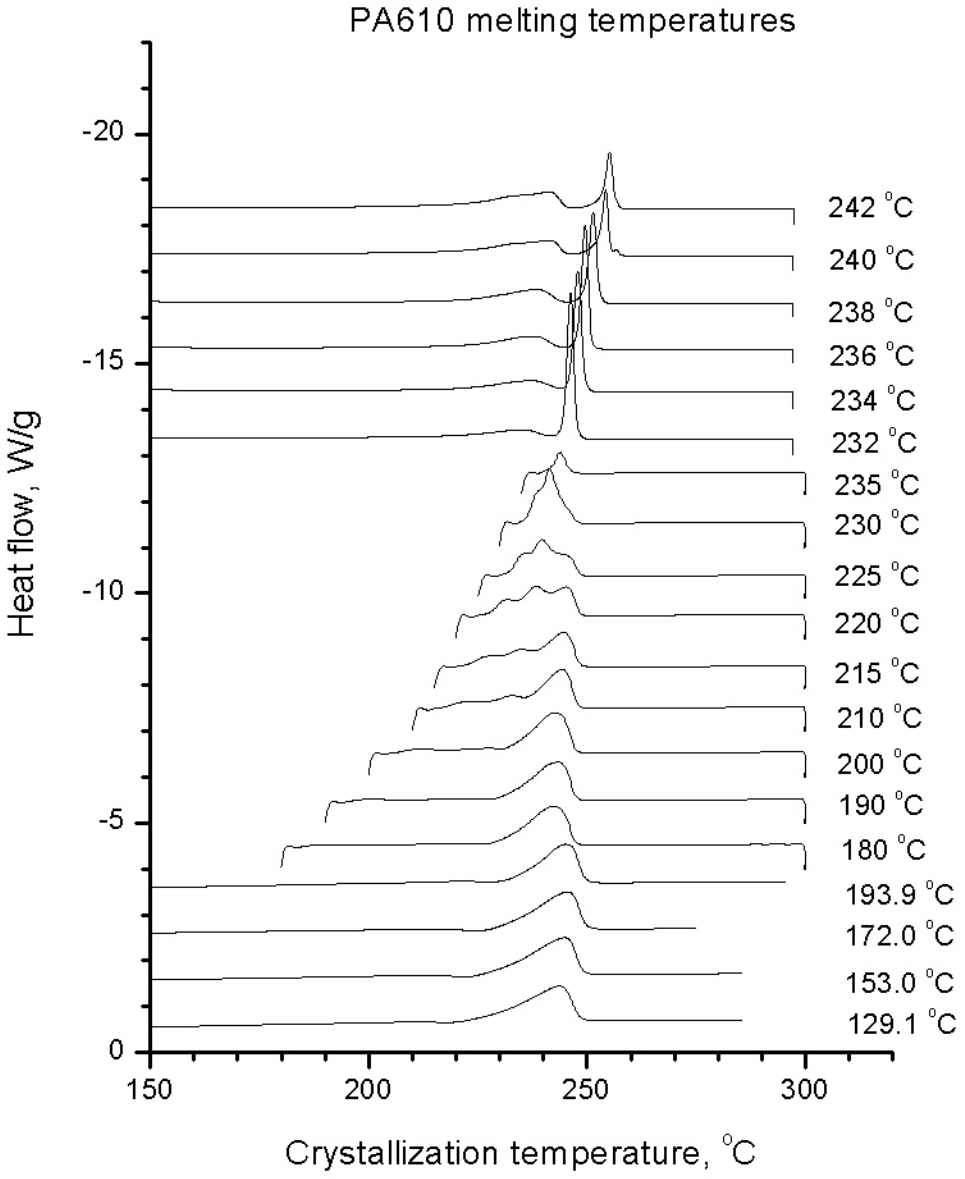

Figure 5.36 Melting temperatures of PA 66 prepared at different crystallization temperatures.

As to the possible recrystallization mechanism, it should be pointed out that no spherulitic structure change, i.e. apparent spherulite growth as normal in old crystallization of PET, is observed in the heating process of quenched PA66/6 copolymer and similar observation has been reported recently in PA 6 (Medellin-Rodriguez et al 2004). Then it is reasonable to attribute this recrystallization process (or reorganization process) to a perfection process such as H-bonding structure optimizing and lamella thickening process.

As to the isothermal crystallization in DSC, exceptional caution is required on the "isothermal" crystallization temperature. Since polymers can finish the primary crystallization process, as observed in the spherulitic growth process with optical microscopy, during the temperature jump process before reaching the nominal crystallization temperature. This process is demonstrated by a series of experiments on PP (Ding & Spruiell 1997), PE (Wagner & Phillips 2001)and PA 66 at high supercooling.

With this caution in the mind, the dynamic cooling process could be responsible for the primary crystallization, the following isothermal process might only facilitate the secondary crystallization, and annealing in the situation of low Tc. Consequently, these separate processes might be capable to produce different melting temperatures.

5.4.2.2. Typical multiple melting peaks ($220^{o}C<Tc<250\ ^{o}C$)

This temperature range is easily accessible with DSC, and the most well recognized feature is that the melting process has three discernible melting peaks. The first melting peak is ubiquitously observed about 10 ^{o}C above the corresponding

crystallization temperature, therefore it is attributed to melting of crystal structure produced in the annealing process and called as annealing peak (Stouffer et al 1996). A second melting peak first shows up around 220 ^{o}C, whose temperature and magnitude gradually increase with crystallization temperature at the expense of the third peak. It is believed that this peak should be corresponded to the melting process of originally formed crystal structure, therefore it is often taken as the real melting temperature and the peak called as crystallization peak. The third peaks always has a constant peak temperature and are usually believed to be the melting process of metastable crystal structure formed after recrystallization of the original crystal, and it is called as recrystallization peak.

Recently, the melting behavior of PA 6 was considered to be counted for with a step-like mechanism similar as in PET and PEEK (Medellin-Rodriguez et al 2004). The second melting peak was proposed to relate to the secondary crystal. Since the melting processes directly followed with the isothermal crystallization process in DSC, we can confidently exclude secondary crystallization during cooling to room temperature from the possible cause of this secondary crystal.

During the isothermal growth under optical microscopy, for PA 66 spherulites, especially axialites at higher temperature usually show fibrillar structure. The spacing filling process can be clearly observed to follow behind the growth front in the isothermal crystallization. This secondary crystal is probably the “daughter lamella” inserted between the “dominant lamella”, as described by Bassett (Bassett & Hodge 1981b) derived from electron microscopy study. It is therefore possible that isothermal

crystallization itself could produce two types of lamellar crystal with different lamellar thickness.

Therefore, one can relate the second peak and third peak to the subsidiary lamella (daughter lamella) and dominant lamella (mother lamella), respectively. The decreasing intensity of third melting peak can be explained by the decreasing content of primary lamella at increasing crystallization temperature, which is phenomenologically consistent with increasingly open fibrillar structure observed in optical microscopy. Actually this explanation seems also make sense of the rough surface like kinetics and constant lamellar thickness.

However, if the highest meting peak is related to the dominant lamella, another question arise on the constant value of this melting peak: why does the melting temperature does not change with the crystallization temperature at high supercoolings? Will it change with Tc at higher supercooling? The melting studies of a series of negative spherulites of PA 66 copolymer probably could give some hints on these questions.

5.4.2.3. Increasing single peak of negative spherulites (250<Tc<262 ^{o}C)

Optically negative and positive spherulites in polyamides were first reported in PA 610 (Brenschede 1949), negative spherulites in PA 66 were prepared later (Boasson & Woestenenk 1956). The different birefringence under polarized microscope can be accounted for by the spherically symmetrical arrangement of uniaxial index ellipsoids (Keller 1959): spherulite shows positive birefringence when the larger refraction index is in the radial direction; shows negative birefringence when the larger refraction index is in

the tangential direction. The comprehensive work of Magill (Magill 1966) and Khoury (Khoury 1958) summarized the formation of four different types of spherulites. It was found (Ramesh et al 1994b) that the highest melting peak of negative spherulites (Tc>250 °C) actually increased with the crystallization temperature in contrast to the constant melting peak of positive spherulites at lower crystallization temperature (Tc<250 °C).

As shown in Figure 5.32, the melting temperature increases with the negative spherulites forming temperature as reported (Ramesh et al 1994b). This transition is also confirmed in melting curves of all the type of copolymers; see Figure 5.33 and Figure 5.34 for details. This transition always occurs at the same temperature of 250^{o}C as PA 66 for PA 66/6T (both 6% and 12%) copolymer.

However, the transition is at the lower temperature (around 232 ^{o}C) for PA 66/6I copolymer. For PA66/6 copolymers, melting temperatures of negative spherulites also increase with the crystallization temperature but the beginning of this transition occurs at 232 ^{o}C. It is interesting to notice that the positive-negative spherulite transition temperature is about 10 degrees below the constant melting peak temperature of positive spherulite for each polymer.

Another salient feature is that the Tm-Tc plot is almost parallel to the equilibrium Tm=Tc line, see Figure 5.37 and Figure 5.38, as found for the annealing peak, i.e. the first peak of the positive spherulites. This similarity might suggest that negative spherulites should be related to annealing process (or thickening process) in the melt at high temperature.

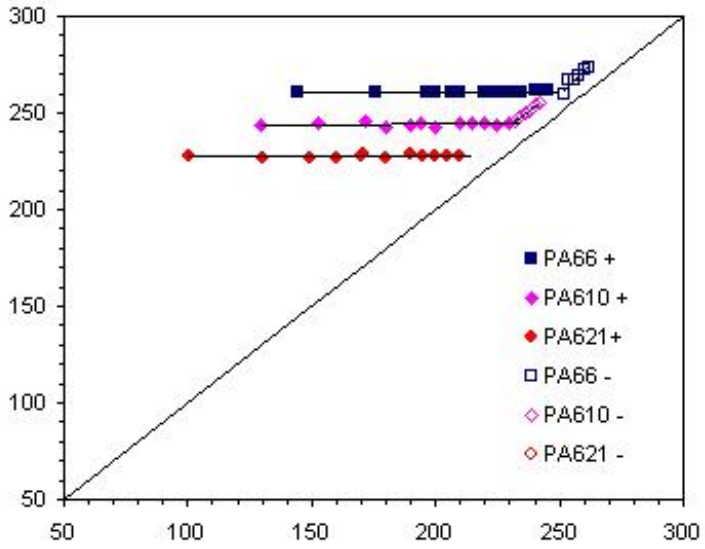

Figure 5.37 Increasing of Tm in negative spherulites of PA66/6 copolymers

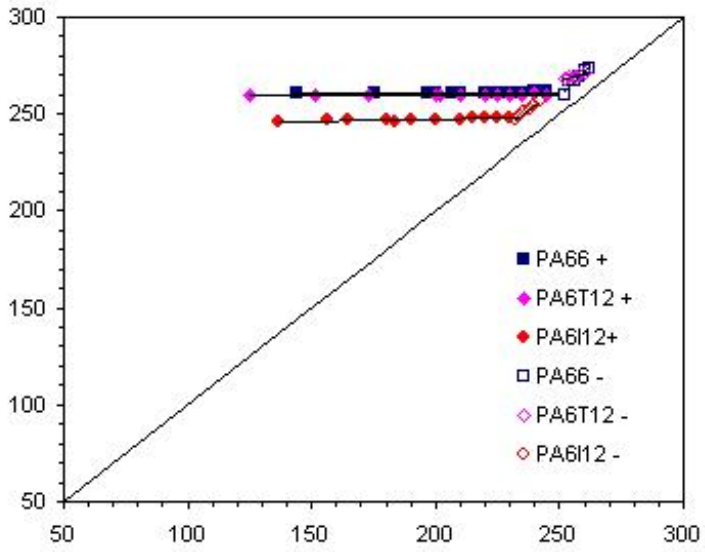

Figure 5.38 Increasing of Tm in negative spherulites of PA66/6T and PA66/6I copolymers

It is well known that residual crystal structure from positive spherulites still exist in the melt before the negative spherulite growth (Ramesh et al 1994a), as well as suggested by IR studies (Garcia & Starkweather 1985). This annealing process is probably analogous to the transition of folded chain conformation to more extended chain conformation by chain unfolding and refolding process.

This conformation change of PA 66 at high temperature is very possible based on following arguments: 1). lamella thickening is well recognized in polyethylene by c-axis diffusion; 2). thickening of PA 66 single crystal has been noticed a long time ago (Hinrichsen 1973, Magill et al 1981). 3). Constant folding length in PA66 is possible due to the difficulty of chain diffusion from the pinning of H-bond at lower temperature. 4). H-bonding is just a physically dynamic crosslinking between polymer chains in contrast to a chemical crosslinking.

From the study of PA 66 chain dynamic by NMR, librational motion of methylene segments is very strong from the Brill transition temperature (Hirschinger et al 1990). Breaking-making process of H-bonding is possible to allow the chain diffusion due to the weakening H-bond force due to the increasing chain distance.

However, this dynamic process could be too fast to be observed with IR. Thickening process should occur in the crystal since there is also low melting peak below 250 °C during cooling, as seen in Figure 5.32, before the negative spherulites impinged with each other.

5.4.3. Hoffman-Weeks analysis

The second melting temperatures were found to increase with crystallization. Occasionally, they were used to estimate the equilibrium melting temperature of PA66 with Hoffman-Weeks plot (Schreiber 1998, Stouffer et al 1996).

When the melting temperatures were extrapolated to intercept with $T_m=T_c$, there equilibrium melting temperature were determined as 264.15 ^oC, 250.79 ^oC and 240.58 ^oC for PA 66, PA 610 and PA 621, respectively.

These values are just slightly higher than the highest melting temperatures, which are generally found constant for each polymer. However, obviously, these temperatures could not mean the equilibrium melting temperature of PA 66 lamellar crystal with infinite lamellar thickness, as the original Hoffman-weeks equation represents in polyethylene. First, melting temperature as high as 270 ^oC has been reported for the lamella from solution crystallization. Secondly, from the results of Ramesh et al and this study on the melting behavior of negative spherulites, the melting temperature of PA 66 negative spherulites can increase to as high as 284 ^oC.

It should be emphasized that the failure of Hoffman-weeks in giving a reasonable Tm^o in this situation does not discredit its reliability in other polymers; whereas lingering ambiguity on the physical meaning of melting behavior in PA 66 is the real cause for the misuse of this effective tool. The melting peak temperatures of positive spherulites are shown in Figure 5.39 (PA66), Figure 5.40 (PA6T06), Figure 5.41 (PA6T12), Figure 5.42 (PA6I12), Figure 5.43 (PA610) and Figure 5.44 (PA621).

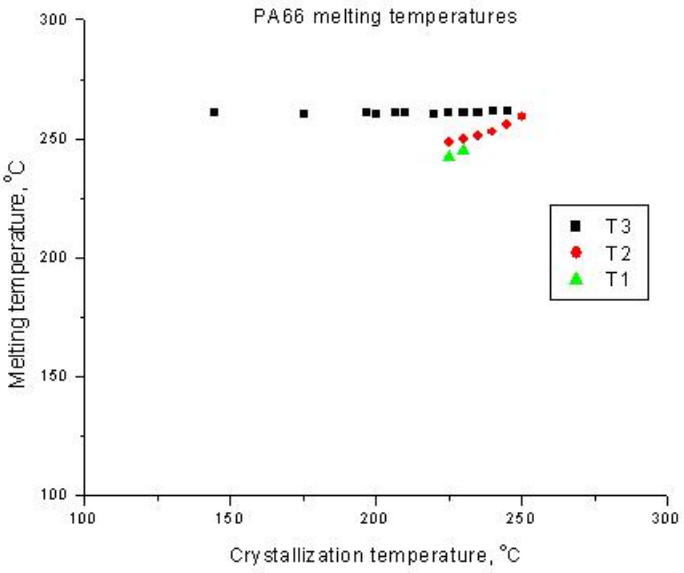

Figure 5.39 Hoffman-weeks analysis of PA66 over a wide rang of crystallization temperature.

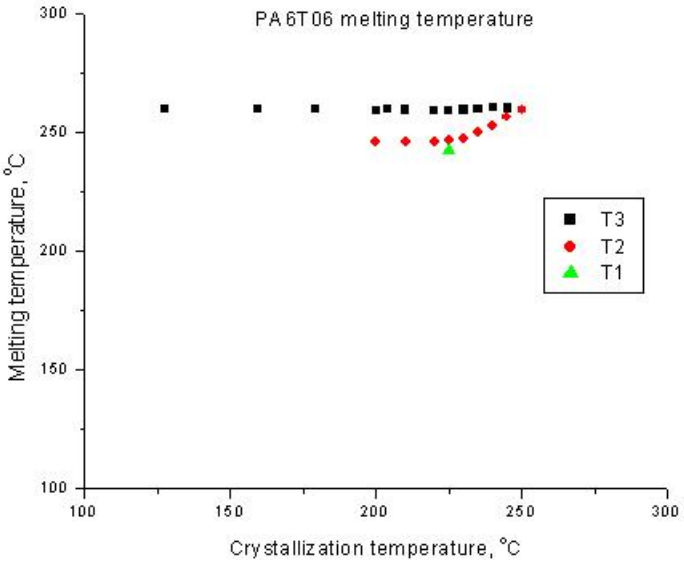

Figure 5.40 Hoffman-weeks analysis of PA6T06 over a wide rang of crystallization temperature.

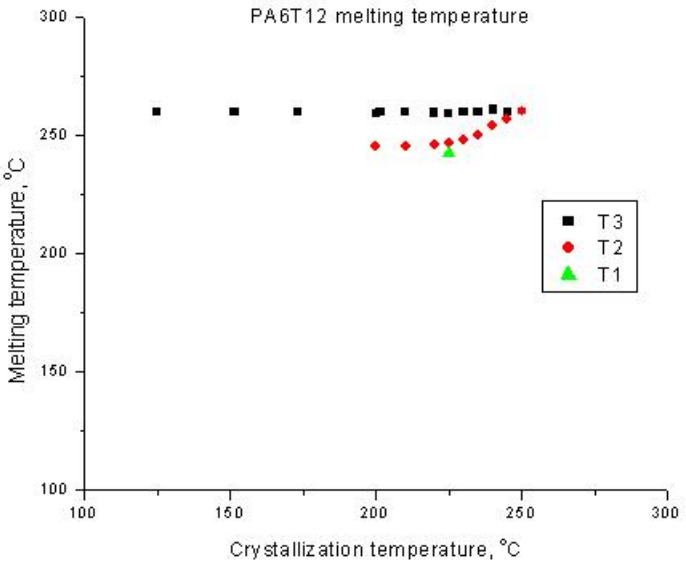

Figure 5.41 Hoffman-weeks analysis of PA6T12 over a wide rang of crystallization temperature.

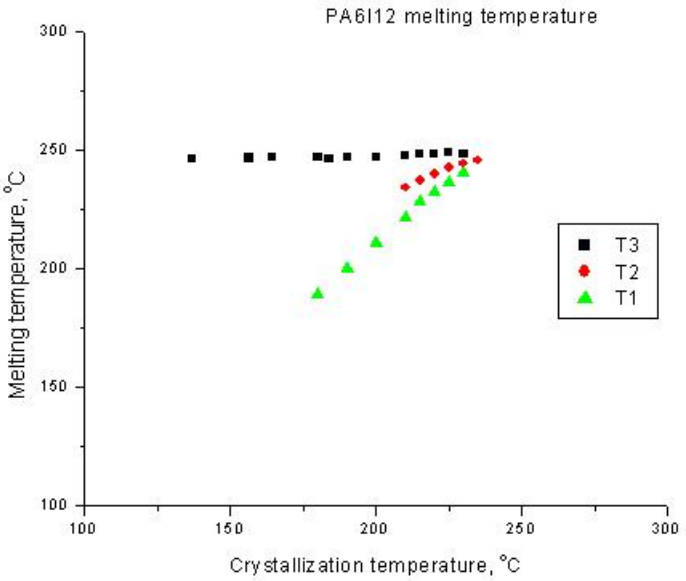

Figure 5.42 Hoffman-weeks analysis of PA6I12 over a wide rang of crystallization temperature.

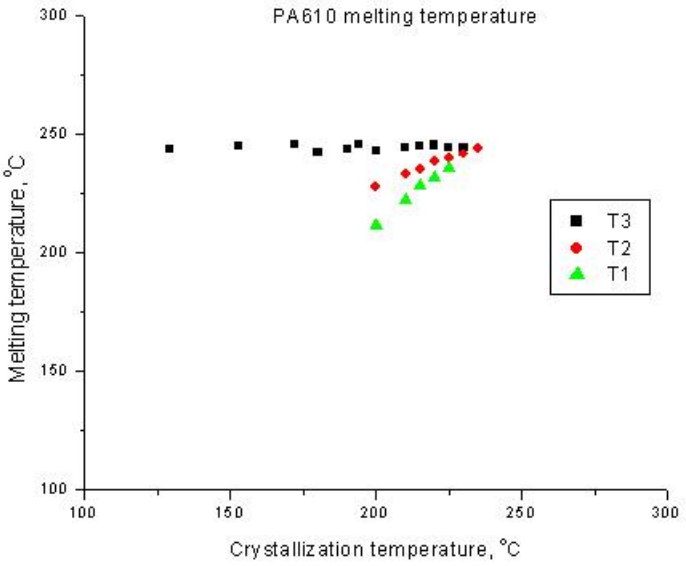

Figure 5.43 Hoffman-weeks analysis of PA610 over a wide rang of crystallization temperature.

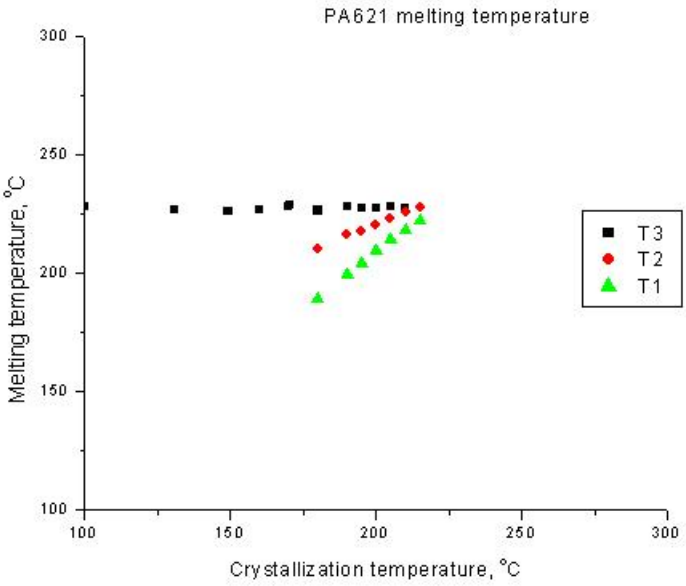

Figure 5.44 Hoffman-weeks analysis of PA621 over a wide rang of crystallization temperature.

It is clearly shown that all of the melting points appear to merge at the specific constant melting temperature with the increasing of crystallization temperature. Therefore, it is possible that the second melting point as well as the lamellar thickness only represent the relative degree of perfection.

5.4.4. Lamellar thickness and melting temperatures

5.4.4.1. Lamellar thickness

If there are at least two different types of lamella formed at isothermal crystallization, as suggested from the spherulitic morphology (Bassett & Hodge 1981b) and melting behavior (Medellin-Rodriguez et al 2004). It is possible that annealing structure also occurs when the crystal is cooling down to room temperature. At different crystallization temperature, the change of relative population will further complicate the situation in melting process of PA66.

Unfortunately, SAXS could only give an estimate of average lamellar thickness in such a complex crystal system. Due to generally high content of secondary lamella develop behind the growth front, therefore SAXS is expected to give an estimate of l_c close to the secondary lamella rather than the primary crystal, which relate the kinetics of spherulite growth.

Some annealing effect may exist during the isothermal crystallization, which is probably responsible for the higher lamellar thickness. The extensive SAXS study of Schreiber found that the lamellar thickness is relatively constant with about 2 repeat units (long period about 6-7 repeat units). It is also found that Gibbs-Thompson relationship

still hold between the changing lamellar core thickness and the second melting peak temperatures.

5.4.5. Hypothesis of crystallization with constant folding length

If we assume that the third melting peak is the melting peak of dominant crystal formed at the stage of morphology development, the constant melting temperature implies constant lamellar thickness of primary crystals over a wide range of supercoolings, which in turn implies constant folding length during the crystallization process of PA66.

Constant folding length has been reported (Dreyfuss & Keller 1973) to be constant (4 repeat units) over a wide range of crystallization temperatures in solution crystallization of nylon 66. It was further found that the constant folding length is different in different solution and consistent with the Gibbs-Thompson equation. Corresponding to constant melting temperature of 262 ^{o}C in PA66, a constant fold length of 5 repeat units (67.5 Å) is expected.

The major features of these melting mechanism are listed in Table 5.3.

5.4.6. Controlling factors of melting temperatures in PA66 and its copolymers

5.4.6.1. H-bonding (comonomer type)

H-bonding is the most dominant factor affecting the melting temperature of PA66. Without H-bonding the melting temperature of methylene segment will possess a melting temperature as low as polyethylene (about 142 °C).

Table 5.3 Comparison of melting mechanisms proposed in polyamides

Spherulitic Morphology	Melting peak	Recrystallization (reorganization) Mechanism	Step-like melting of morphology	Lamella thickness distribution	Constant Folding length
Positive spherulite (Tc<250 °C)	1st Peak	Annealing in amorphous phase	Annealed structure	Short-range order of H-bond (1 r.u.)	Annealing in amorphous
	2nd Peak	Original lamella	Secondary lamella	Lamella core (2 r.u.)	Ordered core within folding
	Constant Tm peak	Reorganized metastable crystal	Dominant lamella	Lamella thickness (5 r.u.)	Breakup of constant folding length of 5 r.u.
Negative spherulite (250<Tc<264 °C)	Increasing Tm peak			Lamella Thickening	Folding length beyond 5 r.u.

5.4.6.2. Average sequence length of PA66 (comonomer content)

For the copolymer with comonomer capable of disturbing the H-bonding, decreasing average sequence length of PA66 will reduce the melting temperature significantly. However, for PA66/6T copolymer the average sequence length has little effect on the melting temperature probably due to the integrity of the H-bonding in these copolymers as in PA 66 homopolymer.

5.4.6.3. Chain folding length at different supercooling (crystallization temperature)

The melting behavior of PA66 copolymer changes dramatically with the crystallization temperature. Understanding of chain folding process in PA66 at different crystallization condition is helpful to put the melting behavior of PA66 into perspective.

For the crystallization below 250 °C (positive spherulites range), the crystallization process involves adding crystal stem at constant stem length, which is probably related to persistence length in the melt. The resulting lamellar structure keeps constant folding length over a wide range of crystallization conditions.

On the one hand, shorter folding length will apply additional tension on the folds; on the other hand, longer folding length requires enough chain mobility to fulfill the unfold–refold process. Therefore folding length is kept constant from the consideration of minimum free energy. It would be expected that folding length of PE could exist in a very wide range due to its high chain flexibility to easily folding and much higher mobility without the restriction of H-bonding.

Nevertheless, the degree of order inside the folding might be different due to the different relative content of dominant lamellae and secondary lamellae as well as the condition allowed for further perfection.

At high crystallization temperature, the content of dominant lamellae is lower; perfection capability is high due to the weakening H-bonding between polymer chains. At lower crystallization, the relative content of dominant lamella is higher, which is manifested by the dense fibrillar spherulitic structure, but the annealing ability is restricted by the restricted chain mobility.

The melting process could be explained as step-like process corresponding to the crystal morphology: first melting peak is due to the crystal structure produced by annealing, which are formed chains that are not crystallized during morphology forming (by dominant lamellae) and following space filling (by secondary lamella).

The second melting peak is corresponding to the melting of secondary lamella formed behind the growth front. While the third melting peak is the result of the melting of dominant crystals, which are of metastable lamellar structure probably with folding length of 5 repeat units.

For the negative spherulites, dense spherulitic structures imply very low content of secondary lamellae. Lamellar folding length exceeds the constant length of 5 repeat units due to annealing and thickening process. The melting process of lamellar thickness will directly lead to the breakup of lamellar structure.

5.5. Relaxation behavior

5.5.1. Relaxation behavior of PE copolymers

5.5.1.1. Effect of branch content on the relaxation temperatures

The relaxation temperatures from deconvolution of iso-choral (equal frequency) experiments were plotted vs. the comonomer content to show the changing of the temperatures with the branch content, melting temperatures (T_m) from DSC were also added for comparison (Figure 5.45a).

All of the relaxation temperatures were found to decrease with the increasing branching content. It appears that tanδ curves produce higher relaxation temperatures than those of E" curves for the same relaxation.

Due to the dramatic change of loss modulus (several decades in magnitude) with temperature, it was difficult to separate the relaxation by fitting loss modulus curves, therefore only the major loss peak could be accurately determined (see Figure 5.45b).

Since the relaxation temperature of LPE and L04 are much higher (about 50 ^oC) than that of the other copolymers with higher branch content, it is concluded that the major relaxation should be $\alpha 1$ relaxation in LPE and L04, but β relaxation in the copolymer with higher branch content.

This seems reasonable from the modest increase of β relaxation temperature at higher branch content, which is also confirmed by the significantly different activation energies.

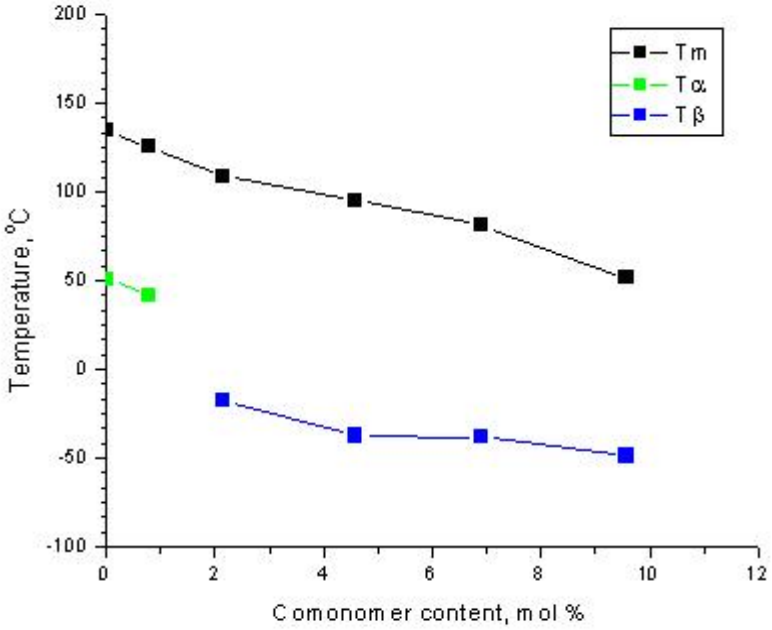

(a)

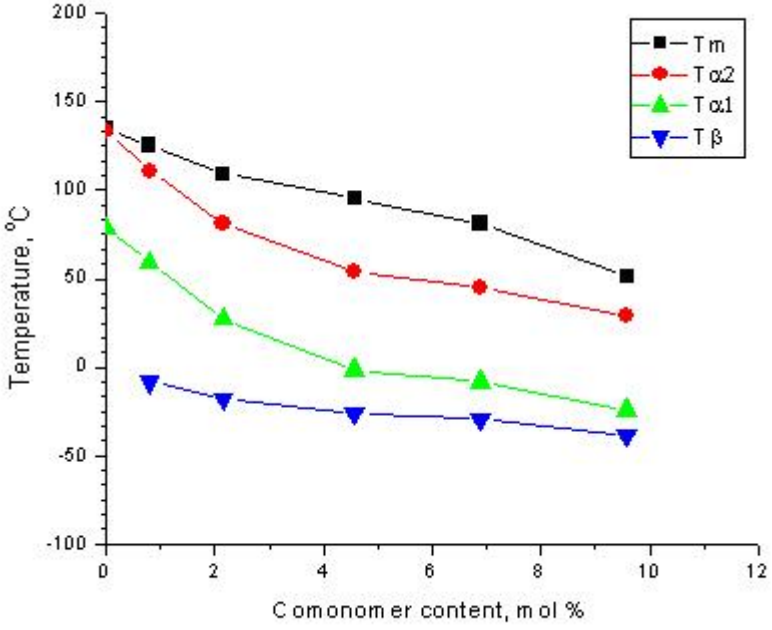

(b)

Figure 5.45 Relaxation temperature of polyethylenes determined: (a) from loss modulus curves (E’’); (b) from loss factor curves (Tanδ).

Loss factor curve (Tan δ) can be easily deconvoluted to different components probably because it could provide a horizontal baseline by representing the ratio of loss modulus to the storage modulus (see Figure 5.45b). Actually it was suggested (Stachurski & Ward 1969) that Tan δ should be preferred to E" or S_{33}" in assigning the relaxations temperature due to the consideration of phase structure in isotropic crystalline polymer.

The results of relaxation temperature, from the loss factor curves deconvolution, are consistent with that determined from loss modulus curves and provide more details on the α relaxations due to the feasibility of deconvolution. β relaxation temperatures of copolymers were found to increase linearly from –36.7 ^{o}C to –8.5 ^{o}C with the decreasing branch content, which is consistent with results of branched polyethylenes (Willbourn 1958) and recent results of homogeneous ethylene copolymers (Clas et al 1987).

This could be explained from the increasing restraints effect of crystalline phase on the β relaxations of amorphous phase as Boyd proposed (Boyd 1985a, Boyd 1985b). It should be noticed that β relaxation temperatures in chlorinated low density polyethylenes decrease first then increases rapidly due to the two effect of chlorine on the relaxations (McCrum et al 1967, Schmieder & Wolf 1953).

The relaxation behavior is first dominated by steric effect of chlorine similar as methyl group which decreases Tg, then dominated by the dipolar interaction between C-Cl dipoles which can increase Tg. Similar results were reported (Nielsen 1960) on the copolymer of ethylene and vinyl acetate.

The α relaxation temperature was found to decrease with increasing branch content. The decrease is more significant at the low branch content than at the high branch content.

It is interesting that a transition of spherulitic morphologies from fully impinged spherulites to isolated crystals is observed at L24. It is possible that this morphology transition correlated to the transition from α dominant relaxation to β dominant relaxation.

5.5.1.2. Effect of supercoolings on the dynamic mechanical properties

To discuss the effect of crystallinity and lamellar thickness on the dynamic mechanical properties, the relaxation temperatures were plotted vs. crystallinity and lamellar thickness (see Figure 5.46), respectively.

Basically crystallinity and lamellar thickness have similar effect on the relaxation temperatures for each polymer, but lamellar thickness is more likely to be the cause of the change in relaxation temperatures, as reported (Popli et al 1984).

5.5.1.3. Assignment of relaxations and the molecular origins

After review of the relaxation temperatures and activation energies of a full spectrum of dynamic mechanical behavior, some comments on the assignment of the β, α_1, and α_2 relaxation are meaningful, which are also the motivations to check dynamic mechanical behavior of a series of structures regular metallocene polyethylene copolymers.

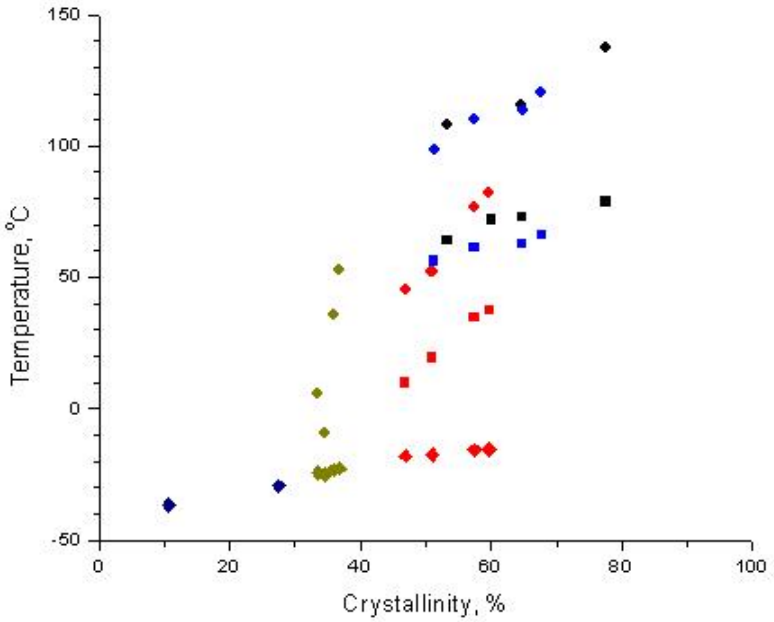

(a)

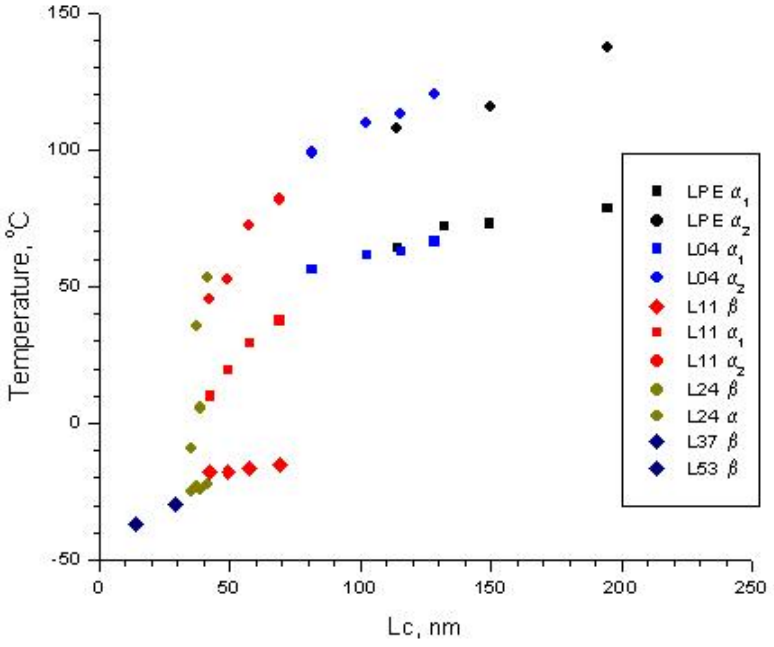

(b)

Figure 5.46 Dynamic mechanical relaxation temperatures of PE copolymers plotted with: (a) Crystallinity; (b) Lamellar thickness

β relaxation: The continuous decreasing of intensity and slightly increasing relaxation temperatures as shown in Figure 5.45, confirmed that β relaxation could be traced from completely amorphous phase to fairly detectable β relaxation in linear polyethylenes (Boyd 1985a). The experimental results seem to lend support to the assignment of β relaxation to amorphous region. In spite of apparent similarity between β relaxation in LDPE (L11) and the α_1 relaxation in HDPE (LPE38) existing as the major relaxation, they were assigned to different origins rather than to the same mechanism. The significantly different relaxation temperatures lend support to assign the major loss peaks of LPE, L04 as α_1 relaxation, but assign the major loss peaks in L11 and L24 as β relaxations.

α_1 (α') *relaxation*: Considerable uncertainty on the origin of α_1 relaxation could be attributed to the elusive nature of α_1 relaxation in crystalline polyethylenes from our assignments. α_1 relaxation can always only be inferred from the apparent shoulder of α_2 relaxations in HDPE such as LPE and L04. It is further screened in LDPE by the increasing intensity of β relaxation as well as less regular lamellar structure in LDPE, which results in lower necessity of lamellar slip in responding to tension.

α_2 (α or α_c) relaxation: the mechanism of α_2 relaxations could be clearly determined if the α1 relaxation had actually been ignored as a lot of researchers usually did, especially in LDPE. The clear dependence of the α_2 on lamellar thickness had naturally led to the conclusion of c-shear within the crystals as the molecular origin.

5.5.1.4. About the glass transition temperature of PE

The original objective of DMA studies on PE is to check the effect of crystal structure and morphology on the α relaxations, which is usually affected by the crystallinity and lamellar thickness and morphology. However, during the course of the experiment and subsequent analysis, it was realized that the complex relaxation behavior of polyethylene could be better understood in the context of a spectrum of branch content and diverse spherulitic morphology. Therefore, it is meaningful to have a brief discussion on the glass transition temperature of polyethylene regarding to the present experimental results.

It should be mentioned that the glass transition temperature has been a controversial topic(Boyer 1973a, Boyer 1973b, Popli et al 1984, Stehling & Mandelkern 1970) for a long time. Even the glass transition itself is not a significant experimental phenomenon for the crystalline polyethylene; it still stimulates great enthusiasm and sometime bitter arguments in the polymer physics field due to the importance of polyethylene.

In general, there has been three amorphous transition temperatures (Boyer 1973b) taken as the glass transition temperature: 145 ± 10 K, 195 ± 10 K, and 240 ± 10K. The two temperatures of 145 K and 240 K are usually corresponding to γ and α relaxation, respectively; and the 195 K is usually extrapolated either from the amorphous ethylene copolymer or from bulk crystallized polyethylene with different crystallinity (Illers 1972). It was suggested (Boyer 1973a, Boyer 1973b) that semi-crystalline polyethylene should have double glass transitions: an upper one, Tg(U), around 240K and a lower one,

Tg(L) around 195K (see Figure 5.47), which continuously vary with crystallinity and merge at 195 K for totally amorphous polyethylene. In consistence with chain folding crystal structure, it was further proposed that the double transitions aroused from different morphological feature in melt crystallized polyethylene: Tg(U) was associated with loose loops and tie chains; Tg(L) was associated with cilia of one free end. It was also implied that other phase structures could also cause double glass transition temperature such as smectic or paracrystaline phase (Takayanagi & Matsuo 1967) and fringed micelle as tentatively proposed in amorphous PET (Yeh & Geil 1967).

The direct evidence of glass transition of linear polyethylene was not available until the successful quenching of polyethylene melt into amorphous with liquid nitrogen (Hendra et al 1975)The infrared data revealed that the quenched amorphous state began to transform into crystalline structure around 180 K. The torsion braid analysis of utlra-quenched LPE (Lam & Geil 1978) confirmed the double glass transition hypothesis of Boyer that a Tg(L) at 190 K corresponded to the real glass transition temperature and a Tg(U) at 260 K due to the amorphous regions constrained by crystalline region (Figure 5.48).

In the light of this evidence, it seems that the β relaxation temperature determined from DMA should be related to the Tg(U) rather than the real glass transition temperature Tg(L). For comparing with the β relaxation temperature from DMA, the glass transition temperatures of polyethylene copolymers were also determined by DSC (Figure 5.49). It is clearly shown that the glass transition temperature is clearly detectable for copolymers with high branch content.

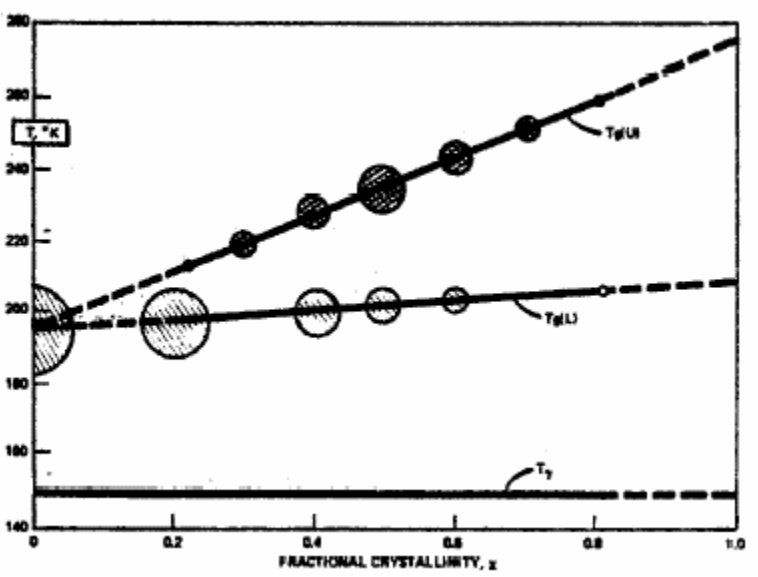

Figure 5.47. The double glass transition: Tg(L) and Tg(U) (Boyer 1973b), the size of the circles indicates the intensity of the two glass transitions.

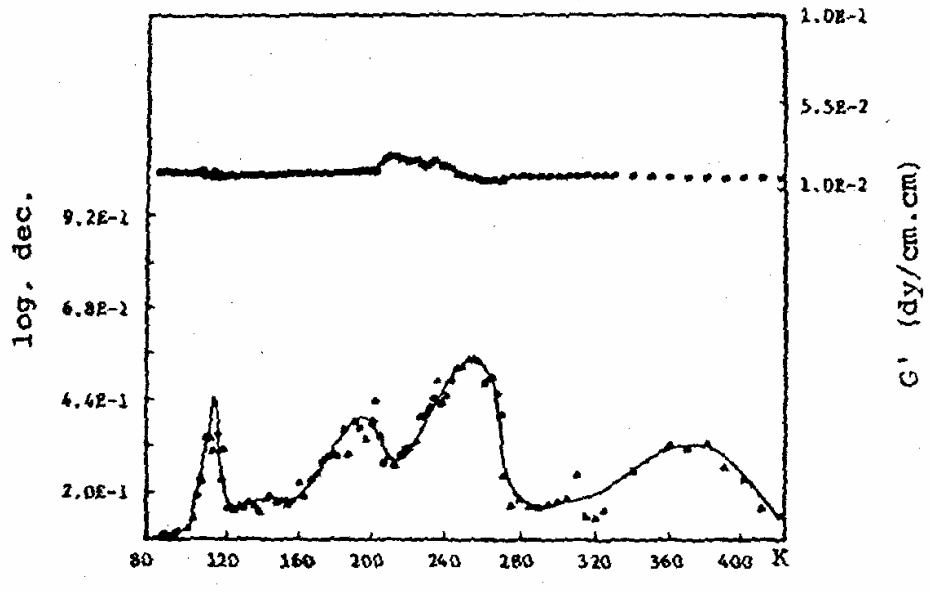

Figure 5.48. Double glass transitions observed in ultra-quenched LPE(Lam & Geil 1978)

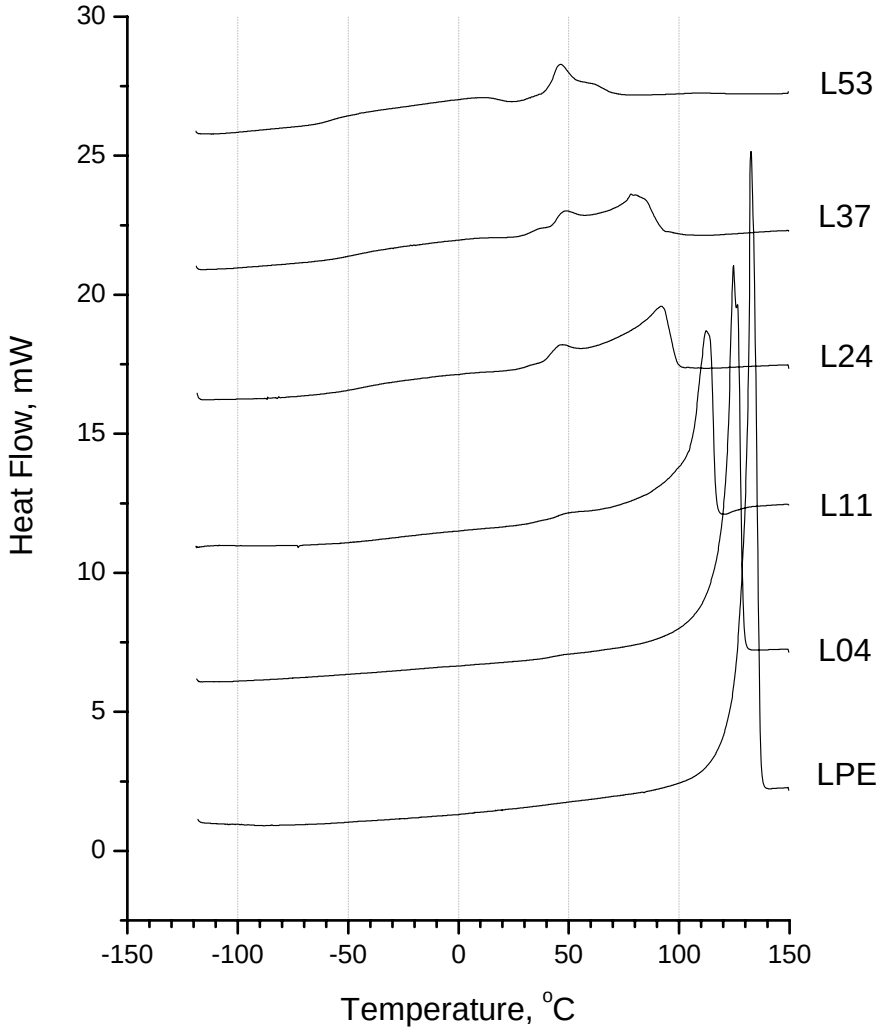

Figure 5.49. DSC heating curves of polyethylenes across glass transition region.

The Tg data determined by DSC were plotted together with the β relaxation temperatures versus the crystallinity determined with WAXD (Figure 5.50). It is clearly shown that the glass transition temperatures from DSC are close to β relaxation temperatures. Both temperatures increase with crystallinity probably due to the increasing constraint effect of crystalline phases.

It should be mentioned that neither the DSC result nor the DMA results clearly show the apparent double glass transition as the case of ultra-quenched LPE. It could be the results of the very close value at low crystallinity or the amorphous structure in our studies is significantly different from the ultra-quenched structure, which could still maintain the chain conformation and distance in the melts in the contrary to the slowly transformed amorphous structure in this study.

Another feature should be noted that the β relaxation temperatures of L11 and L24 do not change significantly with the crystallinity by changing supercoolings. Therefore, it is possible that free volume, due to varying branch content, rather than crystallinity actually play important role in the β relaxation.

5.5.2. Relaxation behavior of PA66 copolymers

5.5.2.1. Relaxation mechanism of PA66

The relaxation behavior of PA66 is well summarized in by McCrum, Read and Williams (McCrum et al 1967). Generally, three loss peaks (labeled as γ, β and α) can be observed with increasing temperature around -140 °C, -60°C and 80°C.

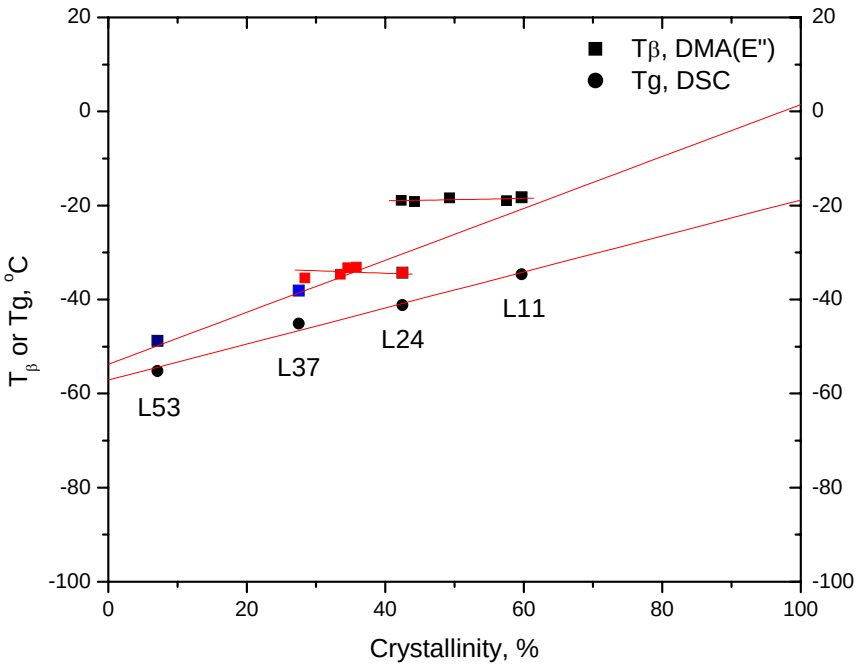

Figure 5.50. β relaxation temperature and glass transition temperature (from DSC) with crystallinity.

The γ peak of PA66 peak is a little broader but occurs at the similar temperature and frequency as the γ peak of polyethylene. Therefore, it is widely accepted that γ relaxation of PA66 is due to the motion of methylene segments between amide groups. However, the existence of γ relaxation in dielectric experiments of Curtis (1961) implied that dipolar amide groups were partially involved in the γ relaxation.

The β relaxation was originally assigned to the motions of chain segments including amide groups that are not hydrogen bonded by Woodard et al (1957). Based on the observation that β relaxation magnitude increased with water content, however, Curtis (1961) proposed that β relaxation involves the motions of water-polymer complex. That still could be due to the effect of H_2O molecules H-bonding to amide group to remove H-bonding between molecular chain as suggested (Khanna & Kuhn 1997).

The α relaxation is related to the motions of long chain segments in amorphous phase, which is corresponding to the β relaxation of polyethylene. Boyd (1959) estimated that they contained about 15 amide groups from the disappearing of α relaxation in the dielectric experiment of irradiation-crosslinked PA66.

The α relaxation is usually related to amorphous glass transition (Tg) from its dependence on the content of amorphous phase. However, Willbourn (1959) suggested that Tg for polyamide is below –36 °C since PA66 can still crystallize below the temperature of α regions.

Takayanagi (1963) proposed that a relaxation involved crystalline phase for a shoulder located at high temperature side of the α relaxation in PA6 samples with very high crystallinity, and an additional crystalline relaxation might exist around 190 °C. Due to the relative low crystallinity (<50 %) usually encounter in polyamides, these high temperature relaxations are not conclusively established (McCrum et al 1967).

5.5.2.2. Effect of water

It is well known that the α, β and γ decrease when the water content is increased as shown in Figure 5.51. The α is the most sensitive to the water content and its relaxation temperature can decrease from 80°C in dry sample to -15°C for water saturated sample.

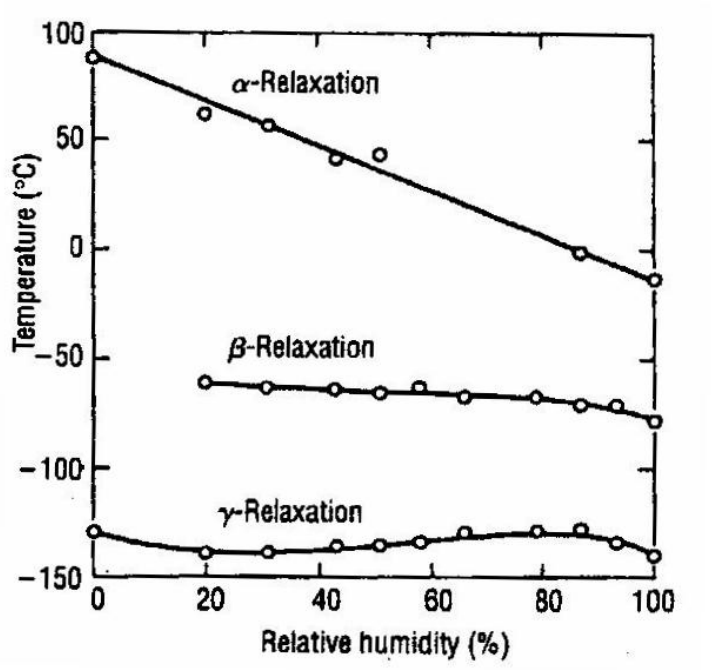

Figure 5.51 Effect of relative humidity on the relaxation temperatures of PA66 (Starkweather 1995)

The β relaxation temperature can decrease from -60°C to –80 °C over the humidity range, while γ relaxation temperature just change little (Starkweather 1995). In addition to the reduction of relaxation temperature, the magnitude of β relaxation is also found to increase significantly. This phenomenon is usually explained with the plasticizing effect of water. It is believed that water molecules enter into the amorphous region to form H-bonding with the amide groups of PA66 chains.

Therefore the inter-chain cohesive force will decrease as a result of breaking H-bonding between PA66 chain that is ultimately responsible for the decrease of relaxation temperatures (McCrum et al 1967). It should be mentioned that this plastic effect is different form the free volume explanation since the density of PA66 actually increase as a result of the water content, probably due to the closer packing between molecular chains.

5.5.2.3. Effect of chemical structure and supercooling

From the relatively high relaxation temperature and weak magnitude of β relaxation, it is reasonable to believe that water effect is not significant with the procedure of drying sample in vacuum oven before DMA tests.

Therefore, the relaxation behavior of PA66 copolymer can be attributed to the chemical structure and the supercooling with considerable degree of confidence. As to the chemical structure of comonomer, the relaxation temperatures of PA66/6T and PA66/6I copolymer appears to both increase slightly with the inclusion of comonomer

which is expected from the higher glass transition of PA6T (125 °C) and PA6I (118°C) than PA66 (80 °C).

Since the α and β relaxations are believed to be related to the amorphous region, the isomorphism effect as discussed in PA66/6T copolymer should not have any effect on the relaxation temperatures. The relaxation temperature of PA66/6 copolymer seems to decrease slightly from 82.2°C of PA66 homopolymer to 78.6 °C, which is also expected from the lower glass transition temperature of PA6 (48 °C). It therefore could be inferred that, during the melt crystallization, PA66/6T copolymer should have higher relative supercooling than PA66 whereas PA66/6 copolymer should have lower relative supercooling at the same crystallization temperature.

For the effect of supercooling, the relaxation peaks appear slightly stronger and sharper but they do not seem to be as sensitive as polyethylene, probably due to the weak crystalline relaxation in copolymer because of the lower crystallinity. The shoulder on the α relaxation seems to decrease with the increase of supercooling, especially in PA66 and PA610, which might be attributed to decreasing crystalline relaxation, as proposed by Takayanagi (1963).

CHAPTER 6. CONCLUSIONS

6.1. Temperature gradient at high supercooling

1) Linear growth rates were found during the rapid cooling of PA 66 and PET despite no temperature plateau in the cooling curve.

2) Further instantaneous growth rate analysis revealed that steady temperature gradient at the growth front of spherulites could lead to the linear growth.

3) This behavior shows that crystallization is controlled by a temperature gradient at the growth face, and not by the measured temperature.

4) The results of this study have profound implications for our understanding of polymer crystallization.

6.2. Crystallization kinetics

1) In general, the PA66/6T copolymers have almost the same growth rates as PA66 homopolymer over a wide range of supercoolings;

2) The growth rates seem to be slightly higher at very low supercooling probably due to the increased nucleation effect; and lower at very high supercooling due to decreased chain diffusion ability. Both effects could result from the existence of benzyl ring.

3) The crystallization temperatures of copolymers move to lower temperature at equivalent cooling condition, and growth rate is significantly decreased with decreasing average sequence length of PA66 at the same time.

4) With increasing cooling rate, the crystallization temperatures of copolymers move to lower temperature and have lower growth rate values than PA 66 homopolymer at equivalent cooling conditions.

6.3. Crystal morphologies

1) The final spherulitic morphology of PA 66 and PA6 copolymer could be changed from impinged spherulites to isolated spherulites with decreasing size until total amorphous.

2) Crystallinity and melting temperature were found to be lower at lower crystallization temperature from the result of DSC and WAXD.

3) These can be explained from the chain irregularities introduced by the PA 6 random comonomer, which is excluded from the crystal.

6.4. Melting behavior

1) The PA66/6T copolymers have a relatively constant melting temperature independent of comonomer content while the PA66/6I and PA66/6 copolymer decrease linearly with the increasing content of comonomer.

2) The different melting temperature dependence on comonomer content has been attributed to the isomorphism of PA66/6T copolymers; and attributed

to the conventional exclusion mechanism of PA6 and PA6I segments from the PA66 crystal core.

3) PA66/6I and PA66/6 copolymer seems to follow the same linear relationship, which might imply that their melting temperatures could both be related to the average sequence length of crystallizable PA66.

6.5. Relaxation behavior

1) It was confirmed that the relaxation behavior of copolymers varied continuously with branch content: the magnitude of the β relaxation increases with branch content, while the intensity of the α relaxation decreases with branch content; relaxation temperatures decrease with the branching in the copolymers. Copolymer films prepared at different cooling conditions were further examined and strikingly continuous changes were also found.

2) The β relaxation was believed to correlate with the long-range chain movements of the amorphous phase. With reduced branching content, the increase of the β relaxation temperature may result from the increased constraint of crystalline phase because of increased crystallinity and increased structural regularity. α_1 and α_2 relaxations are associated with the inter-lamellar slip and intra-crystalline c-shear respectively.

3) The α relaxation temperatures of PA66/6T and PA66/6I copolymers appear to increase slightly with the inclusion of comonomer; whereas PA66/6 copolymers decrease somewhat. The α relaxation peaks of PA66 copolymers appear slightly stronger and sharper but they do not seem to change significantly with supercooling as polyethylenes, probably due to the weak crystalline relaxation in copolymer because of the lower crystallinity.

REFERENCES

Abo el Maaty M. I., Bassett D. C. 2001. On fold surface ordering and re-ordering during the crystallization of polyethylene from the melt. *Polymer* 42: 4957

Abo el Maaty M. I., Bassett D. C., Olley R. H., Jaaskelainen P. 1998. On cellulation in polyethylene spherulites. *Macromolecules* 31: 7800

Armistead J. P., Hoffman J. D. 2002. Direct Evidence of Regimes I, II, and III in Linear Polyethylene Fractions As Revealed by Spherulite Growth Rates. *Macromolecules* 35: 3895

Armistead K., Goldbeck-Wood G. 1992. Polymer crystallization theories. *Advances in Polymer Science* 100: 219

Bassett D. C. 2003. Polymer spherulites: a modern assessment. *Journal of Macromolecular Science, Physics* B42: 227

Bassett D. C., Hodge A. M. 1981a. Morphology of melt-crystallized polyethylene. I. Lamellar profiles. *Proceedings of the Royal Society of London, Series A: Mathematical, Physical and Engineering Sciences* 377: 25

Bassett D. C., Hodge A. M. 1981b. Morphology of melt-crystallized polyethylene. III. Spherulitic organization. *Proceedings of the Royal Society of London, Series A: Mathematical, Physical and Engineering Sciences* 377: 61

Bassett D. C., Hodge A. M., Olley R. H. 1981. Morphology of melt-crystallized polyethylene II. Lamellae and their crystallization conditions. *Proceedings of the Royal Society of London, Series A: Mathematical, Physical and Engineering Sciences* 377: 39

Bassett D. C., Olley R. H. 1984. On the lamellar morphology of isotactic polypropylene spherulites. *Polymer* 25: 935

Benard A., Advani S. G. 1995. Energy equation and the crystallization kinetics of semi-crystalline polymers: regimes of coupling. *International Journal of Heat and Mass Transfer* 38: 819

Benard A., Advani S. G., Schultz J. M. 1996. Solidification of semicrystalline polymers using a variable interface temperature model. *Journal of Polymer Science, Part B: Polymer Physics* 34: 471

Boasson E. H., Woestenenk J. M. 1956. Negative spherulites in nylon 66 (polyhexamethylene adipamide). *J. Polymer Sci.* 21: 151

Boasson E. H., Woestenenk J. M. 1957. Aspects of the crystallization of nylon 66. *J. Polymer Sci.* 24: 57

Boyd R. H. 1985a. Relaxation processes in crystalline polymers: experimental behavior. *Polymer* 26: 323

Boyd R. H. 1985b. Relaxation processes in crystalline polymers: molecular interpretation - a review. *Polymer* 26: 1123

Boyer R. F. 1973a. Apparent Double Glass-Transition in Semicrystalline Polymers. *Journal of Macromolecular Science-Physics* B 8: 503

Boyer R. F. 1973b. Glass Temperatures of Polyethylene. *Macromolecules* 6: 288

Brenschede W. 1949. *Kolloid-Z.* 114: 35

Bunn C. W., Garner E. V. 1947. The crystal structures of two polyamides. *Proceedings of the Royal Society of London, Series A. Mathematical and Physical Sciences* 189: 39

Burnett B. B., McDevit W. F. 1957. Kinetics of spherulite growth in high polymers. *J. Appl. Phys.* 28: 1101

Burton W. K., Cabrera N., Frank F. C. 1949. Dislocations in crystal growth. *Nature (London, United Kingdom)* 163: 398

Cahn J. W., Hillig W. B., Sears G. W. 1964. The molecular mechanism of solidification. *Acta Met.* 12: 1421

Calvert P. D. 1983. Fibrillar structures in spherulites. *Journal of Polymer Science, Polymer Letters Edition* 21: 467

Chui S. T., Weeks J. D. 1978. Dynamics of Roughening Transition. *Physical Review Letters* 40: 733

Clas S. D., McFaddin D. C., Russell K. E. 1987. Dynamic mechanical properties of homogeneous copolymers of ethylene and 1-alkenes. *Journal of Polymer Science, Part B: Polymer Physics* 25: 1057

Cooper S. J., Atkins E. D. T., Hill M. I. 1998. Structures for monodisperse oligoamides. A novel structure for unfolded three-amide nylon 6 and relationship with a three-amide nylon 6 6. *Journal of Polymer Science, Part B: Polymer Physics* 36: 2849

Ding Z., Spruiell J. E. 1996. An experimental method for studying nonisothermal crystallization of polymers at very high cooling rates. *Journal of Polymer Science, Part B: Polymer Physics* 34: 2783

Ding Z., Spruiell J. E. 1997. Interpretation of the nonisothermal crystallization kinetics of polypropylene using a power law nucleation rate function. *Journal of Polymer Science, Part B: Polymer Physics* 35: 1077

Dole M., Wunderlich B. 1959. Melting points and heats of fusion of polymers and copolymers. *Makromolekulare Chemie* 34: 29

Dreyfuss P., Keller A. 1970. A. *Journal of Macromolecules Science, Physics B.* 4

Dreyfuss P., Keller A. 1973. Invariance of the long spacing-crystallization temperature dependence of polyamides precipitated from solution. *Journal of Polymer Science, Polymer Physics Edition* 11: 193

Dreyfuss P., Keller A., Willmouth F. M. 1972. Novel diffraction effects in the combined wide-angle and low-angle x-ray diffraction patterns of solution-grown nylon crystals. *Journal of Polymer Science, Polymer Physics Edition* 10: 857

Eder G., Janeschitz-Kriegl H., Liedauer S. 1990. Crystallization processes in quiescent and moving polymer melts under heat transfer conditions. *Progress in Polymer Science* 15: 629

Edger O. B., Hill R. 1952. The p-Phenylene linkage in linear high polymers:some structure -property relationship. *Journal of Polymer Science* 8: 1

Edwards B. C., Phillips P. J. 1975. High-pressure phases in polymers. II. Spherulitic growth morphology in cis-polyisoprene. *Journal of Polymer Science, Polymer Physics Edition* 13: 2117

Flocke H. A. 1962. 180: 118

Flory P. J. 1949. Thermodynamic of Crystallization in High Polymers. IV. A Therory of Crystalline States and Fusion in Polymer, Copolymers, and Their Mixture with Diluents. *Journal of Chemical Physics* 17: 223

Flory P. J. 1969. *Statistical Mechanis of Chain Molecules*. New York: Intersciences

Garcia D., Starkweather H. W., Jr. 1985. Hydrogen bonding in nylon 66 and model compounds. *Journal of Polymer Science, Polymer Physics Edition* 23: 537

Geil P. H. 1960. Nylon single crystals. *Journal of Polymer Science* 44: 449

Geil P. H. 1963. *Polymer single crystals*. New York: Intersciences

Gill W. N. 1989. Heat transfer in crystal growth dynamics. *Chemical Engineering Progress* 85: 33

Gilmer G. H. 1976. *Journal of Crystal Growth* 36: 15

Glicksman M. E., Lupulescu A. O. 2004. Dendritic crystal growth in pure materials. *Journal of Crystal Growth* 264: 541

Guan X., Phillips P. J. 2003. *Crystallization behaviors of nylon 66 and nylon 66 copolymers at high supercoolings*. Presented at Annual Technical Conference - Society of Plastics Engineers

Harvey E. D., Hybart F. J. 1970. Rates of crystallization of copolyamides. II. Random copolymers of nylons 66 and 6. *Journal of Applied Polymer Science* 14: 2133

Harvey E. D., Hybart F. J. 1971. Melting and crystallization of copolymers of nylon-66 and nylon-610 with poly(hexamethylene terephthalamide) (nylon-6T). *Polymer* 12: 711

Hendra P. J., Jobic H. P., Holland-Moritz K. 1975. Low temperature crystallization in polyethylene and the value of Tg. *Journal of Polymer Science, Polymer Letters Edition* 13: 365

Hinrichsen G. 1973. *Die Makromolekulare Chemie* 166: 291

Hirschinger J., Miura H., Gardner K. H., English A. D. 1990. Segmental dynamics in the crystalline phase of nylon 66: solid state deuterium NMR. *Macromolecules* 23: 2153

Hobbs J. K., McMaster T. J., Miles M. J., Barham P. J. 1998. Direct observations of the growth of spherulites of poly(hydroxybutyrate-co-valerate) using atomic force microscopy. *Polymer* 39: 2437

Hoffman J. D. 1985. Growth rate of extended-chain crystals: the lateral surface free energy of pure n-C94H190 and a fraction .apprx.C207H416. *Macromolecules* 18: 772

Hoffman J. D., Davis G. T., Lauritzen J. I., Jr. 1976. The rate of crystallization of linear polymers with chain folding. *Treatise Solid State Chem.* 3: 497

Hoffman J. D., Miller R., L. 1997. Kinetics of crystallization from the melt and chain folding in polyethylene fractions revisited: theory and experiment. *Polymer* 38: 3151

Hosier I. L., Bassett D. C., Vaughan A. S. 2000. Spherulitic Growth and Cellulation in Dilute Blends of Monodisperse Long n-Alkanes. *Macromolecules* 33: 8781

Illers K. H. 1972. Glass temperature in the amorphous region in partially crystalline polymethylene. *Kolloid Zeitschrift & Zeitschrift fuer Polymere* 250: 426

Illers K. H., Haberkorn H. 1971. Specific volume, heat of fusion, and crystallinity of nylon 66 and nylon 8. *Makromolekulare Chemie* 146: 267

Jackson K. A. 1969. Theory of crystal growth: fundamental rate equation. *Journal of Crystal Growth* 5: 13

Jackson K. A. 1984. Crystal growth kinetics. *Materials Science and Engineering* 65: 7

Keith H. D., Padden F. J., Jr. 1963. A phenomenological theory of spherulitic crystallization. *Journal of Applied Physics* 34: 2409

Keith H. D., Padden F. J., Jr. 1964a. Spherulitic crystallization from the melt. I. Fractionation and impuritiy segregation and their influence on crystalline morphology. *Journal of Applied Physics* 35: 1270

Keith H. D., Padden F. J., Jr. 1964b. Spherulitic crystallization from the melt. II. Influence of fractionation and impurity segregation on the kinetics of crystallization. *Journal of Applied Physics* 35: 1286

Keller A. 1959. The morphology of crystalline polymers. *Die Makromolekulare Chemie* 34: 1

Keller A. 1968. Polymer crystals. *Reports of Progress in Physics* 31: 626

Khanna Y. P., Kuhn W. P. 1997. Measurement of crystalline index in nylons by DSC: complexities and recommendations. *Journal of Polymer Science, Part B: Polymer Physics* 35: 2219

Khoury F. 1958. Formation of negatively birefringent spherulites in poly-(hexamethylene adipamide) (Nylon 66). *Journal of Polymer Science* 33: 389

Koenig J. L., Agboatwalla M. C. 1968. Infrared studies of chain folding in polymers. IV. Poly(hexamethyleneadipamide). *Journal of Macromolecular Science, Physics* 2: 389

Kohan M. I. 1995. *Nylon Plastics Handbook*. New York: Hanser

Lam R., Geil P. H. 1978. The Tg of amorphous linear polyethylene: a torsion braid analysis. *Polymer Bulletin (Berlin, Germany)* 1: 127

Langer J. S. 1989. Dendrites, Viscous Fingers, and the Theory of Pattern-Formation. *Science* 243: 1150

Lauritzen J. I., Hoffman J. D. 1973. *Journal of Applied Physics* 44: 4340

Lauritzen J. I., Jr., Hoffman J. D. 1960. Theory of formation of polymer crystals with folded chains in dilute solution. *J. Research Natl. Bur. Standards* 64A: 73

Leung W. M., Manley R., Panaras A. R. 1985. Isothermal growth of low molecular weight polyethylene single crystals from solution. 3. Kinetic studies. *Macromolecules* 18: 760

Lindegren C. R. 1961. Spherulites in nylon 610 and nylon 66. *Journal of Polymer Science* 40: 181

Lock G. S. H. 1994. Latent Heat Transfer: An introduction to fundamentals. New York: Oxford University Press

Lovinger A. J. 1978a. Crystallographic factors affecting the structure of polymeric spherulites. I. Morphology of directionally solidified polyamides. *Journal of Applied Physics* 49: 5003

Lovinger A. J. 1978b. Crystallographic factors affecting the structure of polymeric spherulites. II. X-ray diffraction analysis of directionally solidified polyamides and general conclusions. *Journal of Applied Physics* 49: 5014

Magill J. H. 1962. Crystallization kinetics study of nylon 6. *Polymer* 3: 655

Magill J. H. 1966. Formation of spherulites in polyamide melts. III. Even-even polyamides. *Journal of Polymer Science, Polymer Physics Edition* 4: 243

Magill J. H., Girolamo M., Keller A. 1981. Crystallization and morphology of nylon-6,6 crystals. 1. Solution crystallization and solution annealing behavior. *Polymer* 22: 43

Mann J., Roldan-Gonzalez L. 1962. Orientation in nylon spherulites-x-ray diffraction. *Journal of Polymer Science* 60: 1

McCrum N., G. , Read B. E., Williams G. 1967. *Anelastic and Dielectric Effects in Polymeric Solids*. New York: Wiley

McLaren J. V. 1963. Kinetic study of the isothermal spherulitic crystallization of poly(hexamethylene adipamide). *Polymer* 4: 175

Medellin-Rodriguez F. J., Larios-Lopez L., Zapata-Espinoza A., Davalos-Montoya O., Phillips P. J., Lin J. S. 2004. Melting behavior of polymorphics: moldecular weight dependence and steplike mechanism in nylon-6. *Macromolecules* 37: 1799

Mitomo H. 1988. Correspondence of lamellar thickness to melting point of nylon-6,6 single crystal. *Polymer* 29: 1635

Mullins W. W., Sekerka R. F. 1963. Morphological stability of a particle growing by diffusion or heat flow. *Journal of Applied Physics* 34: 323

Naterer G. F. 2000. *Heat Transfer in Single and Multiphase Systems,*. Boca Raton, Florida: CRC Press

Ngai K. L., Magill J. H., Plazek D. J. 2000. Flow, diffusion and crystallization of supercooled liquids: Revisited. *Journal of Chemical Physics* 112: 1887

Nielsen L. E. 1960. *Journal of Polymer Science* 42: 357

Phillips P. J. 1990. Polymer crystals. *Reports of Progress in Physics* 53: 549

Phillips P. J. 1994. Spherulitc Crystallization in Macromolecules. In *Handbook of Crystal Growth,* ed. D. T. J. Hurle, pp. 1168

Point J. J., Kovacs A. J. 1980. A critical look at some conceptual aspects of kinetic theories of polymer crystal growth. *Macromolecules* 13: 399

Popli R., Glotin M., Mandelkern L., Benson R. S. 1984. Dynamic mechanical studies of a and b relaxations of polyethylenes. *Journal of Polymer Science, Polymer Physics Edition* 22: 407

Porter D. A., Easterling K. E. 2001. *Phase Transformations in Metals and Alloys*. Cheltenham: Nelson Thornes

Prabhu N., Schultz J., Advani S. G., Jacob K. I. 2001. Role of coupling microscopic and macroscopic phenomena during the crystallization of semicrystalline polymers. *Polymer Engineering and Science* 41: 1871

Raimo M., Cascone E., Martuscelli E. 2001. Melt crystallization of polymer materials: the role of the thermal conductivity and its influence on the microstructure. *Journal of Materials Science* 36: 3591

Ramesh C., Keller A., Eltink S. J. E. A. 1994a. Studies on the crystallization and melting of nylon 66: 2. Crystallization behavior and spherulitic morphology by optical microscopy. *Polymer* 35: 5293

Ramesh C., Keller A., Eltink S. J. E. A. 1994b. Studies on the crystallization and melting of nylon 66: 3. Melting behavior of negative spherulites by calorimetry. *Polymer* 35: 5300

Sadler D. M., Gilmer G. H. 1984. A model for chain folding in polymer crystals: rough growth faces are consistent with the observed growth rates. *Polymer* 25: 1446

Sadler D. M., Gilmer G. H. 1986. Rate-theory model of polymer crystallization. *Physical Review Letters* 56: 2708

Schmieder K., Wolf K. 1953. *Kolloid-Z.* 134: 149

Schreiber S., Phillips P. J. 1998. Acceleration of spherulite growth rates of nylon 6,6 by comonomer addition. *Annual Technical Conference - Society of Plastics Engineers* 56th: 2060

Schreiber S. L. 1998. *Crystallization of random copolymers based on poly (hexamethylene adipamide)*, University of Tennessee, Knoxville, Knoxville

Schultz J. M. 1991a. Roles of 'solute' and heat flow in the development of polymer microstructure. *Polymer* 32: 3268

Schultz J. M. 1991b. Theory of crystallization in high-speed spinning. *Polymer Engineering and Science* 31: 661

Sekerka R. F. 1968. Morphological stability. *Journal of Crystal Growth* 3-4: 71

Sifleet W. L., Dinos N., Collier J. R. 1973. Unsteady-State Heat Transfer in a Crystalline Polymer. *Polymer Eng. Sci.* 13: 10

Sombatsompop N., Chonniyom D., Wood A. K. 1999. Temperature gradients in molten polymers during the cooling process. *Journal of Applied Polymer Science* 74: 3268

Stachurski Z. H., Ward I. M. 1969. Anisotropy of viscoelastic relaxation in low-density polyethylene in terms of an aggregate model. *Journal of Macromolecular Science, Physics* 3: 427

Starkweather H. W., Jr. 1995. Transitions and relaxations [of nylon plastics]. *Nylon Plastics Handbook*: 139

Starkweather H. W., Jr., Jones G. A. 1981. Crystalline transitions in powders of nylon 66 crystallized from solution. *Journal of Polymer Science, Polymer Physics Edition* 19: 467

Starkweather H. W., Jr., Whitney J. F., Johnson D. R. 1963. Crystalline order in Nylon 66. *Journal of Polymer Science: Part A* 1: 715

Starkweather H. W., Jr., Zoller P., Jones G. A. 1984. The heat of fusion of 66 nylon. *Journal of Polymer Science, Polymer Physics Edition* 22: 1615

Stehling F. C., Mandelkern L. 1970. Glass temperature of linear polyethylene. *Macromolecules* 3: 242

Stockmayer W. H. 1973. Dynamics of local motions. *macromolecular Chemistry* 8: 379

Stouffer J. M., Starkweather H. W., Jr., Hsiao B. S., Avakian P., Jones G. A. 1996. Copolymer modification of nylon-6,6 with 2-methylpentamethylenediamine. *Polymer* 37: 1217

Strobl G. R., Schneider M. J. 1980a. *J. Polym. Sci. Polym. Phys. Phys. Ed.* 18: 1343

Strobl G. R., Schneider M. J. 1980b. *J. Polym. Sci. Polym. Phys. Phys. Ed.* 18: 1361

Takayanagi M. 1974. Some Morphological Factors in Thermomechanical Analysis of Crystalline Polymers. *Journal of Macromolecular Science, Physics* 9: 391

Takayanagi M., Matsuo T. 1967. Studies of Fien Structure of Viscoelastic Crystalline Absorption in Polyethylene Single Crystals. *Journal of Macromolecular Science, Physics* 1: 407

Tiller W. A. 1991. *The Science of Crystallization: microscopic interfacial phenomena*. Cambridge: Cambridge University Press

Tiller W. A., Jackson K. A., Rutter J. W., Chalmers B. 1953. The redistribution of solute atoms during the solidification of metals. *Acta Met.* 1: 428

Tiller W. A., Schultz J. M. 1984. Crystallization of polymers under high tension: a dendrite model. *Journal of Polymer Science, Polymer Physics Edition* 22: 143

Vonk C. G. 1988. *Macromolecular Chemistry, Macromolecuar Symposium* 15: 215

Wagner J., Abu-Iqyas S., Monar K., Phillips P. J. 1999. Crystallization of ethylene-octene copolymers at high cooling rates. *Polymer* 40: 4717

Wagner J., Phillips P. J. 2001. The mechanism of crystallization of linear polyethylene, and its copolymers with octene, over a wide range of supercoolings. *Polymer* 42: 8999

Willbourn A. H. 1958. *Trans. Faraday Soc.* 54: 717

Wunderlich B. 1980. *Macromolecuar Physics*. New York: Academic Press

Xenopoulos A., Wunderlich B. 1990. Thermodynamic properties of liquid and semicrystalline linear aliphatic polyamides. *Journal of Polymer Science, Part B: Polymer Physics* 28: 2271

Xenopoulos A., Wunderlich B. 1991. Conformational motion and disorder in aliphatic nylons. The case of nylon 6.6. *Colloid and Polymer Science* 269: 375

Yeh G. S. Y., Geil P. H. 1967. Crystallization of poly(ethylene terephthalate) from the glassy amorphous state. *J. Macromol. Sci., Part B.* 1: 235

Yu A. J., Evans R. D. 1959. Isomorphous replacement in copolyamides systems: homologs of adipic and terephalic acids. *Journal of American Chemical Society* 81: 5361

VITA

Xiaoping Guan was born in Jingmen, Hubei Province of China in December 1972. He graduated from Hubei Polytechnic University in Wuhan, China with a B.E. in Chemical Engineering in July, 1994. Then he went to Shanghai Jiao Tong University and graduated with a M.S. in Polymeric Materials Science and Engineering in March, 1997. He had worked for two years in Yanfeng Visteon Automotive Trim Company as a polymer process engineer.

He entered the Polymer Engineering program in Department of Materials Science and Engineering at University of Tennessee, Knoxville in August, 1999. He married Dr. Ying Chen on January 29, 2003. He completed all the requirements for the Doctor of Philosophy degree in Polymer Engineering by August 2004.